UNIVERSITÀ
DEGLI STUDI
DI PADOVA

Sede Amministrativa: Università degli Studi di Padova

Dipartimento di Ingegneria Industriale

SCUOLA DI DOTTORATO DI RICERCA IN INGEGNERIA INDUSTRIALE
INDIRIZZO: INGEGNERIA DELL'ENERGIA
CICLO: XXVII

POWER PLANTS BEHAVIOUR DURING TRANSIENT OPERATING CONDITIONS

Direttore della Scuola: Ch.mo Prof. Paolo Colombo
Coordinatore d'indirizzo: Ch.mo Prof. Luisa Rossetto
Supervisore: Ch.mo Prof. Anna Stoppato
Co-Supervisore: Ch.mo Prof. Alberto Mirandola

Dottorando: Alberto Benato

UNIVERSITÀ
DEGLI STUDI
DI PADOVA

Sede Amministrativa: Università degli Studi di Padova

Dipartimento di Ingegneria Industriale

SCUOLA DI DOTTORATO DI RICERCA IN INGEGNERIA INDUSTRIALE
INDIRIZZO: INGEGNERIA DELL'ENERGIA
CICLO: XXVII

POWER PLANTS BEHAVIOUR DURING TRANSIENT OPERATING CONDITIONS

Direttore della Scuola: Ch.mo Prof. Paolo Colombo
Coordinatore d'indirizzo: Ch.mo Prof. Luisa Rossetto
Supervisore: Ch.mo Prof. Anna Stoppato
Co-Supervisore: Ch.mo Prof. Alberto Mirandola

Dottorando: Alberto Benato

Acknowledgements

I would like to take this opportunity to acknowledge those who have supported me during my Ph.D. course.

Firstly, I would like to thank my supervisors, Professor Anna Stoppato and Professor Alberto Mirandola, for giving me this opportunity, for their constant support and encouragement throughout, and for their belief that I would complete my work profitably.

A particular acknowledgement for the support during my external stay at the Technical University of Denmark is to Professor Fredrik Haglind, Ing. Leonardo Pierobon and Dr. Martin Ryhl Kærn.

I would also like to thank the members of the Energy Conversion Systems and Machines group at the University of Padova for their help and support.

Finally, I wish to thank Maria and my family, my parents for their encouragement and support, and my brother.

Abstract

System dynamic modelling and simulation is becoming a powerful and essential design tool. For this reason, this Ph.D. Thesis is devoted to analyse the transient operation conditions' effects using power plant dynamic models.

In the first part of this dissertation, the dynamic analysis is the core of a procedure developed to predict lifetime reduction on traditional power plant devices. In particular, the plant dynamic model, and its capability of evaluating the trends of the main thermodynamic parameters, which describe the plant operation during transient conditions, is the base point to identify the most stressed plant devices.

Being fundamental the role played by combined cycle power plants in the liberalized electricity market scenario, a combined cycle power plant is selected as test case. The dynamic model of a single pressure combined cycle power unit is built and the proposed procedure is tested. The results show that the procedure can be considered as a valuable innovative tool to assist power plant designers and operators in order to improve the plant's flexibility without excessively compromising the integrity of devices subjected to high thermo-mechanical stresses.

The second part of this work underlines the essential role played by the dynamic analysis during the design phase of innovative small-medium size waste heat recovery units on isolated grid. In particular, after a design optimization process, the dynamic behaviour of gas turbines coupled with waste heat recovery units (ORC, SRC and ABC power units) is tested to verify the grid stability and, in the case of an ORC unit, the working fluid thermochemical stability.

In conclusion, in this dissertation, two different software tools are proposed. In both cases the core is the plant dynamic model. The first tool is able to predict the plant thermodynamic variables and compute the components lifetime reduction caused by load changes while the second one performs a design and optimization of different waste heat recovery units for stand-alone offshore facilities. The entire plant is then dynamically analysed in order to verify the grid stability and, in the case of ORC unit, the working fluid thermochemical stability.

Riassunto

La simulazione dinamica sta diventando uno strumento sempre più potente ed essenziale sia nella fase di design che durante il processo di ottimizzazione e gestione dei sistemi di produzione dell'energia. Da questa nuova necessità è nata l'idea di studiare gli effetti indotti dalle variazioni di carico sui componenti che costituiscono gli impianti energetici. A tal fine si devono sviluppare dei modelli di impianto in grado di simulare il comportamento dinamico del sistema in esame.

Nella prima parte di questo elaborato, l'analisi dinamica è il cuore di una procedura integrata sviluppata allo scopo di prevedere la riduzione di vita utile dei componenti maggiormente sollecitati degli impianti termoelettrici. In particolare, il modello dinamico dell'impianto, capace di simulare l'andamento delle principali grandezze termodinamiche e quindi il comportamento del sistema durante le variazioni di carico, è l'elemento centrale della procedura poichè consente di identificare i componenti maggiormente soggetti a fenomeni di stress derivante da fatica termo-meccanica.

Dato che gli impianti a ciclo combinato sono la tecnologia attualmente più efficiente e maggiormente diffusa tra i produttori di energia operanti nel mercato liberalizzato della produzione, il caso studio selezionato per testare la procedura sviluppata è proprio un impianto a ciclo combinato a singolo livello di pressione. I risultati ottenuti dimostrano che la procedura è un metodo innovativo in grado di assistere sia i progettisti che gli operatori degli impianti poichè in grado di simulare il comportamento dinamico del sistema e fornire indicazioni fondamentali sugli effetti indotti dall'esercizio flessibile.

Tuttavia, l'analisi dinamica riveste un ruolo centrale anche nel caso di progettazione di impianti medio-piccoli di recupero del calore di scarto. Questi impianti vengono generalmente impiegati per incrementare le prestazioni del sistema e ridurre contestualmente i consumi di combustibile e le emissioni inquinanti rilasciate in atmosfera. La seconda parte di questo elaborato si focalizza quindi sull'utilizzo e l'integrazione dell'analisi dinamica nel processo di design e gestione degli impianti di piccola potenza inseriti in reti stand-alone di piattaforme oil and

gas. In particolare, dopo l'individuazione del case study (impianto costituito da tre turbine a gas in ciclo semplice) ed una fase di studio delle possibili configurazioni (tre turbine a gas alternativamente affiancate da differenti sistemi di recupero: ABC, SRC, ORC), differenti tipologie di impianto sono state progettate utilizzando una ottimizzazione multi-obiettivo. A partire da questi dati di design, sono stati costruiti i modelli dinamici delle diverse configurazioni di impianto al fine di verificare la stabilità della rete elettrica e, nel caso di un sistema di recupero basato sulla tenologia ORC, del fluido termovettore impiegato nel ciclo sottoposto.

In conclusione, nella presente tesi di dottorato vengono sviluppati due differenti computer tools. In entrambi i casi il cuore è costituito dal modello dinamico dell'impianto di produzione dell'energia. Nel primo tool software è implementata una procedura innovativa sviluppata con lo scopo di simulare il comportamento dell'impianto durante le variazioni di carico, predire il trend delle principali grandezze termodinamiche, individuare i componenti maggiormente sollecitati e calcolare la riduzione di vita utile indotta sui componenti. Il secondo tool, invece, realizza prima una progettazione ottimizzata di differenti tipologie di unità di recupero del calore di scarto per stand-alone offshore facilities. Quindi, il comportamento dinamico dell'impianto viene simulato in maniera tale da verificare la stabilità della rete elettrica e, nel caso di una unità ORC, la stabilità termochimica del fluido operativo di ciclo.

Contents

List of Tables

List of Figures

Nomenclature

A	area [m^2]
A_{ff}	free flow area [m^2]
C_T	turbine constant [$kg \cdot K^{0.5} \cdot s^{-1} \cdot Pa^{-1}$]
C_o	dimensionless parameter in Eq. 5.3
D	total creep-fatigue damage [-]
D_{CF}	cumulative fatigue damage index [-]
D_L	limit damage [-]
D_c	creep damage [-]
D_h	hydraulic diameter [m]
F	parameter in Eqs. 3.8 and 5.31
F_{cu}	copper loss fraction [-]
F_t	temperature correlation factor [-]
G	mass flux [$kg \cdot m^{-2} \cdot s^{-1}$]
H	fin height [m] or pump Head [m]
I	total capital cost [$] or moment of inertia [$kg \cdot m^2$]
I_{CO2}	income saved CO_2 emissions [$\cdot yr^{-1}$]
I_{fuel}	income saved fuel consumptions [$\cdot yr^{-1}$]
L	flow length [m]
$Load$	platform load [W] or gas turbine load [-]

M_{f}	maintenance factor [-]
N	dimensionless parameter in Eq. 5.3 or number of stages [-]
N_0	number of cycles before failure [cycle]
Np	number of plates [-]
Nt	number of parallel tubes [-]
P	power [W]
P_r	Prandtl number [-]
R	thermal conduction resistance [K $\cdot$ W^{-1}] or yearly income [\$$\cdot$ yr^{-1}]
R_e	Reynolds number [-]
T	temperature [°C]
U	overall heat transfer coefficient [W $\cdot$ m^{-2} $\cdot$ K^{-1}] or internal energy [J]
V	volume [m^{-3}]
W	weight [kg]
X	operand in Eq. 5.22
$\bar{J}$	arrays of objective functions
$\bar{X}$	arrays of variables
$\dot{Q}$	heat rate [W]
$\dot{V}$	volumetric flow rate [m^3 $\cdot$ s^{-1}]
$\dot{m}$	mass flow rate [kg $\cdot$ s^{-1}]
Bo	Boiling number [-]
Fr	Froude number [-]
Nu	Nusselt number [-]
b_1, b_2	parameters in Eq. 5.29

c	speed of sound [m $\cdot$ s^{-1}]
c_p	specific heat capacity [J $\cdot$ kg^{-1} $\cdot$ K^{-1}]
d	diameter [m]
f	Fanning factor [-]
f_D	Darcy friction factor [-]
f_l	fin length [m]
g	gravity acceleration [m $\cdot$ s^{-2}]
h	enthalpy [J $\cdot$ kg^{-1}] or heat transfer coefficient [W $\cdot$ m^{-2} $\cdot$ K^{-1}]
h_{LG}	heat of vaporization [J $\cdot$ kg^{-1}]
i	discount rate or operand in Eq. 1.10
j	Colburn factor [-]
j_{sf}	shell side friction factor [-]
j_{sh}	shell side heat transfer factor [-]
j_{tf}	tube side friction factor [-]
j_{th}	tube side heat transfer factor [-]
k	heat capacity ratio in Eqs. 4.1 and 4.2
l	length [m]
m_{CO2}	CO_2 emissions [ton $\cdot$ d^{-1}]
n	rotational speed [rpm] or lifetime of the investment [year] or equipment lifespan [-]
nf	number of fins per meter [m]
p	pressure [Pa]
p_t	tube pitch [m]
pt	plate thickness [m]

q	interest factor
q''	heat flux [$W \cdot m^{-2}$]
r_e	expansion ratio [-]
r_c	compression ratio [-]
s	entropy [$J \cdot kg^{-1} \cdot K^{-1}$]
t	fin thickness [m] or time [s]
t_r	time of failure [yr]
tw	thickness [m]
u	velocity [$m \cdot s^{-1}$]
x	steam moisture content [-]

Abbreviations

CO_2	carbon dioxide
ABC	air bottoming cycle
AC	air compressor
AHX	air to gas heat exchanger
AMA	arithmetic mean average
AT	air turbine
CC	combustion chamber
CCPP	combined cycle power plant
CFC	chlorofluorocarbons
DC	direct costs
ECO	economizer
EGS	engineered geothermal system
EU	European Union

EVA	evaporator
FCI	fixed-capital investment
FLC	fatigue life calculation
GA	genetic algorithm
GEN	electric generator
GHG	greenhouse gases
GT	gas turbine
GWP	global warming potential
HC	hydrocarbons
HCFC	hydrochlorofluorocarbons
HFC	hydrofluorocarbons
HFE	hydrofluoroethers
HPC	high pressure compressor
HPT	high pressure turbine
HRSG	heat recovery steam generator
HX	heat exchanger
IC	indirect costs
LHV	lower heating value [$J \cdot kg^{-1}$]
LMTD	logarithmic mean temperature difference
LPC	low pressure compressor
LPT	low pressure turbine
NPV	net present value
ODP	ozone depletion potential
OMTS	O-methyltransferases

ORC	organic Rankine cycle
OTB	once-through boiler
PEC	purchased-equipment cost
PFC	perfluorocarbons
PFHX	plate-fin heat exchanger
PSO	particle swarm optimizer
PT	power turbine
PV	photovoltaic
REC	recuperator
RSD	relative standard deviation
SH	superheater
SRC	steam Rankine cycle
T	turbine
TCI	total capital investment
TFC	trilateral flash cycle
TMF	thermo-mechanical fatigue
TUR	turbine or expander
WHRU	waste heat recovery unit
WHRU-SG	waste heat recovery unit for steam generation

Greek letters

Δ	difference
η	efficiency
γ	dimensionless parameter in Eqs. 1.16, 3.3, 4.26 and 5.28
λ	thermal conductivity [$W \cdot m^{-1} \cdot K^{-1}$]

μ	viscosity [N $\cdot$ m^{-2}]
ω	rotational speed [rad $\cdot$ s^{-1}]
Φ	parameter in Eq. 5.29
ρ	density [kg $\cdot$ m^{-3}]
σ	stress [MPa]
ε	strain [$\mu\varepsilon$]
φ	operand in Eq. 5.22

Subscripts

0	outlet
a	air
b	baffle
C	compressor or cold
d	dirt
des	design
e	exhaust gases
eco	economizer
el	electric
eva	evaporator
exh	exhaust
f	fuel or fin or fouling
G	gas
g	exhaust gases
H	hot
i	inner

i_{th}	i-esimo
in	inlet
is	isentropic
L	liquid
lm	logarithm mean
net	net
o	overall
out	outlet
p	pump
r	recuperator
S	static
s	shell side
sh	shell and tube
sup	superheater
T	turbine or total
t	tube side
$t0$	bare tube surface
th	throat
tw	tube wall
w	wall
wet	wet
wi	inner wall
wo	outer wall
cb	convective boiling
nb	nucleate boiling

Introduction

In the last few decades, the global energy demand has risen to a level never reached before. This, in turn, has led to several environmental problems such as air pollution, global warming, the reduction of the ozone layer and the depletion of fossil fuels.

These aspects and the increasing concerns over climate change, have forced the international administrations to adopt stringent environmental protection measures and energy efficiency policies. The first international agreement was the Kyoto Protocol but, since the 1990s, the European Commission released Directives devoted to the energy sector liberalization, the environmental protection, the operators competition and the renewable sources' diffusion. One of the most important package was released in March 2007, and is called European "20-20-20" Climate and Energy package. It defines targets of primary energy consumption and Greenhouse Gases (GHG) reduction [1]. The three ambitious targets for 2020 set in the Directive are: a 20 % reduction in EU greenhouse gas emissions from 1990 levels, an increase of EU energy consumption produced from renewable resources to 20 % and a 20 % improvement in the EU's energy efficiency. Obviously, as outlined in [2, 3], in order to fulfil these targets it is fundamental to introduce the following modifications in the current energy systems:

- Reducing buildings and industries energy consumptions.
- Shifting from fossil fuels toward electricity especially in the transportation sector.
- Generating heat and power through renewable sources.
- Reinforcing grids capacity and interconnections.
- Exploiting waste heat or using cogeneration.

To this purpose, Government incentives for wind, solar, biomass, fuel efficient vehicle, plug-in electric vehicles, waste heat recovery and efficiency have been established.

The most significant result of this process is a high diffusion of power plants fed by unpredictable renewable energy sources such as wind and solar. However, unpredictable renewable energy plants have a great impact on the electricity market.

In fact, the context of the deregulated energy market and the rapid expansion of non-predictable energy sources, are stressing the necessity of improving the flexibility of power generation systems.

New power technologies play an essential role in improving flexibility but, on the one hand, in the case of power plants design for base-load the implementation of flexible strategies is a difficult task especially if they have to compete with the latest combined cycle gas turbine units. On the other hand, flexible operation and high energy conversion efficiency are mandatory for stand alone systems.

In this context, system dynamic modelling and simulation is becoming a powerful and essential design tool. For this reason, this Ph.D. thesis is devoted to analyse the transient operation conditions' effects using power plants dynamic models.

The dynamic analysis is the core of a procedure developed to predict the lifetime reduction on traditional power plant devices. Furthermore, the dynamic analysis is used to test the possibility of introducing innovative waste heat recovery units on offshore facilities with isolated grid. In particular, after a design optimization process, the dynamic behaviour of gas turbines coupled with waste heat recovery units is tested to verify the grid stability. Being organic Rankine cycle one of the most promising technologies, the dynamic analysis is used also to investigate the thermochemical stability of the working fluid.

Chapter 1

CCPP: Dynamic Analysis and Residual Life Estimation

In the recent years, the flexibility of fossil fuels power plants and the resulting components' lifetime reduction have became of primary importance.

As presented in literature and enhanced by industrial companies the context of the deregulated energy market, as a consequence of the Directives 2003/54/EC [4] and 2009/72/EC [5], and the increasing quota of electrical capacity supplied by non-predictable renewable sources [6], require strongly, irregular and discontinuous operation of thermal power plants in order to meet the users demand and compensate the variability of renewable sources.

Delarue et al. [7] studied the influence of wind turbines on energy costs and CO_2 emissions in Belgium. They take into account the operation constraints (minimum operation load, start-up and shut-down minimum times, maximum contribution to spinning reserves) and costs related to frequent start-ups of fossil fuels plants due to sudden generation losses caused by windmills. In addition, depending on wind operation profile, different levels of cost and emission reduction are observed. Furthermore, as discussed in [8], in the last decades several national support strategies are employed to increase the diffusion of photovoltaic (PV) solar systems and create the conditions to make it competitive for the energy market. These actions create, on the one hand, a significant increase of the PV installed capacity but, on the other hand, contribute to increase the production variability and reduce start-up/shut-down periods of thermal power plants. As deeply explained by St Pierre [9], this operation mode guarantees high profits in the short term, but causes a lifetime reduction of the most critical devices due to thermo-mechanical fatigue (TMF), creep and corrosion. Since the proper goal of good management practices is to obtain the plant's best average performance during the whole life of

the system, the decision makers need suitable software tools able to give information about the long-term consequences of the operation choices. Obviously, strong difficulties are met to comply with strict environmental standards also at low load and during transient periods, as stated by the Directive 2010/75/EU [10].

In the recent years, many efforts were done to develop new and more flexible devices and power plants' arrangements especially to increase the range between peak power and technical minimum load. As suggested by Henkel et al. [11], high operational flexibility is an essential prerequisite to ensure economic success in the liberalized electricity market and requires the ability to meet the requested fast start-ups and steep changes of load. The existing plants are called to move from base load to flexible operation and this involves the need to check if they can be suited to this operation mode. Therefore new plant management strategies able to reduce problems related to flexibility must be studied, implemented and tested.

In this context, combined cycle power plants fed by natural gases are the most concerned in flexible operation problems since in many countries they provide and will likely supply the main contribution to the electricity production in the next future. This is happening in the European electricity market scenario, where operational flexibility, high part-load efficiency and fast start-up capabilities are more and more required to combined cycle units in order to compensate the variability of renewable sources. Indeed, combined cycle plants are fairly suited to spinning and cold service, because they are intrinsically more flexible than traditional steam power plants [12]. In addition, cycling requirements in terms of fast start-up and number of start-ups per year are considerably increasing. Nowadays, to be competitive in the electricity market, flexibility capabilities are fundamental. But, load cycling brings damages to the components and the accumulated damages cause frequent breakdowns and unplanned maintenance. As known, the start-up and shut-down procedures influence the reliability and life expectancy of the plants. For these reasons, many efforts have to be done in order to develop efficient algorithms to improve start-up/shut-down performances and decrease lifetime reduction. Moreover, the dynamic simulation is an essential step to achieve the desirable performance under the various kinds of constraints related to system design, plant operation and environmental impacts.

Tica et al. [13] presented a methodology for transforming a physical model of a power plant designed for simulation into an optimization-oriented model and then used in an algorithm to improve the performances during the start-up of a single pressure level combined plant. Alobaid et al. [14] present and validate, by measured data, a static and dynamic simulation model of a three pressure levels

heat recovery steam generator. In [15], an approach is presented and tested as an on-line support tool during start-up operation, while in [16] a brief review of the modelling and simulation techniques for the analysis of both static and dynamic operation of power plants is presented. An example of application is also described: single device models are built and then linked into the whole plant model.

Superheaters/reheaters in Heat Recovery Steam Generators (HRSGs) and gas-steam turbines are subject to severe thermo-mechanical cycles due to an increase of heating gradients and of the number of transitional periods. Steam drums are also stressed because they present great thickness and many weak points such as down-comers, risers and steam pipes connected to the main body. Indeed, during transient operation, they are subject to pressure and temperature variations which induce low-cycle fatigue. However, as pointed out by Madejski et al. [17], superheaters are the most stressed devices in the plants, being exposed to high temperatures and pressures. Considering a severe start-up, the superheater (SH) is exposed to high temperature on the outside surface of pipes and headers whereas inside may still be cool, while at shut-down cool gases are in contact with hot surfaces. Similarly, after a shut-down, the condensed steam in the pipes impinges on hot surfaces if condensate remains inside.

The availability of procedures able to predict the residual life, considering the combined effects of creep, thermo-mechanical fatigue, corrosion and oxidation, as a function of the past and the forecast operation strategy, is essential to optimize power plants' operation and maintenance scheduling.

1.1 The procedure

With the purpose of predicting the power plant components' lifetime reduction, a procedure able to investigate the relations between a plant's operation and its components' lifetime reduction is proposed. The procedure's key points can be summarized as follows:

- Analysis of the plant's management strategy. A particular focus on the production scheduling can be done in order to compute the number of fast start-ups, shut-downs and load variations, and the plant efficiency.
- Dynamic simulation of the plant annual operation via a dynamic mathematical model.
- Detailed analysis of the thermodynamic variables trend.

- Identification of the most stressed components.
- Stress and strain calculation and evaluation of the lifetime reduction of the identified most stressed components.
- Insertion of more flexible and efficient components and implementation of new management strategies in order to guarantee better performance and reasonable components' life.

As outlined by Benato et al. [18], the core of the aforementioned procedure is the dynamic model of the plant. The capability of evaluating the trends of the main thermodynamic parameters (flow rates, temperatures and pressures), which describe the plant operation during different transient conditions, is the base point to identify the stressed plant devices. For this reason, several plants models with different component specifications are built and tested.

Combined gas-steam power plants are the most efficient and widespread technology. Then, reducing characteristic time of start-up and shut-down, extend the range of possible operating conditions by increasing the peak power, and reducing the technical minimum load and increasing ramp rate have become prerogatives. For these reasons, the attention and the modelling efforts are focused on this technology.

Only with the availability of plants' dynamic models, able to simulate design, part-load and dynamic operating conditions, new load ramp rates can be tested and the effects of these conditions on the plants' devices can be found. By analysing the results of this fundamental step, the most stressed devices can be identified and the lifetime reduction computed.

In the proposed procedure creep and thermo-mechanical fatigue damage are evaluated according to the present Design Standards: some of the most important are the ASME code [19], the R5 British procedure [20], the UNI EN 12952 Standard [21] and the German boiler regulation TRD 301 [22].

Creep damage is caused by a prolonged exposure to high temperature and stress. Creep may be the only process which is not caused or enhanced by cycling. However if the creep is coupled with fatigue due to cycling, the damage will be much higher than that occurring if the same fatigue or creep were working alone. The creep damage is computed by means of the following equation:

$$D_c = \frac{t}{t_r(\sigma)} \tag{1.1}$$

where $t_r(\sigma)$ is the time to failure at the equivalent stress σ, and the subscript "σ" is computed according to a proper model: since a multi-axial stress state occurs, the

Von Mises equivalent stress [20] has been considered. The creep stress is mainly due to the inside pressure, the weight of the device itself and the temperature differential among different points.

Fatigue damage is the most prevalent action affecting the boiler life and is a direct consequence of cycling. For example, during fast start-ups, the superheater tubes and heaters are exposed to high temperature on the outside surface whereas inside may still be cool. On the contrary, during shut-downs cool gases are sent on hot surfaces. Similarly, the condensed steam in the tubes after shut-downs impinges on hot surfaces if condensate remains in the tubes. Additionally, the high pressure components are more vulnerable to top fatigue effects due to higher thickness. The fatigue damage is computed according to the ASME code [19]. The equivalent strain range is calculated for the "i_{th}" fatigue cycle as:

$$\Delta\varepsilon_{equiv,i} = \frac{\sqrt{2}}{2 \cdot (1+\nu)} \cdot \{[\Delta(\varepsilon_1 - \varepsilon_2)_i]^2 + [\Delta(\varepsilon_2 - \varepsilon_3)_i]^2 + [\Delta(\varepsilon_1 - \varepsilon_3)_i]^2\}^{\frac{1}{2}} \quad (1.2)$$

where ε_1, ε_2 and ε_3 are the principal strains of the drum at the "i_{th}" fatigue cycle, while "ν" for the steel used in the HRSG is equal to 0.5.

As suggested by Stoppato et al. [23], during load variations, the maximum and minimum strain are computed taking into account the wall temperature variation along the tube, the variable temperature gradient between inside and outside of the tube metal wall and the variation of internal pressure.

Following the methodology outlined in [24], the strain ranges are used to compute the number of cycles before failure (N_0) by the use of Manson-Coffin curve or database [25] at the specific working temperature.

According to the ASME Code, creep and fatigue damages are added using a linear rule:

$$D = \sum_{j=1}^{p} \left(\frac{N}{N_0}\right)_i + \sum_{k=1}^{q} \left(\frac{t}{t_r}\right)_k \leq D_L \quad (1.3)$$

where D is total creep-fatigue damage and D_L is the "limit damage" defined for different materials, which accounts for creep and fatigue interaction. D is then used to evaluate the cumulative mechanical damage for each single component. The effect of the current management strategy is therefore evaluated in terms of residual life reduction. In this manner several management strategies can be implemented and the related effects evaluated.

This methodology is adopted to evaluate the stress and strain which occurred in the heat exchangers tube bank (i.e. superheater devices) while to compute

the drum's thermal and mechanical stresses the software tool described in [18] is employed.

The fatigue life calculation tool (FLC) is implemented in Matlab environment [26, 27] and considers a simple cylindrical geometry for the steam drum: an inner metal cylinder and an outer insulation cylinder. The presence of discontinuities in the metal structure of the component (due to the connection of downcomers and risers and to the drum end plates) is taken into account by assuming suitable stress concentration factors. FLC is developed according to the EN 13345 Standard [28]. The fatigue life calculation procedure implemented in FLC tool can be summarized as follows:

1. Calculation of temperature and thermal-mechanical stresses (radial, circumferential and axial components), on the basis of the trend of steam pressure and temperature inside the drum, for each coaxial metal layer in which the cylinder has been divided.

2. Calculation of the three principal structural stresses for each metal layer.

3. Calculation of the signed Tresca equivalent stress for each metal layer.

4. Application of the "Rainflow Counting Method" to the signed Tresca equivalent stress, in accordance with the ASTM E 1049 Standard [29], to identify fatigue cycles for the more stressed metal layer.

5. Analysis of the results of Step 4 for each i_{th} fatigue cycle. The stress range $\Delta\sigma_l$, the mean stress $\Delta\sigma_{m,i}$, the maximum stress $\Delta\sigma_{max,i}$, the value n_i (that is equal to 0.5 if the stress range $\Delta\sigma_l$ is counted as a half cycle or to 1 if it is counted as one cycle), the starting time $t_{0,i}$, the period τ_l and the average temperature T_i^*.

6. Application of the life reduction calculation procedure, developed in accordance with the EN 13445 Standard, to each fatigue cycle (identified by Steps 4 and 5) in order to compute the allowable number of fatigue cycles N_i and, as a consequence, the "cumulative fatigue damage index" D_{CF} for the examined transient by applying the Palmgren-Miner rule which indicates to sum the fatigue damage indexes $LC_i = n_i/N_i$ of each cycle.

In conclusion, plants' cycling operations guarantee high profits in the short-term but cause a reduction of the lifetime due to thermo-mechanical fatigue, creep and corrosion effects in the medium-long time. In this context, the availability of a procedure based on the dynamic simulation and able to predict the residual life

is essential to optimize the power plants' operation and maintenance scheduling. Clearly, the plant dynamic model needs to be built in an appropriate environment. To this purpose, DYMOLA constitutes a valid alternative to the in-house code being a very powerful simulation tool with commercial, open-source and fully extendible libraries.

1.2 The modelling language

As said, an effective way to build dynamic models is to use the commercial software DYMOLA [30]. Dynamic Modeling Laboratory or DYMOLA (version 2014) is the commercial Modelica simulation environment based on the open Modelica language developed by the Swedish company Dassault Systemes AB [31]. DYMOLA environment allows to build Modelica models with components collected in Modelica libraries and provides integration algorithms which are used to solve the model.

Modelica [32–34] is a free language developed by the non-profit Modelica Association since 1996. In Modelica simulation environment each Icon represents a physical component (electrical resistance, mechanical device, pump, etc.) while a Connection Line represents the actual physical coupling (wire, fluid flow, heat flow, etc.). A component consists of connected sub-components (hierarchical structure) and/or is described by equations. These equations can be differential, algebraic, and discrete equations. By symbolic algorithms, the high level Modelica description is transformed into a set of explicit differential equations which can be easily solved.

In practise, the Modelica language allows to build differential equation models without state form; from which state equations are derived automatically [32]. It is a freely available, fully modular, object-oriented language for modelling large, complex, and heterogeneous physical systems. From a user's point of view, models are described by schematic, also called object diagrams. These features facilitate the development of advanced models as pre-defined components (e.g. pipes) that can be directly used as sub-components in more complex models (e.g. heat exchangers).

In a nutshell, Modelica language allows, firstly, to carry out the modelling task reliably and in a short time, by leveraging on existing and well-tested libraries of reusable component models. Secondly, the equation-based approach of the language enables to easily customize the models for specific requirements at hand.

For these reasons, the dynamic models presented in this dissertation (i.e. gas

turbine, air bottoming cycle unit, organic Rankine cycles turbogenerator and heat recovery steam generator unit for on grid and stand-alone units) are developed using base and extended components available on existing Modelica packages: Thermal Power library (TPL), ThermoPower library (TP) and the Modelica ORC package.

Thermal Power library is a commercial Modelica library, developed by Modelon AB [35], for the unsteady state simulation of power plants and their components. The library covers the complete steam cycle (including steam and combined cycle power plants), as well as a wide range of flue gases after-treatment technologies such as desulphurization, NOx-removal and CCS technologies (for more details see [35]). Well-known correlations are employed for the heat transfer and pressure drop estimations for flue gases, steam and liquid water. Steam and flue gases medium models come from the Modelica.Media library [36, 37]. Obviously, the package includes components for the conventional steam power plants' modelling but, to better characterize the dynamic behaviour of these devices, the base models need to be extended by the user. This library is very detailed but presents an important drawback: it does not allow to load and use fluids which are not included in the package. This aspect limits the range of applications, therefore, only the heat recovery steam generator models are built with components available on Thermal Power library. The other models (i.e. gas turbine, organic Rankine cycle unit) are developed with components available on ThermoPower library.

ThermoPower library is an open-source package, developed at Politecnico di Milano, for modelling thermo-hydraulic processes and power plants [38]. It is a fully open library where the users can create and extend components, and import and use the fluids that are wanted. Starting from the components available on ThermoPower, a Modelica ORC package was developed [39]. As for the other libraries the ORC package components can be extended in order to fulfil the users requirements.

1.3 Case study

The case study selected to test the procedure presented in Chapter 1.1 is a gas-steam combined cycle power plant (CCPP) consisting of a gas turbine (GT) and a single pressure level heat recovery steam generator (HRSG) unit. Figure 1.1 shows the plant scheme while Table 1.1 lists the plant design point characteristics. This is a real plant operating in the Italian liberalized electricity market, but only few design data are available. For this reason, the missing parameters are assumed

based on data available in literature or by well-known design procedures.

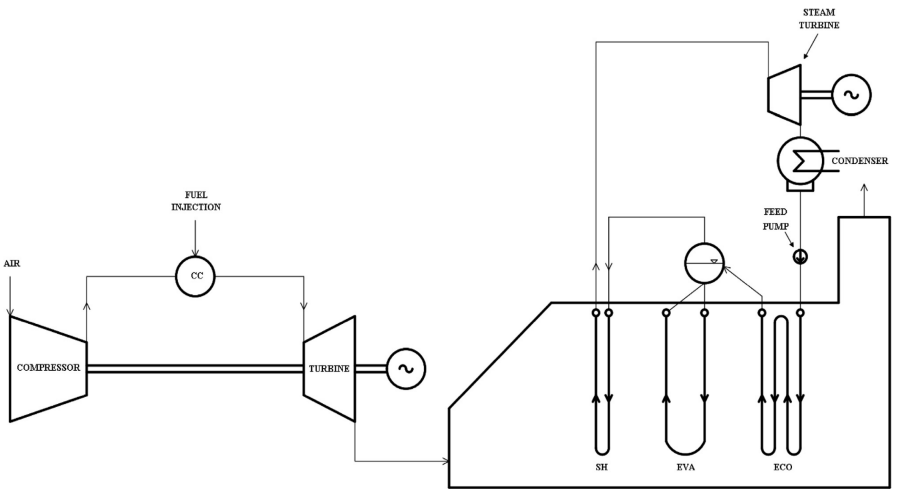

Figure 1.1: Scheme of the single pressure combined cycle power plant.

Table 1.1: Combined cycle power plant design specifications.

Parameter	**Value**
GT exhaust gases mass flow	191.4 kg · s^{-1}
GT exhaust gases temperature	582.8 °C
Stack exhaust gases temperature	140.2 °C
Steam mass flow	28.5 kg · s^{-1}
Evaporating pressure	38 bar
Condensing pressure	0.05 bar
CCPP design power	97,8 MW
CCPP electric efficiency	50.0 %
Fuel	Natural gas

The HRSG dynamic behaviour is strictly dependent on the gas turbine performance, therefore both the GT and the HRSG models are built and tested.

1.3.1 The gas turbine model

The gas turbine dynamic model is developed in DYMOLA environment coupled with ThermoPower library. The library components are extended in order to better describe the GT unit.

The gas turbine model is based on data available in the open literature [40, 41]. Table 1.2 reports the gas turbine design point specifications while the Modelica object diagram of the engine is shown in Figure 1.2.

Table 1.2: Gas turbine design-point specifications.

Model	**Siemens SGT-1000F**
Year	1996
Compressor ratio	15.8
Exhaust gases temperature	582.8 °C
Exhaust gases mass flow	191.4 kg · s^{-1}
Rotational speed	5400 rpm
Electric power output	67.7 MW
Thermal efficiency	35.8 %
Fuel	Natural gas

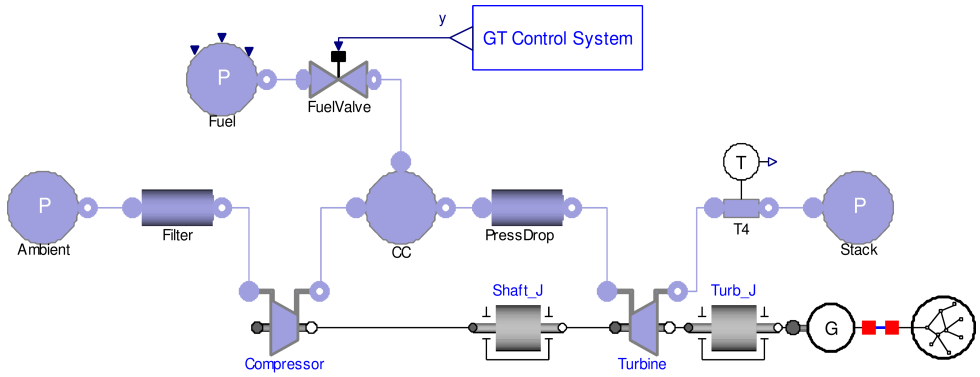

Figure 1.2: Modelica object diagram of the gas turbine.

The compressor and the turbine are described as zero-dimensional components adopting steady state and offdesign characteristics.

The compressor is described by quasi-static component, employing the maps of axial compressors provided with the commercial software GASTURB, compiled from data available on the open literature [42]. In particular, these maps are represented by tables stating values for flow coefficient, pressure ratio, isentropic efficiency and speed of revolution for the complete operating range of the device. Following the methodology proposed by Kurzke [43], maps are scaled in order to represent the part-load characteristics of the axial compressor installed on the gas turbine. Being the compressor a multistage machine equipped with variable inlet guide vanes (VIGVs), the compressor sub-model is extended and appropriate equations able to consider the VIGVs effect are implemented.

The equation proposed in 1992 by Stodola [44] is employed to describe the turbine behaviour. The equation expresses the relation between inlet and outlet pressure, mass flow rate and inlet temperature in offdesign operating conditions (see Equation 1.4).

$$C_T = \frac{\dot{m}_g \cdot \sqrt{T_{in}}}{\sqrt{p_{in}^2 - p_{out}^2}} \tag{1.4}$$

where C_T is the turbine constant, $\dot{m}_g$ is the mass flow of the combustion products and T_{in} is the turbine inlet temperature. The inlet and outlet pressure are expressed with p_{in} and p_{out}, respectively.

The turbine's offdesign conditions are predicted with the correlation proposed by Schobeiri [45]. The correlation expresses the relation between the isentropic efficiency (η_{is}) and the dimensionless flow coefficient.

$$\eta_{is} = \eta_{is,des} \cdot \sqrt{\frac{\Delta h_{is,des}}{\Delta h_{is}}} \cdot \left(2 - \frac{n}{n_{des}} \cdot \sqrt{\frac{\Delta h_{is,des}}{\Delta h_{is}}}\right) \tag{1.5}$$

The isentropic efficiency is a function of the rotational speed n and the isentropic enthalpy drop Δh_{is}. The subscript "des" refers to the value computed at the design point conditions.

The electric generator part-load performance is predicted by the equation proposed by Haglind and Elmegaard [46].

$$\eta_{el} = \frac{Load \cdot \eta_{el,des}}{Load \cdot \eta_{el,des} + (1 - \eta_{el,des}) \cdot [(1 - F_{cu}) + F_{cu} \cdot Load^2]} \tag{1.6}$$

where η_{el} and $Load$ are the electric generator efficiency and the gas turbine load

expressed in percent, respectively. F_{Cu} represents the losses in the copper of the generator.

The combustion chamber (CC) unit is modelled assuming a perfect mixing between the air and fuel streams and a combustion process that takes place in a constant volume. Besides, it is assumed complete and adiabatic combustion but the mass and energy conservation equations are expressed including the dynamic terms. The mass and the internal energy are computed using the thermodynamic properties of the products leaving the combustion chamber as suggested in [47]. The mass and internal energy equations implemented into the combustion chamber component are

$$V_{CC} \cdot \frac{d\rho_{CC}}{dt} = \dot{m}_a + \dot{m}_f - \dot{m}_g \tag{1.7}$$

$$\frac{dU_{CC}}{dt} = \dot{m}_a \cdot h_a + \dot{m}_f \cdot (h_f + LHV) - \dot{m}_g \cdot h_g \tag{1.8}$$

where V_{CC} is the combustion chamber volume while ρ_{CC} is the density of the products exiting the combustor. $\dot{m}_a$, $\dot{m}_f$ and $\dot{m}_g$ are the air, fuel and exhaust gases mass flow rate. LHV is the fuel lower heating value while U_{CC} is the internal energy of the combustion chamber. The specific enthalpy of air, fuel and exhaust gases exiting the combustion chamber are denoted with h_a, h_f and h_g, respectively.

The CC pressure drops are lumped in an external component. As shown in Equation 1.9 a quadratic dependence on the volumetric flow rate is assumed.

$$\frac{\Delta p}{\Delta p_{des}} = \left(\frac{\dot{V}}{\dot{V}_{des}}\right)^2 \tag{1.9}$$

where Δp and $\dot{V}$ are the pressure drop and the volumetric flow rate, respectively.

The shaft dynamic balance, reported in Equation 1.10, is employed to model the spools dynamics.

$$\frac{d\omega}{dt} = \frac{\sum_{i=1}^{n} (P_{in,i} - P_{out,i})}{I \cdot \omega} \tag{1.10}$$

where the rotational speed and the inertia of the shaft are ω and I, while P_{in} and P_{out} are the mechanical power given and provided to the shaft, respectively.

The values of the inertia of the rotating masses (shaft, blades and generator) are set, as for the combustion chamber volume, according with data published in the open literature.

1.3.2 The single pressure HRSG model

Due to the need of evaluating the components' lifetime reduction, caused by load variation, fast start-ups and shut-downs, it is essential to build plant models with detailed components (i.e. heat exchangers and drums geometry, pumps maps, etc.). Of course, a plant model with detailed components' description needs long simulation time and appropriate devices' sub-models. Components' models with a detail geometry are available on Thermal Power library (TPL) but not in ThermoPower (TP).

Therefore, with the aim of analysing both the components' lifetime reduction and the mathematical and computational aspects introduced by the implementation of devices geometry, two models of the same HRSG unit are built and then compared.

Thermal Power HRSG model

Figure 1.3 shows the Modelica object diagram of the single pressure heat recovery steam generator built with sub-models available on Thermal Power library (TPL model). The distinctive trait of this model is the heat exchanger model. In it the geometry is fully implemented and used to compute heat transfer coefficients, pressure drops, heat fluxes, and so on. The heat exchanger model command windows are shown in Figure 1.4.

Note that the gas turbine engine is modelled as a gas source that acquired the simulation results coming from the GT model described in Chapter 1.3.1.

The HRSG has a horizontal gas pass design; it is composed by three heat exchangers (the economizer (ECO), the evaporator (EVA) and the superheater (SH)), the drum, two pumps (FeedPump and CircPump), pipes ($Tube\_1$ to $Tube\_5$), the steam turbine (ST), the condenser (CONDENSER) and a spray attemperator. In Table 1.3 the geometry and the wall material of the economizer, evaporator, superheater and drum are summarized.

The wall and fins material characteristics are also included into the HX model because they are fundamental to evaluate the heat transfer among exhaust gases, water/steam and tubes metal wall.

As pointed out in Table 1.3, the drum dimensions and wall characteristics are also included into this plant model.

The steam turbine is modelled using the Stodola's equation [44]. The design operating conditions (such as mass flow rate, inlet and outlet temperature and pressure), the mechanical and the isentropic efficiency are set to describe the turbine's behaviour. Pumps are built using a module which describes a centrifugal

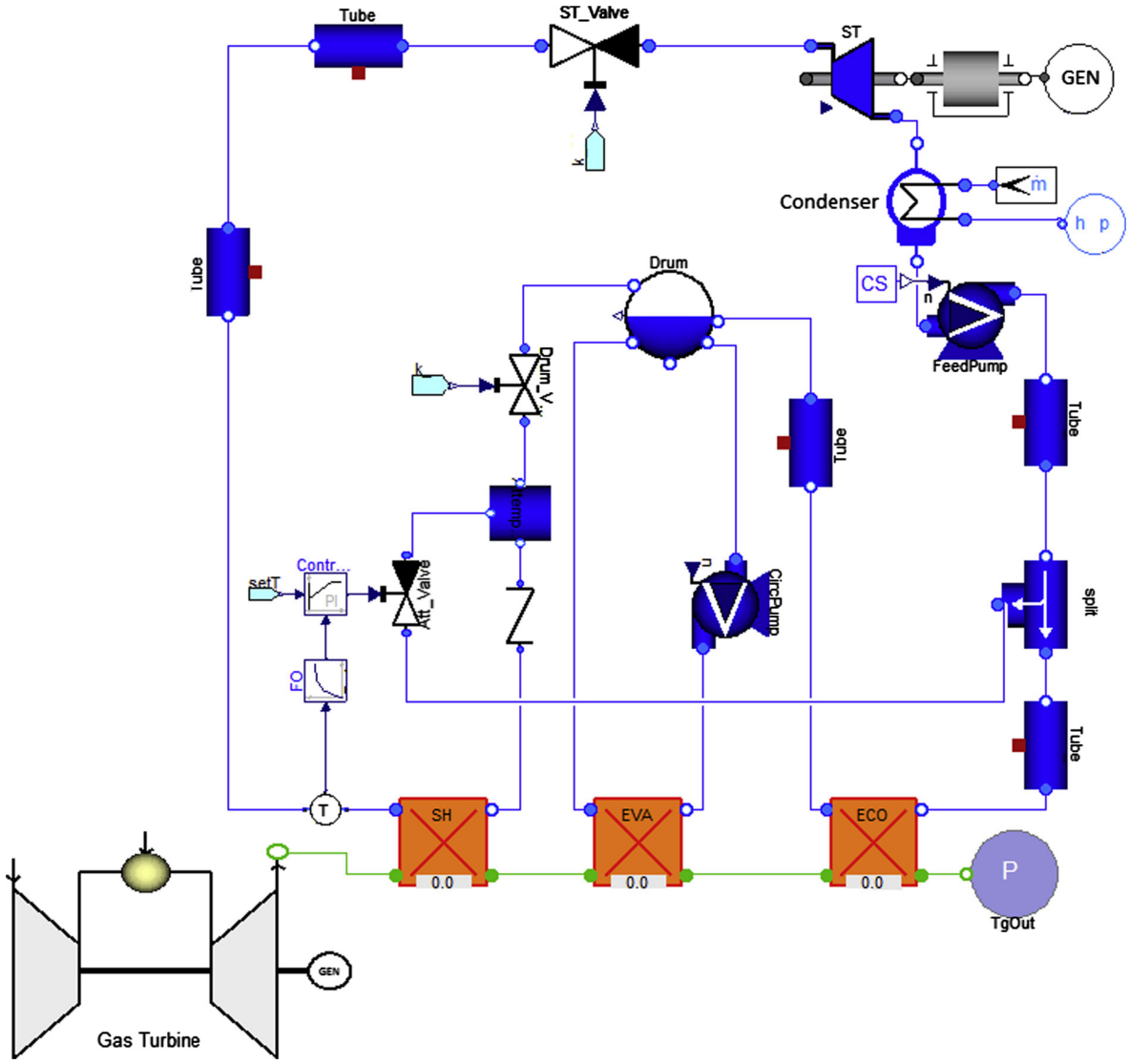

Figure 1.3: Modelica object diagram of the single pressure heat recovery steam generator.

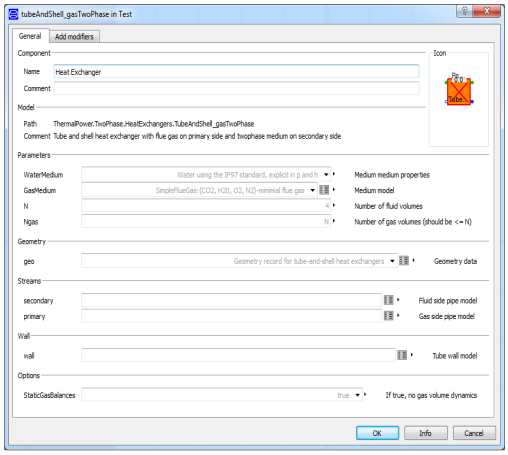

(a) Main window

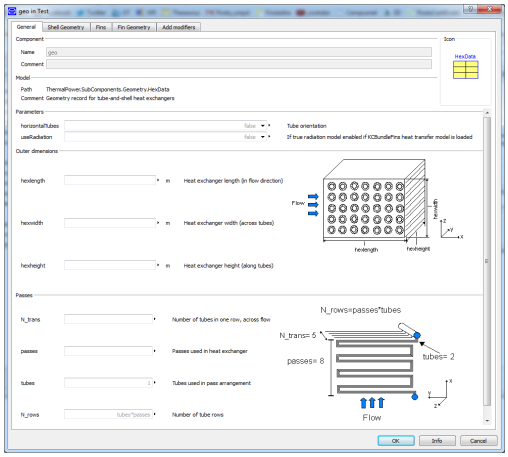

(b) Geometry general window

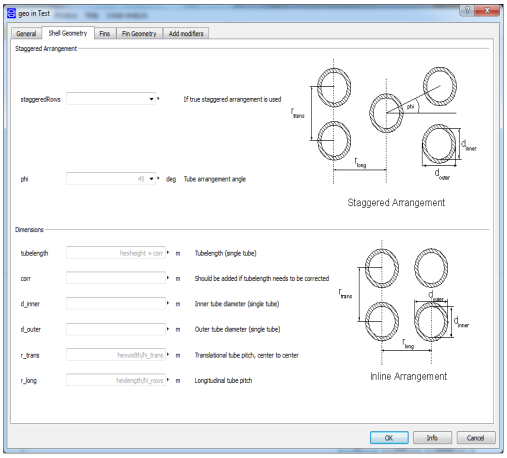

(c) Shell geometry window

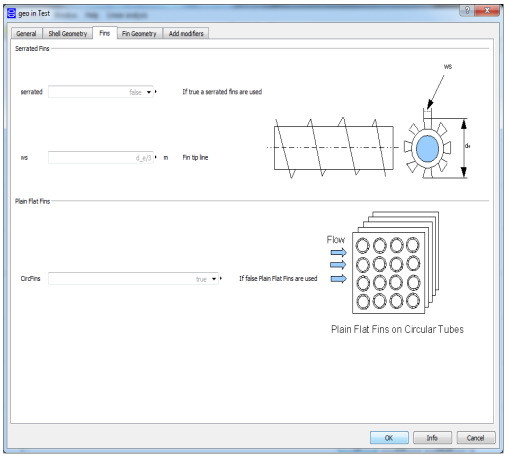

(d) Fins geometry window 1

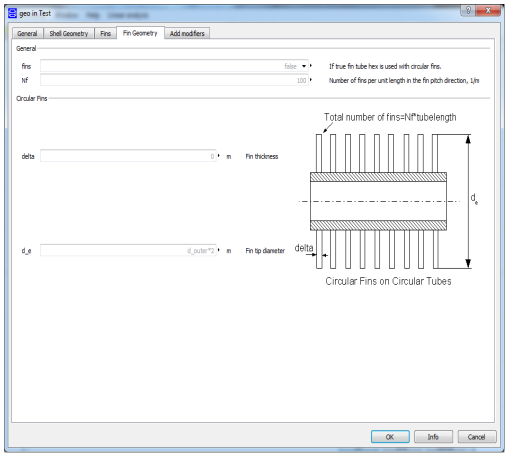

(e) Fin geometry window 2

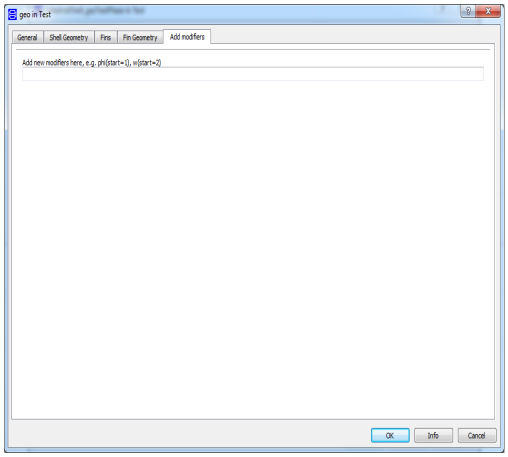

(f) Geometry modification window

Figure 1.4: Shell and tube heat exchanger model available on Thermal Power library.

Table 1.3: Heat exchanger geometry data.

Device	**Parameter**	**Value**
Economizer	Material	AISI 304
	Outer diameter	25.0 mm
	Tube thickness	2.5 mm
	Tube length	10.0 mm
	Number of tubes	7560
	Longitudinal tube pitch	78 mm
	Traversal tube pitch	90 mm
	Number of fins	236 fins $\cdot$ m^{-1}
	Fin dimension	12x4x1.2 mm
	Fin pass	4.24 mm
Evaporator	Material	AISI 304
	Outer diameter	25.0 mm
	Tube thickness	2.5 mm
	Tube length	7.0 mm
	Number of tubes	12960
	Longitudinal tube pitch	78 mm
	Traversal tube pitch	90 mm
	Number of fins	236 fins $\cdot$ m^{-1}
	Fin dimension	12x4x1.2 mm
	Fin pass	4.24 mm
Superheater	Material	AISI 304
	Outer diameter	38.0 mm
	Tube thickness	6.0 mm
	Tube length	5.0 mm
	Number of tubes	2080
	Longitudinal tube pitch	78 mm
	Traversal tube pitch	90 mm
	Number of fins	236 fins $\cdot$ m^{-1}
	Fin dimension	12x4x1.2 mm
	Fin pass	4.24 mm
Drum	Material	P355GH
	Internal radius	750 mm
	Wall thickness	30 mm
	Length	10800 mm

pump with ideally controlled speed, either fixed or provided by an external signal. The circulation pump is inserted to assist circulation into the evaporator tubes and works at a fixed speed while the feed pump works at variable speed. This pump is controlled by a PI controller (see Figure 1.5) which provides to maintain the drum level on a prefixed value. The pump, as said, is centrifugal and its speed can change from 1500 to 3500 rpm. During load variation, the level of the drum is kept under control by changing the rotational speed of the feed pump. In both cases the pump's maps are implemented into the component and are derived by fitting data of existing machines designed for similar volumetric flows and heads.

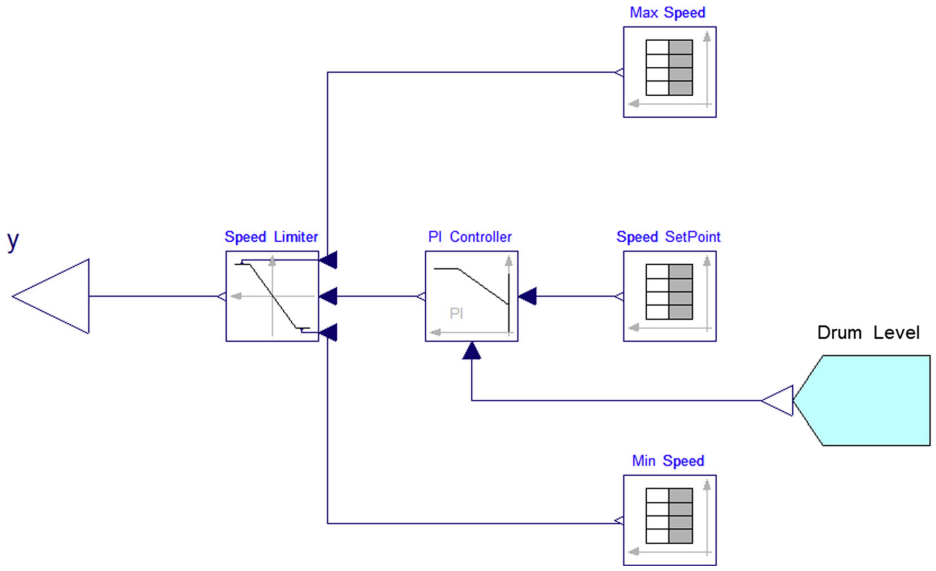

Figure 1.5: Modelica object diagram of the pump control system.

The dynamics of the shaft is modelled by applying the shaft dynamic balance; also the value of the moment of inertia of this component is set.

The model includes all the control systems, whose role is very important during cycling operation mode. Drum vent, admission valves and pump speed control are implemented. They are in charge of maintaining the correct water level in the drum. The plant operates in sliding pressure mode. Steam attemperator is needed to avoid high steam temperature at the outlet of the HRSG. As said, during load variation, the level of the drum is kept under control by changing the pump rotational speed while the steam turbine is maintained at 3000 rpm.

The composition of the exhaust gases is modelled adopting NASA Extended Exhaust Gas Model which is implemented into Thermal Power library while for water/steam fluid model, the IF 97 water model is employed [48].

Note that the heat exchangers are in cross-flow arrangement and each HX

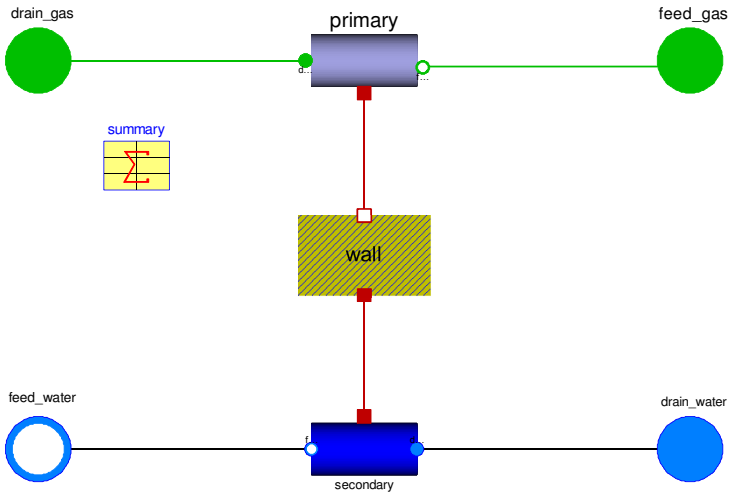

Figure 1.6: Modelica object diagram of the heat exchanger model.

model is discretized in "n" identical segments (see Figure 1.6.) Each segment is constituted by a gas volume (called "primary"), a wall and a water/steam volume (called "secondary"). The volume exchange information via thermal port to wall and via fluid connectors to the other fluid volumes. In each volume the fluid properties, the heat transfer coefficients and pressure drops, etc. are computed with appropriate equations. For example, the heat transfer coefficient can be fixed equal to a constant value or computed with an equation or evaluated with a user implemented correlation. In this work, the heat transfer coefficient for the water/steam side in the economizer and superheater components is computed for each pipe segment with the equation:

$$h_c = Nu_m \cdot \frac{\lambda}{d_{hyd}} \tag{1.11}$$

where λ is the fluid conductivity and d_{hyd} is the hydraulic diameter of the pipe. Nu_m is the average Nusselt number and is computed by means of Reynolds number using an equation put forward by Gnielinski [49] for heat transfer during turbulent flow of gases and liquids through pipes [50].

$$Nu_m = \frac{\left(\frac{\xi}{8}\right) \cdot Pr \cdot Re}{1 + 12.7 \cdot \sqrt{\frac{\xi}{8}} \cdot \left(Pr^{\frac{2}{3}} - 1\right)} \cdot \left[1 + \left(\frac{d_i}{l}\right)^{\frac{2}{3}}\right] \tag{1.12}$$

where l and d are the pipe length and diameter. The parameter ξ is given by:

$$\xi = (1.8 \cdot log_{10}(Re) - 1.5)^{-2} \tag{1.13}$$

Note that Equation 1.12 was obtained by modifying an equation that was derived from the theory of momentum transport by Petukhov and Kirillov [51] and is valid for completely developed pipe flow. It was enlarged by a factor proposed by Hausen [52] to take into account the dependence of the heat transfer coefficient on the length of the pipe. According to Konakov [53], the friction factor for turbulent flow in smooth pipes may be calculated from Equation 1.13. Ranges of validity are reported as follows:

$$\frac{d_i}{l} \leq 1 \qquad 10^4 < Re < 10^6 \qquad 0.1 < Pr < 10^3 \tag{1.14}$$

where Re and Pr is the Reynolds and Prandtl number, respectively.

The heat transfer coefficient during evaporation processes (which occur into the pipes) is computed with the correlation for convective boiling in vertical and horizontal tubes with a Froude number $Fr > 0.05$. It uses a modified Dittus-Boelter equation for the heat transfer coefficient of the liquid and is multiplied by an enhancement factor which depends on the steam quality and the Boiling number. For horizontal tubes and Froude lower than 0.05 it also contains a multiplicative correction term (see [50, 54]). Note that, the correlations are implemented into the heat exchangers models and, based on the fluid regime and state, the solver selects the appropriate equation.

The heat transfer coefficient on the gas side of the three heat exchangers, can be obtained with several correlations available in the open literature for solid or serrated finned tubes. Some equations for finned tubes with serrated and solid fins were developed by e.g. ESCOA [54] (Extended Surface Corporation of America) as well as by Nir [55]. The correlation proposed by ESCOA [54], to evaluate the Nusselt number for serrated and solid fins in staggered tube arrangement is employed.

$$Nu = \frac{1}{4} \cdot Re^{0.65} \cdot Pr^{\frac{1}{3}} \cdot C_3 \cdot C_5 \cdot \left(\frac{T_{gm}}{T_s}\right)^{\frac{1}{4}} \cdot \left(\frac{d_a + 2 \cdot h_f}{d_a}\right)^{\frac{1}{2}} \tag{1.15}$$

where d_a and h_f are the outside diameter and the average fin height, respectively. The coefficient C_3 and C_5 are computed according to the methodology outlined in [54, 56].

Pressure drops are also computed in the heat exchanger model with appropriate

correlations taken from [50, 54, 56].

In conclusion, the model developed with Thermal Power Library is able to simulate the plant steady state, part-load and transient behaviour and predicts the trends of the main thermodynamic flow parameters (such as mass flow rates, pressures, temperatures, etc.). It is also able to compute the temperature values along the thickness of the HX walls, pipes and drum. Once the variation over time of the thermodynamic variables is evaluated, the associated trend of the underlying mechanical parameters (stresses and strains in each component) can be computed using the well-known relationships as a function of pressure, temperature difference between internal and external radius of pipes or drum, temperature gradient along tube length and considering the variations of these parameters over time.

ThermoPower HRSG model

In this case, the model is developed again with the commercial software DYMOLA but components are taken from ThermoPower library (TP model). The Modelica object diagram is depicted in Figure 1.7.

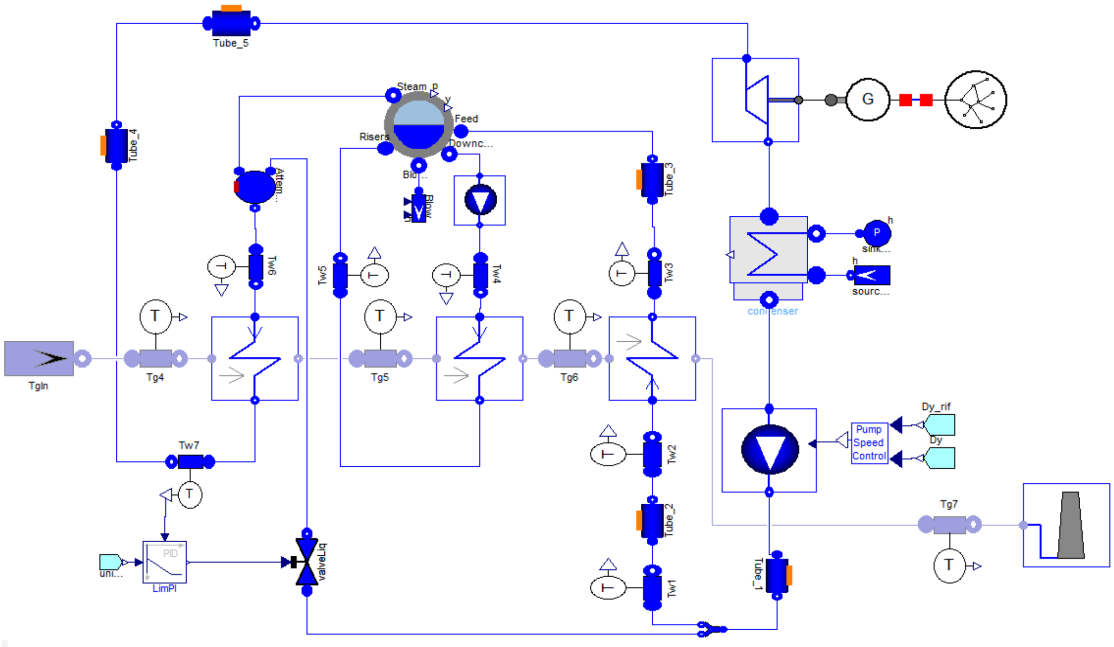

Figure 1.7: Modelica object diagram of the single pressure heat recovery steam generator.

The HRSG has the same configuration and control system modules described in Chapter 1.3.2 but, in this model, the heat exchangers geometry is not inserted. In practice, the heat exchanger is implemented by combining basic ThermoPower modules, see Figure 1.8: 1D-flow models for the gas side (top) and fluid side

(bottom of the figure), and the 1D-thermal model for the tube bundle (middle). The exchange of thermal power is modelled with the so-called 1D-thermal ports (in orange in the figure); the counter-current model establishes the topological correspondence between the control volumes on the tube walls, and the control volumes on the gas flow model. The tube metal wall is modelled by a 1D dynamic heat balance equation, discretized by finite volumes. The flow models contain one-dimensional dynamic mass and energy balance equations, discretized by the finite volume method, assuming a uniform pressure distribution; the relatively small friction losses are lumped in an external component model. Here, the pressure drops at offdesign conditions are estimated assuming a quadratic dependency on the volumetric flow. As reported by [57], due to their relatively small contributions, the thermal resistance in the radial direction and thermal diffusion in the axial direction are thus neglected in the dynamic models. The heat transfer coefficient between the gas and the outer pipe surface is much lower than the one between the inner pipe surface and the working fluid flow. Therefore, the overall heat transfer is essentially dependent on the gas side only, and the working fluid temperature is always close to the inner surface temperature of the pipe. For this reason, the heat transfer coefficient at the interface between the gas and the metal wall, at offdesign conditions, is evaluated with the relation proposed by Incropera et al. [58].

$$h = h_{des} \left(\frac{\dot{m}}{\dot{m}_{des}} \right)^{\gamma} \tag{1.16}$$

where $\dot{m}$ is the mass flow rate of the water/steam side. The subscript "des" refers to the value at design operating conditions, while the variable γ is the exponent of the Reynolds number. In the equation γ is assumed equal to 0.6. The thermal interaction between the wall and the working fluid is described by specifying a sufficiently high constant heat transfer coefficient, so that the fluid temperature is close to the wall temperature, and the overall result is dominated by the gas side heat transfer (more details can be found in [58]).

The input parameters of the heat exchanger models are the mass and the heat capacity of the tube metal wall, the volumes occupied by the exhaust gases, and the water/steam, the design-point heat transfer coefficients on the hot and cold side and the hot and cold surface areas. Reasonable figures for these variables are obtained applying the well-documented standardized design-procedure for shell and tube heat exchangers outlined in Coulson et al. [59].

The steam turbine, the condenser, the pumps and the other components are implemented into the model as outlined in Chapter 1.3.2 while water/steam and

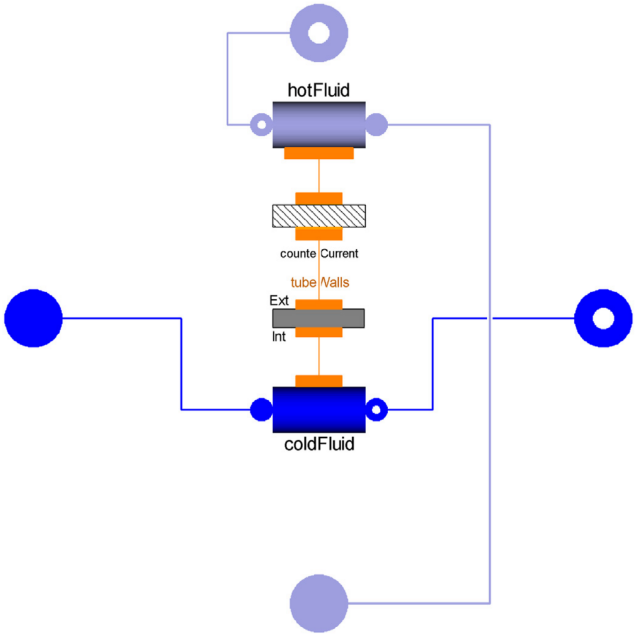

Figure 1.8: Modelica object diagram of the heat exchanger model.

exhaust gases are implemented with models described in [36].

1.4 Models validation

The validation process is a fundamental step during the model's developing phase. Normally, an example is used to test the new model. In this case, after a literature review (see i.e. [24, 60–64]) only Bracco et al. [24] presented a similar work. They propose a mathematical model (called MSM model) of a HRSG similar to the one built in Modelica with ThermoPower components. With the aim of developing dynamic power plant models, able to help in the evaluation of components' lifetime reduction, an on-going collaboration was established.

As outlined in [24], this model is built by means of the Matlab/Simulink software and is based on a non-linear lumped parameter mathematical model, described by a set of algebraic and partial differential equations, for power plants and particularly for combined cycle plants in [65] (see Figure 1.9).

The gas turbine is modelled in a simple way using the characteristic curves of the turbomachinery; this block provides as input to the HRSG the exhaust gas flow rate and temperature at the gas turbine discharge. Furthermore, the gas composition is computed in order to correctly evaluate enthalpy and specific heat. The equations which describe the HRSG behaviour take into account the thermal storage in the metal parts of each heat exchanger. It is important to remark that,

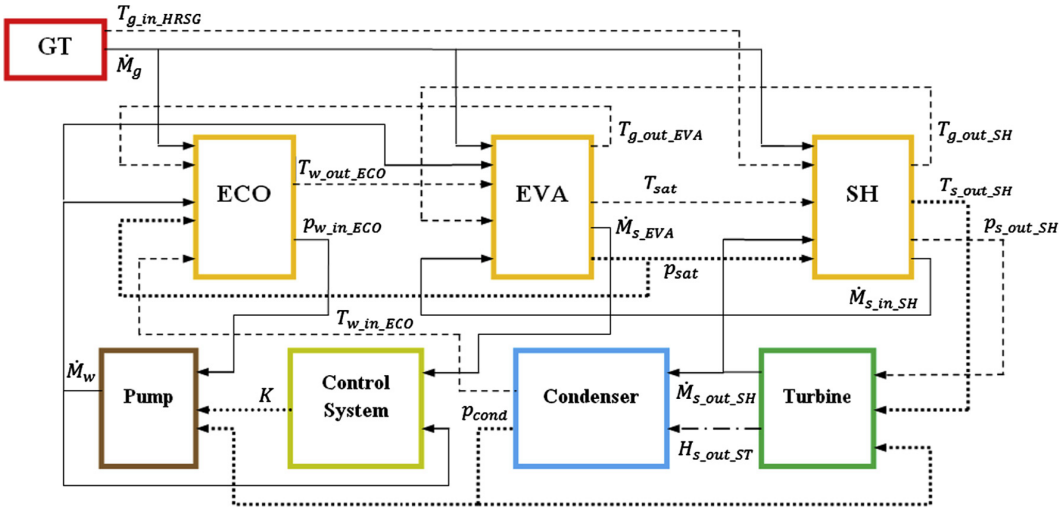

Figure 1.9: Scheme of the single pressure heat recovery steam generator model.

in the model, the economizer and the superheater are not characterized by a single wall temperature since it has been necessary to divide them into multiple sections (respectively five and three); this guarantees, for all operating conditions, that the wall temperature of each section is greater than the water/steam outlet temperature and lower than the gas outlet temperature. The water/steam properties are computed by means of the XSteam tool [66].

The steam turbine is modelled as an algebraic block, analogously to the Modelica model. The components of the plant that work at low temperature are represented in a simple way: the condenser pressure is calculated as a function of the steam flow rate, whereas the feed-water system (represented by the pump, characterized by its head-volumetric flow rate curve, and the valve downstream) is managed by a PI controller which work in the same way as the one installed into the Modelica models.

The comparison between the three models (the two developed in Modelica language and the one in Matlab/Simulink environment) is performed considering the transient condition shown in Figure 1.10.

The selected transient consists in a step variation of the exhaust gases temperature at the HRSG inlet from 582 °C to 552 °C while the exhaust gas mass flow rate is assumed constant. Some interesting results of the simulation processes are reported in the following figures.

The three models have a different response in term of pressure while the trends of the temperature at the exit of the superheater are the same. As shown in Figure 1.11, the models developed in Modelica have similar pressure trends despite the different way to model the inertia into the heat exchangers while the model

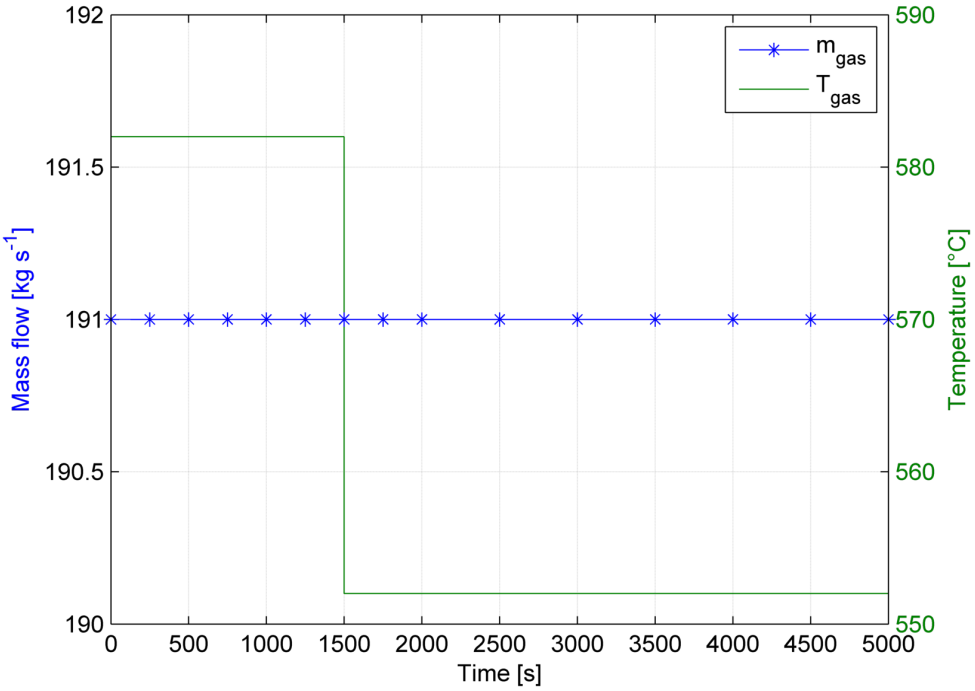

Figure 1.10: Mass flow rate and temperature of the exhaust gases at the HRSG inlet section.

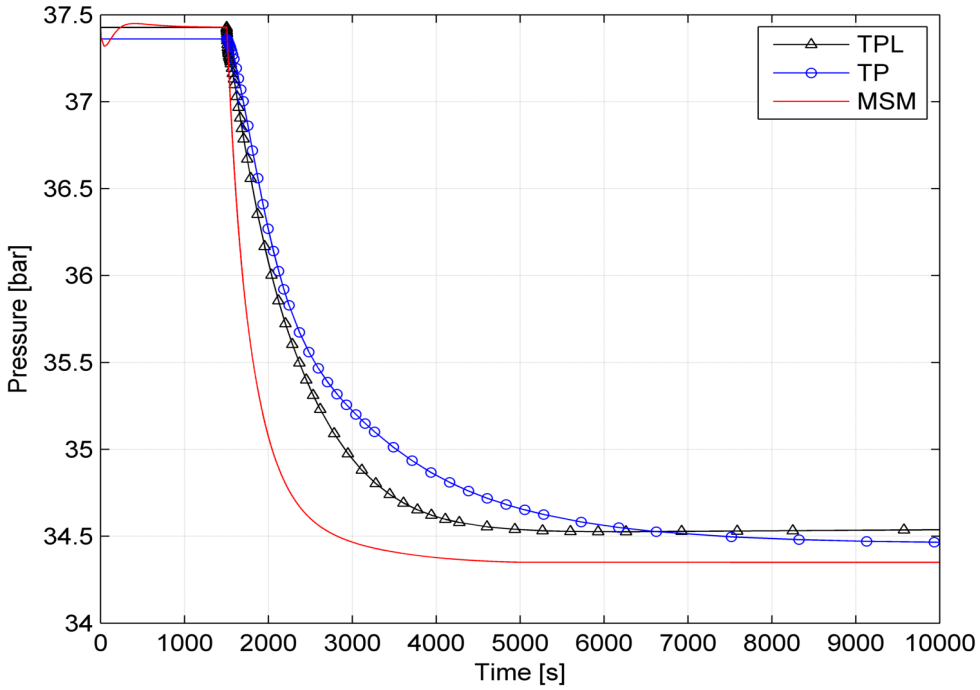

Figure 1.11: Steam pressure at the drum inlet.

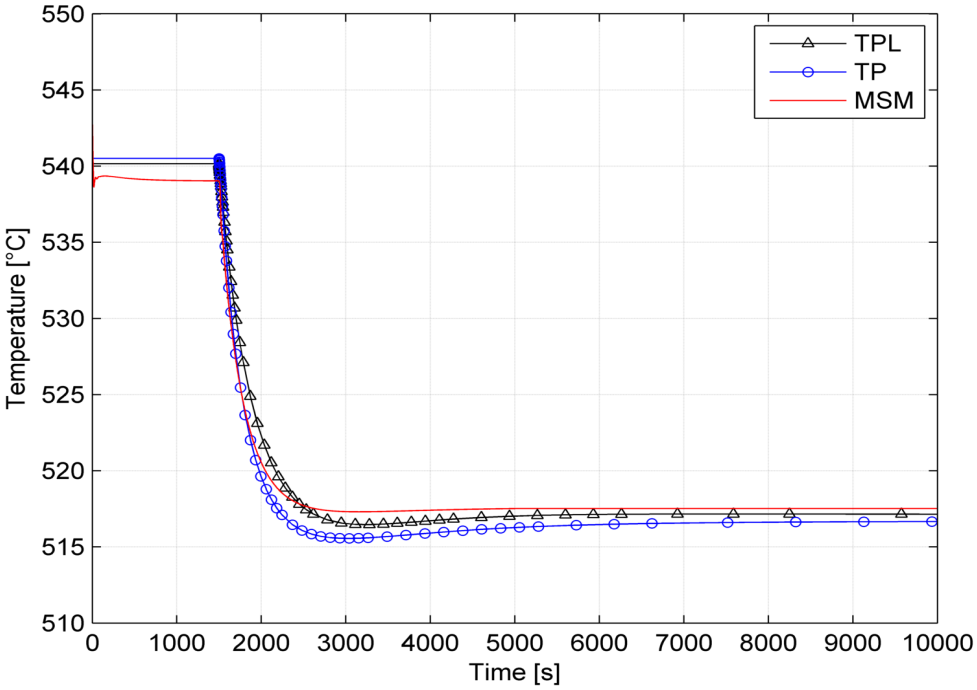

Figure 1.12: Steam temperature at the superheater outlet section.

developed in Simulink has a faster response mainly due to the different control system. In addition the feed pump into the TPL model is an ideal pump but is able to take into account the inertia phenomena into the machine; effect which is not implemented into the TP model. As reported in 1.12 the trends of the temperature at the exit of the superheater are more or less the same for the three models therefore the heat transfer coefficients and the relative heat transfer areas are computed in the correct way in the three models. Obviously, it is not necessary to introduce the heat transfer areas into the TPL model because the heat exchanger component computes these surfaces starting from the inserted geometry. On the other hand, developing a model where the entire geometry of the components is taken into account is computationally expensive; in particular the simulation time is three times faster for the TP model in comparison of the TPL model. Furthermore, it is important to underline that, to evaluate the thermal stresses and the residual life, it is essential to build a detailed model that permits to determine the pressures and temperatures trends into the single part of the device; as a consequence, only the model developed in DYMOLA coupled with Thermal Power library (TPL) is able to predict thermodynamic variables with this grade of detail. However, in order to understand the geometry's influence the dynamic analysis and the lifetime estimation are performed using both the DYMOLA model (components from Thermal Power library) and the Simulink one. The MSM model because uses a different approach during the equations' solving process instead of

the one built in DYMOLA with components taking from ThermoPower library (TP). In this manner, the dynamic behaviour is predicted with two different models based on two different approaches and built from two different research groups.

1.5 Dynamic analysis

The trend of the exhaust gases mass flow rate and temperature at the HRSG inlet is taken from the gas turbine model described in Chapter 1.3.1. The GT compressor, which is equipped with variable inlet guide vanes (VIGVs), is able to maintain the exhaust gases mass flow approximately constant for a gas turbine load from 0 % to 50 % while the temperature increases up to the design value. On the other hand, from 50 % to 100 % of the gas turbine load, the gas flow rate increases (due to the VIGVs opening) while the temperature remains constant (see Figure 1.13).

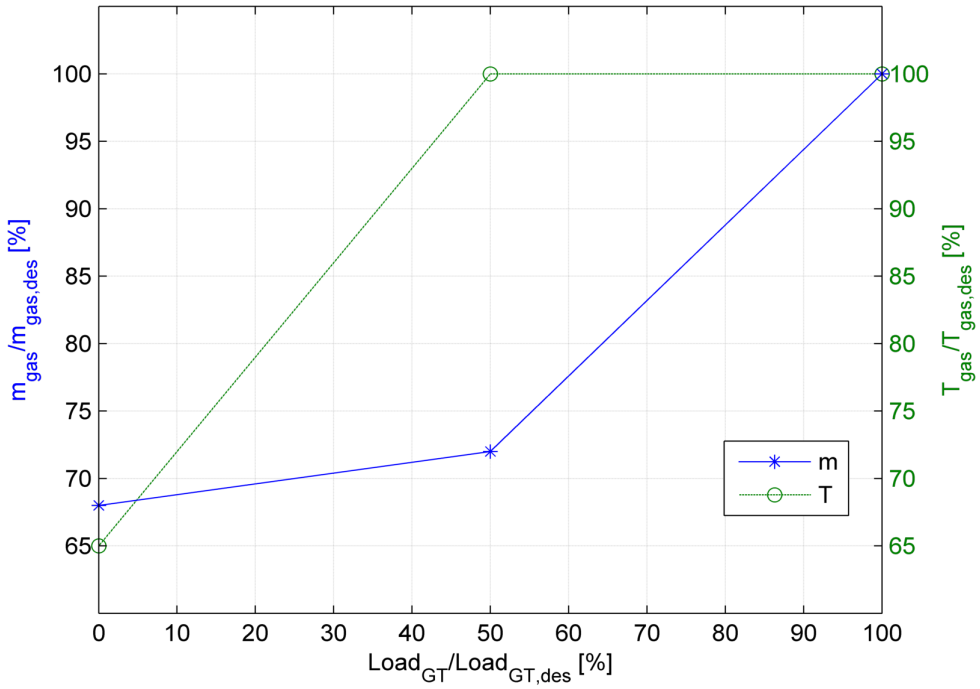

Figure 1.13: Flow rate and temperature of the gases entering the HRSG as a function of GT load [40].

In Figure 1.14 two typical transient conditions, supplied by an operator of the Italian electricity market and indicated by the acronyms “Tr. A and “Tr. B”, are sketched. The two transients coincide till 2500 s from the simulation start time, when the exhaust gases mass flow rate (and thus the steam turbine power) is equal to 84 % ($160\,kg \cdot s^{-1}$) of the rated value, thereafter they become specular: in “Tr. A” the gases mass flow rate decreases up to $140\,kg \cdot s^{-1}$, whereas in “Tr. B” it

increases again up to $180\,kg \cdot s^{-1}$. In both transients, the gases temperature at the inlet of the HRSG remains constant and equal to the rated value (582 °C). As shown in Figures 1.15 and 1.16, which report respectively the steam drum pressure and the steam turbine power output, there is a complete correspondence between the Simulink model and the one developed with Thermal Power library.

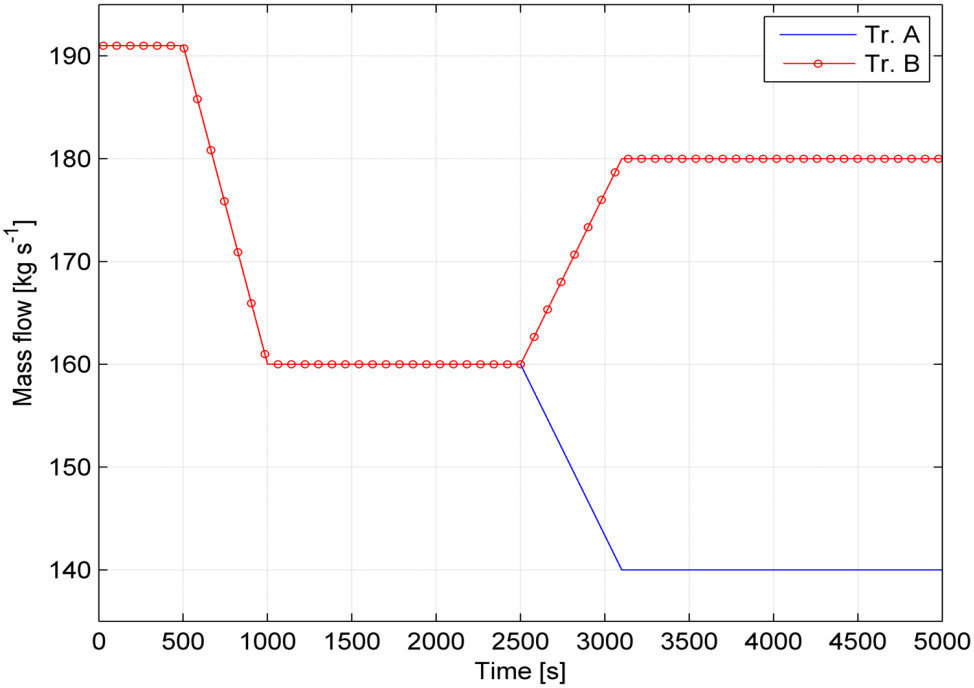

Figure 1.14: The exhaust gases mass flow rate at the HRSG inlet for transients Tr. A and Tr. B.

1.6 Lifetime calculation

In the selected test case, the analysis of the thermodynamic variables shows that superheater and drum are the most stressed components. For this reason, the output values of the dynamic simulation models are used as input for the mathematical tools able to evaluate the steam drum's life reduction (due to low-cycle fatigue) and the superheater lifetime reduction (due to creep and thermo-mechanical fatigue).

For this analysis, other three more strict transient operating conditions are selected (see Figure 1.17). All of them consider a plant load reduction from the rated value to about 55 %, but they differ for the decreasing time values. In particular, transient "Tr. 1" is selected as reference case (the flow rate decreases from 191 to $130\,kg \cdot s^{-1}$ in 37.5 minutes and temperature from 582 °C to 515 °C in 6.25 minutes), whereas transients "Tr. 2" and "Tr. 3" can be considered respectively as a "less" and a "more" stressed operating condition. They are characterized by

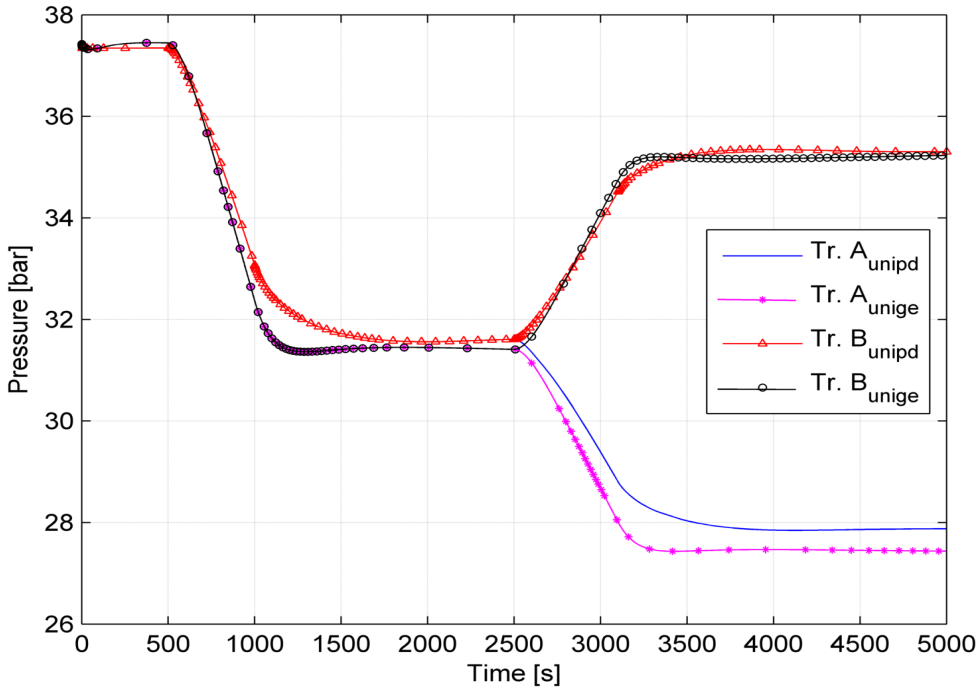

Figure 1.15: The steam drum pressure during transients Tr. A and Tr. B.

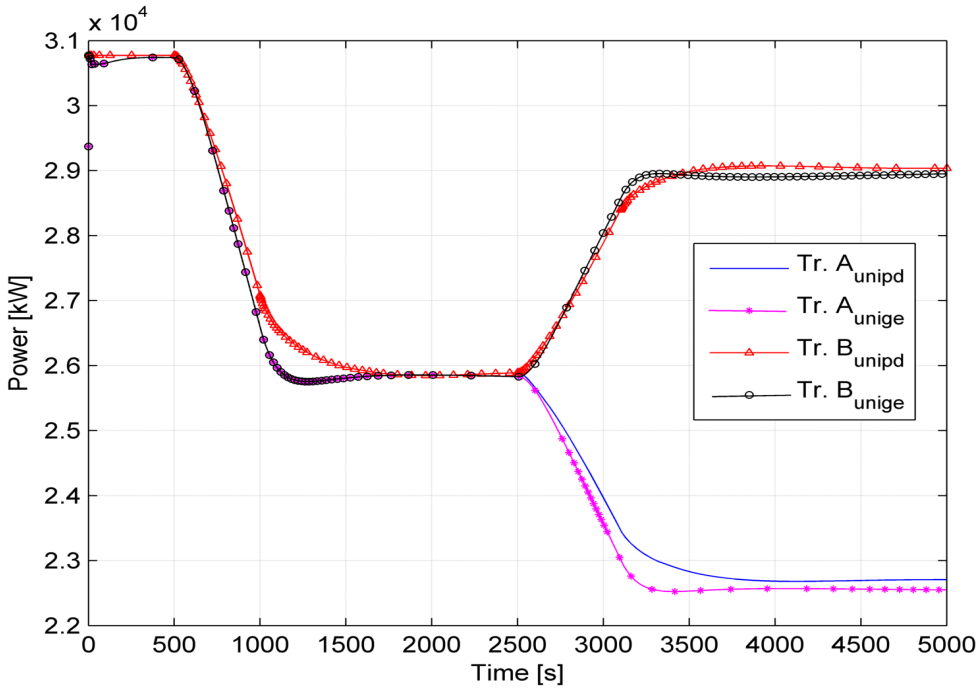

Figure 1.16: The steam turbine power output during transients Tr. A and Tr. B.

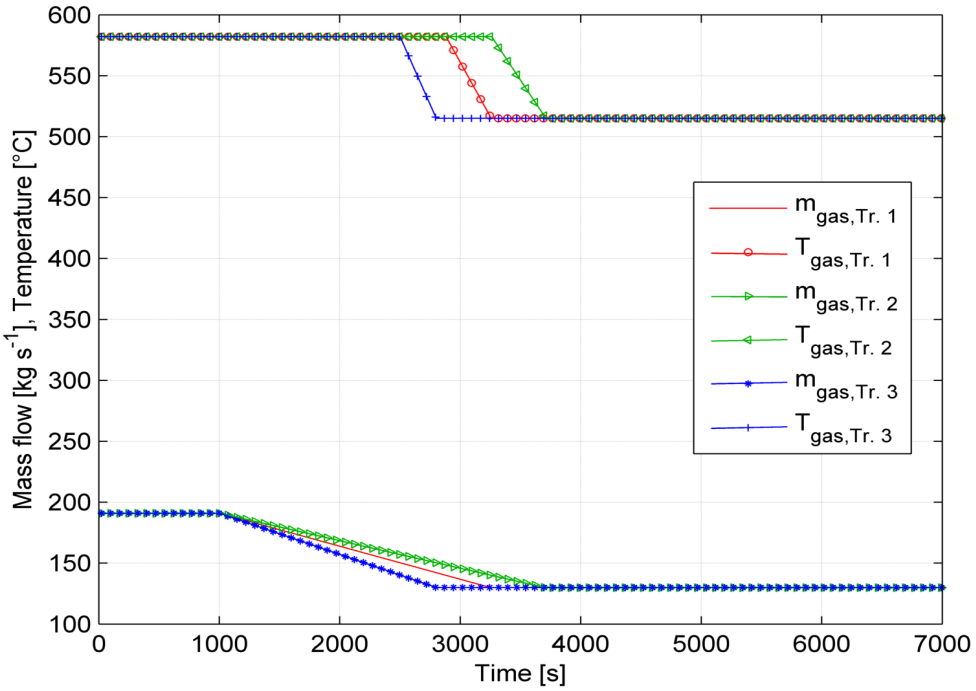

Figure 1.17: Mass flow rate and temperature of exhaust gases at the HRSG inlet during transients Tr. 1, Tr. 2 and Tr. 3.

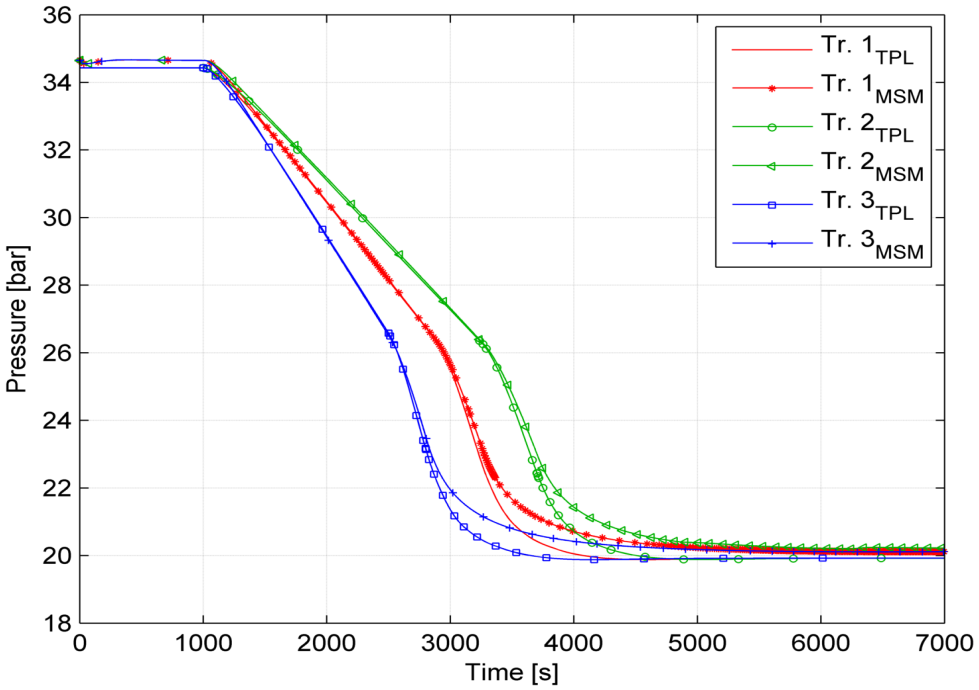

Figure 1.18: Steam pressure at the superheater exit during transients Tr. 1, 2 and 3.

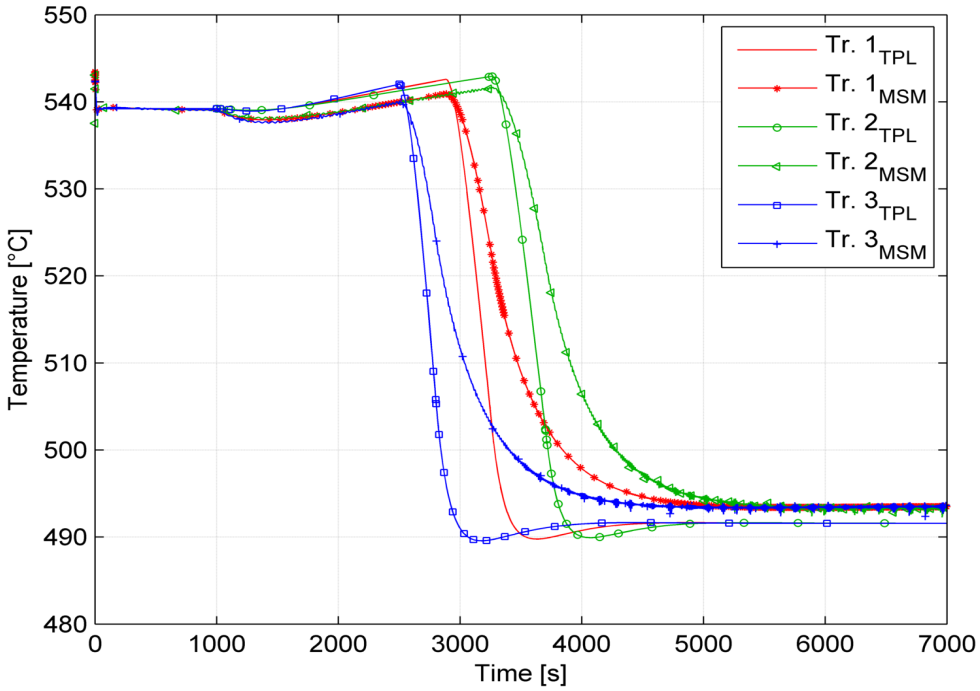

Figure 1.19: Steam temperature at the superheater exit during transients Tr. 1, Tr. 2 and Tr. 3.

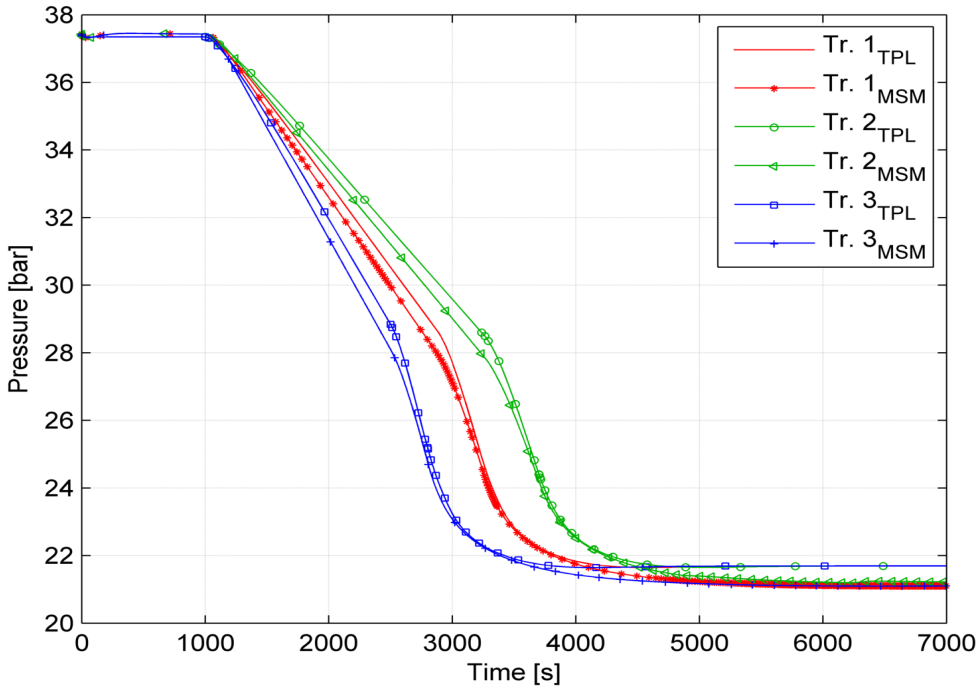

Figure 1.20: Steam pressure into the drum during transients Tr. 1, 2 and 3.

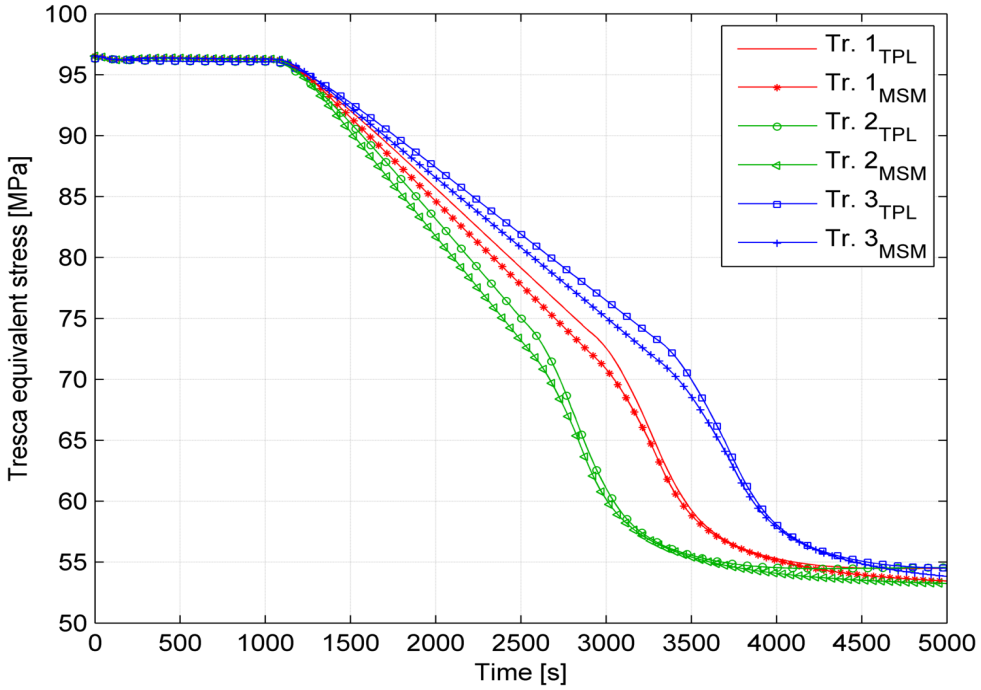

Figure 1.21: The signed Tresca equivalent stress during transients Tr. 1, 2 and 3.

decrease time values 25 % higher and lower respectively than that of "Tr. 1". As shown in Figure 1.17, it is assumed that in all the three transients the gases temperature starts diminishing when the mass flow rate attains the value of $140\,kg \cdot s^{-1}$; this hypothesis is in accordance with data supplied by combined cycle operators. In particular, the selected test cases have been chosen in order to investigate the dependence of the residual life reduction on the slope of the load reduction curve.

The good accordance between the two models (Simulink and Thermal Power) is proved also by analysing the simulation results related to the three aforesaid transients; to this end, Figures 1.18 and 1.19 plot the thermodynamic conditions of steam at the superheater exit as a function of time.

Considering the interest of estimating the steam drum residual life, in the following the analysis is focused on this purpose. In Figure 1.20 the trend of the steam drum pressure is depicted; this signal, together with that of the steam saturation temperature, is the main input of the fatigue life calculation tool. The trend of pressure is very similar to that of the signed Tresca equivalent stress, the latter shown in Figure 1.21 for the most stressed metal layer: this is mainly due to the fact that, in the three examined transients, the mechanical stress (due to pressure) is predominant on the thermal stress (due to thermal gradients) since the exhaust gases temperature gradient, and so that of steam, is not so high; only near the time instant of 3000 s it can be noticed a certain deviation of Tresca signal (see Figure 1.21) compared to the pressure signal (see Figure 1.20) because

at that time the maximum thermal stress is occurs.

From the life reduction calculation, it derives that, in comparison with the transient "Tr. 1" (that is the reference case) the transient "Tr. 2" is less severe since it determines a decrease in the life reduction of about 9.4 %, whereas the transient "Tr. 3" leads to an increase of about 5.3 %.

The superheater lifetime is estimated using the methodology outlined in Chapter 1.1. The trends of the pressure and temperature computed at the outlet section of the device with the Modelica model are used to calculate the creep and thermo-mechanical fatigue stress. Considering a management strategy aimed at maximizing the production during periods where the electricity price is high (from 9 am to 6 pm) and maintaining the plant at minimum load from 6 pm to 9 pm, the results show a life time reduction of about 5 % and an increase of 7 % if the hypothesis is to adopt "Tr. 2" or "Tr. 3" instead of "Tr. 1".

1.7 Discussion

The role played by combined cycle power plants in the scenario of the liberalized electricity market is a fundamental aspect to take into account. The issue of the plant's life reduction has been pointed out as a consequence of more and more frequent cycling operations. In this context, the availability of dynamic simulation models of power plants, able to test different operating conditions and evaluate their impact on the residual life of plant devices, is paramount. At this purpose, three different flexible simulation models for the same single pressure level combined cycle unit are developed, tested and successfully validated.

Then, the dynamic analysis results are used in a procedure able to estimate thermo-mechanical stresses and the associated devices' life-time reduction. The proposed tools can be considered as valuable innovative instruments to assist power plant designers and operators in order to improve the plant's flexibility without excessively compromising the integrity of devices subjected to high thermo-mechanical stresses. Furthermore, another key factor is the user-friendly interface of the life reduction calculation tool proposed in this dissertation and its short run-time in comparison with finite elements analysis tools.

1.8 Computational issues

As previously said, Modelica is an effective language to build power plant dynamic models because the user can exploit and extend existing models or build new ones.

Customers can build very detailed models or implement more simple ones to grossly describe the system. Obviously, the grade of detail depends on both the application and the aim of the study. However, the higher is the model complexity, the slower is the computational speed.

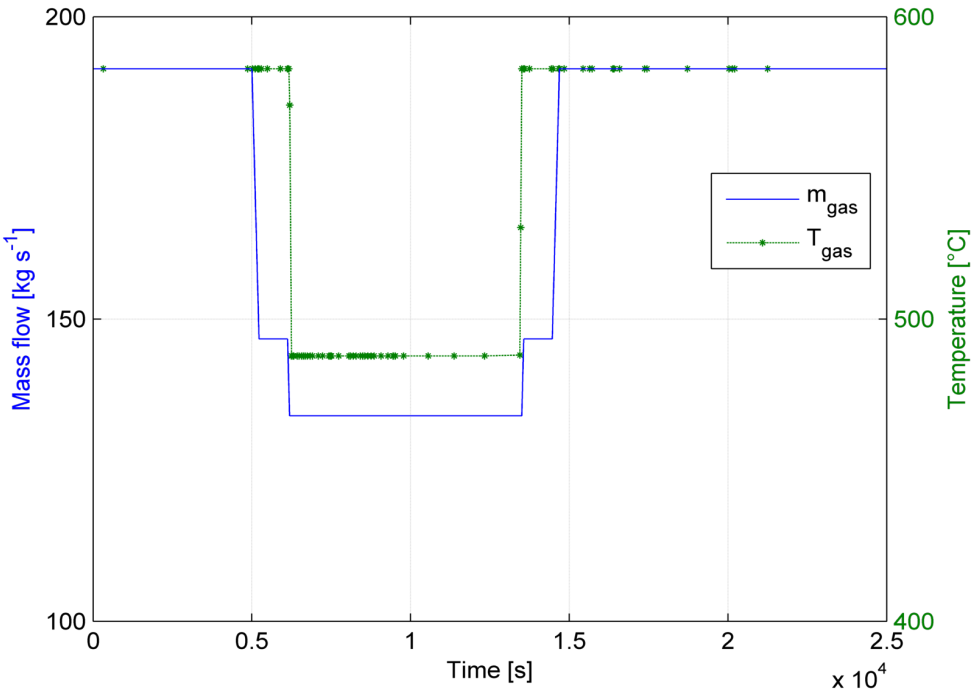

Figure 1.22: Exhaust gases mass flow and temperature during load variation.

In the present work, the implementation of a detailed geometry doubles the simulation time but guarantees a higher results accuracy. In addition, a detailed geometry coupled with a high discretization of the device, allowed to show thermodynamic variables in each volume.

As an example, the fluids and wall temperatures trend in the first volume of the superheater are shown in Figure 1.23 while the wall mean temperatures along one of the SH tubes are depicted in Figure 1.24

However, high complexity induce numerical instability into the model, which means, in particular cases, infeasible results. A particular load variation (see Figure 1.22) is selected as test case and the results are outlined in the following. During the dynamic simulation, due to the low tolerance (10^{-8}) and the numerical instability into the correlations used to compute the heat transfer coefficients, the pump control system is not able to control the drum level properly (see Figure 1.25). The feed pump continuously changes the rotational speed; consequently pressures and water mass flow are unstable. Figures 1.26 and 1.27 depict these trends. In order to solve these numerical issues, different interpolation method of the fluid tables and smooth correlations are introduced and coupled with an

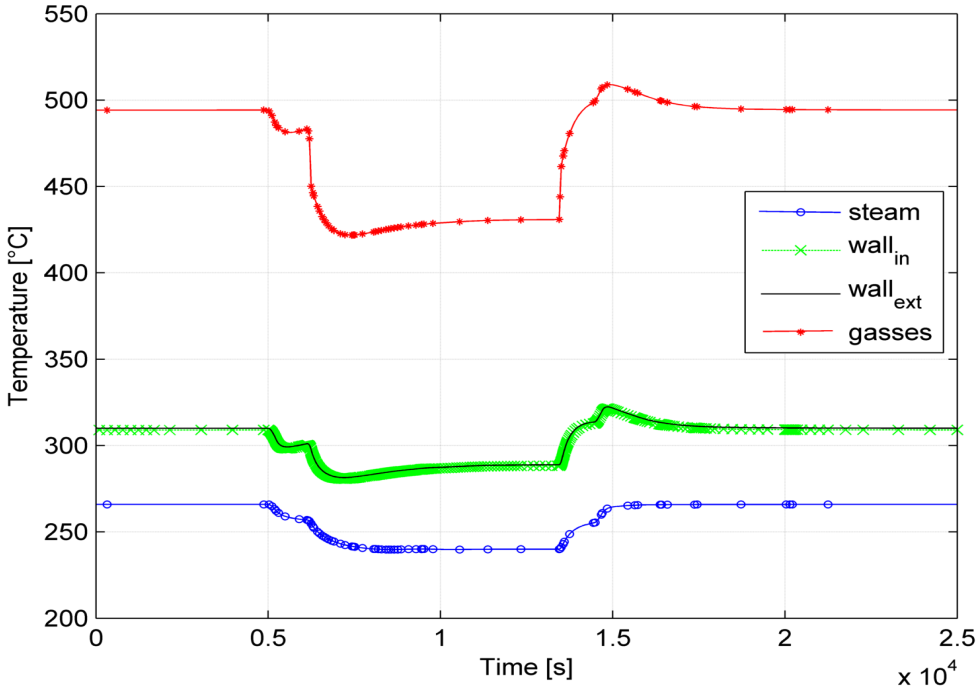

Figure 1.23: Steam, internal and external wall and exhaust gases temperatures trend in the first volume of the superheater.

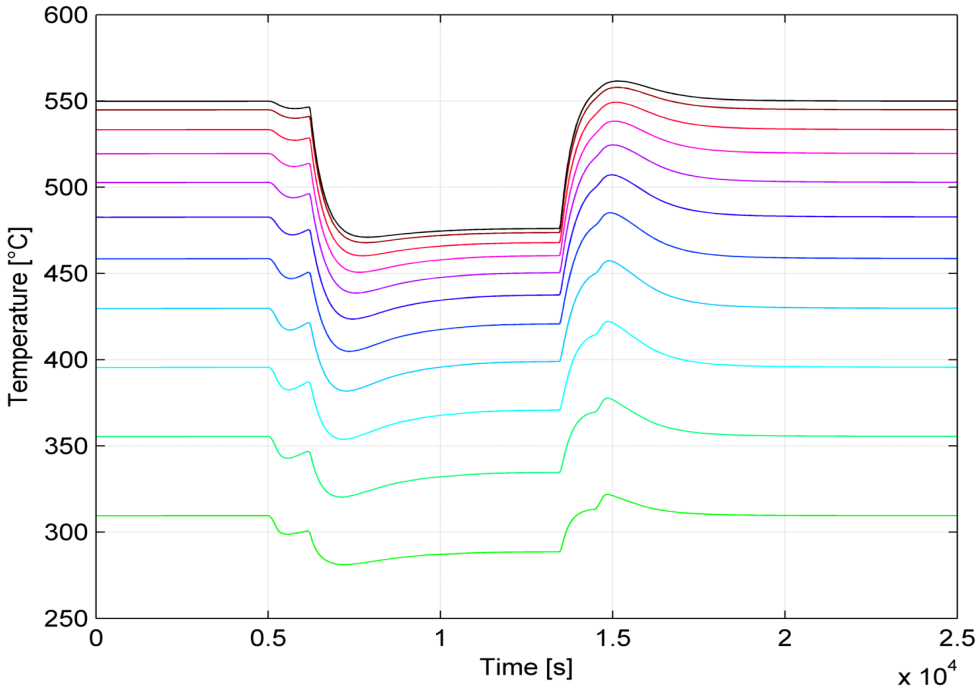

Figure 1.24: Superheater wall temperatures trend from steam inner to outer section. Each value is computed in the middle of the wall volume.

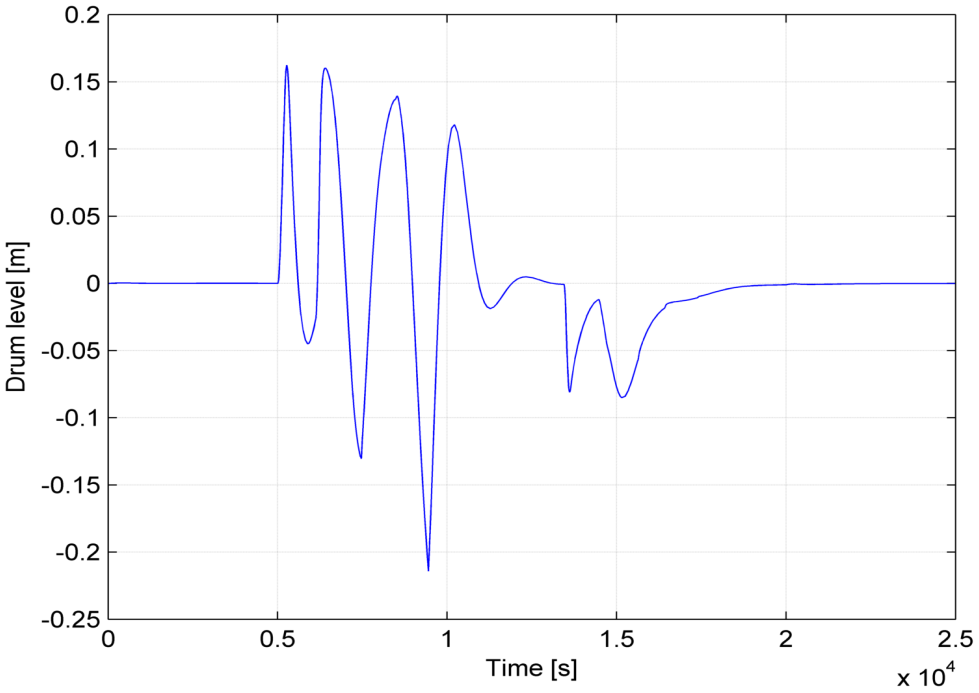

Figure 1.25: Drum level fluctuation.

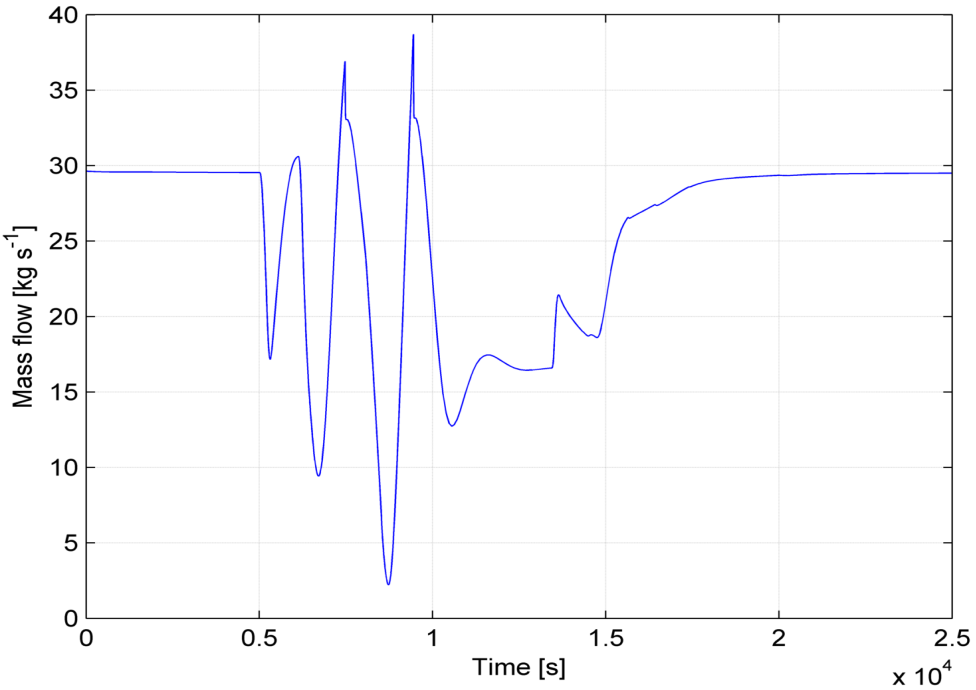

Figure 1.26: Pump mass flow.

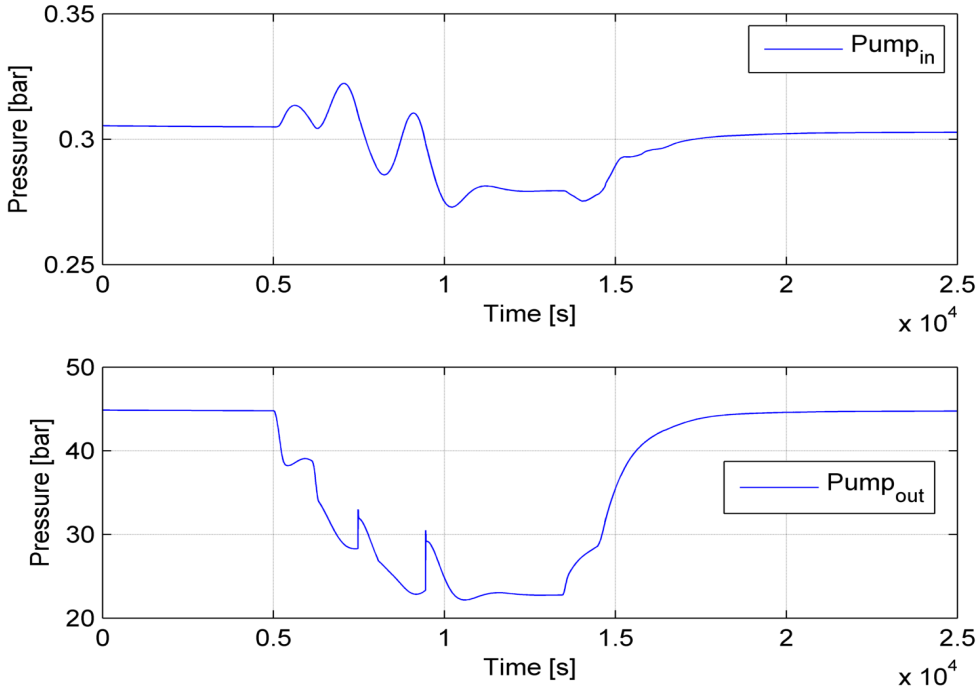

Figure 1.27: Pump inner and outer pressure.

algorithm suitable for solving stiff systems.

1.9 Future work

The dynamic analysis in DYMOLA environment is a very complicated but powerful method to predict the plants' behaviour during start-up, shut-down and load variation. Nevertheless, developing and setting models is really complicated without plants operators' skill and real data.

At present, two types of analysis are in progress within our research team. The first one is devoted to the dynamic investigation of a three pressure level heat recovery steam generator with reheating. The Modelica object diagram is depicted in Figure 1.28.

The main problems that limit the development of this model are: the definitions of the control systems' parameters, the implementation of appropriate correlations and the computational speed.

The other research line is focused on the evaluation of thermal stresses in specific plant devices by finite elements tools. The parameterization of the drum and superheater models is done with data computed with the Modelica model of the entire plant. As for the previous analysis, the selection and implementation of appropriate correlation and the computational speed are the main obstacles. In Figures 1.29 and 1.30 the three dimensional models built for the ongoing analysis

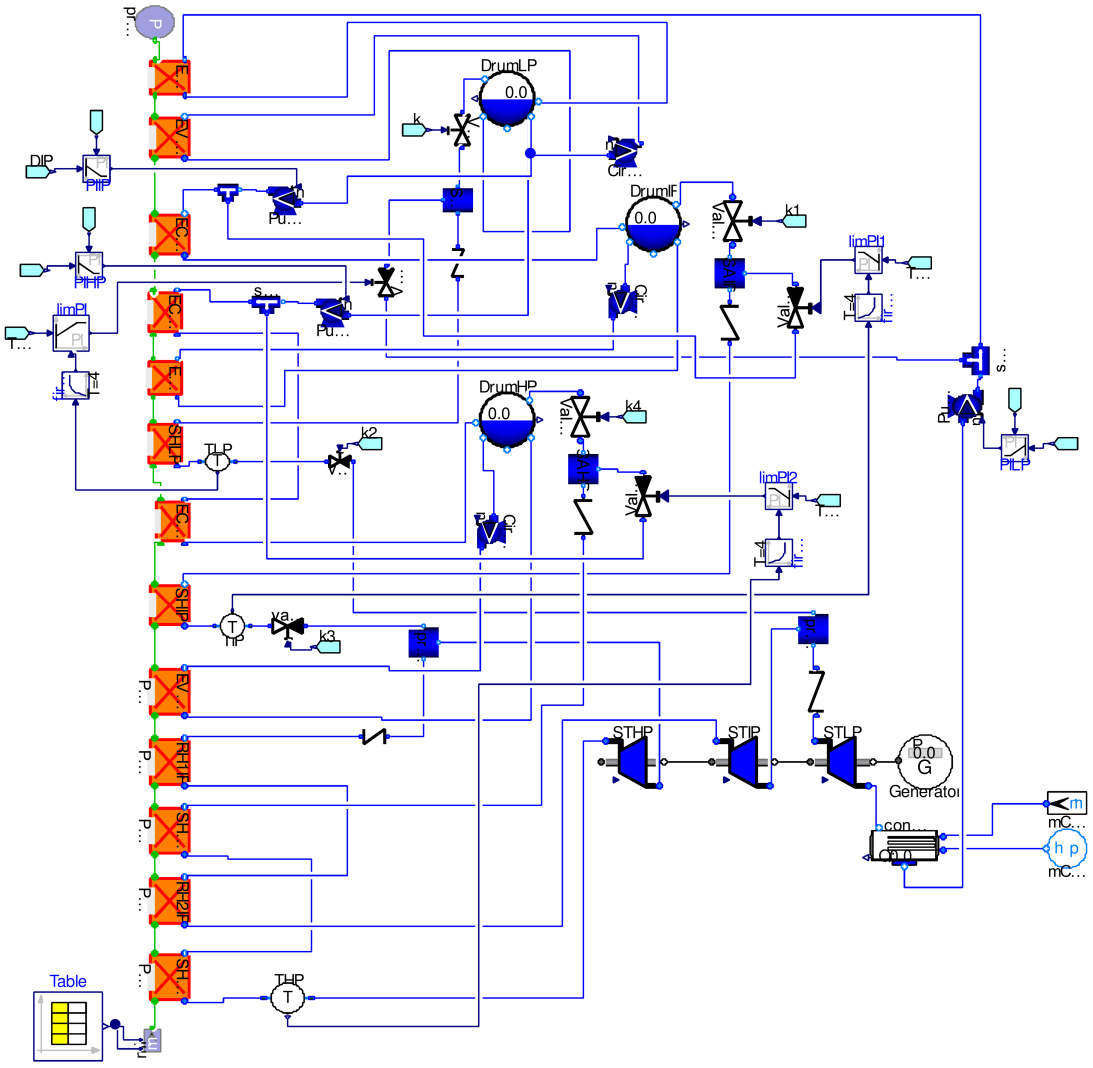

Figure 1.28: Object diagram of the three pressure level heat recovery steam generator.

are shown.

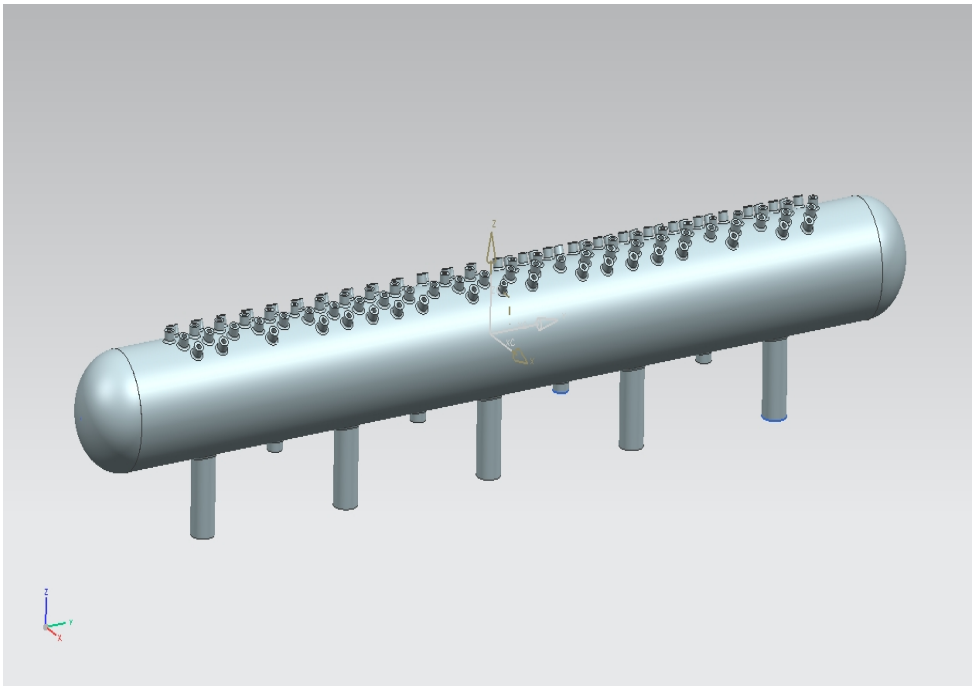

Figure 1.29: 3D model of the drum.

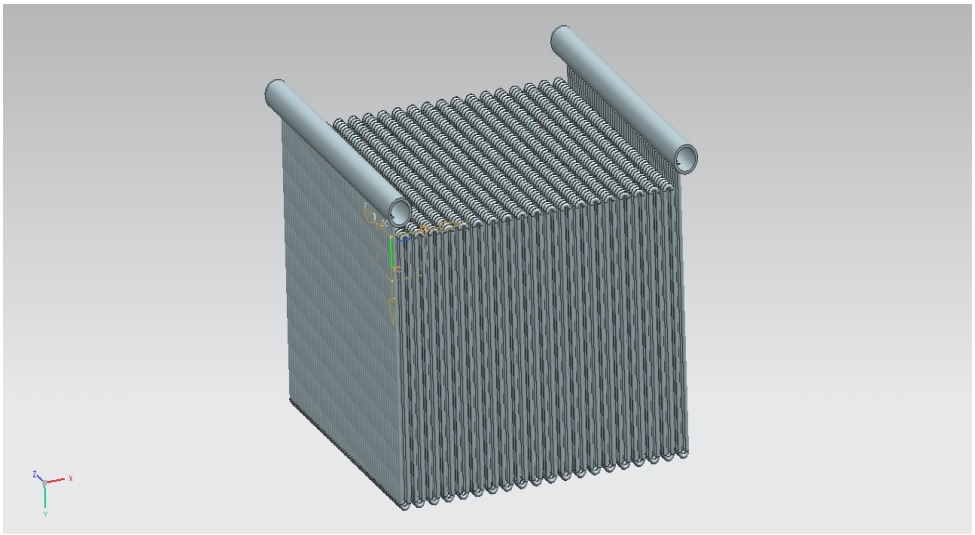

Figure 1.30: 3D model of the superheater.

Chapter 2

Waste Heat Recovery Units

2.1 Context

In the recent years, the world energy consumption has risen to a level never reached before. As previously said, to satisfy the energy demand is necessary to use fossil fuels. But, this intense use in energy sector has caused a huge release of CO_2 in atmosphere [67]; a greenhouse gas with a great contribution to global warming [68]. Therefore, the increased concerns about climate change, has forced international administrations to adopt stringent environmental protection measures and energy efficiency policies.

Although remarkable contribution to the electricity production is expected to be provided by wind and solar power, the efficient recovery of waste heat from fossil sources is also going to play a key role in the future scenario. As reported in [69], the European civil, industrial and transportation sectors discharge approximately 140 TWh/y of high- and low- temperature waste heat, corresponding to a potential CO_2 reduction of about 14 Mt/y. In the U.S. the industrial sector accounts for about one-third of the total energy consumed and is responsible for about one-third of fossil fuel related greenhouse gas emissions [70]. It is also estimated that from 20 to 50 % of U.S. industrial energy input is lost as waste heat in the form of hot exhaust gases, cooling water, and heat lost from hot equipment surfaces and heated products.

It is fundamental to underline that the waste heat temperature is a key factor because determines waste heat recovery feasibility. In Table 2.1 the typical heat sources and temperature range are listed.

On account of this, during the years, many researchers developed several methods for converting waste heat into electricity, each one with its advantages and drawbacks. Notwithstanding, independently of the technical problems, the main

Table 2.1: Temperature classification of waste heat sources [70].

Categories	**Heat Source**	**Temperature**
High temperature (T>650 °C)	Nickel refining furnace	1370–1650 °C
	Steel electric arc furnace	1370–1650 °C
	Basic oxygen furnace	1100–1200 °C
	Aluminum reverberatory furnace	1100–1200 °C
	Copper refining furnace	760–820 °C
	Steel heating furnace	930–1040 °C
	Copper reverberatory furnace	900–1090 °C
	Hydrogen plants	650–980 °C
	Fume incinerators	650–1430 °C
	Glass melting furnace	1300–1540 °C
	Coke oven	650–1000 °C
	Iron cupola	820-980 °C
Medium temperature (230 °C<T<650 °C)	Steam boiler exhaust	230–480 °C
	Gas turbine exhaust	370–540 °C
	Reciprocating engine exhaust	320–590 °C
	Heat treating furnace	430–650 °C
	Drying & baking ovens	230–590 °C
	Cement kiln	450–620 °C
Low temperature (T < 230 °C)	Exhaust gases exiting recovery devices in gas-fired boilers ethylene furnaces, etc.	70–230 °C
	Process steam condensate	50–90 °C
	Cooling water from:	
	furnace doors	30–50 °C
	annealing furnaces	70–230 °C
	air compressors	30–50 °C
	internal combustion engines	70–120 °C
	air conditioning and refrigeration condensers	30–40 °C
	Drying, baking and curing ovens	90–230 °C
	Hot processed liquids/solids	30–230 °C

obstacle limiting the diffusion of medium and low temperature waste heat recovery units is the high initial investment cost which in turn results in high payback times and poor economic revenue. However, there is an industrial area where the implementation of waste heat recovery units could be really interesting because it shows the largest energy recovery potential [71] and high taxation per ton of CO_2 emitted: the oil and gas sector.

2.2 Case study

Among all the industrial areas, oil and gas sector has the largest energy recovery potential. According to Campana et al. [71] a high emissions' reduction can be achieved, for example, by augmenting the performance of gas compressor stations. However, on offshore facilities the principal contributor to the overall emissions is the power generation system which typically releases a large amount of heat and CO_2 to the environment. As estimated by Nguyen et al. [72], in 2011, the North Sea oil and gas platforms were responsible for about 25 % of the total CO_2 emissions in Norway.

In order to reduce the CO_2 emissions, since 1991, the Norwegian Government established a carbon tax on hydrocarbon fuels. Furthermore, in 2013, the Norwegian Government has increased this tax by 200 NOK per ton of CO_2 [73]. Thus, with a tax of 60 $ per ton of CO_2, increasing the performance of the offshore platform power generation systems has become a focus area from an environmental and economic perspective [74].

Most of the oil and gas platforms are isolated systems where the electric grid operates in island (stand-alone system). The platform power generation unit normally consists of one or more redundant engines. A standard configuration is characterized by three gas turbines in simple cycle where only a small fraction of the heat contained in the exhaust gases released by the GTs is recuperated.

For security reasons the platform load is covered by two units, which run at the same time covering 50 % of the load each, while the third one is in stand-by or on maintenance.

On the one hand, this management strategy reduces the system performance because the GTs efficiency is in the range from 20 % to 30 %. On the other hand, a high power generation system's reliability guarantees a reduction of system failure and the consequent high economic loss.

With the declared intent of studying alternative power unit able to increase the platform performance and reduce CO_2 emissions, a four years research project was

funded [75] and the author was involved in this project during his external stay at Technical University of Denmark. The Draugen oil and gas offshore platform (see Figure 2.1) was selected as case study.

Figure 2.1: Draugen offshore oil and gas platform (by courtesy of A/S Norske Shell [76]).

Figure 2.2 shows the Draugen oil field, that is located in the Haltenbanken area of the North Sea and belongs to the Norwegian continental shelf. So, the Draugen platform is located approximately 150 km from Kristiansud in the Norwegian Sea, where, in 1984, the production license was acquired by Royal Dutch Shell [76].

The reservoir was discovered in 1984, is made of sand stone which is located 1650 m below the sea bed. The platform was installed in 1993, it is a monopile gravity based structure trusted 5 m into the sea bed at a water depth of 251 m. The structure has seven large concrete oil tanks situated on the seabed, which keep the platform in place. The oil tanks are connected to an off-loading buoy. Figure 2.3 shows tge Draugen field and the platform monopile.

The platform is operated by A/S Norske Shell and produces gas (exported via Åsgar gas pipeline to Kårstø) and oil (which is firstly stored in tanks at the bottom of the sea and then shipped, once every one or two weeks, via shuttle tanker) [74, 77].

The on board power generation system is composed by three Siemens SGT-500 gas turbines. Table 2.2 lists the GT design point specifications as provided by the manufacturer [78, 79].

Figure 2.2: Draugen field location (by courtesy of A/S Norske Shell [76]).

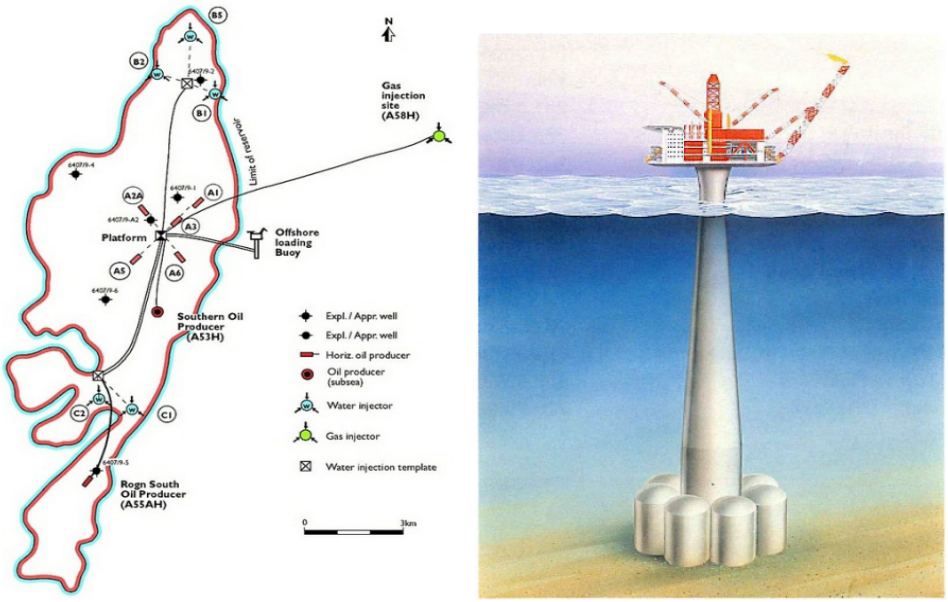

Figure 2.3: Draugen field and the platform monopile (by courtesy of A/S Norske Shell [76]).

Table 2.2: Design-point specifications for the twin-spool gas turbine installed on the Draugen offshore oil and gas platform.

Model	**Siemens SGT-500**
Low pressure compressor stages	10
High pressure compressor stages	8
Low pressure turbine stages	1
High pressure turbine stages	2
Power turbine stages	3
Turbine inlet temperature	850 °C
Exhaust gas temperature	379.2 °C
Exhaust gas mass flow	91.5 kg $\cdot$ s^{-1}
Electric power output	16.5 MW
Thermal efficiency	31.3 %
Fuel	Natural gas

In Figure 2.4 the layout of the platform power generation system is depicted. As reported in [79], the three shaft industrial gas turbine SGT-500 is a light weight, high efficiency, very flexible, heavy duty machine. It employs two coaxial shafts coupling the low pressure compressor (LPC) with the low pressure turbine (LPT) and the high pressure compressor (HPC) with the high pressure turbine (HPT). The power turbine (PT) transfers mechanical power through a dedicated shaft to the electric generator (GEN). The fuel is natural gas and is burned into the combustion chamber (CC).

The SGT–500 gas turbine compressors are not equipped with variable inlet guide vanes. Consequently, the engine load can only be controlled by opening/closing the fuel valve. Therefore, the exhaust temperature drops down when the load decreases.

The platform normal electric demand is equal to 19 MW. A typical yearly platform electric demand is plotted in Figure 2.5, where the dimensionless values are referred to the normal electric load. During oil export activities the demand increased up to 25 MW, that is the peak load demand [80]. In order to reduce grid failure during load changes, the platform owner has established that the maximum frequency undershooting can be equal to 5 % compared to the steady-state value (50 Hz). In addition to this, another critical performance metric parameter, the so call "rise time", needs to be checked. For clarity, the rise time is defined as the time required to the frequency to return back at the 99 % of the value at steady-state (50 Hz).

In this context, with the particular requirements imposed by the platform operator, the only viable solution able to increase the platform performance and reduce

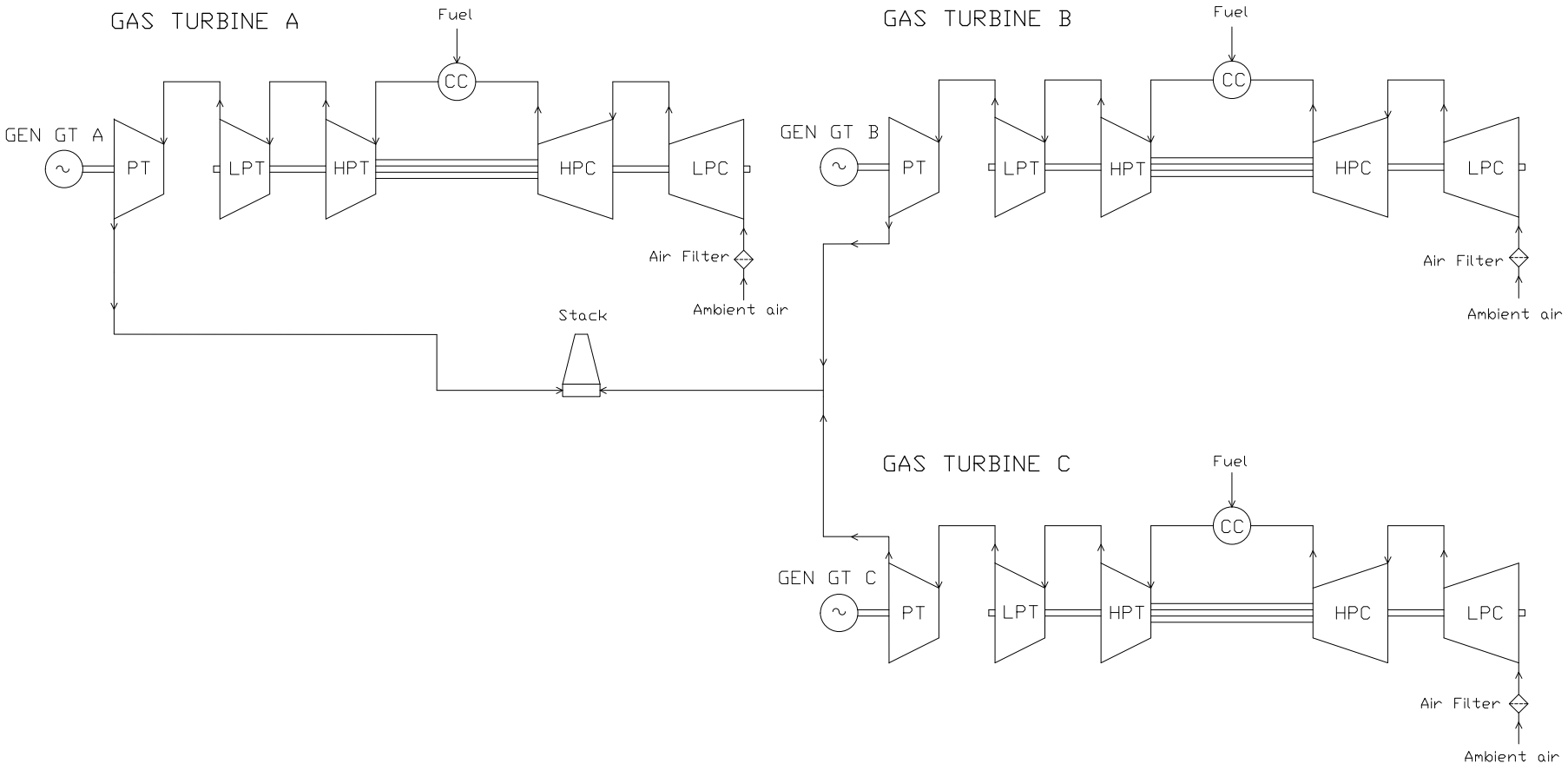

Figure 2.4: Layout of the power system installed on the Draugen oil and gas platform.

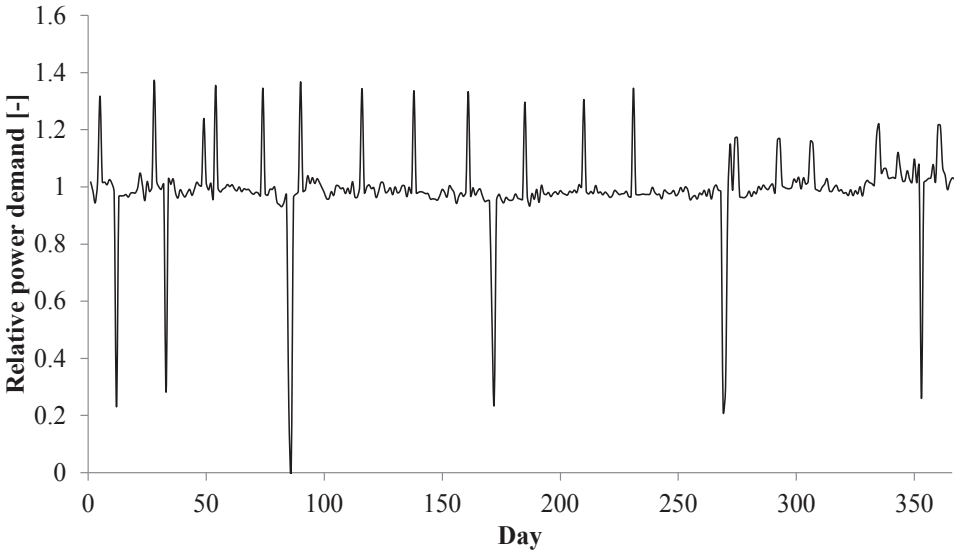

Figure 2.5: Relative electric power demand in the Draugen offshore oil and gas platform in 2012. Daily average value are shown.

the CO_2 emissions is the installation of one or more waste heat recovery units on the gas turbines outlet sections.

2.3 WHRU state of the art

During the years, several researchers have developed different thermodynamic cycles to recover waste heat and increase the plant overall performance.

Steam Rankine cycle (SRC) is probably the most adopted cycle, while Air Bottoming Cycle (ABC) and Organic Rankine Cycle (ORC) are mature alternatives that can easily compete with SRC. Kalina cycle, trilateral flash cycle (TFC) and supercritical CO_2 cycle are very promising and can become competitive alternatives in the next future.

2.3.1 Steam Rankine cycle

Steam Rankine cycle (SRC) is the most common waste heat recovery method. It is a mature and widely adopted technology especially in large and medium scale onshore power plants due to the very high efficiency that can be achieved compared to each of the other cycles alone.

The main SRC's drawback is the complexity that makes it both bulky and heavy due to the need of an evaporator and a condenser [81]. However, this is not an issue on onshore applications where space is available but in offshore facilities

high space and weight mean high costs. Therefore, this disadvantage is caused by the use of water as working fluid.

Water is classified as a "wet" fluid (which means that the saturated vapour curve has a negative slope as can be seen in Figure 2.6) with the following thermodynamic characteristics:

- Critical point: 647 K – 22.06 MPa
- Triple point: 273.16 K – 0.611 kPa
- Boiling point: 373.16 K – 101.325 kPa
- Freezing point: 273.15 K – 101.325 kPa
- Latent heat: 2256.6 kJ · kg^{-1} – 101.325 kPa
- Molecular weight: 18 kg · $kmol^{-1}$

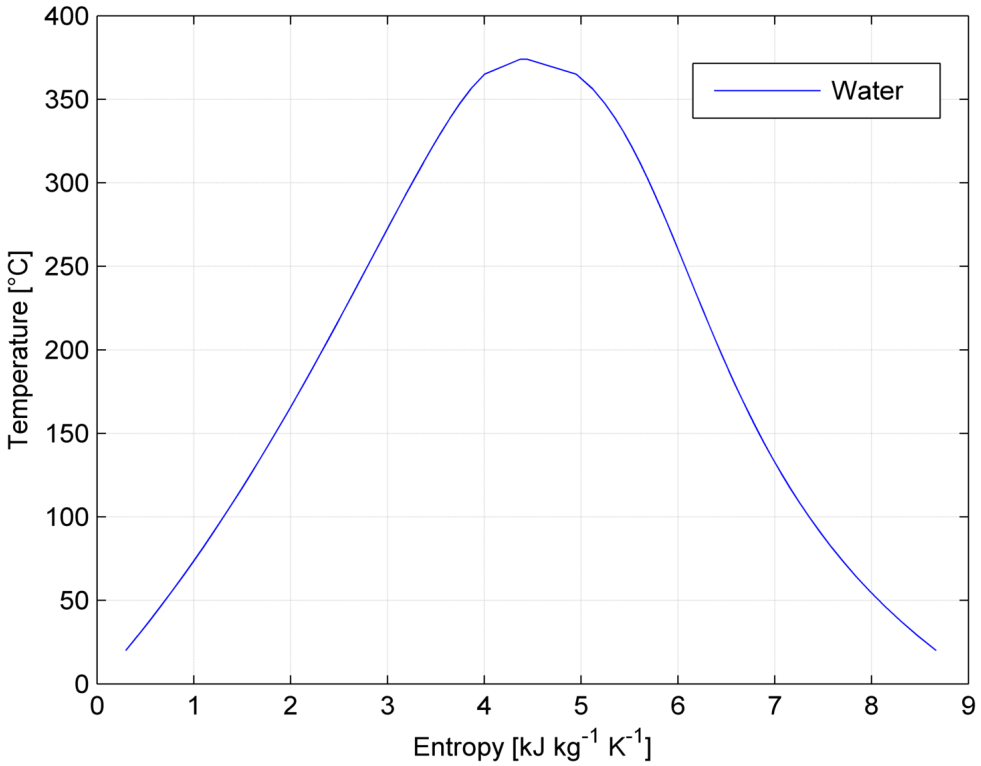

Figure 2.6: T-s diagram of water.

Using water as working fluid presents numerous advantages in many cases [82]:

- Good thermal and chemical stability: there is no risk of thermochemical decomposition of the fluid.

- Low viscosity: the required pumping work is really small.
- Good energy carrier: the latent and specific heat are high.
- Non-toxic fluid.
- Non-flammable fluid.
- Zero ODP and GWP.
- Abundant and cheap fluid.

However, the use of this fluid have drawbacks [83]:

- High evaporating pressure.
- Needs of superheating: the fluid superheating is needed to prevent condensation during the expansion process; phenomenon that causes erosion in turbine blades.
- Complex and expensive expander devices.

For these reasons, although water/steam can offer higher pressure ratios and better heat transfer properties than other fluids, standard pressure and temperature at the inlet of the steam turbine are 100 bar and 450 °C [84]. Therefore, using water as working fluid is more suitable in large on-shore power plants. However, SRCs are also used as waste heat recovery units in small and medium size power plants.

In any case, the water/steam combined cycle concept is simple: it is a combination of the gas turbine and the steam turbine process. The exhaust gases normally leave the GT at high temperature (discharging big amount of energy) which is recovered by producing steam in a waste heat recovery unit. The steam is sent to the steam turbine, which produces mechanical power. The low-pressure steam exiting the steam turbine is condensed, and then sent back to the WHRU for steam generation.

Despite the technical problems, the SRC waste heat recovery unit was the first type of WHRU employed in an offshore oil and gas platform. Kloster [85] described the existing SRC units in the Oseberg, Eldfisk and Snorre B offshore platforms. In these cases the steam bottoming cycle is a drum-type heat recovery steam generator (see Figure 2.7) and is divided into two skids: the first one is a single list skid for the WHRH-SG (see Figure 2.8) while the other one includes the steam turbine, instruments, auxiliary and monitoring equipment. Obviously, the main obstacle to set up combined cycle in offshore plants is the required space and the weight of devices.

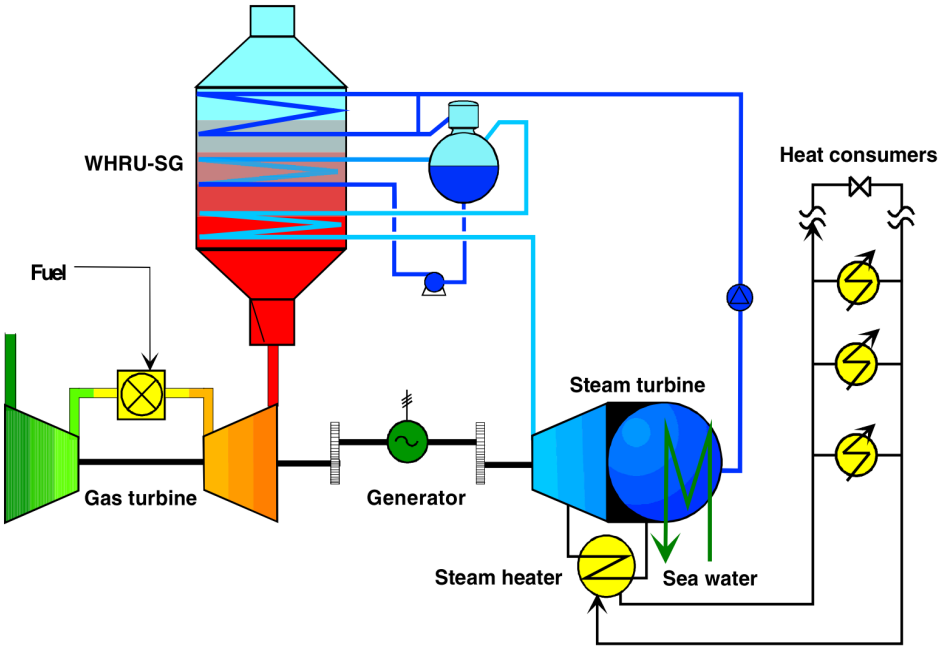

Figure 2.7: Scheme of an offshore Combined Heat and Power Cycle where steam heater and heat consumers represent the Oseberg option. The HRSG is a drum-type module [85].

Figure 2.8: The double-inlet, single lift Oseberg WHRU-SG [85].

Aiming at minimizing the weight of the heat transfer equipment, Nord and Bolland [86] proposed a steam cycle with a single pressure once-through boiler (OTB) instead of the conventional and heavier drum type heat recovery steam generator (see Figure 2.9).

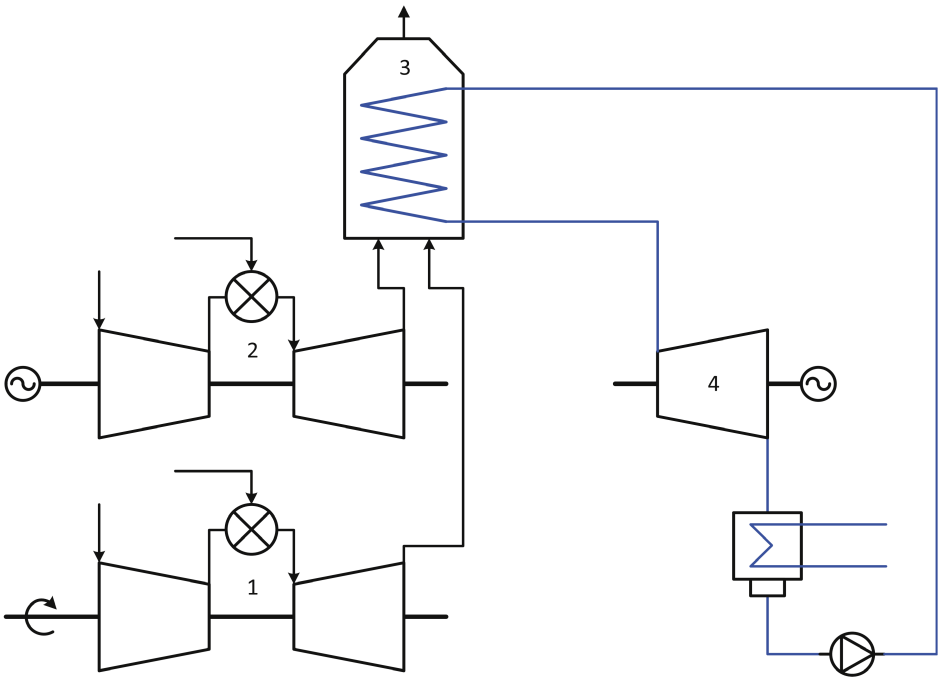

Figure 2.9: Layout of combined cycle for offshore installations with two gas turbines and one dual-inlet once-through HRSG [86]. The mech. drive gas turbine and the gen. drive gas turbine are identified with 1 and 2, respectively. The single-pressure OTSG and the steam turbine are pinpointed with 3 and 4, respectively.

Nord and Bolland [86] also performed a comparison between a drum-type HRSG and a once-through HRSG for offshore applications and concluded that a suitable HRSG design could be a single pressure once-through boiler (see Figure 2.10). This configuration guarantees plant flexibility and the possibility to avoid the bypass stack while allowing for dry HRSG operation. On the contrary, the presence of evaporator and condenser remains an issue considering the platform space and weight limitations.

2.3.2 Air bottoming cycle

The air bottoming cycle turbogenerator is a valuable alternative to the conventional steam Rankine cycle unit due to its high compactness and low weight.

The simplest configuration of an ABC unit is depicted in Figure 2.11; it is composed by an air compressor (AC), a heat exchanger (AHX) and an air turbine (AT).

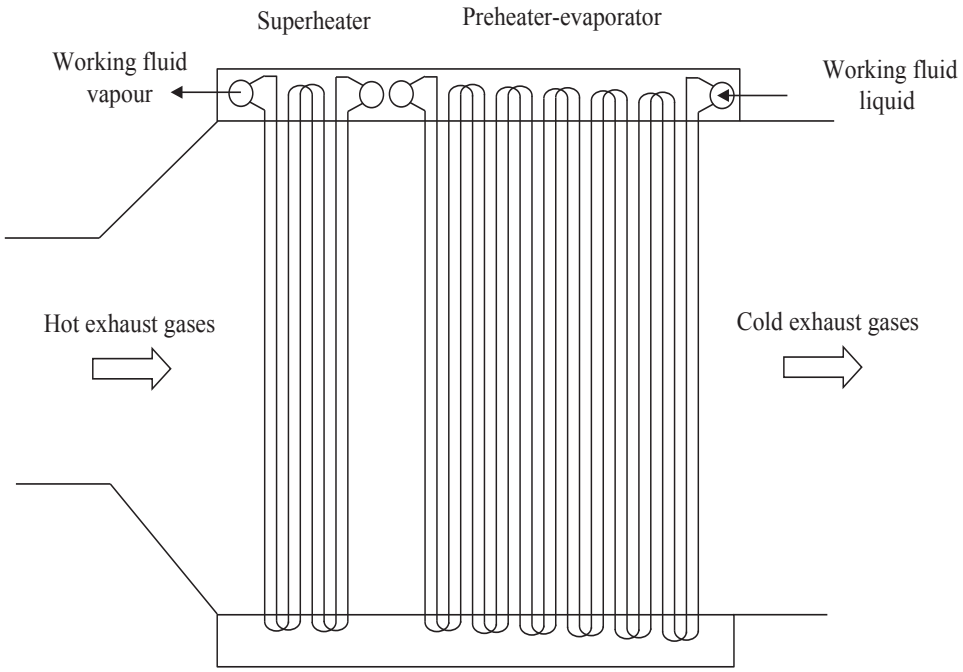

Figure 2.10: Once-through boiler typical layout.

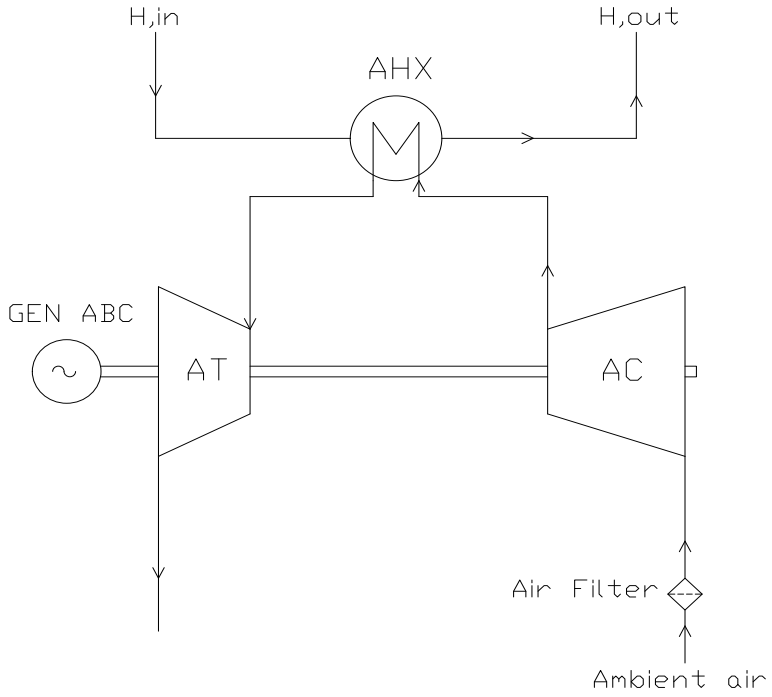

Figure 2.11: Air bottoming cycle layout.

This cycle uses the same principle as the well-known Brayton cycle where the combustion chamber is replaced by a gas to gas heat exchanger where air is heated up by e.g. the exhaust gases exiting from a gas turbine or a boiler.

The ABC power module was invented by Farrell (General Electric) in 1988; a year later he patented the ABC in the United States [87] and then (1992) in Europe [88]. During the decades, a large variety of ABC configurations were proposed. As an example, in Figure 2.12 the ABC module with one intercooler, two intercoolers and with two spools configuration are shown. Note that, an ABC unit consisting of an air turbine, that drives the air compressor, and another one which drives the electric generator (called "power turbine"), is the plant scheme that guarantees the highest efficiency at part-load conditions.

In literature extensive surveys can be found about the use and the thermodynamic potential of a large variety of ABC configurations, see i.e. [89–94]. However, the first authors who proposed the use of ABC for gas turbine waste heat recovery on oil and gas platforms were Bolland et al. [95]. They performed a thermodynamic analysis of the whole platform power generation system, including gas turbines and an ABC with varying numbers of intercoolers. It was concluded that the configuration with two intercoolers increased the plant thermal efficiency by 10.5 % compared to the case with the gas turbine alone where the thermal efficiency was 36.1 %. The ABC itself had an efficiency of 23.2 % and the plant total power was increased by 30 %. In this manner, Bolland et al. demonstrate that, despite the low gain in performance, the low weight (the unit does not require condenser as it operates as open-cycle) and the use of a non-toxic and not-flammable working fluid guarantees low investment costs and, consequently, short pay-back time. In addition, the use of an ABC unit in an offshore platform was economically feasible due to the high CO_2 taxes applied in Norway at that time.

Other investigations on the use of ABC units in oil and gas field are presented in [96, 97] while in [98] the ABC is employed to boost the performance of a high-speed ferry which uses gas turbines as power train.

As presented before, at the beginning researchers focused their attention on the thermodynamic design and optimization of different ABC configurations with the aim of improving the system performance. After that, their attention was devoted to devices' configurations with a particular focus on the gas to gas heat exchanger module. As known, in oil and gas platform volume and weight play a key role: low weight means high compactness and low costs. For this reason, the selection of the heat exchanger's type is a crucial aspect. In fact, the heat exchanger configuration and its dimensions are parameters that influence its ability to transfer heat, the

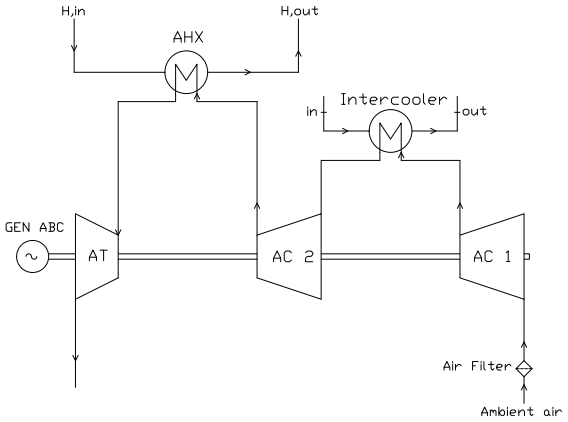

(a)

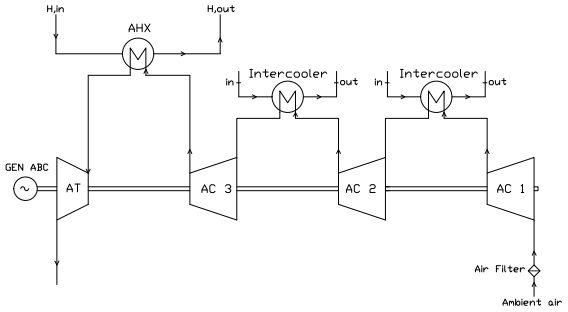

(b)

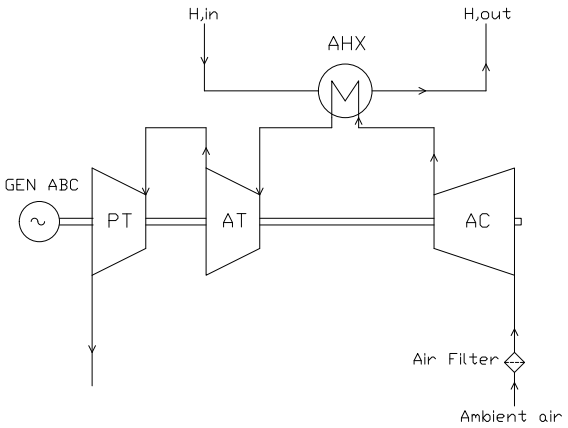

(c)

Figure 2.12: Different configurations of the air bottoming cycle unit.

efficiency and the performance of the whole system.

There are two different types of heat exchanger that can be used to recover a hot gaseous stream with another cold gaseous flow [95]: a regenerator or a recuperator. In a recuperator, the heat is transferred through walls that separate the streams, while in a regenerator, the heat transfer surface is alternately exposed to the two flows. Kays and London [99] list four advantages for the regenerators over the recuperators:

1. A much more compact heat transfer surface can be employed.
2. The heat transfer surface is substantially less expensive per unit of transfer area.
3. The surface tends to be self-cleaning due to the periodic flow reversals that avoid the flow stagnation.
4. They require only light-gage containment for the low pressure exhaust gas over most of their volumes.

In addition, recuperators need heavy-gage containment over their entire volume; but they are a much more proven technology compared to the regenerators in this type of application and size range.

Kays and London [99] also list the regenerators' drawbacks:

1. There is some mixing between the hot and cold fluid due to the leakage and carry-over.
2. If the fluids operate at high pressure the sealing problem of a regenerator is a difficult task.

In ABC units the fluid mixing and leakages are not acceptable. Note that, with an air leakage of 3 %, the combined gas turbine and ABC efficiency decreases by 1 %. These are the main reason why recuperators have been favored over regenerators to recover gas turbines' waste heat.

In literature, different types of recuperator can be found for different pressures and temperatures range [50, 58, 99–102]: the shell and tube heat exchanger (see Figure 2.13(a)) and the plate-fin heat exchanger (PFHE) (see Figure 2.13(b)). The shell and tube heat exchanger is widely adopted in ABC where a large difference in pressure ratio between the two streams is observed, while the PFHX, due to the extended surface (fins are used on both flow sides), is used when large amounts of heat need to be transferred with a small volume.

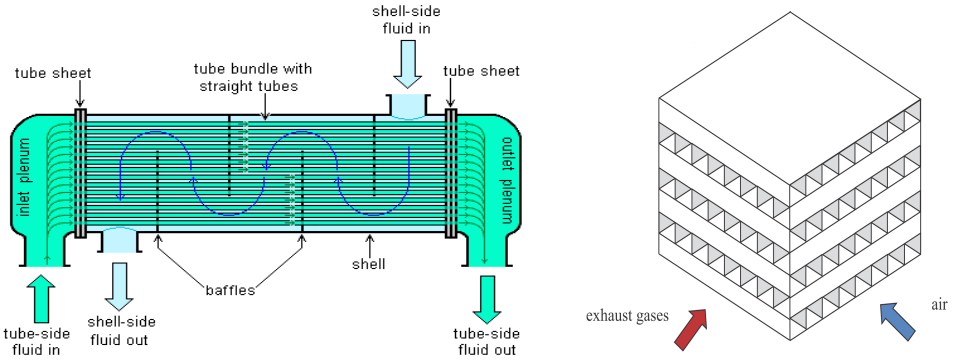

(a) (b)

Figure 2.13: (a) Shell and tube heat exchanger layout, (b) plate-fin heat exchanger unit.

2.3.3 Organic Rankine cycle

Although investigated since the 1880s, Organic Rankine Cycles (ORC) have never been popular until today's growing interest on medium and low grade energy recovery systems where cycles using water as working fluid fails for technical and economic reasons [103, 104].

The technical problems encountered with water can be mitigated by selecting an appropriate organic fluid, i.e. refrigerants and hydrocarbons. These compounds are characterized by higher molecular mass and lower critical temperature than water, aspects which can make a small and medium scale power plant technologically and economically feasible .

Notwithstanding, an ORC unit is similar to the conventional steam Rankine cycle: the liquid working fluid at high pressure is firstly evaporated, then is expanded to a lower pressure thus releasing mechanical work. The cycle is closed by condensing the low pressure vapour (coming from the turbine outlet) and pumping the liquid back to the high pressure. Hence, the ORC unit is fundamentally made up by the same devices as a conventional steam power module: an evaporator, an expander, a condenser and a pump.

Nevertheless, an organic Rankine cycle has several advantages over steam power plant [82]:

- Less heat is needed during the evaporation process.
- The evaporation process takes place at lower temperature and pressure.
- The expansion process ends in the vapor region, so superheating is not required and the risk of turbine blades erosion is avoided.

- The smaller temperature difference between evaporation and condensation means that the pressure drop/ratio will be much smaller and thus simple single stage turbines can be adopted.

ORCs, owing to their low operating temperature, are suitable for recovering heat from sun's radiations [105–113], ocean warm layers [114–118], hydro-thermal and engineered geothermal systems (EGS) [119–122], abandoned oil fields [123–125], biomass [126–130], and industrial processes [103, 131, 132].

Obviously, the type and temperature of the heat source significantly influences the choice of the working fluid which in turn determines the configuration, the performance and the economics of the plant [133].

This aspect justifies the abundant literature dedicated to fluids selection and plant configurations for different heat sources. In the following a brief review is presented.

Working fluid selection

The fluid selection is a complicated task owing to the following two reasons [134]:

- The heat source type and the working conditions vary widely: from low-temperature to high-temperature heat sources (e.g. 80<T<500 °C).
- Hundreds of substances can be used as working fluid candidates (hydrocarbons (HC), hydro-fluorocarbons (HFC), hydro-chlorofluorocarbons (HCFC), chlorofluorocarbons (CFC), per-fluorocarbons (PFC), siloxanes, alcohols, aldehydes, ethers hydrofluoroethers (HFE), amines, zeotropic and azeotropic mixtures and inorganic fluids).

However, the working fluids can be categorized according to the saturation vapor curve. The curves' type is one of the crucial characteristics [103]. It affects the fluid applicability, the cycle efficiency, and the arrangement of power unit's equipment [135]. There are three types of vapour saturation curves in the Temperature-entropy (T-s) diagram: a "dry" fluid with positive slopes (i.e. cyclohexane), a "wet" fluid with negative slopes (e.g. water), and an "isentropic" fluid with nearly infinitive large slopes (i.e. R141b). In Figure 2.14 the three types of saturated curves are shown.

With isentropic and dry fluids the superheating is not needed given that the fluid remains saturated or superheated at the turbine outlet section, respectively. The features of persistent saturation throughout the expansion process eliminate the concerns of impingement of liquid droplets on the expander blades. Moreover,

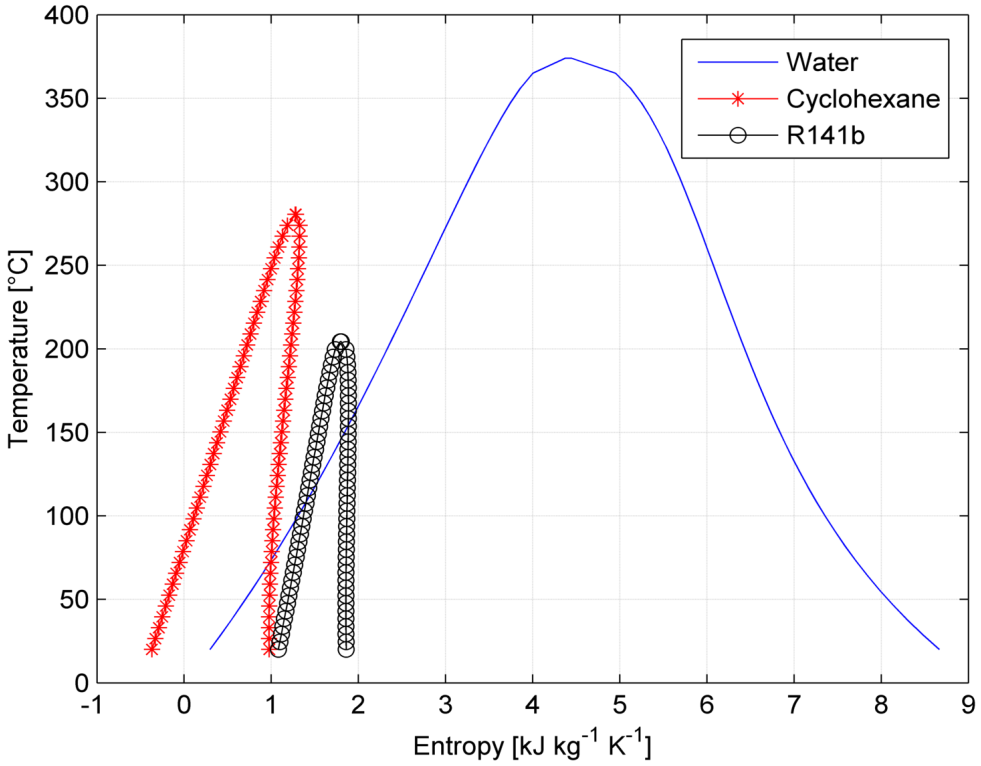

Figure 2.14: Diagram T-s for fluids (Water) wet, (R141b) isentropic and (Cyclohexane) dry.

the superheating apparatus is not needed. Therefore, the working fluids with dry or isentropic saturation curves are more adequate for ORC systems than wet fluids [136, 137]. A drawback of this aspect is that the expanded vapour leaves the turbine with superheat, which is necessary to dissipate in the condenser. In this manner, the plant efficiency is reduced. To mitigate this aspect a recuperator is usually inserted to increase the cycle efficiency; as a consequence the initial investment and the plant complexity are increased.

The methodology adopted for the selection of working fluids in ORC applications is the so called "screening method". It is the most implemented method and consists in building steady-state simulation model of the ORC cycle and run it with different working fluids [138]. A candidate fluid can be a pure fluid or a mixture: an extensive review can be found in [134].

Even though in the scientific literature a broad range of working fluids are analysed, only a few fluids are actually employed in commercial ORC plants [138]. These fluids are

- HFC–134a, N-pentane → geothermal applications.
- HFC–134a → very low temperature waste heat recovery.

- HFC–245fa, N-pentane, Solkatherm, Toluene → waste heat recovery.
- N-pentane solar ORC power plant.
- OMTS → CHP power plants.

According to Bao and Zhao [134], there is not a working fluid suitable for any ORC system but the characteristics that can be expected from a good candidate are:

1. Vapour saturation curve with zero o positive slope → isentropic o dry fluids → no superheating is needed.
2. High latent heat of vaporization → small equipment.
3. High density.
4. High specific heat.
5. Appropriate critical temperature and pressure → 100–200 °C.
6. Appropriate boiling temperature → 0–100 °C.
7. Good heat transfer properties (low viscosity and high thermal conductivity).
8. High thermal and chemical stability.
9. Good compatibility with materials (non corrosive).
10. High thermodynamic performance.
11. Low environmental impact → low ODP and GWP.
12. Good safety characteristics (non toxic and non flammable).
13. Good availability and low cost.

In conclusion (see a survey by Qiu [139]), the candidate working fluid for ORC applications must have not only thermophysical proprieties that match the application but also meet safety requirement and economic costs.

ORC applications and layouts

The layout of the ORC unit is somewhat similar to the layout of the SRC module described in Chapter 2.3.1: there is no drum connected to the boiler, and a single heat exchanger is used to perform the preheating, evaporation and superheating phases. This heat exchanger is, as for the steam cycle, a once-through boiler (See Figure 2.10). The variations of the plant architecture are more limited: superheating is generally not employed and a recuperator can be installed as liquid preheater between the pump drain and expander outlet section. In Figure 2.15 the ORC plant scheme with and without the recuperator are depicted.

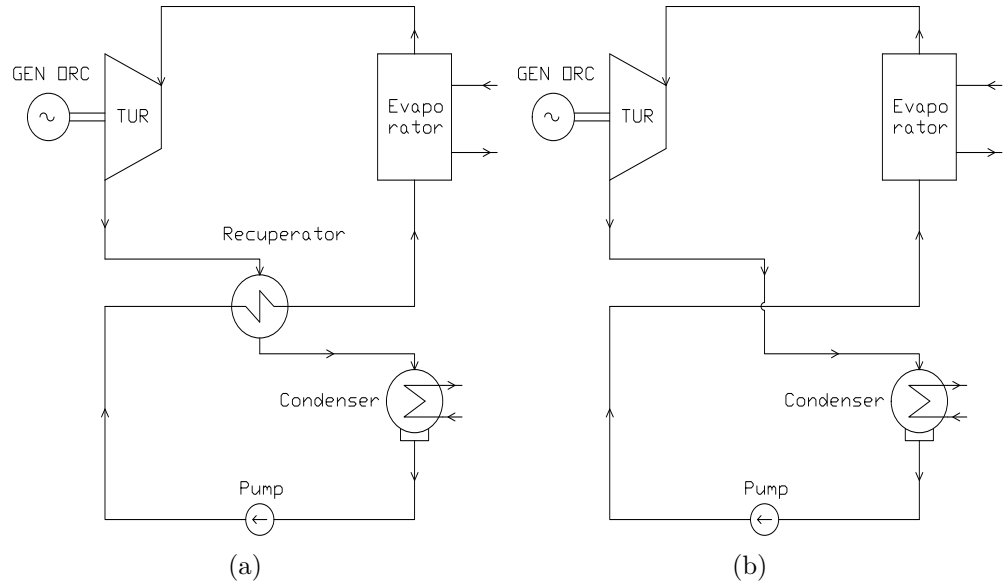

Figure 2.15: Schematic view of an ORC with (left) and without (right) recuperator.

In the following a brief overview of the different ORC applications is reported with respect to the nature of the heat source focusing the attention on the configuration adopted in waste heat recovery systems.

A review of the ORC binary geothermal power plants including temperatures of the heat sources, plant schemes and the ORCs working fluids selection is presented in [82, 140].

Solar ORC-RO desalination systems, duplex-Rankine cooling systems and ocean thermal energy conversion systems are also outlined in [82, 140].

Plant configurations and ORC devices for solar thermal power systems are studied, for example, in [141–144] and in [145–147], respectively.

Regarding the use of ORCs in waste heat recovery applications a wide range of energy recovery technologies has been developed to recover the large amounts of wasted heat. In Table 2.1 the possible heat sources and the temperatures range are

presented. However, the heat transfer from these hot sources to the ORC module can be done in two ways: the hot fluid can exchange directly with the ORC working fluid in the same heat exchanger (see Figure 2.16(b)) or an oil loop is integrated to avoid risk of contact between hot fluid and, usually, flammable ORC working fluid (see Figure 2.16(a)). The first layout is widely adopted to recover waste heat from gas turbine, internal combustion engines, etc. while, the oil loop configuration is extensively used in biomass power plants (see Figure 2.17). Obviously, the ORC module in both configurations can be equipped with or without the recuperator.

A short list of ORC waste heat recovery plants currently in operation and their capital costs can be found again in [82, 140].

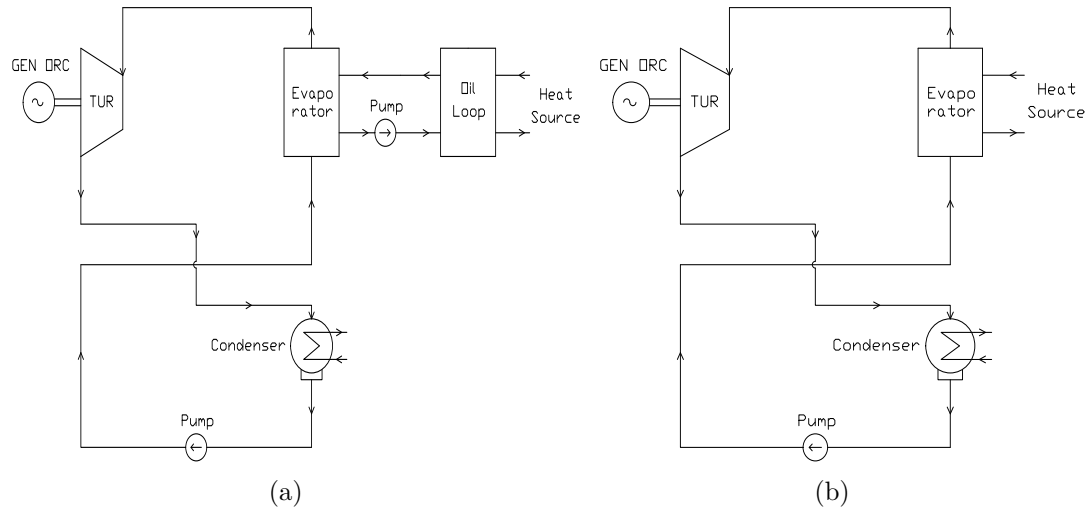

Figure 2.16: Schematic view of an ORC with (left) and without (right) oil loop.

In conclusion, the organic Rankine cycles are a really promising solution to recover waste heat from medium and low temperature sources and, due to their advantages, can become emergent technologies especially on offshore facilities.

2.3.4 Other innovative cycles

In early 1980s, Alexander Kalina proposed a new family of thermodynamic cycles using as working fluid an ammonia-water mixture [148–150]. In 1985, Alexander Kalina patented the so called "Kalina Cycle" [151]. As said by Zhang et al. [152], the Kalina cycle is the most significant improvement in thermal power plant design since the advent of the Rankine cycle. This cycle improves the efficiency of thermal power plants by 15 % to 50 % depending on the particular application [152–156]. In literature, several layouts of the Kalina cycle can be found but it is principally a "modified" Rankine cycle. In practice, the modifications that permit the

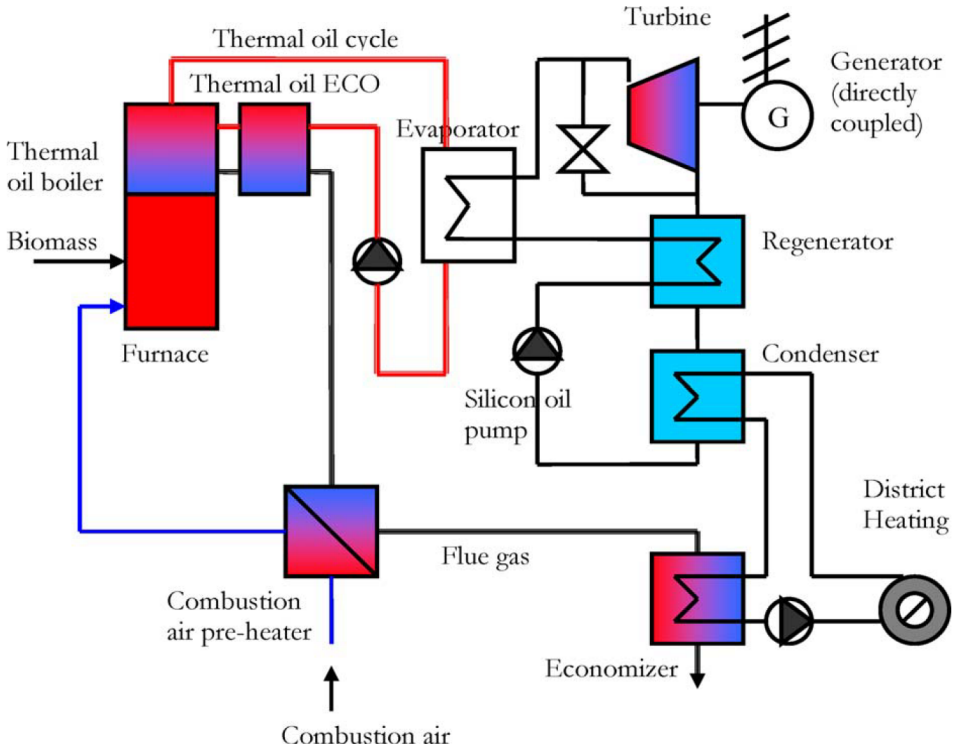

Figure 2.17: Scheme of a biomass power plant with ORC power unit [82].

transformation from Rankine to Kalina consist of proprietary system design that specifically exploit the virtues of the ammonia-water working fluid. For a detailed review of the Kalina cycle working principle, configurations and applications see e.g. [152].

Trilateral flash cycle (TFC) and Supercritical CO_2 cycle are other innovative methods proposed and under development to recover waste heat from medium and low temperature heat sources.

Trilateral flash cycle is a power recovery system from single-phase low-grade heat sources. The TFC system can produce outputs of up to 80 % more than simple Ranking cycle systems in the recovery of power from hot liquid streams in the temperature range from 100 °C to 200 °C. The estimated cost per unit net power output is approximately equal to that of Rankine cycle systems and the preferred working fluids are light hydrocarbons. For more details about this cycle see i.e. [110, 157–159].

In [160] the authors proposed two types of supercritical CO_2 Rankine cycles with and without internal heat exchanger to recover low and medium temperature industrial heat recovery. Kim et al. [161], analyzed transcritical or supercritical CO_2 cycles using both low- and high-temperature heat sources, while Yamaguchi et al. [162] analyzed a solar energy powered Rankine cycle using supercritical CO_2 for

combined production of electricity and thermal energy. A design optimization of supercritical CO_2 power cycle using genetic algorithm and artificial neural network is performed in [163].

These types of innovative cycles are really promising but, at the moment, are not commercially available and only prototypes are under development. Therefore no implementation in offshore platforms are carried out and, consequently, they do not represent a viable solution for the case under analysis.

2.4 Discussion

The possible heat sources and technologies that can be exploited to recover waste heat and reduce the world energy consumption have been presented. The oil and gas sector presents a great potential due to the high quantity of released heat and the high taxation. These aspects forced several companies to study systems able to increase the power generation system performance. The most promising idea is to add a bottoming cycle to the gas turbines constituting the generation unit. After a brief presentation of the possible waste heat recovery technologies, a particular case is presented and the possible waste heat recovery units are selected: SRC, ABC and ORC.

Starting from this background, in Chapter 3 a multi-objective optimization procedure is adopted to find the most suitable waste heat recovery technology for existing and future offshore facilities.

Notwithstanding, an oil and gas platform has a stand-alone grid with specific concerns during load changes and engines failures. At this purpose, a dynamic analysis of the gas turbines and ABC unit is performed in Chapter 4.

The same study is conduced with the gas turbines and ORC unit, but in this case the attention is devoted not only to the grid but also to the thermochemical decomposition of the ORC working fluid. This work is presented in Chapter 5.

Chapter 3

Waste Heat Recovery Technologies for Offshore Platforms

3.1 Context

Oil and gas sector presents the largest energy recovery potential and, due to the high taxation per ton of CO_2 emitted, represents an industrial sector where the implementation of waste heat recovery units is economically feasible.

As known, in offshore platforms the main contribution to the overall emissions is given by the power generation system: a power unit normally constituting of gas turbines in open cycle.

Therefore, in order to increase the power generation system efficiency and reduce the heat and CO_2 emitted, a waste heat recovery unit is suggested as the most feasible solution.

In this Chapter, a methodology able to find the most suitable waste heat recovery technologies for existing and future offshore facilities is proposed.

A multi-objective optimization approach is employed to attain optimal designs for different waste heat recovery units by selecting specific objective functions tailored to the oil and gas sectors.

Obviously, there are several technologies that can be adopted to recover the waste heat in an oil and gas platforms. However, after the detailed literature review presented in Chapter 2.3, only the steam Rankine cycle, the air bottoming cycle and the organic Rankine cycle are considered as feasible solutions. Additionally, in the literature, there is a lack of a extensive comparison among waste heat recovery technologies for offshore applications.

A great motivation in conducting the comparison between the waste heat recovery technologies depends on all the aforementioned aspects.

3.2 Methodology

The waste heat recovery technologies for offshore applications are compared by employing the DYNDES tool [57]. It is a simulation program which couples steady state and dynamic software models to provide an integrated tool for the optimal design of power systems, including dynamic criteria. The evaluation of the systems dynamic response is not included in the present work: the program is used for design point optimization. Figure 3.1 depicts the architecture of the DYNDES design and optimization tool [74].

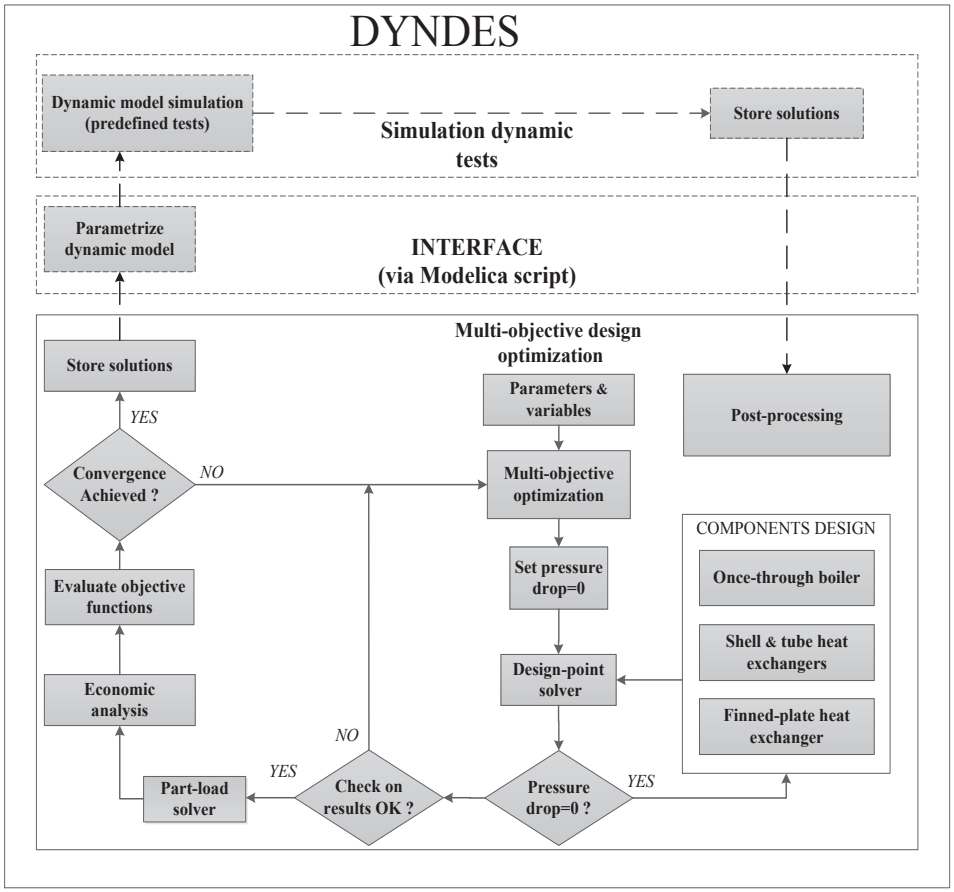

Figure 3.1: Structure of the DYNDES design tool.

The multi-objective optimization procedure coupled with the genetic algorithm is utilized to find the optimal design of the power generation system of each technology. The selected technologies are the ABC, SRC and ORC while the objective functions are the economic revenue, the bottoming cycle weight and the daily

CO_2 emissions. A detailed design, including geometry and materials, of the heat transfer equipment is essential to evaluate the WHRU volume and weight. At this purpose, the devices' geometric quantities are included into the optimization variables. Moreover, for a correct evaluation of the CO_2 emissions over the entire year and of the profitability of the alternative investments, a part load model needs to be implemented into the optimization routine.

At the begging, a Genetic Algorithm (GA) generates the initial population using pseudo random values for the optimization variables. These values are into the ranges fixed by the user. The variables are then passed to the bottoming cycle design solver that computes thermodynamic variables (such as pressures, temperatures, etc) in the nodes of the cycle (see i.e. Figures 3.2, 3.3 and 3.4). The cycle is solved with no pressure drop in the heat transfer devices. Subsequently, the heat transfer equipment are designed by acquiring the inlet and outlet temperatures and pressures, the mass flow rates in each side and the optimization variables related to the heat exchanger geometry. The results of this step are the geometry and the pressure drops of the heat transfer equipment and the bottoming cycle weight. The bottoming cycle design solver is thus run again, considering the pressure drops in the heat transfer equipment. The results are checked with respect to the first and second law of Thermodynamics, therefore it is verified that the velocity of the cold and hot stream in the heat transfer devices is in the admissible range. If the vapour quality is higher than 84 % and the previous tests on the results are positive the part load simulation is performed. The design point constrains (such as heat exchangers pinch point and turbine inlet pressure) are replaced by $U - values$ and Stodola's constants and the components' efficiency is expressed as a function of the operating conditions. With these specifications the part load solver computes the CO_2 emissions. The procedure continues with the economic analysis. Then, the algorithm terminates when the maximum number of generations is reached or when the average change of the solution is lower than a specified tolerance.

A perfect test case for this procedure is the power generation system installed on Draugen oil and gas platform. As described in Chapter 2.2, the power generation system is composed by three Siemens SGT–500 gas turbines which operate in open cycle. The gas turbines design point specifications provided by the gas turbine manufacturer is listed in Table 2.2.

In order to increase the plant efficiency and reduce the CO_2 emissions, it is supposed to add a steam Rankine cycle, an air bottoming cycle or an organic Rankine cycle to recover the exhaust gases produced by one gas turbine. Note that, for weight and space limitation, only one WHRU is supposed to be installed

on the platform. In addition, the bottoming cycle units should have the capability to harvest the waste heat alternatively from all the engines. Figures 3.2, 3.3 and 3.4 depict the layout of the the power generation system with the additional SRC, ABC and ORC unit recovering the heat contained in the exhaust gases.

3.2.1 The bottoming cycle design solver

The design point multi-objective optimization procedure starts with the calculation of the waste heat recovery units thermodynamic cycle. The plants are illustrated in Figures 3.2, 3.3 and 3.4. Such step is accomplished by applying the first Law of Thermodynamics and the mass balance equation to each plant device, thus yielding the computation of the thermodynamic states at the inlet and outlet of each plant component.

Figures 3.5, 3.6 and 3.9 report the T–s diagrams of one design for each waste heat recovery technology.

The steam Rankine cycle unit is composed by: a single pressure non reheat once-through boiler (OTB), a steam turbine (ST), the sea water cooled shell and tube condenser and the feed pump. The OTB configuration is selected as it guarantees a minimization of the space and of the heat exchanger weight.

The air bottoming cycle is a two spools turbogenerator that includes an air compressor (AC) sucking ambient air, a recuperator where the air is heated up, an air turbine (AT) which drives the air compressor and a power turbine (PT) which drives the electric generator (GEN ABC). The recuperator is a plate fin heat exchanger (PFHX). This device offers better performances and compactness for the gas to gas heat transfer compared to the shell and tube and the flat plate heat exchanger. A two spools configurations is selected for the ABC unit, it allows better performance at part load conditions compared to the single spool arrangement.

The organic Rankine cycle module uses cyclopentane as working fluid. The selected layout is similar to the one presented for the SRC module. In this unit a shell and tube recuperator is inserted to decrease the energy contained in the superheated vapour exiting the ORC expander (TUR).

Remember that, due to a negative slope of the saturation curve (wet fluid), in the SRC bottoming cycle solver it is necessary to introduce an equation taking into account the performance reduction due to liquid droplets. To be more precise, as liquid droplets deteriorate the performance of the last steam turbine stages, the design point isentropic efficiency is penalized employing a correlation factor

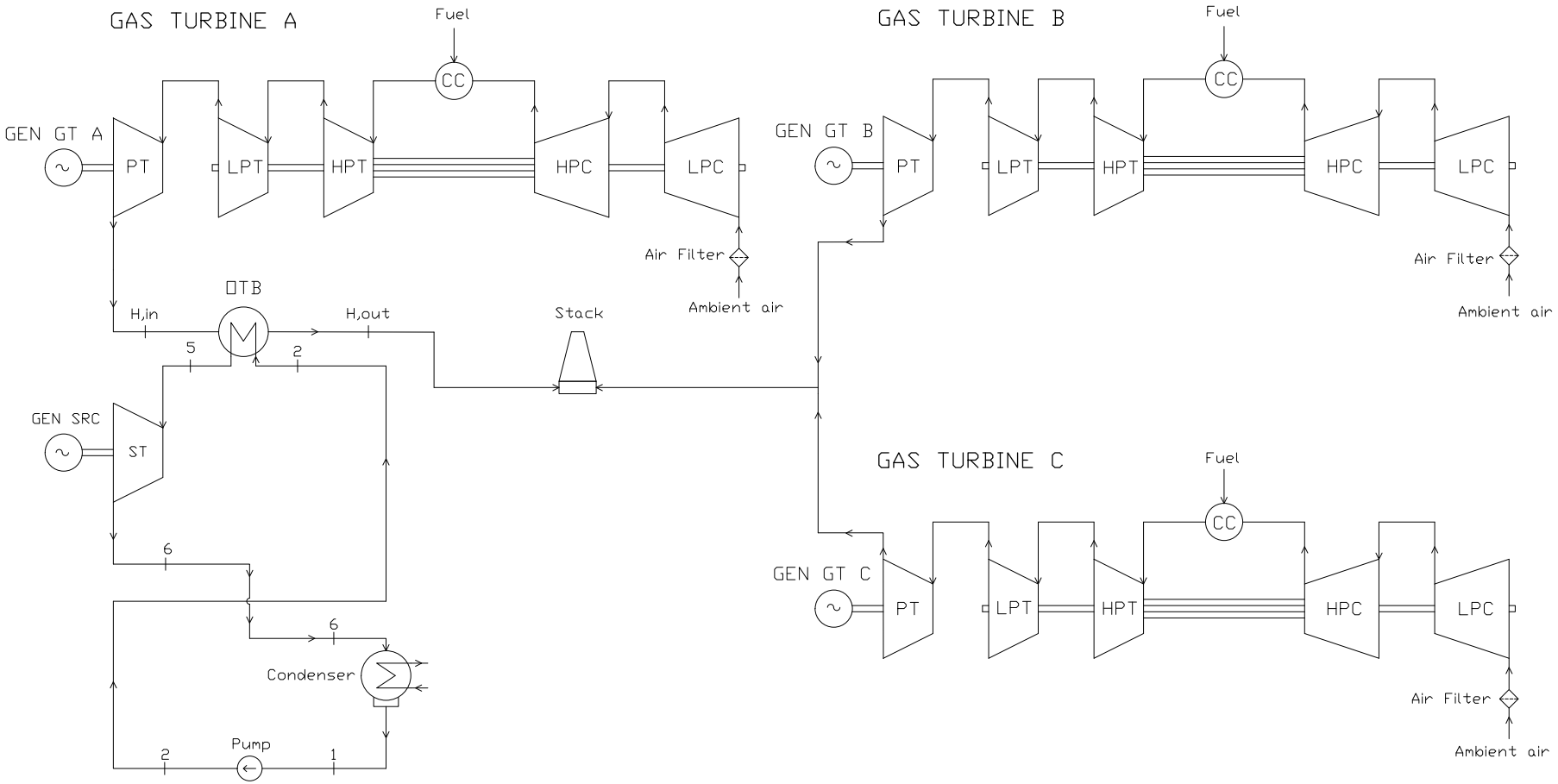

Figure 3.2: Simplified layout of the novel power system with a steam Rankine cycle as waste heat recovery unit.

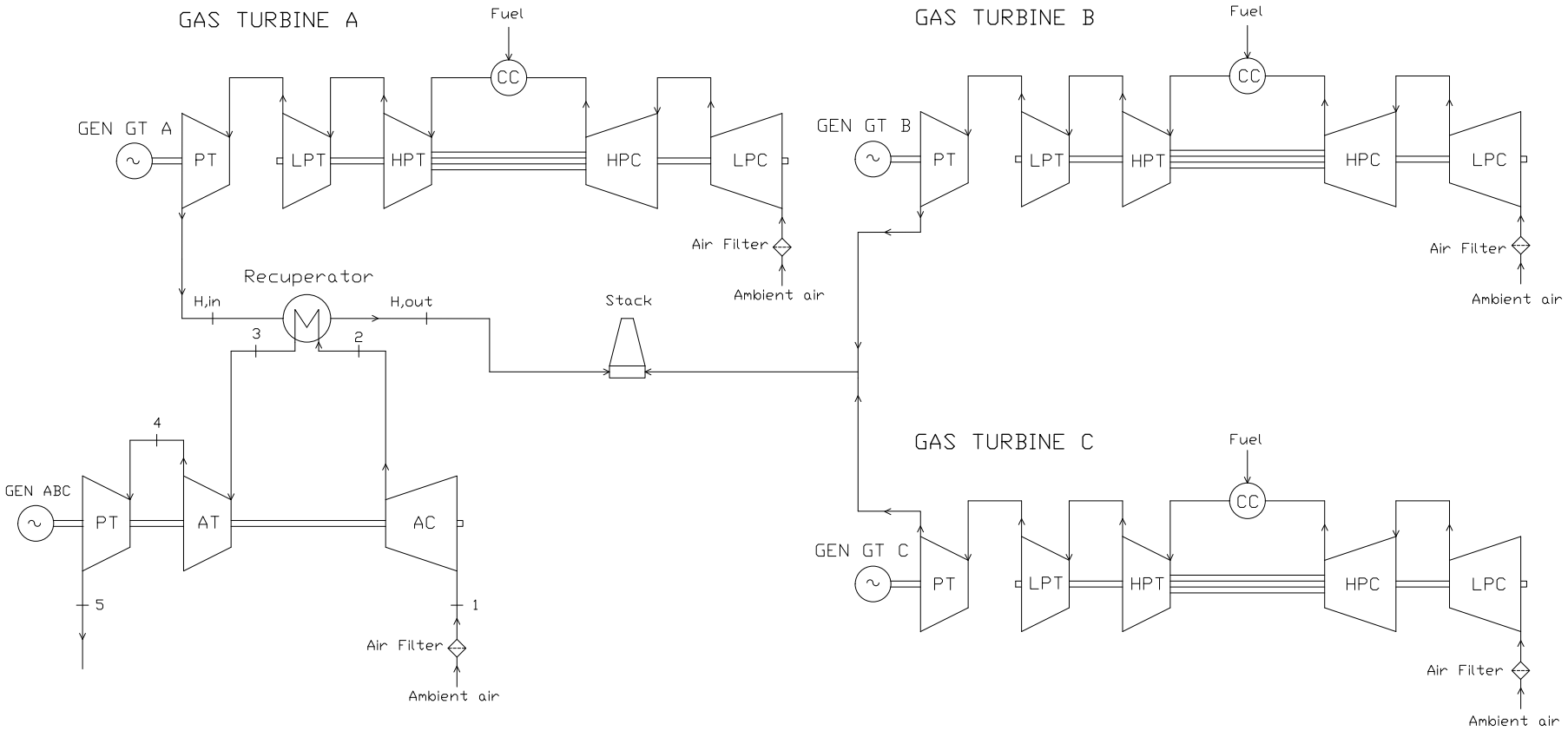

Figure 3.3: Simplified layout of the novel power system with a two spools air bottoming cycle as waste heat recovery unit.

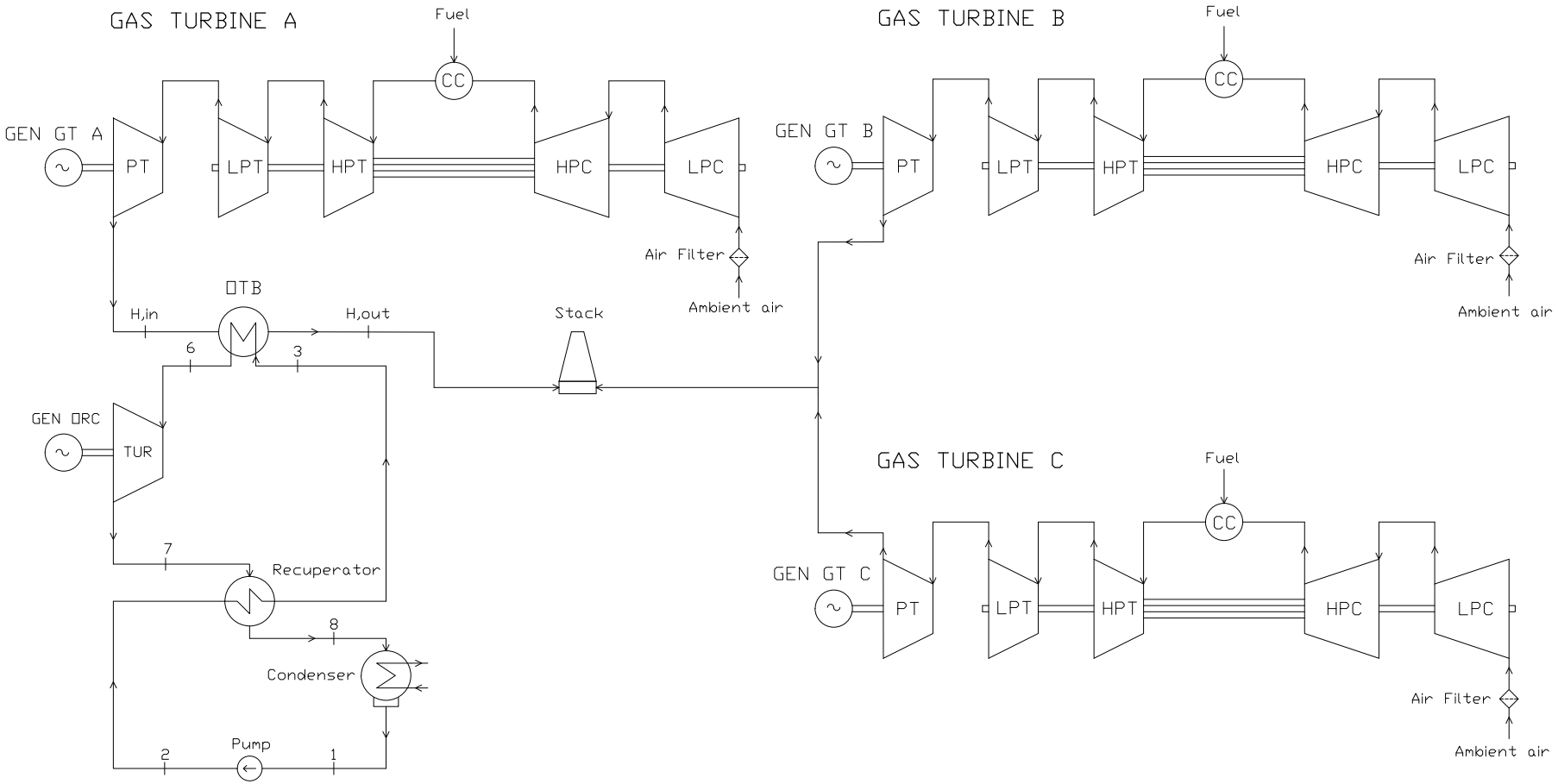

Figure 3.4: Simplified layout of the novel power system with an organic Rankine cycle as waste heat recovery unit.

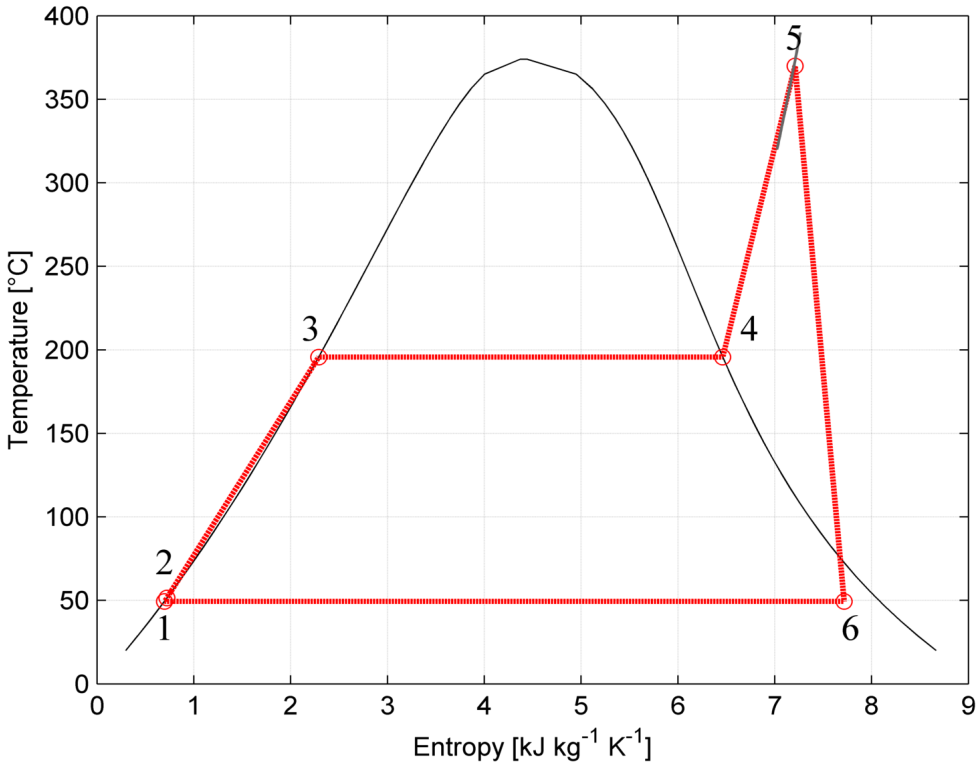

Figure 3.5: T–s diagram with the thermodynamic cycle state points of one design candidate steam Rankine cycle waste heat recovery unit.

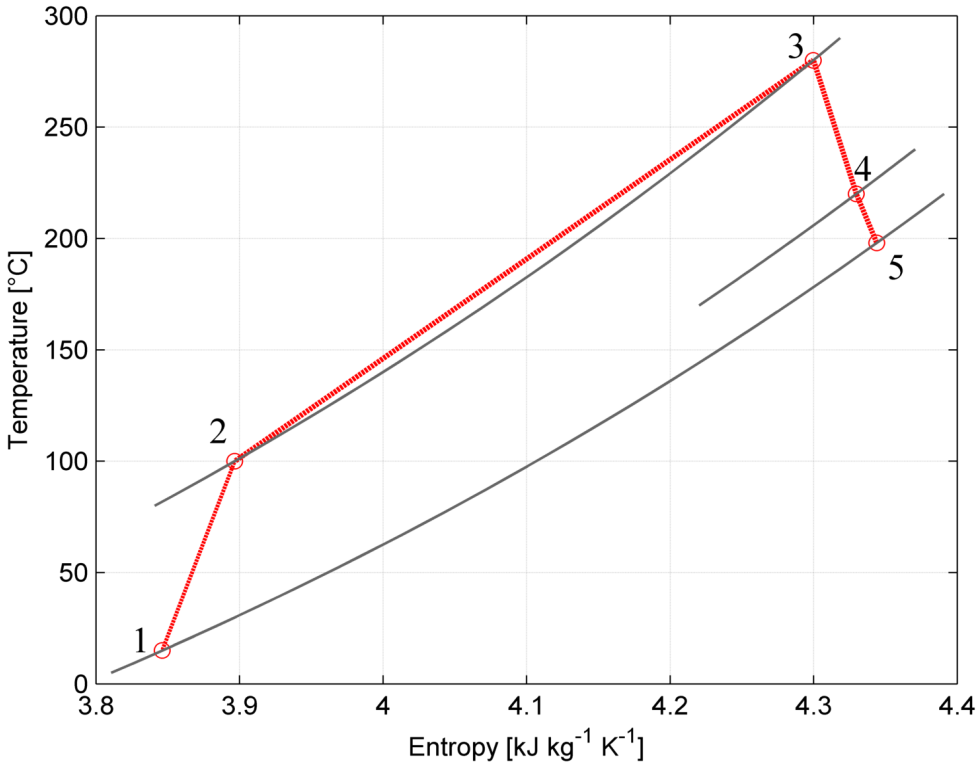

Figure 3.6: T–s diagram with the thermodynamic cycle state points of one design candidate air bottoming cycle waste heat recovery unit.

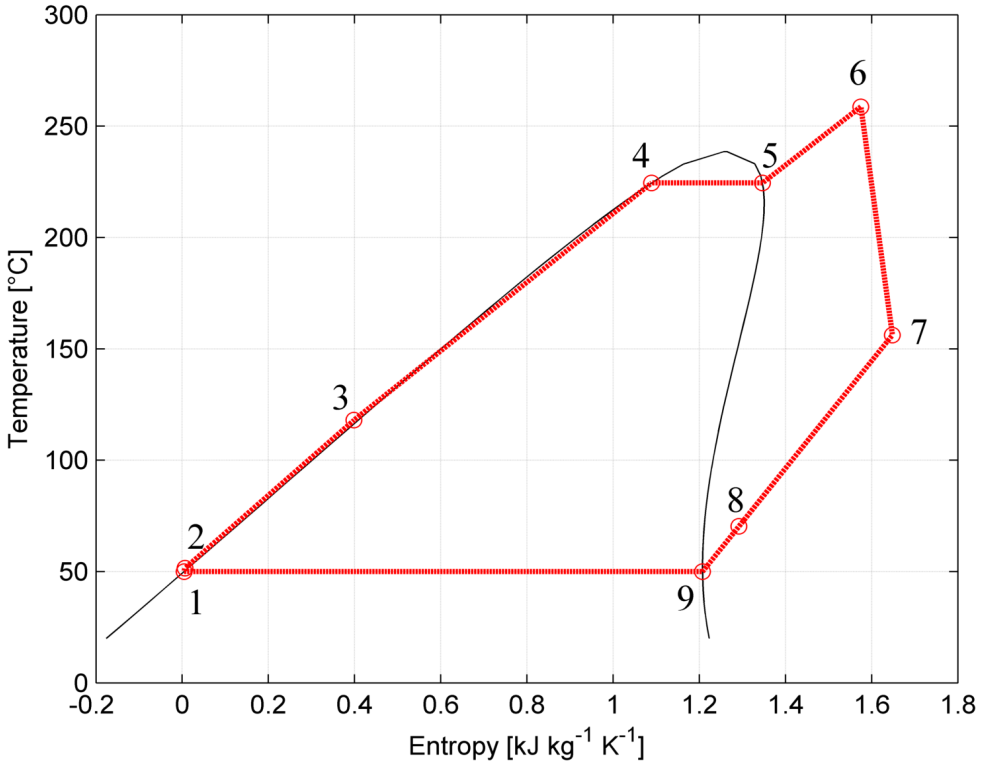

Figure 3.7: T–s diagram with the thermodynamic cycle state points of one design candidate organic Rankine cycle waste heat recovery unit.

expressed as a function of the steam quality x at the turbine outlet [164].

$$\eta_{is,T,wet} = \eta_{is,T} - 2 \cdot (1 - x) \qquad 0.984 < x < 1.0 \qquad (3.1)$$

$$\eta_{is,T,wet} = \eta_{is,T} - 0.032 - 0.76 \cdot [1 - (x + 0.016)] \qquad x < 0.984 \qquad (3.2)$$

Thermodynamic and transport properties of water, cyclopentante and air are computed according to the models implemented in the open source software developed by Bell et al. [165]. For the calculation with the exhaust gases a constant pressure specific heat of $1100\, J \cdot kg^{-1} \cdot K^{-1}$ is assumed.

In this way the bottoming units are designed from the thermodynamic point of view considering no pressure losses in the devices but neither the cycles nor the heat transfer equipment are optimized.

3.2.2 Design of the heat transfer devices

The once-through boiler, adopted in the SRC and ORC unit and shown in Figure 3.9, is modelled following the methodology suggested in [166]. The gas side heat transfer is computed using the approach described in [50], originally derived for air in circular finned tube heat exchangers. For sub-cooled liquid and superheated

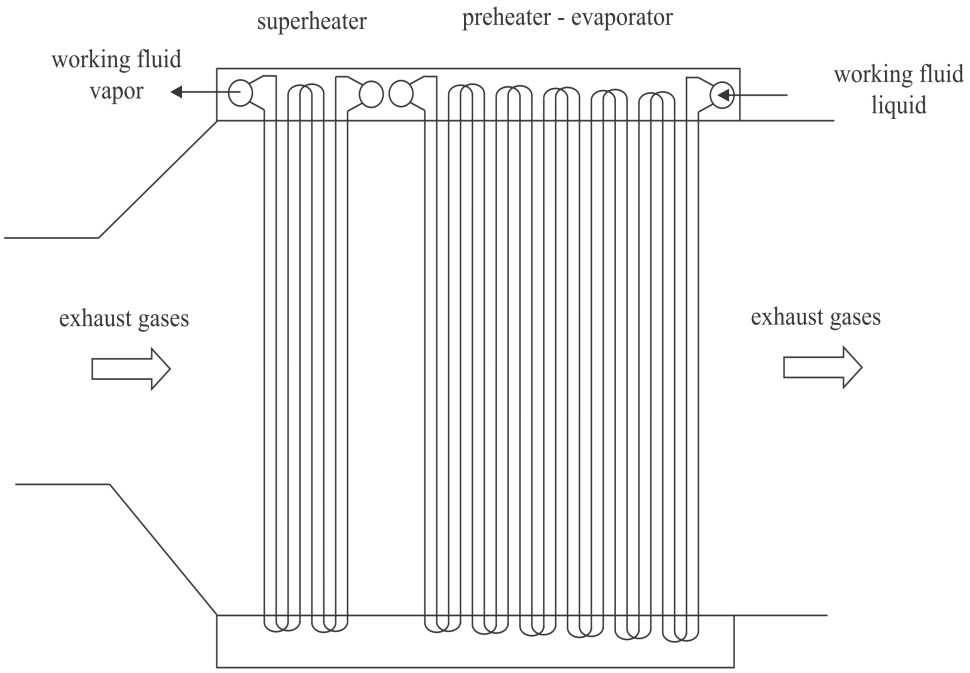

Figure 3.8: Once-through boiler simplified scheme.

vapour the heat transfer coefficient inside the tubes is assessed with the correlations proposed by Gnielinski [167], while in the two phase region the coefficient is evaluated by discretizing the tubes in 50 elements and applying the methodology proposed by Shah [168]. The total pressure drops during evaporation are divided into three contributions: the static one, vanishing for the proposed configuration of horizontal tubes, the kinematic one, and the one due to viscous friction. The last two terms are evaluated according to the equations proposed in [169] and [170], respectively. For the pressure drops in the gas side the correlation given by Haaf [171] is employed. The equation is valid for banks of tubes in cross flow, with plain transverse fins, and can be used for both staggered and in-line arrangement. As regards the transport properties of the exhaust gases, a thermal conductivity of $0.0463\,W \cdot m^{-1} \cdot K^{-1}$ and a density of $0.5763\,kg \cdot m^{-3}$ are assumed.

The condenser in the ORC and SRC module and the recuperator in the ORC unit are shell and tube heat exchangers. The geometry of this equipment can be computed by the iterative design procedure proposed by Richardson and Peacock [59]. The tubes of the recuperator are equipped with fins to enhance the heat transfer coefficient on the shell side, where the fluid is superheated vapour. The Nusselt number on the shell side is computed with the equation reported in [59]. As condensation occurs in both the single- and the two-phase region, the condenser model utilizes two distinct correlations. The approach reported in [59] is adopted for the superheated vapour section while the heat transfer coefficient

during condensation is computed as suggested by Kern [172]. The sea-water heat transfer coefficient (tube side) is evaluated using the correlations outlined in [167]. The pressure drops in the single-phase regions are estimated according to Coulson et al.[59] while those on the condensing side are derived using the method proposed by Kern [172]. The heat transfer coefficient on each side of the plate-fin

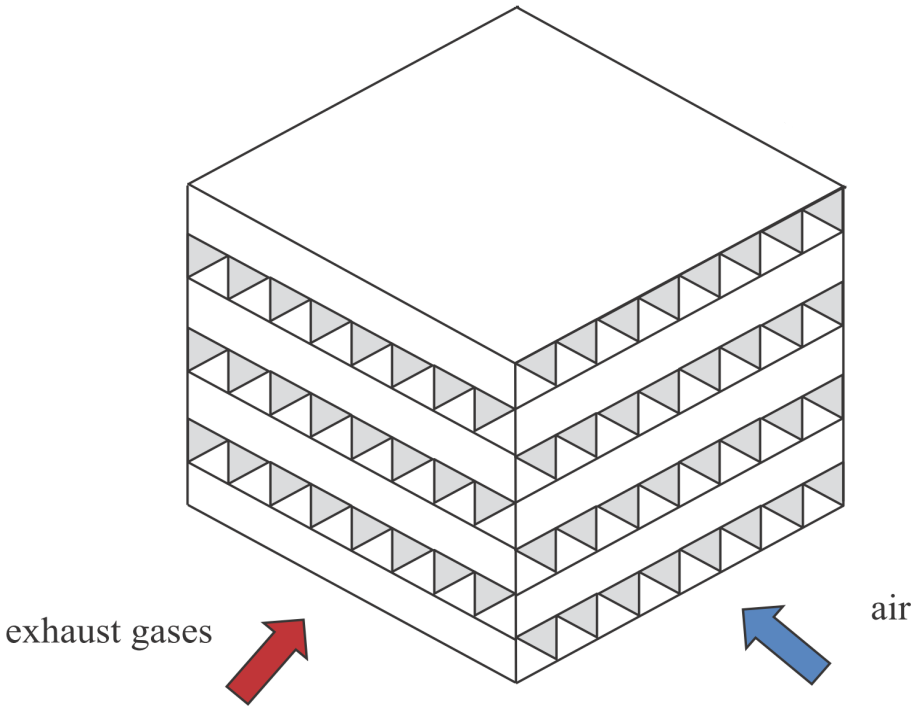

Figure 3.9: Plate-fin heat exchanger simplified scheme.

heat exchanger is computed with the equations proposed by Manglik and Bergles [173]. Regarding the pressure drops' calculation, the approach reported in [174] is employed.

The design models of the shell-and-tube heat exchanger, of the PFHE and of the once-through boiler are validated by comparison with examples outlined in [59], [174] and [166], respectively. The differences between the models' results and the data reported in the references are within 4 % in terms of both overall heat transfer coefficient and pressure drops.

3.2.3 Plants control strategies

The combined cycle behaviour during transient operation depends on the control strategy adopted for the topping unit and the waste heat recovery system.

As described in Chapter 2.2, the SGT–500 compressors are not equipped with variable inlet guide vanes. Consequently, the engine load can only be controlled

by opening/closing the fuel valve. Therefore, the exhaust temperature drops down when the load decreases. Considering this, it was decided to adjust the SRC and ORC units with the sliding pressure mode. The evaporating pressure is governed by the Stodola's cone Law and the rotational speed of the pump can be regulated with a variable frequency electric motor to maintain, for instance, a constant turbine inlet temperature as suggested in [39].

This control strategy is selected for the ORC power module, while for the SRC unit it was decided to maintain a constant superheating approach temperature difference. Owing to the different thermodynamic properties of the working fluids (i.e. water and cyclopentane), the SRC turbogenerator enables to achieve higher turbine inlet temperatures compared to those of the ORC power module. Hence, operating the SRC turbogenerator at fixed turbine inlet temperatures results in an unfeasible heat transfer process (i.e. negative superheating approach temperature difference) when the exhaust gas temperature exiting the gas turbine approaches the steam turbine inlet temperature.

The air bottoming cycle unit does not present any degree of freedom and no operational strategy can be adopted. The pressure ratio and the rotational speed of the air compressor diminish with the load as a results of the interaction between the Stodola's equations and the compressor maps.

With the implemented control strategies, for all the three technologies, the temperatures of the exhaust gases exiting the once-through boiler (SRC and ORC units) and the plate-fin heat exchanger (ABC module) do not vary significantly versus the combined cycle load. Hence, corrosion problems caused by the condensation of sulfuric acid vapour are avoided.

3.2.4 Part-load model

The assessment of the part-load performance of the power systems is the first step towards the evaluation of the total yearly CO_2 emissions, thus enabling to determine the economic feasibility of the alternative investments.

The gas turbines models are built with the data provided by the manufacturer and are verified for the entire operating range of the engines (10–100 %). The numerical data are replaced by interpolating functions selected to ensure a compromise between computational cost and accuracy. The equations provide the fuel consumption, the temperature and the mass flow of the exhaust gases as a function of the engine load at a constant ambient temperature (15 °C) and pressure (101.325 kPa). The coefficient of determination, measuring the discrepancy between interpolating curves and data points, is higher than 99 % for all functions.

For these reasons the gas turbine is considered as a black box, where the thermodynamic and transport properties of the exhaust stream serve as inputs to the part-load model describing the bottoming cycle unit.

For the once-through boiler, the ORC recuperator and the plate-fin heat exchanger the heat transfer coefficients of the cold and hot side, at offdesign conditions, are evaluated with the relation proposed in [101].

$$h = h_{des} \cdot \left(\frac{\dot{m}}{\dot{m}_{des}} \right)^{\gamma} \tag{3.3}$$

where h is the heat transfer coefficient and $\dot{m}$ is the mass flow rate. The subscripts "des" refers to the value at design point conditions while the exponent "γ" is equal to 0.8 in the case of fluid inside the tube banks otherwise equal to 0.6.

In the case of the once-through boiler and the shell and tube recuperator, the heat transfer resistance between the gas and the outer tube surface is the dominant term. Therefore, the conductive term R_{ct} and the heat transfer resistance of the cold stream $\frac{1}{h_{\mathrm{C}} \cdot A_{\mathrm{C}}} + \frac{1}{h_{\mathrm{f,C}} \cdot A_{\mathrm{C}}}$ are neglected when performing part-load simulations.

$$\frac{1}{UA} = \frac{1}{h_{\mathrm{C}} \cdot A_{\mathrm{C}}} + \frac{1}{h_{\mathrm{f,C}} \cdot A_{\mathrm{C}}} + R_{\mathrm{ct}} + \frac{1}{h_{\mathrm{H}} \cdot A_{\mathrm{H}}} + \frac{1}{h_{\mathrm{f,H}} \cdot A_{\mathrm{H}}} \tag{3.4}$$

where A and U are the heat transfer surface and the overall heat transfer coefficient. h is the convective heat transfer coefficient, and R_{ct} is the thermal conduction resistance. The subscripts "C" and "H" stand for the cold and the hot side, while "f" refers to the fouling factor.

The condenser is trivially modelled as a fixed pressure component. This is justified considering the large availability of cooling sea-water, which allows the cooling circuit to be controlled in such a way that the condenser pressure is nearly constant.

For all heat exchangers the pressure drops are lumped at the inlet of each device and are evaluated assuming a quadratic dependence with the volumetric flow rate (see Equation 3.5).

$$\Delta p = \Delta p_{\mathrm{des}} \cdot \left(\frac{\dot{V}}{\dot{V}_{\mathrm{des}}} \right)^{2} \tag{3.5}$$

where the variables $\dot{V}$ and Δp are the volumetric flow rate and the pressure drop inside or outside the tubes. Again, the subscripts "des" refers to the value at design point operating conditions.

The air compressor serving the ABC unit is modelled by employing the maps of axial compressors provided by the commercial software GASTURB [42]. These

maps are represented by tables stating values for reduced flow, pressure ratio, isentropic efficiency and rotational speed within the complete operating range of the component. Following the methodology outlined in [43], the maps are scaled so that they can represent the part-load characteristic of the compressor.

The ABC, SRC and ORC turbines are modelled with the Stodola's cone law, expressing the relation between the pressure at the inlet (p_{in}) and at the outlet (p_{out}) of the expander with the mass flow rate ($\dot{m}$) and the turbine inlet temperature (T_{in}) [44].

$$C_{\mathrm{T}} = \frac{\dot{m} \cdot \sqrt{T_{\mathrm{in}}}}{\sqrt{{p_{\mathrm{in}}}^2 - {p_{\mathrm{out}}}^2}} \tag{3.6}$$

In Equation 3.6 C_{T} is the turbine constant. Remember that, the Stodola's equation relies on the hypothesis that the working fluid is an ideal gas. Preliminary calculations showed that the compressibility factor during the expansion process presented an average value of 0.9 for cyclopentane and 0.95 for water, thus confirming the validity of the aforementioned assumption. To predict the turbines offdesign performance, the correlation relating the isentropic efficiency and the non-dimensional flow coefficient proposed in [45] is utilized.

$$\eta_{\mathrm{is,T}} = \eta_{\mathrm{is,T,des}} \cdot \sqrt{\frac{\Delta h_{\mathrm{is,des}}}{\Delta h_{\mathrm{is}}}} \cdot \left(2 - \frac{n}{n_{\mathrm{des}}} \cdot \sqrt{\frac{\Delta h_{\mathrm{is,des}}}{\Delta h_{\mathrm{is}}}}\right) \tag{3.7}$$

In Equation 3.7 the isentropic efficiency ($\eta_{\mathrm{is,T}}$) is given as a function of the rotational speed n (in rpm) and the isentropic enthalpy drop Δh_{is}. As previously, the subscript "*des*" refers to variables computed at design point conditions.

The isentropic efficiency of the ORC and SRC pumps at part-load is derived using the method proposed in [175]:

$$\eta_{\mathrm{p}} = \eta_{\mathrm{p,des}} \cdot \left(0.86387 + 0.3096 \cdot F - 0.14086 \cdot F^2 - 0.029265 \cdot F^3\right) \tag{3.8}$$

where η_{p} is the pump hydraulic efficiency and the factor F is defined as:

$$F = \frac{\dot{V}/N}{\dot{V}_{\mathrm{des}}/N_{\mathrm{des}}} \tag{3.9}$$

The part-load characteristic of the electric generator is modelled using the equation suggested by Haglind and Elmegaard [46].

$$\eta_{\mathrm{el}} = \frac{Load \cdot \eta_{\mathrm{el,des}}}{Load \cdot \eta_{\mathrm{el,des}} + (1 - \eta_{\mathrm{el,des}}) \cdot [(1 - F_{\mathrm{cu}}) + F_{\mathrm{cu}} \cdot Load^{\,2}]} \tag{3.10}$$

where η_{el} is the electric efficiency of the generator, *Load* is the mechanical power input and F_{cu} the copper loss fraction.

3.2.5 Economic analysis

With the thermodynamic design points and the heat exchangers geometry data the part load solver is able to compute the CO_2 emissions. Therefore, the optimization procedure continues with the economic analysis.

A feasibility study based on economic criteria requires firstly the estimation of the total capital investment (TCI), then, to compute the total revenue of such investment.

The total capital investment is estimated as described in [176]. The procedure starts by evaluating the purchased-equipment cost (PEC) of the components of the bottoming cycle unit. Subsequently, by incorporating the other direct costs (DC) and indirect costs (IC), thus allowing the estimation of the total capital investment.

Table 3.1 shows the details of the capital investment. The off-site costs are not considered as the installation of bottoming cycle units offshore does not require additional expenses related to the land and auxiliary facilities (e.g. fuel supply).

Table 3.1: Breakdown of the total capital investment.

Total capital investment	
I. Fixed-capital investment (FCI)	
A. Direct costs	
Purchased - equipment costs (PEC)	
Purchased - equipment installation	15 %PEC
Piping	35 %PEC
Instrumentation and controls	12 %PEC
Electrical equipment and materials	13 %PEC
B. Indirect costs	
a) Engineering and supervision	4 %DC
b) Construction costs and contractor's profit	15 %DC
Contingencies	10 %(of a and b)
II. Other outlays	
Startup costs	4 %FCI
Working capital	15 %TCI
Costs of licensing, research and development	7.5 %FCI
Allowance for funds used during construction	7.5 %FCI

The purchased-equipment costs of the once-through boiler (PEC_{OTB}), the air compressor (PEC_{AC}) and the air turbines (PEC_{AT}) are calculated with the equations proposed by Valero et al. [177].

$$PEC_{\mathrm{OTB}} = 3650 \cdot \left[\left(\frac{\dot{Q}_{\mathrm{eva}}}{\Delta T_{\mathrm{lm,eva}}} \right)^{0.8} + \left(\frac{\dot{Q}_{\mathrm{eco}}}{\Delta T_{\mathrm{lm,eco}}} \right)^{0.8} \right] + 11820 \cdot \dot{m} + 658 \cdot \dot{m}_{\mathrm{exh}}^{1.2} \quad (3.11)$$

$$PEC_{\mathrm{AC}} = 39.5 \cdot \dot{m}_{\mathrm{air}} \cdot \frac{r_{\mathrm{c}} \cdot log(r_{\mathrm{C}})}{0.9 - \eta_{\mathrm{is,C}}} \quad (3.12)$$

$$PEC_{\mathrm{AT}} = 266.3 \cdot \dot{m}_{\mathrm{air}} \cdot \frac{log(r_{\mathrm{e}})(1 + exp(0.036 \cdot T_{\mathrm{in}} - 54.4)}{0.92 - \eta_{\mathrm{is,T}}} \quad (3.13)$$

where $\dot{Q}_{\mathrm{eva}}$ and $\Delta T_{\mathrm{lm,eva}}$ are the heat rate and the logarithmic mean temperature difference limited to the vapour-liquid region, while the variables $\dot{Q}_{\mathrm{eco}}$ and $\Delta T_{\mathrm{lm,eco}}$ refer to the liquid-phase zone. The variables $\dot{m}_{\mathrm{exh}}$ and $\dot{m}$ represent the mass flow of the exhaust gases and of the working fluid flowing inside the OTB tubes. The variables $\dot{m}_{\mathrm{air}}$ and r_{e} are the air mass flow and the expansion ratio, respectively. The variable $\eta_{\mathrm{is,C}}$ is the isentropic efficiency of the compressor while $\eta_{\mathrm{is,T}}$ is the isentropic efficiency of the turbine. Equation 3.13 can be also applied to the power air turbine.

The price of the pumps (PEC_{p}) serving the SRC and the ORC power units and the cost of the electric generators (PEC_{gen}) are obtained from [178] and [179], respectively.

$$PEC_{\mathrm{p}} = 378 \cdot \left[1 + \left(\frac{1 - 0.808}{1 - \eta_{\mathrm{p}}} \right)^{3} \right] \cdot P_{\mathrm{p}}^{0.71} \quad (3.14)$$

$$PEC_{\mathrm{gen}} = 60 \cdot P_{\mathrm{gen}}^{0.95} \quad (3.15)$$

where P_{p} and P_{gen} are the pump and the electric power produced by the generator.

For the shell and tube heat exchangers (PEC_{sh}) and for the PFHE (PEC_{PFHE}), the cost is related to the heat transfer area A. The equations reported below are from Hall et al. [180] and Genceli [100].

$$PEC_{\mathrm{sh}} = 30800 + 890 \cdot A_{\mathrm{sh}}^{0.81} \quad (3.16)$$

$$PEC_{\mathrm{PFHE}} = 187 + 25 \cdot A_{\mathrm{PFHE}} \quad (3.17)$$

The ORC and SRC turbines provide a similar range of power (MW–size). Nevertheless, the thermo-physical properties of the working fluids play a key role on determining the final design. This aspect influences the final cost. Consequently, the purchased-equipment cost of ORC expander is evaluated using the expression recently proposed by [181], which has been specifically developed for multi-stage axial turbines employing organic vapours as working fluid. In this equation, the cost of the ORC expander depends on the number of stages "N" and the size parameter $\sqrt{\dot{V}_7}/\Delta h_{\text{is}}^{1/4}$ of the last stage. Remember that, in Equation 3.18, a conversion factor of 1.3 dollars-to-euro has been applied. Considering the size of the ORC unit, the volumetric flow ratios (≈ 30) and the enthalpy drops across the turbine (≈ 160 kJ $\cdot$ kg^{-1}), the expander is a single-stage axial turbine.

$$PEC_{\text{T,ORC}} = 1600 \cdot \left(\frac{N}{2}\right)^{0.5} \cdot \left(\frac{\sqrt{\dot{V}_7}/\Delta h_{\text{is}}^{1/4}}{0.18}\right)^{1.1} \tag{3.18}$$

The price of the steam turbine is determined with the correlation reported in [178]. In this case, the purchased-equipment cost is set as a function of the mechanical power output P_{t}.

$$PEC_{\text{T,SRC}} = 3000 \cdot \left[1 + 5 \cdot exp\left(\frac{T_{\text{in}} - 866}{10.42}\right)\right] \cdot \left[1 + \left(\frac{1 - 0.953}{1 - \eta_{\text{is,T}}}\right)^3\right] \cdot P_{\text{T}}^{0.7} \tag{3.19}$$

As the expressions for the components' cost evaluation derive from different sources, the PECs are adjusted for the same reference year (2014) using the historical price indexes [182] reported in Table 3.2.

Table 3.2: Price index and index factors for the calculation of the purchased-equipment costs [182]. The reference price index is 233.916 (2014).

Year	**Component**	**Price index**	**Index factor**
1993	Steam turbine SRC and ORC pumps	142.6	1.64
1994	Once-through boiler ABC compressor and turbines	146.2	1.60
1999	Plate-fin heat exchanger	164.3	1.42
1988	Shell and tube heat exchangers	115.7	2.02
2010	Electric generators	216.687	1.08
2014	ORC turbine	233.916	1.00

The profitability evaluation is carried out using the net present value (NPV) method, see [176]. The bottoming cycle unit yielding the highest NPV is deemed to

be optimal from an economic perspective. The net present value equation referred to the three power systems described in Chapter 2.2 is

$$NPV = \sum_{z=1}^{n} M_{\mathrm{f}} \cdot (I_{\mathrm{CO2}} + I_{\mathrm{fuel}})/(1+i)^{z} - TCI \tag{3.20}$$

where I_{CO2} and I_{fuel} are the yearly incomes associated to the avoided CO_2 emissions and the fuel saving. Based on information provided by the platform operator, reasonable figures for the discount rate "i" and the lifetime of the investment n are 6 % and 20 years. So as to account for the operating and maintenance costs, the factor "M_f" is set equal to 0.9 [179]. The incomes are assessed by computing first the difference in the yearly fuel consumption between the existing power system consisting of two gas turbines providing 50 % load each and the plant comprising the combined cycle unit and one gas turbine. The part load models are utilized for this purpose. The approach assumes a constant electric power demand on the platform of 19 MW for the entire year. Subsequently, the CO_2 emissions are computed by means of the fuel consumption assuming a conversion factor of 2.45 kg(CO_2) kg(fuel)$^{-1}$, which is derived from operational data provided by the Draugen platform operator. A fuel price of 0.68 NOK (St)m^{-3} [183] and a CO_2 tax of 410 NOK ton(CO_2)$^{-1}$ [73] are considered.

3.2.6 Optimization variables

The multi-objective optimizer runs by acquiring firstly the array of the parameters and of the upper and lower bounds limiting the possible values of the optimization variables vectors $\bar{X}_{\mathrm{SRC}}$, $\bar{X}_{\mathrm{ORC}}$ and $\bar{X}_{\mathrm{ABC}}$, which are

$$\bar{X}_{\mathrm{SRC}} = [p_5, \Delta T_{\mathrm{OTB}}, \Delta T_{\mathrm{c}}, T_{\mathrm{H,out}}, d_{\mathrm{i,OTB}}, d_{\mathrm{i,OTB,sup}}, l_{\mathrm{OTB}}, Nt_{\mathrm{OTB}}, d_{\mathrm{i,c}}, l_{\mathrm{c}}, l_{\mathrm{b,c}}] \tag{3.21}$$

$$\bar{X}_{\mathrm{ABC}} = [r_{\mathrm{c}}, \Delta T_{\mathrm{PFHE}}, T_{\mathrm{H,out}}, F_{\mathrm{h,a}}, nf_{\mathrm{a}}, F_{\mathrm{l,a}}, F_{\mathrm{h,exh}}, nf_{\mathrm{exh}}, F_{\mathrm{l,exh}}, Np_{\mathrm{exh}}, l_{\mathrm{exh}}] \tag{3.22}$$

$$\begin{aligned}\bar{X}_{\mathrm{ORC}} = [&p_6, \Delta T_{\mathrm{r}}, \Delta T_{\mathrm{OTB}}, \Delta T_{\mathrm{c}}, T_{\mathrm{H,out}}, d_{\mathrm{i,OTB}}, d_{\mathrm{i,OTB,sup}}, l_{\mathrm{OTB}}, Nt_{\mathrm{OTB}}, d_{\mathrm{i,r}},\\ &l_{\mathrm{r}}, l_{\mathrm{b,r}}, d_{\mathrm{i,c}}, l_{\mathrm{c}}, l_{\mathrm{b,c}}]\end{aligned} \tag{3.23}$$

where p_6 and p_5 are the ORC and SRC turbine inlet pressures, $T_{\mathrm{H,out}}$ is the outlet temperature of the exhaust gases, ΔT_{c} is the minimum temperature difference in the condenser and ΔT_{OTB} is the temperature difference between the two streams in the once-through boiler, at the location where the working fluid is in saturated liquid condition. The variable Nt_{OTB} is the number of tubes in parallel, while $d_{\mathrm{i,OTB}}$ and $d_{\mathrm{i,OTB,sup}}$ are the tube diameters of the preheater-evaporator and of the superheater OTB sections, respectively. The unknowns ΔT_{r}, l_{b} and l refer to the

minimum temperature difference in the recuperator, the baffle spacing (given as a percentage of the shell diameter) and the length of the tubes. The subscripts "OTB", "r" and "c" refer to the once-through boiler, the recuperator and the condenser. In Equation 3.22, r_c is the pressure ratio of the air compressor and ΔT_{PFHE} is the temperature difference at the inlet of the PFHE. The variables F_h, nf, F_l and Np are the fin height, the number of fins per meter, the fin length and the number of plates of the finned-plate heat exchanger. The subscripts "a" and "exh" refer to the air and the exhaust stream side.

Table 3.3: Lower and upper bound for the variables involved in the multi-objective optimization of the three power systems.

Variable	**Lower bound**	**Upper bound**
Turbine inlet pressure	5 bar	41.1 bar
Pinch point recuperator	10 °C	40 °C
Temperature difference OTB	10 °C	80 °C
Pinch point condenser	10 °C	40 °C
Temperature difference FPHE	10 °C	150 °C
Exhaust gas temperature	140 °C	180 °C
Inlet diameter of the tubes	16 mm	50 mm
Length of the tubes	1.83 m	7.32 m
Baffle spacing	20 %	120 %
Gas velocity	10 m · s^{-1}	70 m · s^{-1}
Pressure ratio	1.5	5
Fin height (FPHE)	2 mm	10 mm
Fin frequency (FPHE)	100 s^{-1}	1000 s^{-1}
Fin length (FPHE)	3 mm	150 mm
Number of plates (FPHE)	1	200
Flow length gas side (FPHE)	1.2 m	3 m

In Table 3.3 the upper and lower bounds of the optimization variables are reported while Table 3.4 lists the parameters which are kept constant during the multi-objective optimization.

Note that the values related to the geometry of the heat exchangers and the velocity of the exhaust gases are set accordingly to the limits reported by [59]. In the case of the FPHE serving the ABC unit the upper and lower bounds are obtained from [174]. As the gas turbine can operate on a wide range of both liquid and gaseous fuels, the final temperature of the exhaust gases exiting the once-through boiler has a lower limit of 140 °C. Hence, the condensation of corrosive compounds, in the case that other fuels (crude oil, heavy fuel oil and naphtha) than natural gas are combusted, is prevented. Since the present work does not deal with

supercritical ORC power modules, the upper bound for the turbine inlet pressure is set equal to 90% of the critical pressure of cyclopentane. Regarding Table 3.4, the fin profile and the configuration of the once-through boiler, the shell-and-tube recuperator and the finned-plate heat exchanger are taken from [166], [59] and [174]. The condensing pressure of the ORC unit is fixed to 1.03 bar so as to avoid infiltration of air into the piping from the surroundings. A condensing temperature equal to 50 °C is selected for the SRC module and for the ORC unit.

The array of the objective functions $\bar{J}$ is

$$\bar{J} = [m_{CO2}, W, NPV], \tag{3.24}$$

where m_{CO2} is the amount of average daily CO_2 emissions of the power system, and W accounts for the total bottoming cycle module weight determined summing the weights of the heat exchangers. NPV is the net present value calculated with Equation 3.20.

Finally, the genetic algorithm parameters are listed: population size 200, generation size 200, crossover fraction 0.8, and migration fraction 0.2. The tolerance is assumed equal to 10^{-3}. These numerical values are selected so as to ensure the repeatability of the solution when different simulations are performed.

3.3 Results and discussion

The results of the multi-objective optimization procedure are listed in Table 3.5.

The arithmetic mean average (AMA), the relative standard deviation (RSD) in percent, and the minimum and maximum values of the optimized variables are reported for the three waste heat recovery technologies. A low RSD means that the variable does not vary significantly with the optimal configurations of the waste heat recovery unit. The pinch point and the baffle length of the condensers, the temperature of the exhaust gases and the numbers of fins per meter of the FPHE present the lowest RSDs. As a practical implication, Table 3.5 provides to the designer figures for the optimal geometry of the heat transfer equipment. Hence, since the dimensions of the heat exchangers are standardized, on the basic of the optimal geometric variables (e.g. tube length) the designer can select the closest standardized values.

In Figure 3.10 the two-dimensional prospect of the Pareto front relating the average daily CO_2 emissions of the power systems with the weight of the corresponding bottoming cycle unit are depicted.

The three curves present a hyperbolic trend. Increasing the heat transfer area

Table 3.4: Parameters assumed for the multi-objective optimization.

Parameter	**Value**
Electric efficiency of the generators	98 %
Ambient conditions	1.01325 bar, 15 °C
OTB, PFHE and Condenser material	Stainless steel
Steam Rankine cycle	
Pump and Turbine isentropic efficiency	80 %
Turbine isentropic efficiency	80 %
Condensing pressure	0.12 bar
Organic Rankine cycle	
Working fluid	cyclopentane
Pump isentropic efficiency	72 %
Turbine isentropic efficiency	80 %
Condensing pressure	1.02 bar
Air bottoming cycle	
Air compressor isentropic efficiency	88 %
Air turbines isentropic efficiency	90 %
Once-through boiler	
Layout	in-line
Material	Stainless steel
Tubes thickness	2.0 mm
Longitudinal pitch	83 mm
Transversal pitch	73 mm
Fin height	24 mm
Fin thickness	0.5 mm
Fin efficiency	95 %
Recuperator	
Layout	triangular pitch
Material	Cupro-nickel
Tube pitch	1.2
Tubes thickness	2.0 mm
Fin pitch	2.0 mm
Fin height	12 mm
Fin thickness	1.0 mm
Fin efficiency	95 %
Condenser	
Layout	triangular pitch
Material	Stainless steel
Temperature cooling water	5.0 °C
Tube pitch	1.4
Tubes thickness	2.0 mm
Plate-fin heat exchanger	
Material	Stainless steel
Fin and Plate thickness	1.0 mm

Table 3.5: Results of the multi-objective optimization.

Variable	Maximum	Minimum	AMA	RSD
SRC				
p_5	12.40 bar	12.09 bar	12.23 bar	0.90 %
ΔT_{OTB}	30.82 °C	25.13 °C	27.02 °C	7.17 %
T_{11}	176.25 °C	170.23 °C	172.73 °C	1.20 %
ΔT_{c}	32.07 °C	31.80 °C	31.96 °C	0.20 %
$d_{\mathrm{i,OTB}}$	0.033 m	0.023 m	0.029 m	11.58 %
l_{OTB}	5.21 m	4.49 m	4.82 m	5.04 %
u_{h}	46.81 m · s^{-1}	43.94 m · s^{-1}	45.82 m · s^{-1}	2.17 %
$d_{\mathrm{i,c}}$	0.050 m	0.039 m	0.043 m	5.85 %
l_{c}	3.99 m	3.70 m	3.82 m	1.76 %
$l_{\mathrm{b,c}}$	102.22 %	99.16 %	101.04 %	0.97 %
ORC				
p_6	29.95 bar	25.67 bar	28.48 bar	5.73 %
ΔT_{OTB}	72.70 °C	42.76 °C	60.59 °C	16.21 %
ΔT_{r}	34.74 °C	20.42 °C	23.96 °C	22.86 %
T_{11}	171.57 °C	144.24 °C	157.45 °C	7.28 %
ΔT_{c}	39.78 °C	37.91 °C	38.96 °C	1.28 %
$d_{\mathrm{i,OTB}}$	0.043 m	0.021 m	0.032 m	22.59 %
l_{OTB}	6.11 m	1.98 m	3.30 m	42.31 %
u_{h}	60.08 m · s^{-1}	44.92 m · s^{-1}	54.63 m · s^{-1}	9.56 %
$d_{\mathrm{i,r}}$	0.028 m	0.024 m	0.026 m	3.84 %
l_{r}	4.76 m	4.03 m	4.25 m	4.32 %
$l_{\mathrm{b,r}}$	73.97 %	73.43 %	73.76 %	0.25 %
$d_{\mathrm{i,c}}$	0.038 m	0.028 m	0.032 m	7.76 %
l_{c}	5.09 m	2.67 m	3.84 m	22.17 %
$l_{\mathrm{b,c}}$	70.16 %	68.65 %	69.14 %	0.64 %
ABC				
r_{c}	2.91	1.99	2.41	11.22 %
ΔT_{FPHE}	116.79 °C	71.57 °C	87.77 °C	15.68 %
T_{11}	163.96 °C	163.45 °C	163.69 °C	0.07 %
$F_{\mathrm{h,a}}$	0.04 m	0.02 m	0.03 m	13.22 %
nf_{a}	246 m · s^{-1}	229 m · s^{-1}	237 m · s^{-1}	1.82 %
$F_{\mathrm{l,a}}$	0.15 m	0.03 m	0.08 m	41.73 %
$F_{\mathrm{h,exh}}$	0.04 m	0.03 m	0.04 m	2.85 %
nf_{exh}	226 m · s^{-1}	202 m · s^{-1}	213 m · s^{-1}	3.48 %
$F_{\mathrm{l,exh}}$	0.13 m	0.10 m	0.12 m	5.60 %
Np_{exh}	152	142	148	2.05 %
l_{exh}	2.69 m	1.79 m	2.17 m	11.87 %

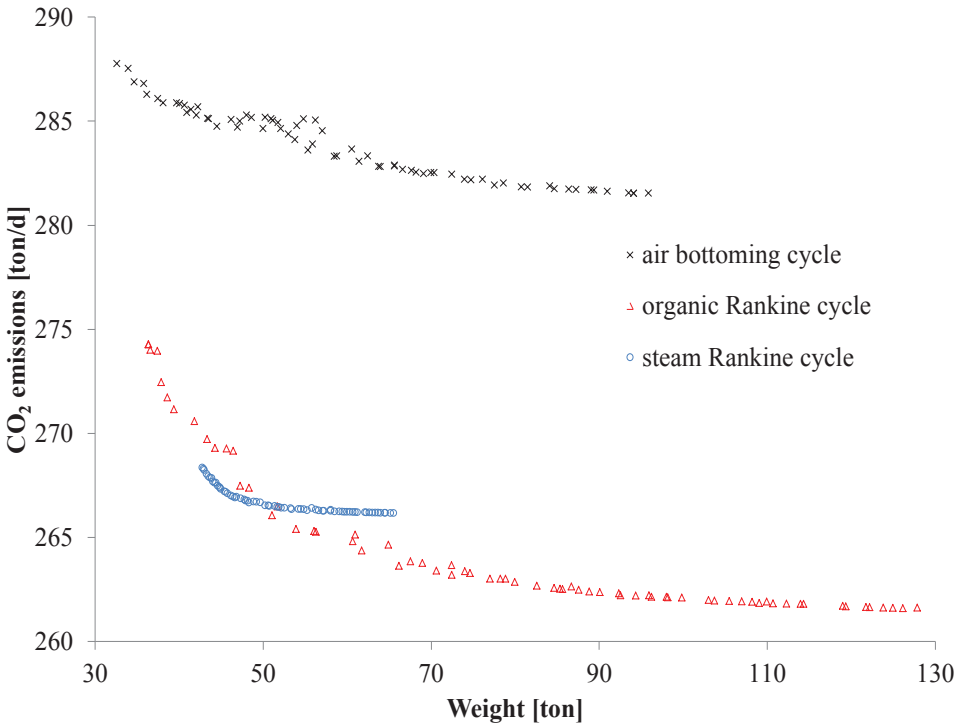

Figure 3.10: Pareto fronts of the three waste heat recovery technologies. The CO_2 emissions (first objective function) are given as a function of the weight of the bottoming cycle units (second objective function).

(i.e. the weight) allows to recuperate more heat from the gas turbine exhaust stream, and to lower the heat transfer irreversibility in the heat exchangers, thus improving the performance of the combined cycle units. The power system employing the ABC unit presents the lowest yearly system performance (highest CO_2 emissions), while it enables to achieve the lowest possible weight (30 ton). For weights between 40 and 50 ton, ORC and SRC units compete in terms of weight and efficiency, while the ORC unit shows better performances compared to both the SRC and ABC technology from 50 to 130 ton. It should be noticed that the steam Rankine cycle curve presents the narrowest Pareto front ranging from 266 to 268 ton d^{-1}. The main reason limiting the applicability of SRC units is the deterioration of the turbine efficiency caused by the liquid content at the turbine outlet. Moreover, the algorithm discards all design solutions which present a vapour quality lower than 84 % at the inlet of the condenser since they will lead to unacceptable mechanical stresses on the blades of the last turbine stages.

In Figure 3.11 the third objective function, i.e. net present value, is plotted as a function of the weight.

For all three waste heat recovery systems the curves initially increase and subsequently flatten out. Since the net present value is a function of the total investment

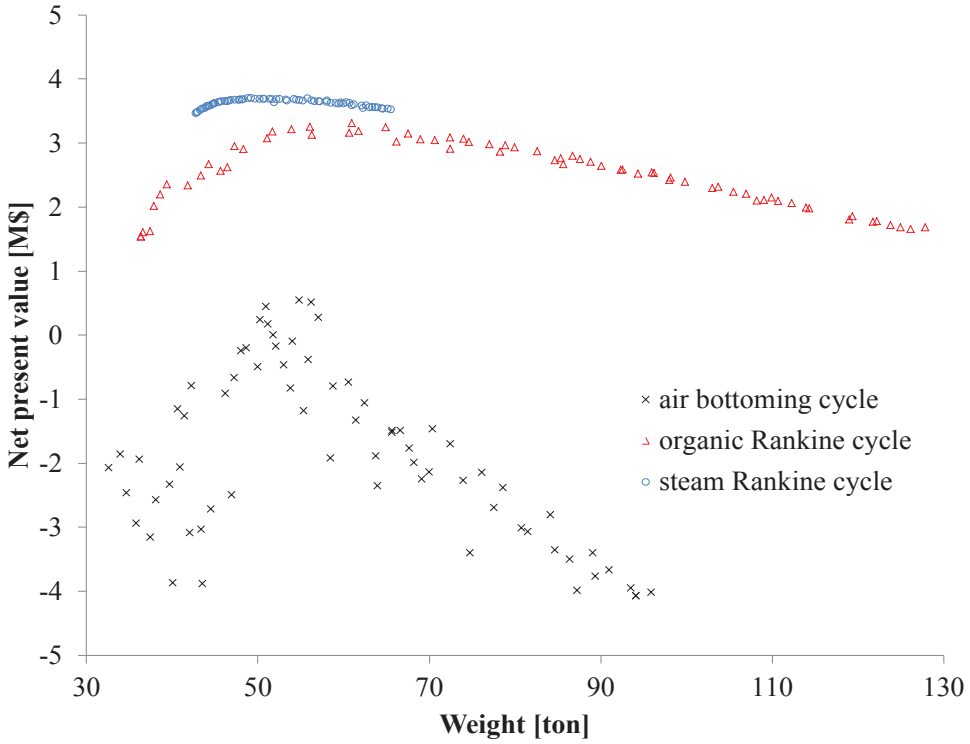

Figure 3.11: Pareto fronts of the three waste heat recovery technologies. The net present value (third objective function) is related to the weight of the bottoming cycle units.

cost and the yearly incomes (dependent on the combined cycles performance), an optimum is reached. After this maximum, enhancing the performance of the bottoming cycle modules by increasing the weight diminishes the economic revenue since the total investment cost becomes too high. The implementation of the ABC unit does not appear economically attractive. In fact, the net present value is negative at low and high weights and the peak is 2-3 times lower than those of the ORC and SRC power modules. The highest economic revenue (0.5 M$) occurs for a combined cycle power of 18.6 MW with a design- and part-load efficiency of 35.1 % and 31.9 %.

The waste heat recovery technology which allows to achieve the highest net present value (3.7 M$) is the steam Rankine cycle. For this solution the combined cycle power is 21.2 MW, and the thermal efficiencies at design- and part-load are 40.1 % and 35.6 %. As regards the ORC technology, the highest economic revenue is obtained for a net power output of 21.3 MW while the design- and part-load efficiencies are 40.2 % and 35.9 %.

Figures 3.12 and 3.13 report the weight and the purchased-equipment cost breakdowns of the three bottoming cycle units designed using the set of variables giving the highest net present value. The weight of the ORC and SRC power mod-

ules is primarily determined by the once-through boiler where stainless steel finned tubes are utilized to cope with the high heat transfer resistance of the exhaust gas stream. The water-cooled condensers and the ORC recuperator contribute with around 20 ton each to the total weight. The heat transfer equipment serving the ABC unit consists only of the finned-plate heat exchanger with a weight of 54 ton. Although an accurate weight calculation of the turbomachinery serving the bottoming cycle units is presently beyond the capability of the developed models, proprietary information from ORC manufacturers indicates that the contribution of the package comprising the turbine and the electric generator is typically around 30 % of the weight of the heat transfer equipment. While the same share is to be expected for the SRC unit, figures for the turbomachinery in ABC modules are instead comparable with those of the finned-plate heat exchanger [95]. In light of such approximate quotations, the benefits of employing the ABC technology for low-weight power systems may diminish because of the larger contribution of the turbomachinery compared to SRC and ORC modules.

Adopting the economic criterion, the ORC is the heaviest power module. Nevertheless, Figure 3.11 shows that for the ORC system the net present value does not vary significantly between 50 and 130 ton. Such trend may lead the plant designer to abate the total weight while maintaining the same economic revenue. Figure 3.13 indicates that the compressor and the two turbines contribute with the largest shares to the purchased-equipment cost of the ABC system. In the case of the SRC and the ORC units, the once-through boiler and the turbine are the most expensive components. Despite the lower daily CO_2 emissions (i.e. higher combined cycle plant part-load performance), the ORC technology exhibits a lower economic revenue compared to the plant configuration including the SRC unit. In fact, the increased incomes related to the CO_2 tax and fuel savings are not sufficient to justify the higher equipment expenses (see Figure 3.13).

Figure 3.11 evidences a more scattered trend for the net present value of the ABC unit compared to those of the ORC and SRC technologies. The different tendency originates from two reasons: i) the PEC of the air bottoming cycle unit is governed both by the compressor and the two turbines while the cost of the SRC and ORC modules primarily relates to the expander (see Figure 3.13); ii) the expressions employed to evaluate the purchased-equipment cost of the turbines and the compressor are a transcendental function of both mass flow and pressure ratio.

It is important to remember that the results are obtained using various correlations, all of which are associated with uncertainties. The assumptions that have

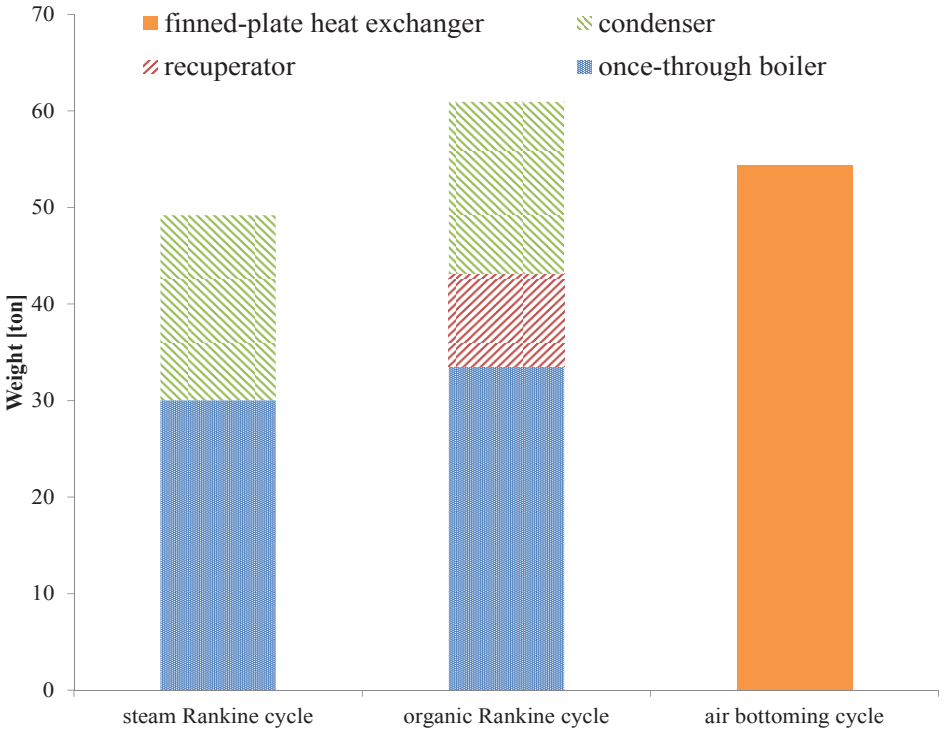

Figure 3.12: Breakdown of the weight for the three waste heat recovery technologies. The weight of the heat exchangers of the bottoming cycle units is reported.

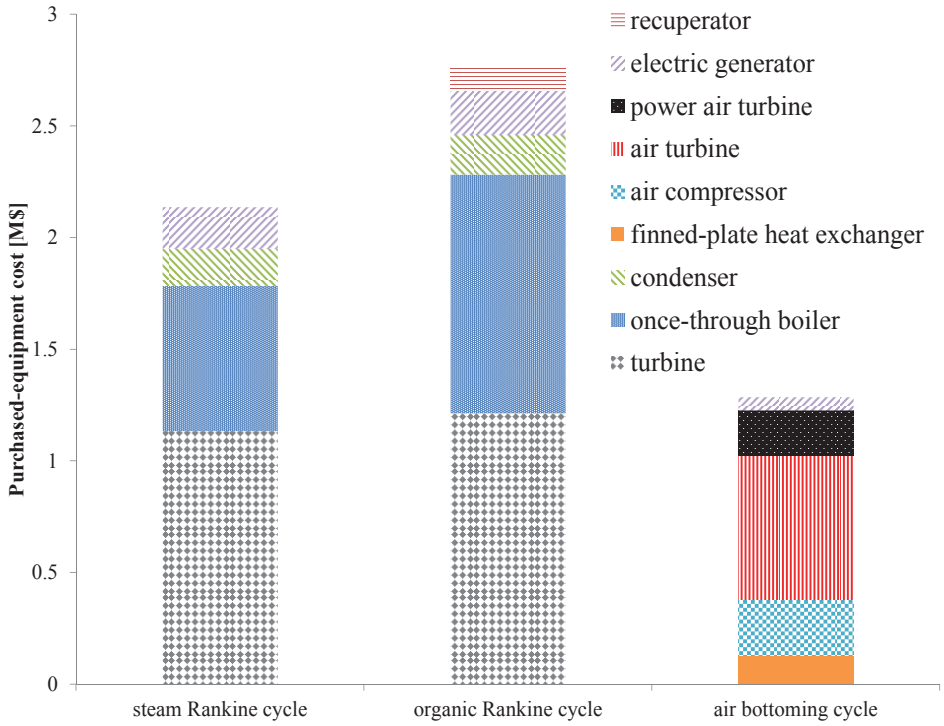

Figure 3.13: Breakdown of the purchased-equipment cost for the three waste heat recovery technologies. The purchased-equipment cost of the components of the bottoming cycle units is indicated.

the largest influence on the results are the equations utilized to estimate the heat transfer coefficients and the purchased-equipment cost of the components constituting the three bottoming cycle units. As en example, in evaluating heat transfer coefficients, average variations of 15%-20% and maximum deviations of about 40% are to be expected [184], thus influencing the weight calculation. Moreover, precise correlations relating the purchased-equipment cost of plant components to design variables and parameters are of paramount importance for an accurate economic analysis. Due to the lack of public available equations characterizing the purchased-equipment costs of all the components considered in this work, generic correlations were adopted, thus resulting in a certain degree of uncertainty. Considering all these aspects, the results of the weight calculation and of the economic study have been utilized to carry out a qualitative comparison of the different waste heat recovery technologies. Nevertheless, preliminary investigations proved that the numerical results hold quantitatively reliable as the weight and the total investment cost per unit of power are within the range of values reported in [86] and [185] for the SRC power unit, in [95] for the ABC system and in [186] and [187] for the ORC power modules.

3.4 Conclusions and future works

The multi-objective optimization approach enabled to compare the use of steam Rankine cycle, organic Rankine cycle and air bottoming cycle power modules to enhance the efficiency of existing and future offshore installations. The performance metrics are the average daily CO_2 emissions, the weight and the economic revenue. The methodology is applied to recover part of the waste heat from the gas turbines-based power system of an offshore oil and gas platform.

The organic Rankine cycle technology exhibits the highest yearly system performance, thus enabling to abate CO_2 emissions and pollutants. The combined cycle design-point and part-load thermal efficiencies are 0.2%-points and 5.1%-points higher compared to the use of the steam Rankine cycle and air bottoming cycle systems. The steam Rankine cycle technology appears to be favourable from an economic perspective as it allows to achieve the highest net present value (3.7 M$). Moreover, the results indicate that the use of ABC power modules is not attractive from an economic and environmental perspective compared to the other two technologies. For all the three bottoming cycle units the heat exchanger recovering the exhaust gases heat is the heaviest component, while the turbines contribute with the largest share to the total cost of the system.

In practice, the steam Rankine cycle and the organic Rankine cycle are competing technologies when targeting at the design of highly-efficient offshore platforms. Advantages in terms of applicability range and system performance seem to lean toward the use of organic Rankine cycle turbogenerators although investment costs have to be reduced to enhance the economic revenue. The implementation of air bottoming cycle units offshore does not appear to be convenient from a performance and economic perspective.

Note that, for a clear comprehensions of the plants' performance is necessary to study the combined cycles dynamic behaviour during load variations. In this analysis, the platform owner's specification can be considered, tested and verified. After that, the real performance of each unit can be found. Then, a clear view of the technologies' potential can be gained.

On that note, the multi-objective optimization approach can be used to compare not only different plants' technologies but also several configurations of the same plant. One of the future developments can be the study of cogenerative power plant configurations and innovative systems (such as supercritical CO_2 cycles, trilateral flash cycles and triple cycles integrated with renewable sources). An additional step can be done in order to reduce the computational time substituting the genetic algorithm with metaheuristic algorithm such as particle swarm optimizer (PSO).

Chapter 4

Dynamic performance of a combined gas turbine and air bottoming cycle plant for offshore platform

After the introduction, by the Norwegian Government, of CO_2 tax for hydrocarbon fuels, the challenge became to improve the performance of the power generation systems installed on offshore facilities.

An oil and gas platform typically operates in island (stand-alone system) and preventing a failure of the power system is a crucial aspect as it may cause a loss of oil and gas production and a drop of the economic revenue. For this reason, the power demand is normally covered by two or more redundant gas turbines. Only a modest fraction of the exhaust gases' thermal energy is recuperated to supply the on board heat demand.

Moreover, despite the considerations outlined in Chapter 3, the air bottoming cycle can be a viable method to enhance the platforms power generation system performance because it employs a non-toxic and non-flammable working fluid. Additionally, ABC units do not require a condenser as they operate as open-cycle, thus leading to high compactness and low weight.

Given that the plant operates in island, restrictions on the minimum and maximum frequency variation and on recovery time during load variation are severe design criteria.

In this context, a feasibility study on the implementation of an ABC requires a detailed analysis of the power system dynamics. Then, a numerical model of the platform's power generation system with the additional bottoming module

is built. This model is capable to simulate the design, part-load and dynamic response of the novel power generation unit. The transient performance of the system is assessed during critical transients, i.e. peak loads, to verify whether requirements and constraints involving dynamic variables are satisfied.

The gas turbine-based power generation system serving the Draugen oil and gas platform, presented in Chapter 2.2, is selected as case study.

4.1 Air bottoming cycle design and optimization

The design point analysis is a fundamental preliminary step to set up the dynamic model of the ABC waste heat recovery unit. Several researchers presented design point analysis but none of them optimized the ABC unit considering the net power output, the compactness and the economic feasibility simultaneously. The minimization of the ABC volume is assessed by introducing a detailed model of the gas to gas heat exchanger including geometric quantities in the set of the optimization variables, as done in Chapter 3.

As deeply explained in Chapter 2.3.2, to recover a hot gaseous stream with a cold gaseous flow there are two different types of technologies: the regenerator and the recuperator. In the present work, a recuperator is selected for two main reasons: no efficiency reduction caused by the leakage and more proven technology for this type of application. Additionally, a shell and tube configuration is preferred over the PFHE do to its advantage of handling applications characterized by large pressure difference between the two streams.

As outlined in [188], the design tool is a mathematical model developed in Matlab environment [27]. The graphic representation of the complete optimization algorithm is depicted in Figure 4.1 [188].

At the begging, the Genetic Algorithm (GA) generates the initial population using pseudo random values for the optimization variables. These values are into the ranges fixed by the user. The variables are then passed to the air bottoming cycle solver that computes thermodynamic variables (such as pressures, temperatures, etc) in the four nodes of the cycle (see Figure 4.2) and the net power output. The cycle is solved with no pressure drop in the recuperator. Subsequently, the recuperator is designed by acquiring the inlet and outlet temperatures and pressures, the mass flow rates on each side and the optimization variables related the heat exchanger geometry. It is verified that the velocities in the tubes and in the shell are in the admissible range. Then the HX volume and the pressure drop on each side are computed. The air bottoming cycle solver re-calculates the net power

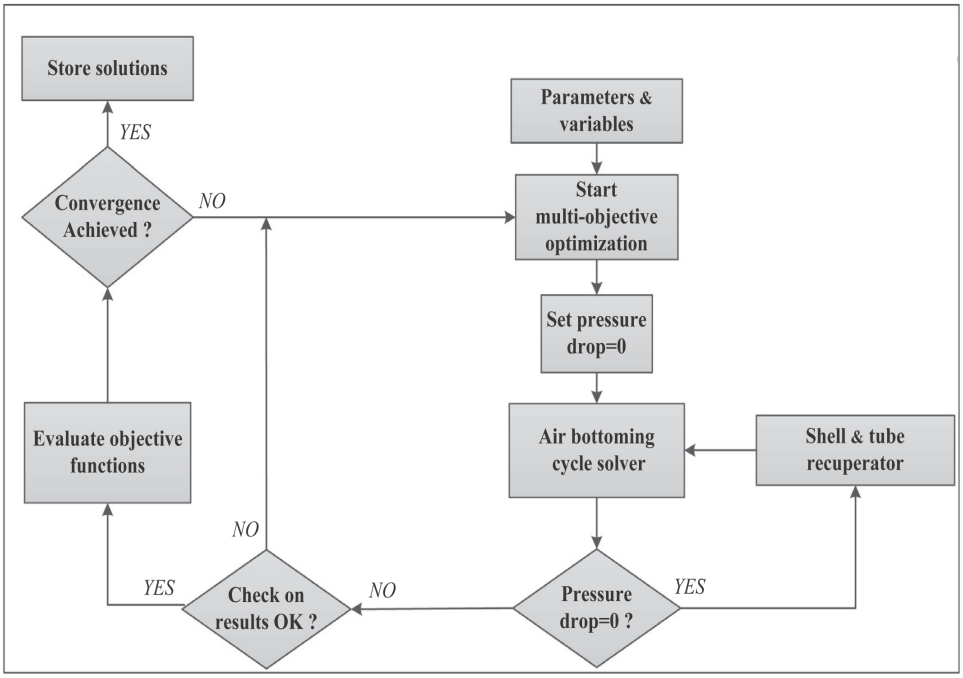

Figure 4.1: Structure of the multi-objective optimization algorithm.

output including the pressure drop of the recuperator. The procedure continues with the evaluation of the investment cost and the net present value. The algorithm terminates when the maximum number of generations is reached or when the average change of the solution is lower than a specified tolerance.

The air bottoming cycle solver is a mathematical model used to compute the thermodynamic design of the plant. Each component is modelled at steady state conditions. The theory of power maximization is employed to maximize the net power output of the single spool ABC unit shows in Figure 4.2. It consists of an air compressor, an air turbine, an air to gas heat exchanger and an electric generator.

Considering a reversible air bottoming cycle with pressure drop and no heat losses, the optimal pressure ratio (r_c) and the hot stream temperature exiting from the recuperator ($T_{H,out}$) can be computed with the theory of power maximization outlined in [189, 190].

$$r_c = \frac{p_2}{p_1} = \frac{\left(\eta_{is,C} \cdot \eta_{is,T} \cdot \frac{T_{H,in} - \Delta T_1}{T_1}\right)^{\frac{k}{2\cdot(k-1)}}}{\sqrt{\frac{p_3}{p_2}}} \tag{4.1}$$

$$T_{H,out} = \Delta T_2 + T_1 \cdot \left(1 - \frac{1}{\eta_{is,C}}\right) + \frac{\sqrt{\frac{\eta_{is,T} \cdot T_1 \cdot \left(T_{H,in} - \Delta T_1\right)}{\eta_{is,C}}}}{\frac{p_3}{p_2}^{\frac{k-1}{2k}}} \tag{4.2}$$

where T_1 and p_1 are the temperature and pressure at the inlet section of the com-

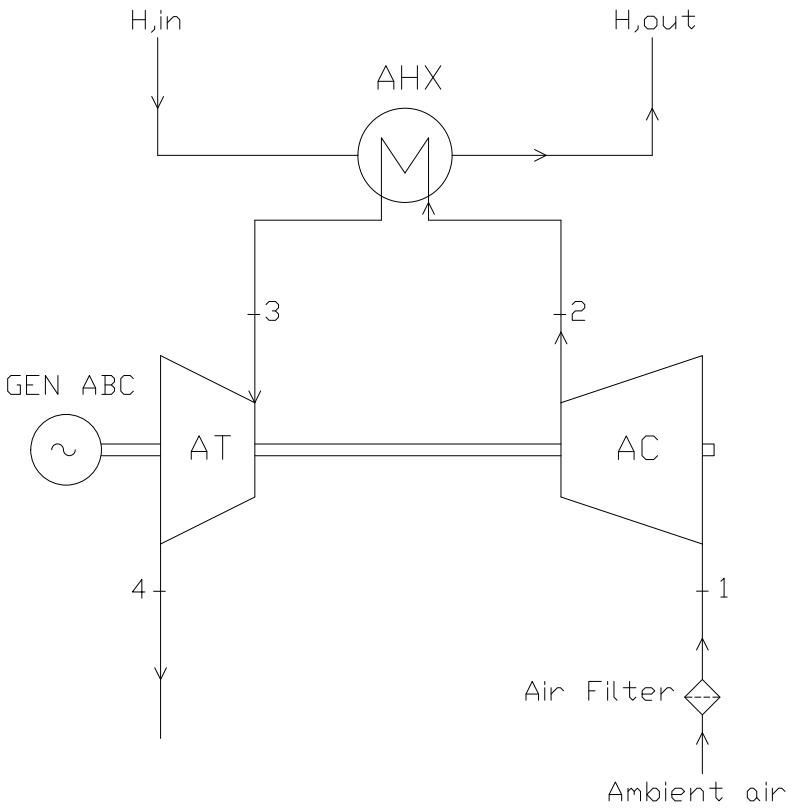

Figure 4.2: Air bottoming cycle layout.

pressor, while p_2 and p_3 are the compressor and recuperator outlet pressure, respectively. $T_{H,in}$ is the recuperator hot stream inlet temperature, k is the heat capacity ratio while $\eta_{is,C}$ and $\eta_{is,T}$ are the compressor and turbine isentropic efficiency. The temperature differences at the inlet and outlet section of the recuperator ΔT_1 and ΔT_2 are given by:

$$\Delta T_1 = T_{H,in} - T_3 \tag{4.3}$$

$$\Delta T_2 = T_{H,out} - T_2 \tag{4.4}$$

where T_2 and T_3 are, respectively, the temperature at the compressor and recuperator outlet section.

The design variables assumed to solve the air bottoming cycle are listed in Table 4.1.

With Equations 4.1 and 4.2, which express the theory of the power maximization, the ABC unit is designed from the thermodynamic point of view but neither the cycle nor the heat exchanger are optimized. As previously presented, the minimization of the ABC volume is assessed by introducing a detailed model of the gas

Table 4.1: Design point specifications assumed for the air bottoming cycle.

Variable	**Value**
Compressor isentropic efficiency ($\eta_{is,C}$)	89 %
Turbine isentropic efficiency ($\eta_{is,T}$)	90 %
Electric generator efficiency (η_{GEN})	98 %
Recuperator inlet temperature difference (ΔT_1)	25 °C
Recuperator outlet temperature difference (ΔT_2)	20 °C
Recuperator relative pressure drop on the tube side (Δp_{REC})	2.0 %

to gas heat exchanger including geometric quantities in the set of the optimization variables.

The geometry of the shell and tube recuperator can be computed with the iterative design procedure proposed by Richardson and Peacock [59]. A triangular pattern for the tubes is the implemented configuration.

1. Evaluation of the heat rate with the following equation:

$$\dot{Q} = U \cdot A \cdot F_t \cdot \Delta T_{lm} \tag{4.5}$$

   where $\dot{Q}$ is the heat rate, U is the overall heat transfer coefficient, A is the heat transfer surface area, ΔT_{lm} is the logarithm mean temperature difference, F_t is the temperature correlation factor with accounts for parallel and cross flow. It is a function of the inlet and outlet cold and hot stream temperatures and of the number of shell passes while F_t is estimated with the method proposed in [191].

2. Initial guess value for the overall heat transfer coefficient U and preliminary evaluation of the heat transfer area A.

3. Calculation of the heat exchanger geometry: tube length l_t, outer tube diameter d_0, tube pitch p_t, tube thickness tw_t and baffle spacing l_b (see Figure 4.3).

4. Calculation of the fluid velocity on tube and shell side and of the heat transfer coefficient on the tube side h_i and on the shell side h_i. These heat transfer coefficients are computed as in the work carried out by Kern [172].

$$h_i = \frac{\lambda_t}{d_i} \cdot j_{th} \cdot Re_t \cdot {Pr_t}^{0.33} \cdot \frac{\mu_t}{\mu_{tw}}^{0.14} \tag{4.6}$$

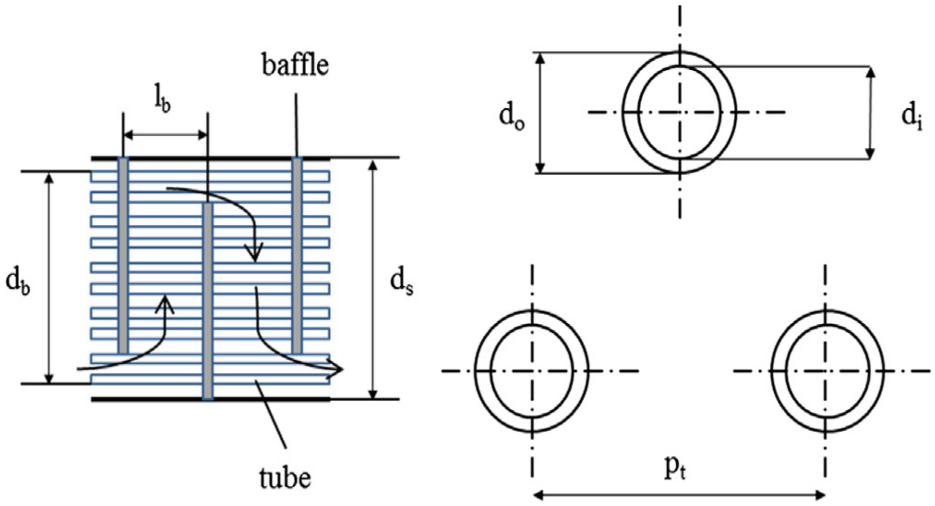

Figure 4.3: Shell and tube recuperator with triangular pattern.

$$h_o = \frac{\lambda_s}{d_s} \cdot j_{sh} \cdot Re_s \cdot {Pr_s}^{0.33} \cdot {\frac{\mu_s}{\mu_{sw}}}^{0.14} \tag{4.7}$$

where the subscripts "s" and "t" refer to the shell side and the tube side, respectively. The variables λ and μ represent the thermal conductivity and the viscosity of the hot and cold fluid.

5. Computation of the overall heat transfer coefficient U (see Equation 4.8) and comparison with the initial guess value of U.

$$\frac{1}{U} = \frac{1}{h_0} + \frac{1}{h_{0d}} + \frac{1}{h_{id}} \cdot \frac{d_0}{d_i} + \frac{1}{h_i} \cdot \frac{d_0}{d_i} + \frac{d_0 \cdot ln\frac{d_0}{d_i}}{2 \cdot \lambda_w} \tag{4.8}$$

where h_0 is the fluid film coefficient outside the tubes and h_i is the fluid film coefficient inside the tubes while h_{0d} and h_{id} are the outside and inside dirt coefficient, respectively. λ_w is the conductivity of the tube wall material while d_0 and d_i are the outer and inner tube diameter. Starting from the considerations outlined in [59] a value of $5000\,\mathrm{W} \cdot \mathrm{m}^{-2} \cdot \mathrm{K}^{-1}$ is selected for h_{id} and h_{0d}.

6. Reiteration of the steps from (2) to (5) until the difference between the two last values of U is lower than a prefixed tolerance.

7. Calculation of the pressure drop on the tube side Δp_t and on the shell side Δp_s. The pressure drop on the shell side is computed with the method proposed by [172] while the ones on the tube side with the modification introduced by Frank [192].

$$\Delta p_t = N_t \cdot \frac{\rho_t \cdot {u_t}^2}{2} \cdot \left[8 \cdot j_{sf} \cdot \frac{l_t}{d_i} \cdot \left(\frac{\mu_t}{\mu_{tw}} + 2.5 \right)^{-m} \right] \tag{4.9}$$

$$\Delta p_s = 8 \cdot j_{sf} \cdot \frac{d_s}{d_e} \cdot \frac{l_t}{l_b} \cdot \left(\frac{\mu_s}{\mu_{sw}} \right)^{-0.14} \cdot \frac{\rho_s \cdot {u_s}^2}{2} \tag{4.10}$$

where u_t and u_s are the velocity inside the tubes and across the shell, N_t is the number of tubes, d_s is the shell diameter, d_e is the equivalent diameter on the shell side and m is coefficient equal to 0.25 for laminar flow ($Re < 2100$) and 0.14 for turbulent flow ($Re > 2100$). j_{tf} and j_{sf} are the friction factors of the tube side and of the shell side and are evaluated with the method outlined in [59].

With the previous equations the ABC unit and the recuperator can be designed but neither the cycle nor the heat exchanger are optimized. As briefly explained before, this issue is easily addressed by employing the a multi-objective optimization. In this work, the object functions are

- The net power output of the ABC (P_{net}). This variable needs to be maximized and is expressed as:

$$P_{net} = P_{GT} + P_{ABC} \tag{4.11}$$

where P_{GT} and P_{ABC} are the net power output to the gas turbine and the air bottoming cycle, respectively.

- The net present value (NPV). Its needs to be maximized and is computed with the equation proposed in [176]:

$$NPV = \sum_{i=1}^{n} \frac{R_i}{(1+q)^i} - I_{TOT} \tag{4.12}$$

where n is the equipment lifespan, q is the investment factor, I_{TOT} is the total capital investment and R_i is the annual income. The compressor and turbine purchase equipment costs (PEC_C and PEC_T) are computed with the equations proposed by Valero et al. [177]. The electric generator and the recuperator purchase equipment costs (PEC_{GEN} and PEC_{REC}) are evalu-

ated with the equations proposed by Lean et al. [179] and Hall et al. [180].

$$PEC_C = \frac{39.5 \cdot \dot{m}}{0.9 - \eta_{is,C}} \cdot \frac{p_2}{p_1} \cdot ln\frac{p_2}{p_1} \tag{4.13}$$

$$PEC_T = \frac{266.3 \cdot \dot{m}}{0.92 - \eta_{is,T}} \cdot \frac{p_3}{p_4} \cdot ln\frac{p_3}{p_4} \cdot [1 + exp\,(0.036 \cdot T_3 - 54.4)] \tag{4.14}$$

$$PEC_{GEN} = 60 \cdot {P_{net}}^{0.95} \tag{4.15}$$

$$PEC_{REC} = 10000 + 324 \cdot {A_{REC}}^{0.91} \tag{4.16}$$

- The volume of the shell and tube recuperator (V_{REC}). It needs to be minimized and is computed assuming a cylinder of diameter d_s and a height l_t for the shell. A correction factor equal to 1.2 considers the space required by the inlet and outlet ducts.

$$V_{rec} = 1.2 \cdot \frac{\pi}{4} \cdot {d_s}^2 \cdot l_t \tag{4.17}$$

The optimization variables and their lower and upper bounds specifications are listed in Table 4.2. The geometry variables bounds are taken from [59].

Table 4.2: Optimization variables lower and upper bounds.

Parameter	**Upper value**	**Lower value**
Recuperator inlet temperature difference	20 °C	70 °C
Recuperator outlet temperature difference	20 °C	70 °C
Pressure ratio	1.1	4.5
Compressor isentropic efficiency	80 %	90 %
Turbine isentropic efficiency	80 %	92 %
Tube outer diameter	10 mm	50 mm
Tube length	1.0 m	7.3 m
Tube thickness	1.0 mm	4.0 mm
Baffle spacing	0.2 d_s	0.2 d_s
Tube pitch	1.15 d_0	2.25 d_0

The optimization procedure results show ABC units, on the one hand, characterized by high compactness and low weight and, on the other hand, by a really poor efficiency especially at part-load conditions. With the aim of increasing the ABC turbogenerator performance the single spool configuration is substituted by a dual spool configuration. The new configuration is implemented in the code while the plant scheme is depicted in Figure 4.4. The ABC thermodynamic solver is modified. The optimization variables, their limits and the object functions remain

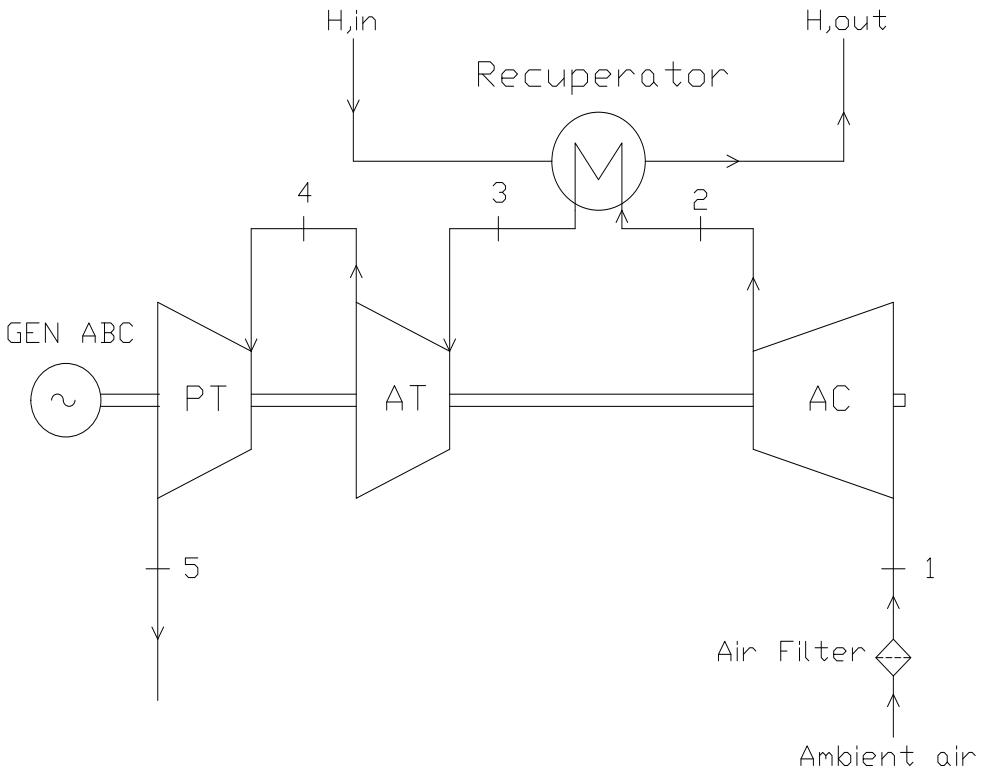

Figure 4.4: Air bottoming cycle with two turbines layout.

the same listed before. Note that this configuration is characterized by two turbines, therefore in the optimization variables and in the NPV equation this aspect is taken into account with an appropriate implementation.

4.2 The SGT-500 Gas Turbine Model

Following the specifications provided by the gas turbine manufacturer the dynamic model is developed in DYMOLA environment. Components available in ThermoPower library are used and extended to build the model. For more detail about the modelling language and the library specifications see Chapter 1.2.

Figure 4.5 depicts the Modelica object diagram of one of the gas turbines installed on Draugen oil and gas platform.

Compressors and turbines are described as zero-dimensional components adopting steady state and offdesign characteristics. As for the model presented in Chapter 1.3.1, the low and high pressure compressors are described by quasi-static components, employing the maps of axial compressors. The maps are scaled in order to represent the part-load characteristics of the axial compressors installed on the SGT-500 gas turbine. In this case the selected maps are originally from Carchedi and Wood [193].

The SGT-500 gas turbine is equipped with three sections: the low and high pressure turbine, and the power turbine. The turbine models are built adopting the equation presented in Chapter 1.3.1.

In the electric generator, as previously mentioned, the equation proposed by Haglind and Elmegaard [46] is implemented.

The combustion chamber volume and the inertia values of the rotating masses (shaft, blades and generator) are set accordingly to data provided by the gas turbine manufacturer.

On the topside of Figure 4.5 the detailed layout of the gas turbine control system, as provided by the GT manufacturer, is sketched. Given that the compressors are not equipped with variable inlet guide vanes, the GT load can be adjusted only by decreasing/increasing the fuel flow by closing/opening the fuel valve. As reported in [57, 194], the difference between the grid frequency and the set point (50 Hz) is measured. The signals deviation passes through a transfer function block and subsequently through the frequency controller which is composed by a gain and a transfer function block, and provides to regulate the opening/closing of the fuel valve. The other gain, the integral block and the other transfer function are used to represent the fuel valve dynamics.

Being Draugen oil and gas platform a stand-alone system with minimum two engines in operation, when the gas turbines run in parallel only one of them stabilized the grid frequency while the remaining machines follow the frequency fluctuation and adjust their load to reach the prefixed set points.

4.3 The ABC Model

The model of the air bottoming cycle unit is developed in DYMOLA coupled with the open source library ThermoPower as outlined in Chapter 1.2. The air compressor and the air and power turbine are described as zero-dimensional components using steady-state and offdesign characteristics. The compressor is modelled by employing the maps of axial compressors provided with the software GASTURB [42] and are scaled with the method proposed by Kurzke [43]. For the turbines the Stodola equation is employed [44]. The part load performance of the electric generator is predicted again with the equation proposed in [46]. The dynamics of the shafts is modelled with the shaft dynamic balance. For more details see Chapter 1.3.1.

The recuperator, as described in Chapter 4.1, is a shell and tube heat exchanger which is implemented by the connection of basic components discretized in the lon-

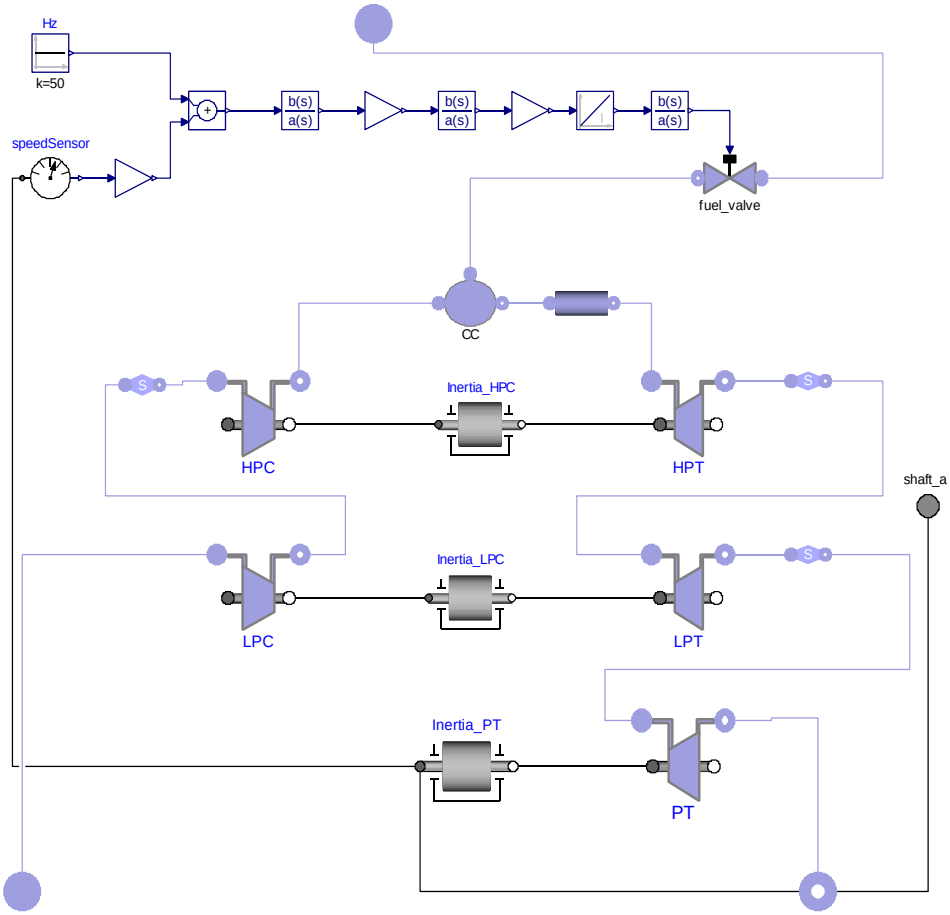

Figure 4.5: Modelica object diagram of the SGT-500 gas turbine.

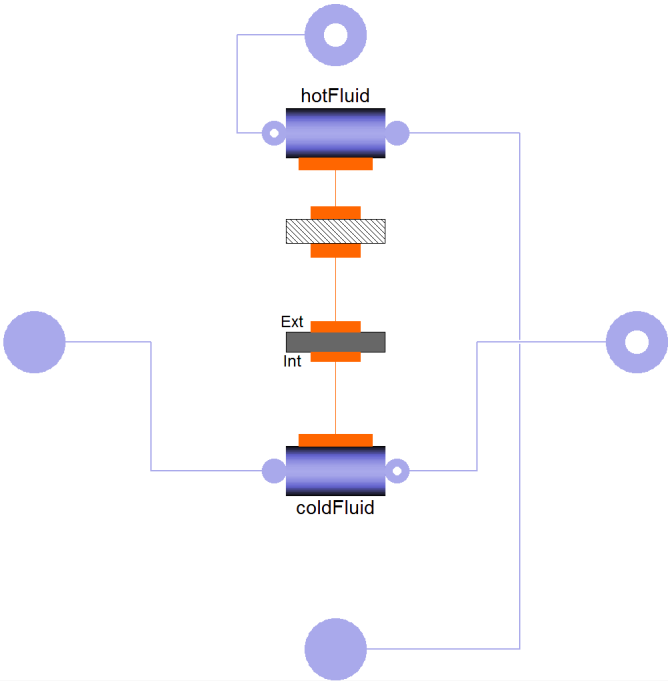

Figure 4.6: Object diagram of the ABC shell and tube heat exchanger model.

gitudinal direction. Figure 4.6 shows the 1D flow models for the gas side (top) and the air side (bottom of the figure), and the 1D thermal model for the tube bundle (middle). These components exchange thermal power through their thermal ports; the counter-current model establishes the topological correspondence between the control volumes on the tube metal walls, and the control volumes on the gas flow model. The tube metal wall is modelled by a one-dimensional dynamic heat balance equation, discretized by finite volumes, neglecting the conductive thermal resistance. The flow models contain one-dimensional dynamic mass and energy balance equations, discretized by the finite volume method, assuming uniform pressure distribution.

The heat transfer coefficients of the cold and hot side, at offdesign conditions, are computed with the following equations:

$$h_{air} = h_{air,des} \left(\frac{\dot{m}_{air}}{\dot{m}_{air,des}} \right)^{0.8} \tag{4.18}$$

$$h_{gas} = h_{gas,des} \left(\frac{\dot{m}_{gas}}{\dot{m}_{gas,des}} \right)^{0.6} \tag{4.19}$$

where h is the heat transfer coefficient and $\dot{m}$ is the mass flow rate. The subscripts "des" refers to the value at design point operating conditions while "air" and "gas" indicate the working fluid air and exhaust gases, respectively. The two exponents are selected based on the fluid location: inside and outside the tubes.

4.4 Models Validation

The model of the gas turbine is validated with a SIMULINK model provided by the GT manufacturer.

The manufacturer model utilizes non-physical transfer functions to represent the dynamic behaviour of the frequency control versus a load change applied to the system. The selected test case foresees that the three gas turbines are sharing a load equal to 24 MW, 8 MW each. In this condition, the gas turbines are running at low load but, if at the same in time, one of the engines trips and the remaining machines have to ramp up in order to supply the whole platform load (12 MW each). The comparison between the two models results show a deviation of 1 % in term of minimum normalized frequency and approximately of 9 % for the rise time.

The gas turbine model is also validated at offdesign conditions in the power range 10–100 % by comparing the steady-state results with the part-load charac-

teristics given by the GT manufacturer. Fuel mass flow rate, combustion chamber pressure and exhaust gas mass flow rate and temperature are monitored during the validation processes. The largest mismatch is observed for the fuel mass flow rate: a relative error of about 15 % is observed when the load is in the range 10–60 % while for load larger than 60 % the error increases up to 15 %.

In summary, the comparison between the Modelica and SYMULINK models shows that the Modelica gas turbine model is able to reproduce both the steady-state and the dynamic behaviour of the components with a reasonable accuracy during the power range 10–100 %. For a better description of the gas turbine validation procedure see [194].

The shell and tube recuperator model is validated using an example outlined in Coulson et al. [59]. At design point conditions, the difference between the simulation results and the data presented in the reference are withing 3 % in term of both the overall heat transfer coefficient and pressure drops.

4.5 Design and dynamic analysis results

In Figure 4.7 the relations between the net power output and the thermal efficiency of the combined gas turbine and ABC plant versus the air compressor pressure ratio are shown. Note that the two variables peak at the pressure ratio of around 2.7 and, for this value, the combined plant thermal efficiency and electric power are 37.2 % and 19.62 MW, respectively.

For this design specifications, the air bottoming cycle solver has computed the plant thermodynamic points listed in Table 4.3. The related T–s diagram of the above mentioned unit is depicted in Figure 4.8.

Table 4.3: Air bottoming cycle state points.

	T	**p**	$\boldsymbol{\rho}$	**h**	**s**
1	15.00 °C	101.32 kPa	1.22 kg · m^{-3}	414.37 kJ · kg^{-1}	3.84 kJ (kg K)$^{-1}$
2	117.73 °C	266.32 kPa	2.37 kg · m^{-3}	517.81 kJ · kg^{-1}	3.87 kJ (kg K)$^{-1}$
3	354.20 °C	261.32 kPa	1.44 kg · m^{-3}	762.25 kJ · kg^{-1}	4.36 kJ (kg K)$^{-1}$
4	255.35 °C	129.47 kPa	0.85 kg · m^{-3}	658.81 kJ · kg^{-1}	4.39 kJ (kg K)$^{-1}$
5	224.70 °C	101.32 kPa	0.70 kg · m^{-3}	627.18 kJ · kg^{-1}	4.40 kJ (kg K)$^{-1}$

The other parameters, computed with the optimization routine, and used to parameterize the plant's dynamic model are listed in Table 4.4. The Modelica object diagram of the novel power generation system composed by three gas turbines and an air bottoming cycle is presented in Figure 4.9.

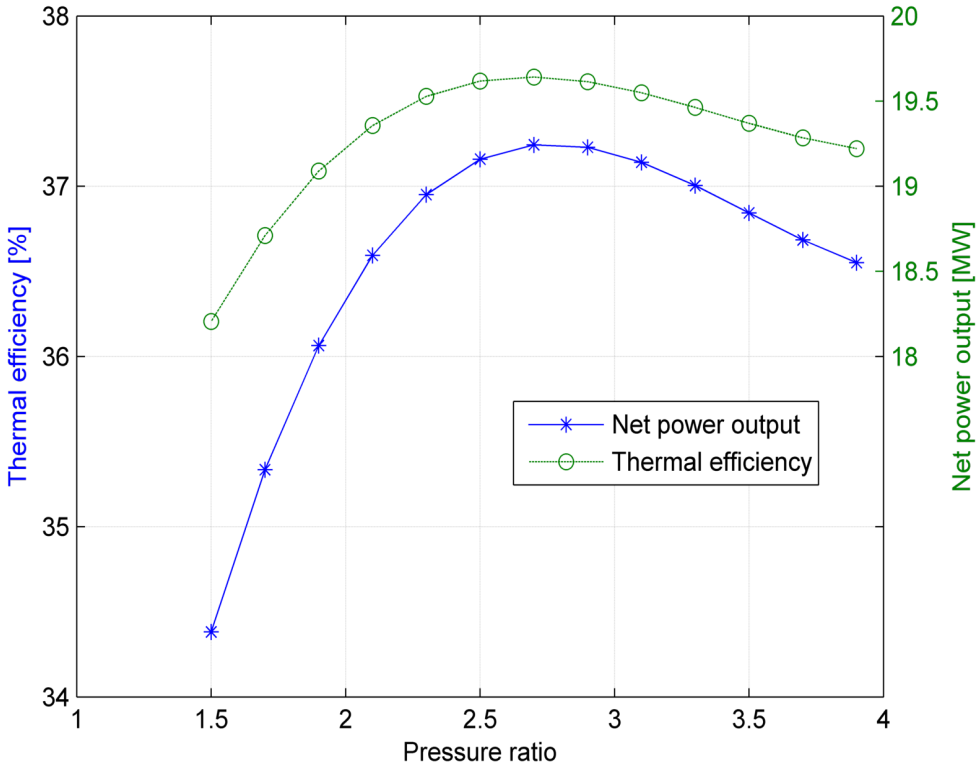

Figure 4.7: Combined gas turbine and air bottoming cycle plant net power output versus air compressor pressure ratio.

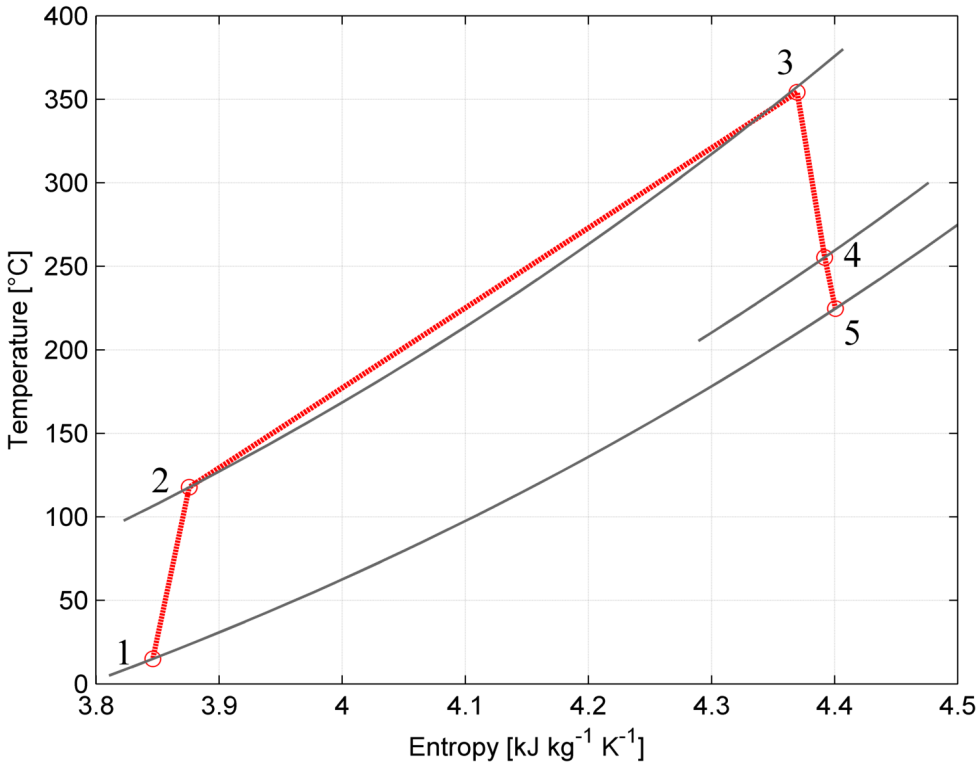

Figure 4.8: Air bottoming cycle T-s diagram.

Table 4.4: Design point parameters of the air bottoming cycle dynamic model.

Parameter	**Value**
Pressure ratio	2.7
Exhaust gases volume	15 m^3
Air volume	10 m^3
Tube material	Stainless steel
Metal wall weight	60 ton
Metal heat capacity	500 $J \cdot kg^{-1} \cdot K^{-1}$
AC - AT shaft inertia	20 $kg \cdot m^2$
PT - GEN shaft inertia	28 $kg \cdot m^2$
ABC electric generator inertia	100 $kg \cdot m^2$
Net power output	19.62 MW
Plant efficiency	37.2 %

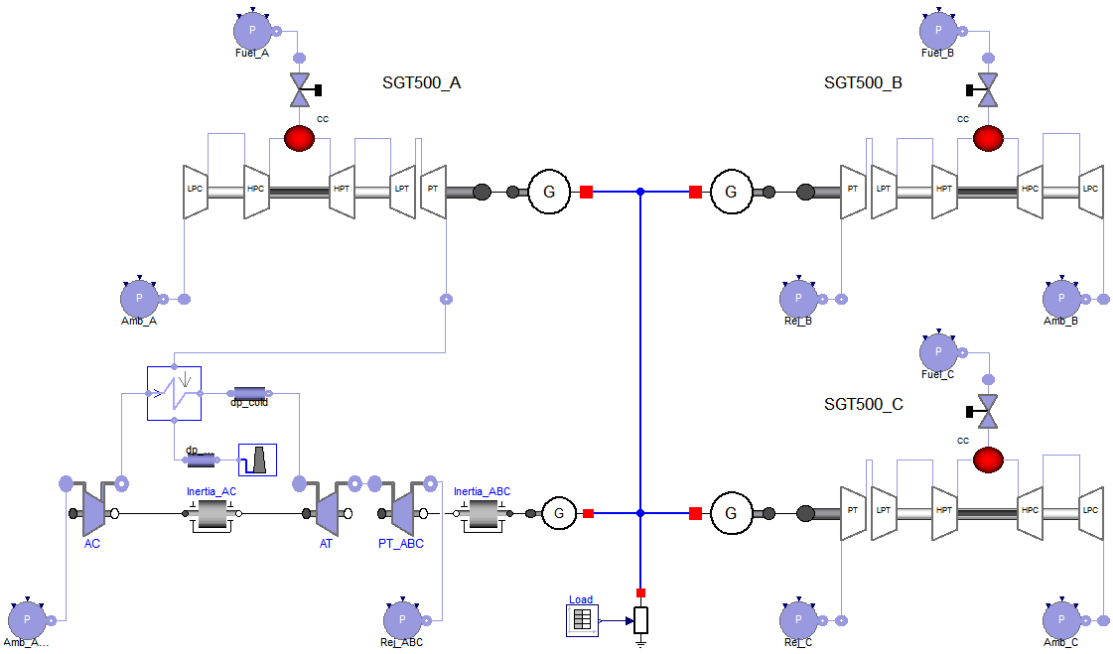

Figure 4.9: Draugen power generation system Modelica object diagram.

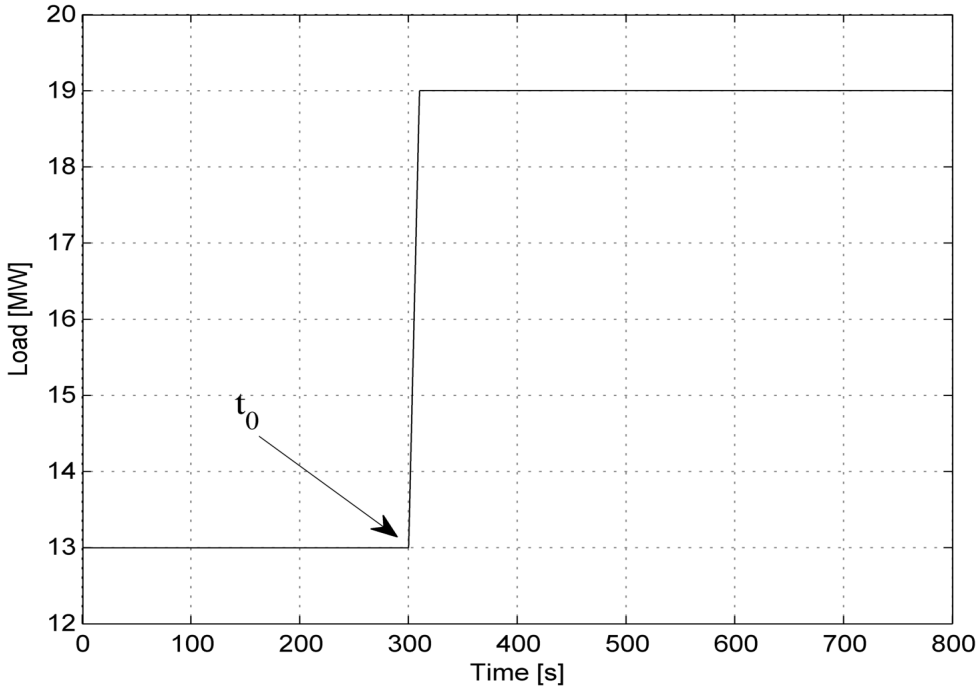

Figure 4.10: GT A + ORC load ramp after the GT B trip.

The test case selected for the dynamic analysis is the trip of one gas turbine. This event is the worst possible scenario which the system has to withstand without compromising the functionality of the power supply system. It is assumed that the combined cycle plant, composed of gas turbine A and the ABC turbogenerator , and gas turbine B supplies the normal load demand (13 and 6 MW, respectively) while gas turbine C is switched off.

As depicted in Figure 4.10, in a given instant of time (t_0), gas turbine B trips and the combined cycle ramps up its load in order to match the total power demand (19 MW), with a transient reduction of the grid frequency. The power of gas turbine B is assumed to drop linearly from 6 to 0 MW in 10 s, as suggested by the gas turbine manufacturer. Hence, in practice, the combined cycle plant undergoes a load set-point increment of $0.6\,MW \cdot s^{-1}$, and it is required to satisfy alone the total normal load, until gas turbine C starts-up. Figure 4.11 relates the set-point power of the combined plant and the frequency of the electric grid with time. For the assumed set-point load increment ($0.6\,MW \cdot s^{-1}$), the frequency exhibits a minimum value (undershooting) of 6 % and a peak (overshooting) of 5 % compared to the steady-state value (50 Hz).

Another critical dynamic performance metric is the rise time, defined as the time required for the frequency to return back to 99 % of the steady-state value. Figure 4.11 indicates that the rise time is approximately 32 s for the considered test case.

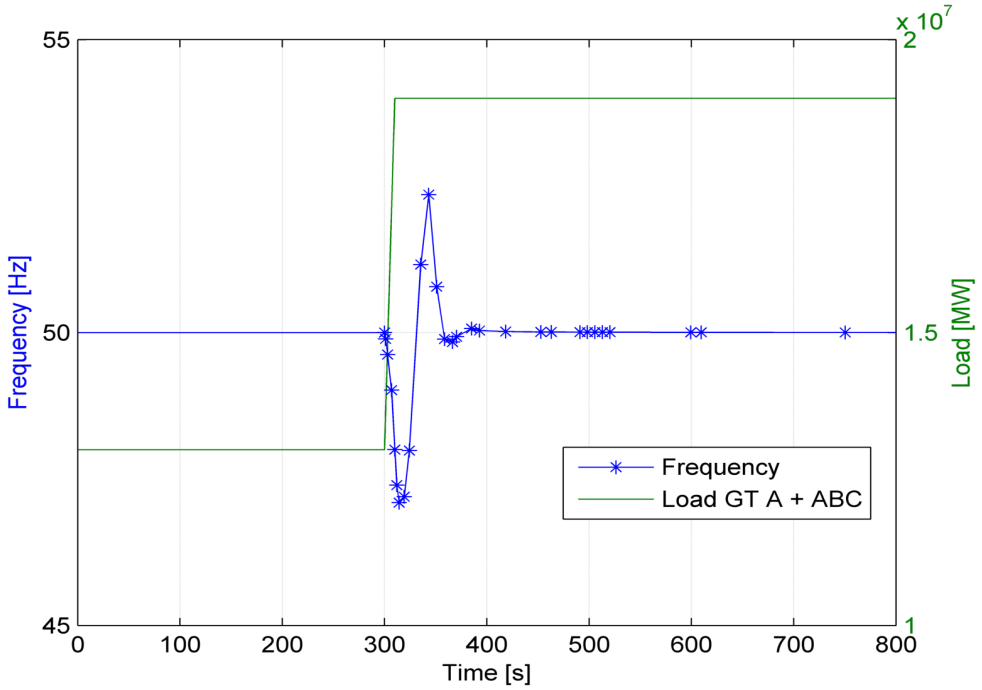

Figure 4.11: Grid frequency and load set-point of gas turbine A and ABC turbogenerator.

Figure 4.12 shows the shares of the combined plant net power output generated by gas turbine A and the ABC power module.

Before the trip of gas turbine B, the topping and bottoming units produce 10.9 MW and 2.1 MW, respectively. After the failure of engine B, gas turbine A increments the net power output up to 16 MW, while the ABC turbogenerator produces 3.0 MW. Figures 4.13 to 4.16 report the inlet and outlet temperatures of the recuperator air side, the air and exhaust gas mass flows, the inlet and outlet temperatures of the ABC power turbine and the pressure ratio of the air compressor. It can be noted that to cope with the new load set point, the pressure ratio of the air compressor rises from 2.3 to 2.6, while the exhaust gases and air mass flow rate increase by around $10\,\mathrm{kg} \cdot s^{-1}$ each; see Figures 4.16 and 4.14.

Equivalently, Figures 4.13 and 4.15 suggest that the air temperature profiles inside the recuperator and the power turbine increase, approaching the design-point values.

The dynamics of the gas turbine is faster than that of the ABC module. For instance, the trend of the ABC air mass flow is approximately five times slower compared to the variation of the exhaust gas mass flow; see Figure 4.14. The main cause of this feature is the thermal inertia of the recuperator which causes a delay in the response of the ABC turbogenerator compared to that of the gas turbine module. This phenomenon can also be observed in Figures 4.12 to 4.16. The contributions of the recuperator thermal inertia are the exhaust gas and air

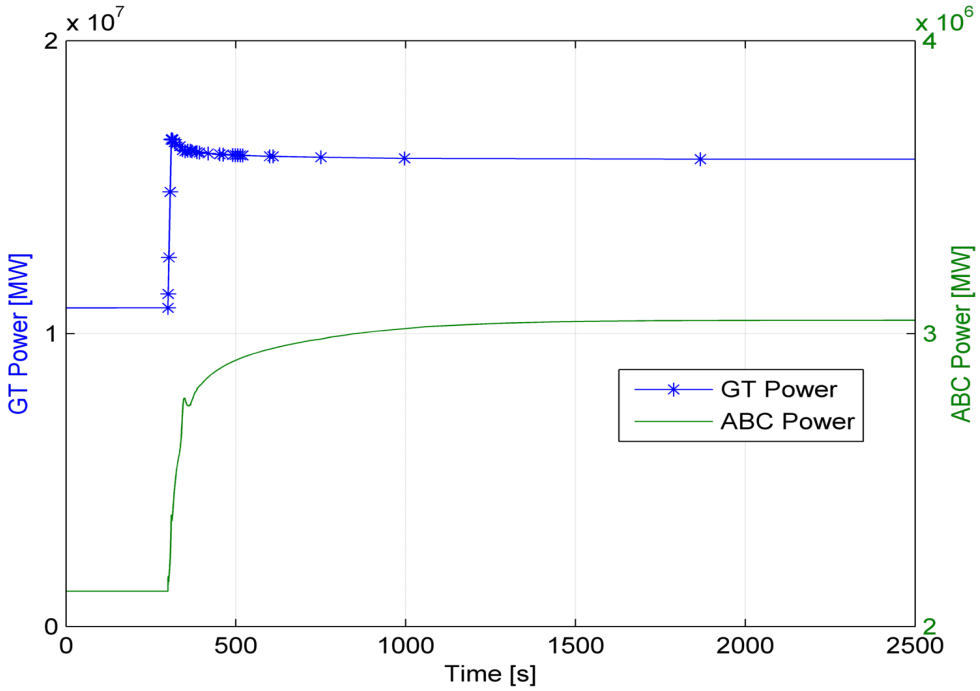

Figure 4.12: Gas turbine A and ABC turbogenerator electric power outputs.

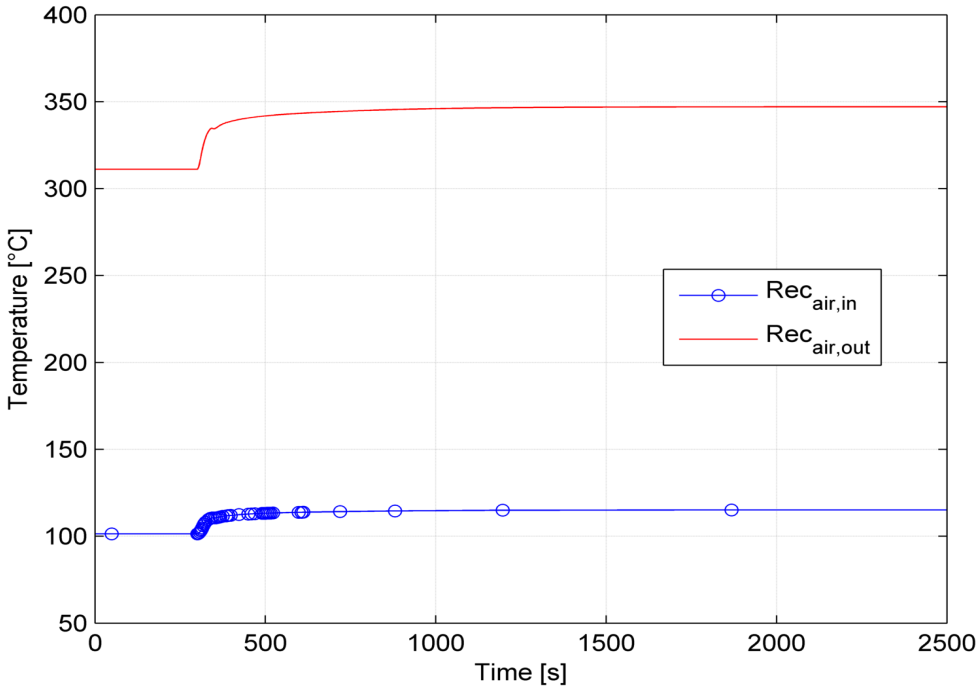

Figure 4.13: Air temperatures (recuperator inlet and outlet).

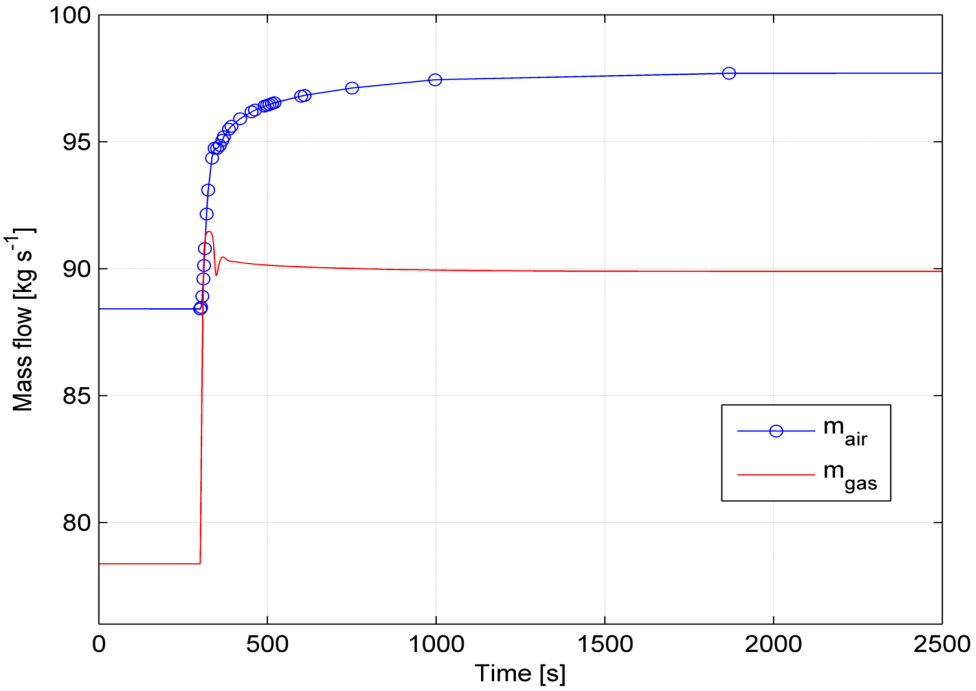

Figure 4.14: Air and exhaust gases mass flows.

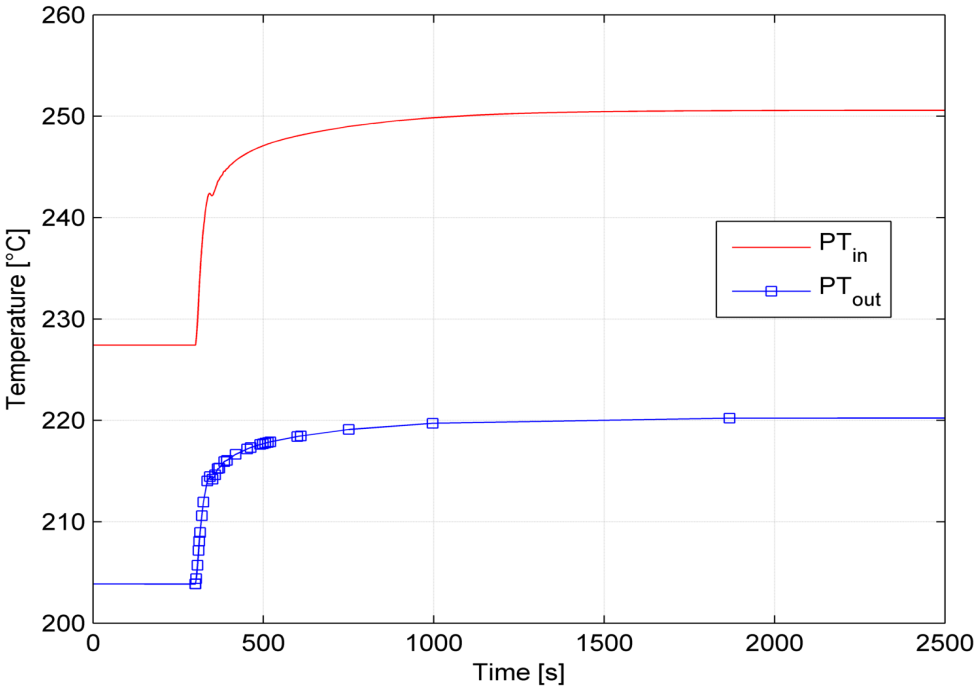

Figure 4.15: Power turbine (PT) inlet and outlet temperatures.

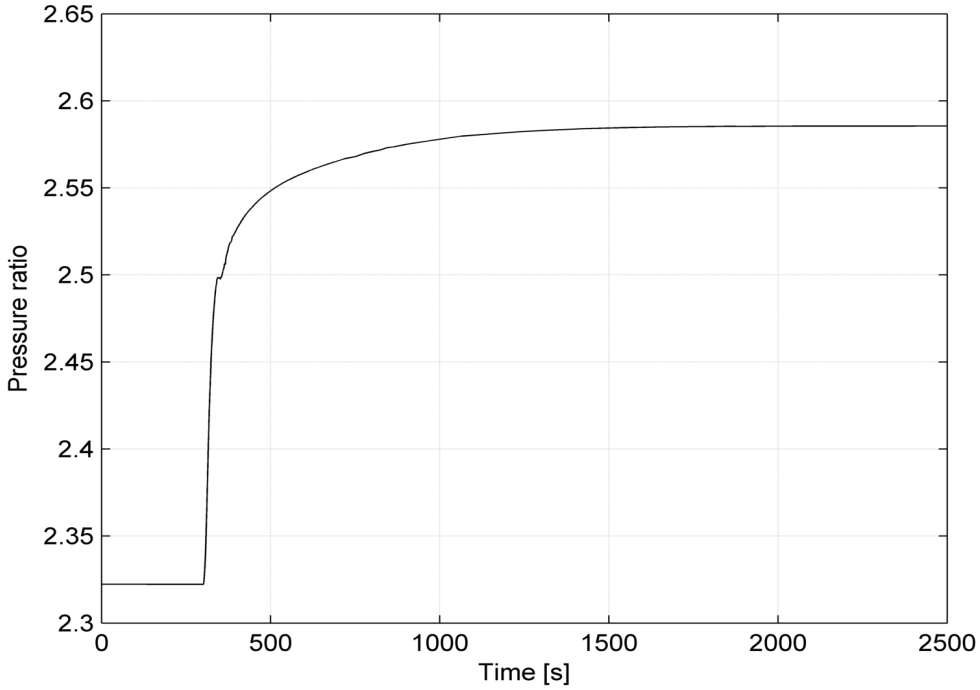

Figure 4.16: Air compressor pressure ratio.

entrained in the hot and cold volumes and the tube metal walls.

Note that the total mass of air and of exhaust gases is negligible as their average density is around 1.8 and 0.7 kg $\cdot$ m^3, respectively. Consequently, the weight of the recuperator is primarily determined by the mass of the tube metal walls which cause the delay of the air bottoming cycle power unit.

In conclusion the results indicate that the ABC power module can boost the thermal efficiency of the SGT-500 gas turbine from 31.3 % up to 37.2 %, corresponding to an increment of around 6 %-points. The total power capacity on board can thus increase up to 52.5 MW, including the remaining two SGT-500 engines. The total weight of the ABC unit, mainly determined by the shell-and-tube recuperator, is estimated to be around 60 ton.

4.6 Discussion

According to the standards for power quality adopted by the platform owner, the frequency undershooting must not exceed 5 % of the nominal value (50 Hz). As results from the dynamic analysis (see Figure 4.11) the implementation of ABC turbogenerator on Draugen may lead to exceed the tolerance of the frequency excursions in case of a 0.6 MW $\cdot$ s $^{-1}$ load set-point variation. Thus, from a reliability perspective, the platform owner should instead operate the power system so that gas turbine A and ABC unit provide 14 MW while gas turbine B sup-

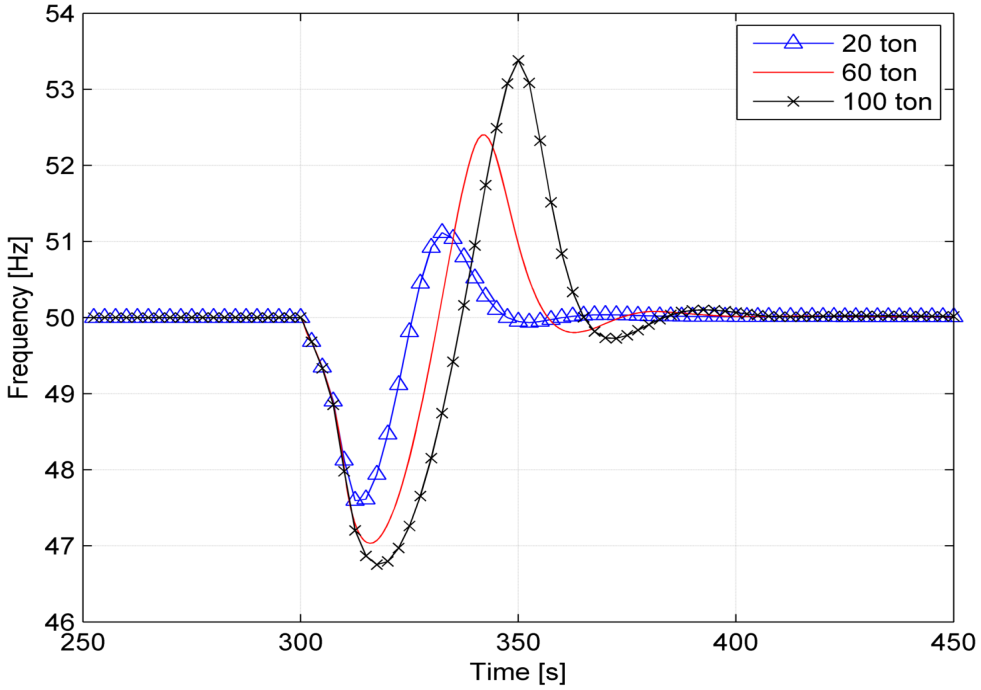

Figure 4.17: Grid frequency versus time for three recuperator core weights. The load set-point variation is 0.6 MW · s $^{-1}$.

plies the remaining power demand (5 MW). The new load set-point variation is 0.5 MW · s $^{-1}$ and the frequency undershooting and overshooting decrease to 4.9 % and 3 %, respectively. Thus, this management strategy ensures that the frequency fluctuations of the electric grid lay within the specified range and the load of gas turbine B is sufficient to prevent surge and chocking in the low and high pressure axial compressors.

A sensitivity analysis is carried out to evaluate the influence of the weight of the recuperator on the frequency undershooting and overshooting. Figure 4.17 shows the trends of frequency versus time for three weights of the shell and tube recuperator. The rate of the load set-point variation of the combined gas turbine and ABC module is 0.6 MW · s $^{-1}$. The higher the weight the larger are the metal wall thermal intertia and the frequency fluctuations. Namely, with a mass of 20 ton the frequency undershooting and overshooting are around 4 and 3 % , thus allowing to comply with the tolerances imposed by the platform operator.

To sum up, due to the presence of the shell-and-tube recuperator, the variables related to the air bottoming cycle module, e.g. pressure ratio and mass flow of the air compressor, present a delay compared to the quantities describing the dynamics of the gas turbine. The principal factor influencing the transient response is the thermal inertia of the tube metal wall of the shell-and-tube recuperator while the total mass of the exhaust gas and air is negligible.

4.7 Ongoing improvements

The sensitivity analysis shows the important role played by the recuperator and, in particular, the influence of its inertia. As outlined in Chapter 2.3.2, the recuperator can be built as a shell and tube or as a plate-fin heat exchanger. In the case analysed in Chapter 2.3.2 a shell and tube configuration was selected and optimized.

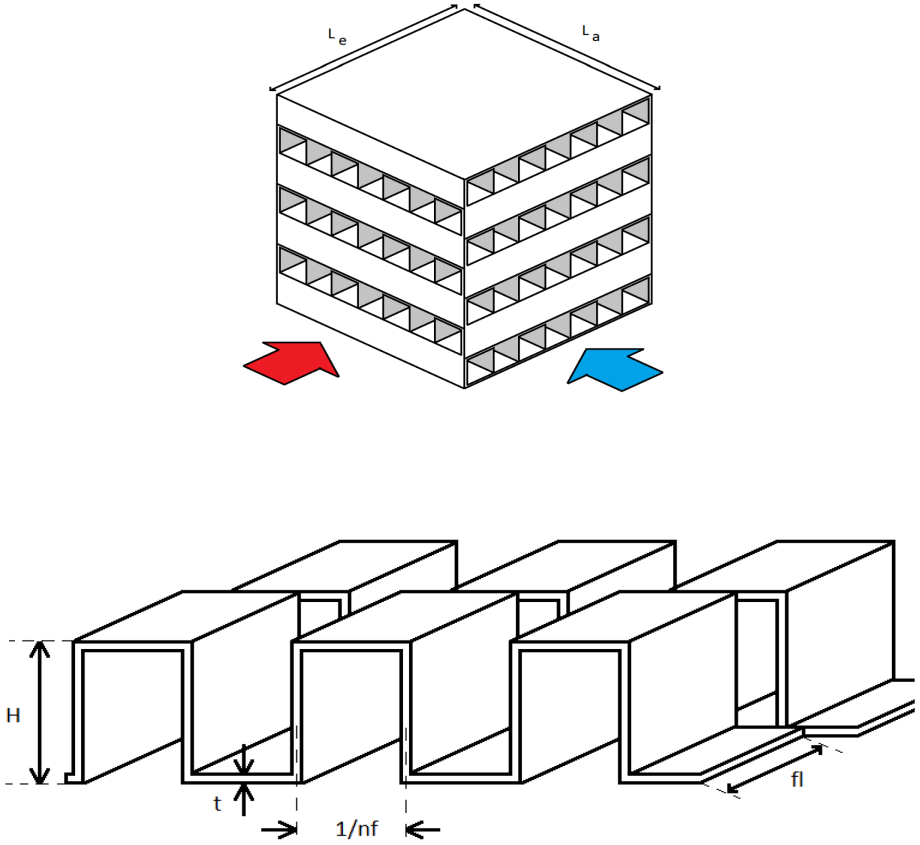

Figure 4.18: Plate-fin dimensions.

To reduce the recuperator inertia the shell and tube configuration is now replaced by a plate-fin heat exchanger recuperator. Following the method outlined in Chapter 3, the two spools ABC unit is design and optimized. The PFHE geometry data are obtained according to [174] while the heat transfer coefficients and the pressure drops are computed with the equations proposed by Manglik and Bergles [173].

These correlations [173] are considered the most accurate for a plate-fin heat exchanger with offset strip fins. The correlations consist of the Colburn factor "j", and the Fanning factor f computed for the air ("a") and exhaust gases ("e") side.

$$j_a = 0.6522 \cdot {Re_a}^{-0.5403} \cdot {\alpha_a}^{-0.1541} \cdot {\delta_a}^{0.1499} \cdot {\gamma_a}^{-0.0678} \cdot \left(1 + 5.269 \cdot 10^{-5} \cdot {Re_a}^{1.340} \cdot {\alpha_a}^{0.504} \cdot {\delta_a}^{0.456} \cdot {\gamma_a}^{-1.055}\right)^{0.1} \tag{4.20}$$

$$j_e = 0.6522 \cdot {Re_e}^{-0.5403} \cdot {\alpha_e}^{-0.1541} \cdot {\delta_e}^{0.1499} \cdot {\gamma_e}^{-0.0678} \cdot \left(1 + 5.269 \cdot 10^{-5} \cdot {Re_e}^{1.340} \cdot {\alpha_e}^{0.504} \cdot {\delta_e}^{0.456} \cdot {\gamma_e}^{-1.055}\right)^{0.1} \tag{4.21}$$

$$f_a = 9.6243 \cdot {Re_a}^{-0.7422} \cdot {\alpha_a}^{-0.1856} \cdot {\delta_a}^{0.3053} \cdot {\gamma_a}^{-0.2659} \cdot \left(1 + 7.669 \cdot 10^{-8} \cdot {Re_a}^{4.429} \cdot {\alpha_a}^{0.920} \cdot {\delta_a}^{-3.767} \cdot {\gamma_a}^{0.236}\right)^{0.1} \tag{4.22}$$

$$f_e = 9.6243 \cdot {Re_e}^{-0.7422} \cdot {\alpha_e}^{-0.1856} \cdot {\delta_e}^{0.3053} \cdot {\gamma_e}^{-0.2659} \cdot \left(1 + 7.669 \cdot 10^{-8} \cdot {Re_e}^{4.429} \cdot {\alpha_e}^{0.920} \cdot {\delta_e}^{-3.767} \cdot {\gamma_e}^{0.236}\right)^{0.1} \tag{4.23}$$

where α, δ and γ are dimension based coefficients given as follow:

$$\alpha_a = \frac{\frac{1}{nf_a}}{H_a} \qquad \alpha_e = \frac{\frac{1}{nf_e}}{H_e} \tag{4.24}$$

$$\delta_a = \frac{t_a}{fl_a} \qquad \delta_e = \frac{t_e}{fl_e} \tag{4.25}$$

$$\gamma_a = \frac{t_a}{\frac{1}{nf_a}} \qquad \gamma_e = \frac{t_e}{\frac{1}{nf_e}} \tag{4.26}$$

where nf is the number of fins per meter, H is the fin height, and fl is the fin length and "t" is the fin thickness. As previously, the subscript "a" and "e" refer to air and exhaust gases, respectively.

The Reynolds number, for air and exhaust gases side, is computed as:

$$Re_a = \frac{G_a \cdot D_{h,a}}{\mu_a} \qquad Re_e = \frac{G_e \cdot D_{h,e}}{\mu_e} \tag{4.27}$$

where D_h is the hydraulic diameter and μ is the dynamic viscosity. G_a and G_e are defined in Equations 4.28 and 4.29 where $\dot{m}$ is the mass flow rate and A_{ff} is the free flow area (see Equations 4.30 and 4.31). L is the flow length and N_p is the number of plates, respectively.

$$G_a = \frac{\dot{m}_a}{A_{ff,a}} \tag{4.28}$$

$$G_e = \frac{\dot{m}_e}{A_{ff,e}} \tag{4.29}$$

$$A_{ff,a} = (H_a - t_a) \cdot (1 - nf_a \cdot t_a) \cdot L_e \cdot N_{p,a} \tag{4.30}$$

$$A_{ff,e} = (H_e - t_e) \cdot (1 - nf_e \cdot t_e) \cdot L_a \cdot N_{p,e} \tag{4.31}$$

The hydraulic diameter, for the air and exhaust gas side, is given in Equations 4.32 and 4.33, respectively [195].

$$D_{h,a} = \frac{4 \cdot fl_a \cdot \left(\frac{1}{nf_a} - t_a\right) \cdot (H_a - t_a)}{2 \cdot \left[\left(\frac{1}{nf_a} - t_a\right) \cdot fl_a + (H_a - t_a) \cdot fl_a + t_a \cdot (H_a - t_a)\right] + t_a \cdot \left(\frac{1}{nf_a} - t_a\right) - {t_a}^2} \tag{4.32}$$

$$D_{h,e} = \frac{4 \cdot fl_e \cdot \left(\frac{1}{nf_e} - t_e\right) \cdot (H_e - t_e)}{2 \cdot \left[\left(\frac{1}{nf_e} - t_e\right) \cdot fl_e + (H_e - t_e) \cdot fl_e + t_e \cdot (H_e - t_e)\right] + t_e \cdot \left(\frac{1}{nf_e} - t_e\right) - {t_e}^2} \tag{4.33}$$

The total height of the heat exchanger is computed with the following equation:

$$H_{PFHE} = N_{p,a} \cdot (H_a - pt) + N_{p,e} \cdot (H_e - pt) \tag{4.34}$$

where N_p is, again, the number of plates and pt is the plate thickness. To reduce the heat loss to the surroundings, is assumed that $N_{p,a} = N_{p,e} + 1$.

The velocities of the streams and the heat transfer area for each side are calculated Equations 4.35, 4.36, 4.37 and 4.38.

$$v_a = \frac{\dot{m}}{A_{ff,a} \cdot \rho_{a,av}} \tag{4.35}$$

$$v_e = \frac{\dot{m}}{A_{ff,e} \cdot \rho_{e,av}} \tag{4.36}$$

$$A_{HX,a} = L_a \cdot L_e \cdot N_{p,a} \cdot (1 + 2 \cdot nf_a \cdot (H_a - t_a)) \tag{4.37}$$

$$A_{HX,e} = L_e \cdot L_a \cdot N_{p,e} \cdot (1 + 2 \cdot nf_e \cdot (H_e - t_e)) \tag{4.38}$$

The sum of the areas computed by 4.37 and 4.38, is the total heat transfer area.

$$A_{tot} = A_{HX,a} + A_{HX,e} \tag{4.39}$$

Regarding the pressure drops, the equations proposed in [174] are employed.

Table 4.5: Air bottoming cycle state points.

	T	p	ρ	h	s
1	15.00 °C	101.32 kPa	1.22 kg · m^{-3}	414.37 kJ · kg^{-1}	3.84 kJ (kg K)$^{-1}$
2	131.31 °C	294.38 kPa	2.53 kg · m^{-3}	531.57 kJ · kg^{-1}	3.88 kJ (kg K)$^{-1}$
3	308.00 °C	293.64 kPa	1.75 kg · m^{-3}	713.60 kJ · kg^{-1}	4.25 kJ (kg K)$^{-1}$
4	194.78 °C	121.96 kPa	0.90 kg · m^{-3}	596.45 kJ · kg^{-1}	4.28 kJ (kg K)$^{-1}$
5	173.40 °C	101.33 kPa	0.79 kg · m^{-3}	574.61 kJ · kg^{-1}	4.29 kJ (kg K)$^{-1}$

$$dp_a = \frac{2 \cdot f_a \cdot L \cdot {G_a}^2}{\rho_a \cdot D_{h,a}} \cdot 10^{-3} \tag{4.40}$$

$$dp_e = \frac{2 \cdot f_e \cdot L \cdot {G_e}^2}{\rho_e \cdot D_{h,e}} \cdot 10^{-3} \tag{4.41}$$

The $LMTD$ method for cross-flow arrangement is used to compute the heat transfer areas of the two sides. The UA value of the heat exchanger is calculated considering the wall and fouling resistances negligible due to their relatively small contributions.

$$\frac{1}{U \cdot A} = \frac{1}{HTC_a \cdot A_a} + \frac{1}{HTC_e \cdot A_e} \tag{4.42}$$

$$U \cdot A = \frac{\dot{Q}}{F \cdot \Delta T_{lm}} \tag{4.43}$$

The parameter F is the correction factor for the cross-flow arrangement. It is computed through a particular function which come from appropriate experimental data reported in graphs available in open literature

With these specifications, the multi-objective optimizer can run and the Pareto front is generated.

The design with the highest core is selected as new test case and investigated. The plant's specifications are listed in Tables 4.5 while the related T–s diagram is shown in Figure 4.19.

The new heat exchanger configuration with a detailed geometry is implemented in Modelica. The HX model is verified following the example implemented in [174]. Then, the ABC turbogenerator model is built in DYMOLA environment and a new gas turbine control system is also introduced into the plant model (see Figure 4.20).

At the time of writing, preliminary analysis have been performed. First of all, a comparison between a model with and without a recuperator with a detailed

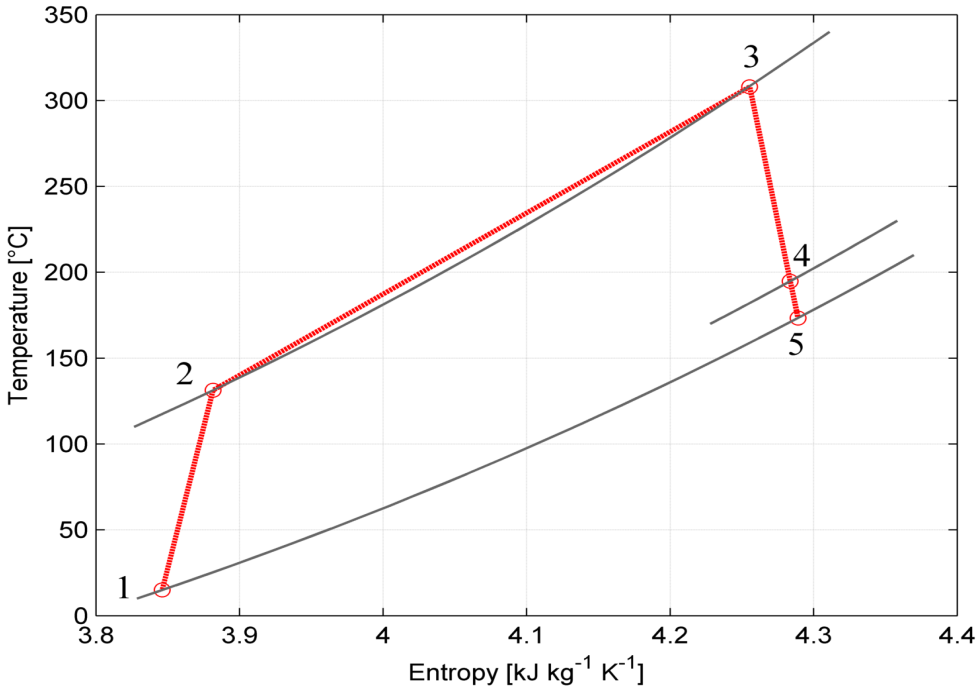

Figure 4.19: Air bottoming cycle T-s diagram.

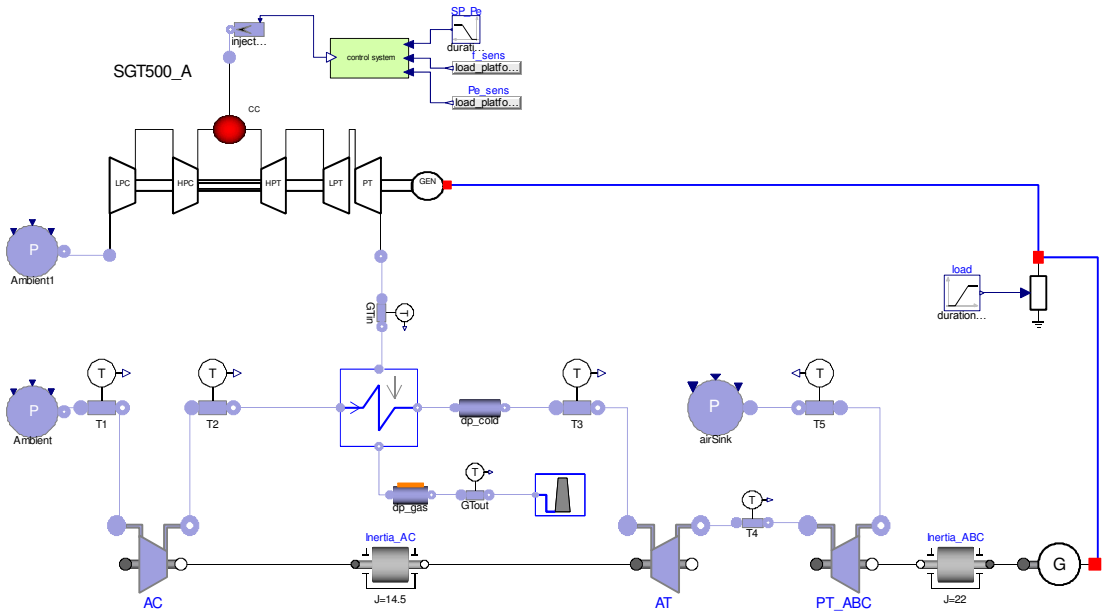

Figure 4.20: Modelica object diagram of one gas turbine and ABC power module.

geometry is investigated.

Figures 4.21 and 4.22 show the temperature trends on the air and exhaust gas side. Note that the model with a detailed geometry of the recuperator is characterized by a temperature trend different from the one with a not detailed recuperator. In addition, the detailed model is able to show the stream temperature maps into the device, as depicted in Figure 4.23. This is a fundamental aspects because it helps identify hot spots and material overheating. In addition, with this map, a clear view of the possible points where exhaust gases can condensate is shown. Its not a negligible issue if the gas turbine burns heavy fuels.

Regarding the frequency trend, the introduction of the AHX geometry does not influence the plant response. Figure 4.24 shows the frequency undershooting and overshooting during a fast load reduction.

As said before, this is an on-going work with the aim of investigating the air bottoming cycle dynamic behaviour. In the next future different ABC configurations (e.g. with one or two intercoolers, etc.) at design, part-load and dynamic conditions will be analyzed. In this manner, the ABC plant configuration performance can be known in steady-state, part-load and dynamic conditions. The practical consequence is a more precise plant configuration selection.

4.8 Conclusions

The dynamic performance of a novel power system serving an offshore oil and gas platform is analysed in this chapter. The system features three gas turbines and an air bottoming cycle unit which recuperates the waste heat released by one of the engines, thus abating the production of carbon dioxide and pollutants on the Norwegian Shelf. Results indicate that the performance of the single gas turbine increases by around 20 %, when it operates in combined cycle mode, while the total power capacity on board increases up to 52.5 MW.

The dynamics of the system is assessed during the trip of one engine, which causes a load set-point variation of the combined gas turbine and air bottoming cycle plant. The transient analysis suggests that the tolerances on the frequency variations can be respected by operating the system so that the combined cycle plant and one gas turbine provide 14 MW and 5 MW, respectively, while the third engine is shut down.

Due to the presence of the shell-and-tube recuperator, the variables related to the air bottoming cycle module, e.g. the pressure ratio and mass flow of the air compressor, present a delay compared to the quantities describing the dynamics of

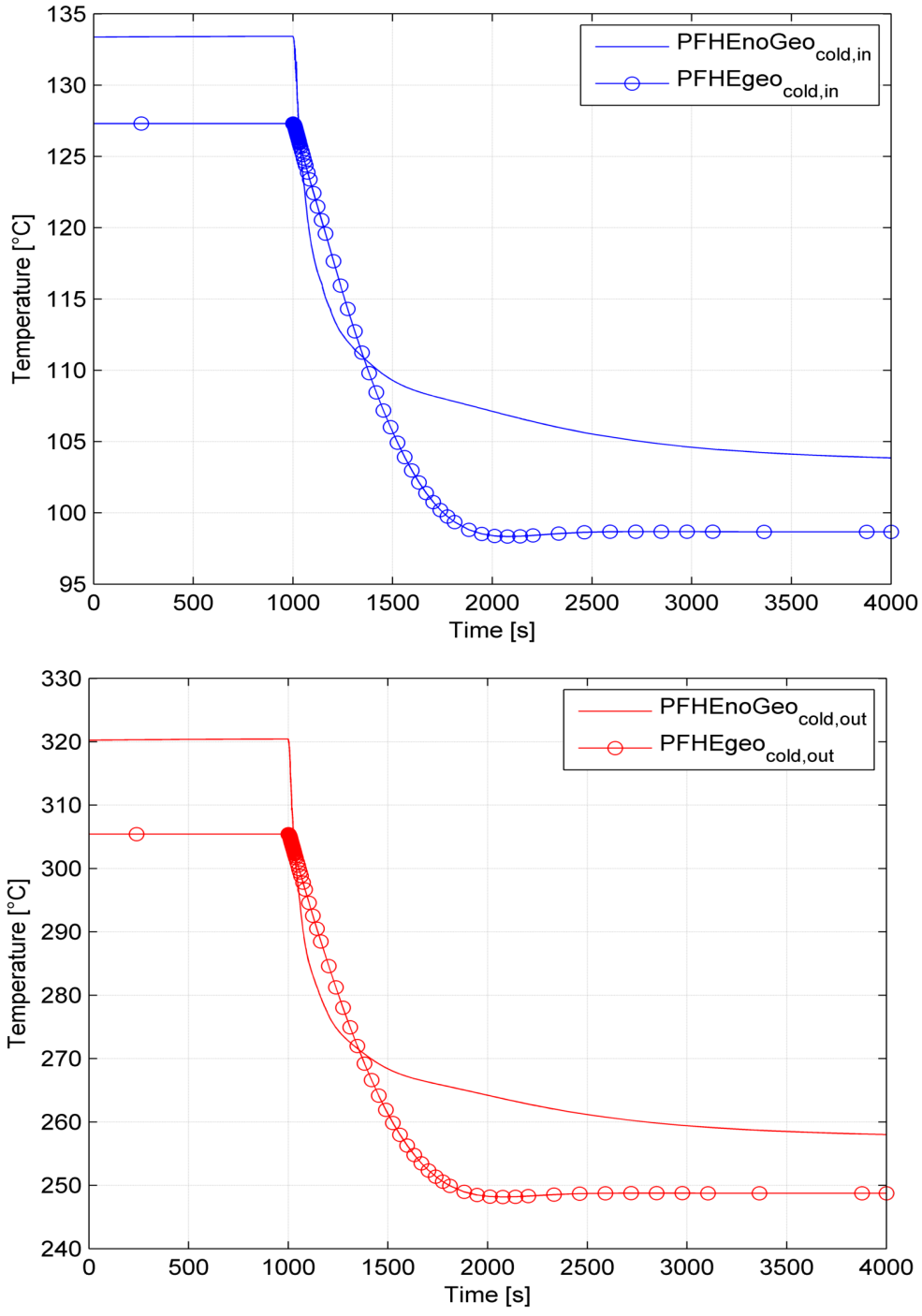

Figure 4.21: Cold fluid temperature trend in the PFHE recuperator.

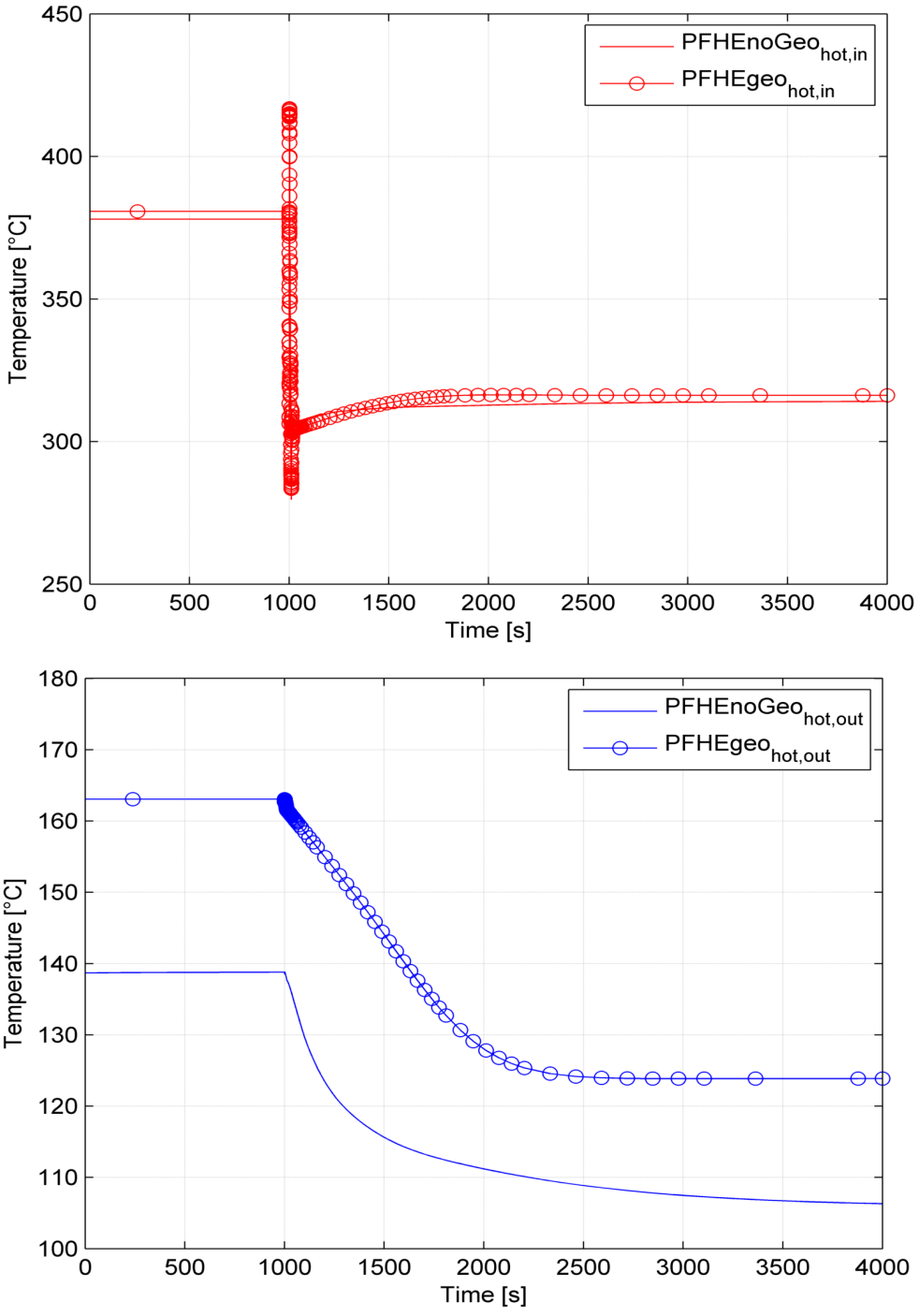

Figure 4.22: Hot fluid temperature trend in the PFHE recuperator.

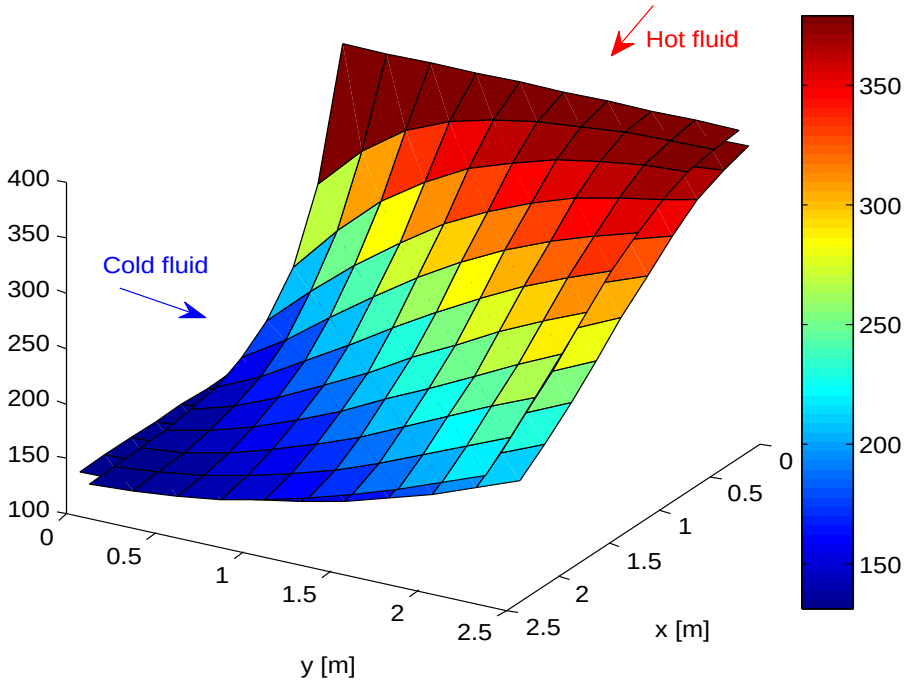

Figure 4.23: Temperature trend in the PFHE recuperator.

the gas turbine. The major factor influencing the transient response is the thermal inertia of the tube metal wall constituting the shell-and-tube recuperator, while the total mass of the exhaust gas and air is negligible.

A sensitivity analysis on the weight of the recuperator indicates that the combined cycle plant can tolerate faster load changes or can operate more reliably (i.e. lower frequency variations) by minimizing the mass of the shell-and-tube bundle.

Finally, the ongoing improvements are reported and discussed.

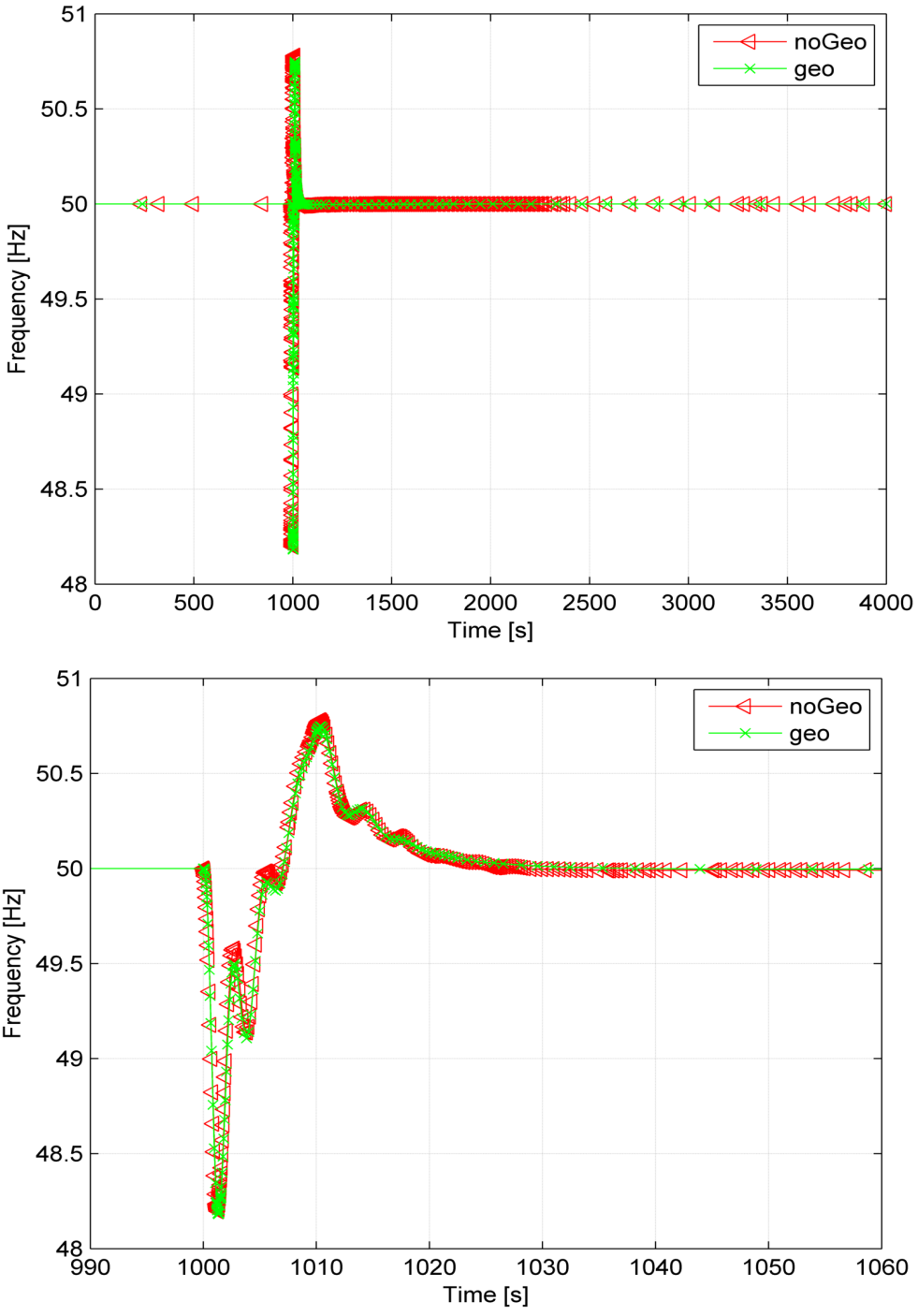

Figure 4.24: Grid frequency trend during a gas turbine trip.

Chapter 5

Analysis of the organic Rankine cycle's dynamic behaviour: effects on grid and fluid

This Chapter is devoted to the investigation of critical dynamic events causing frequency fluctuation and thermochemical decomposition of the working fluid in organic Rankine cycle unit. The case study is the power system serving Draugen oil and gas platform where one of the three gas turbines is combined with an organic Rankine cycle unit so as to increase the overall performance and reduce the CO_2 emissions.

A dynamic model of the plant has been developed with particular emphasis on the once-through boiler recuperating the exhaust heat from the topping engine, for which a distributed cross-flow physical model coupled with local correlations for single- and two-phase heat transfer coefficients is used.

As a practical consequence of this study, guidelines for safe and reliable operation of organic Rankine cycle power modules for offshore installations are suggested.

5.1 ORC working fluid stability

Organic Rankine cycle power systems have recently emerged as an efficient and cost-competitive solution for heat-to-power conversion. Nonetheless, a major obstacle to actual implementation is the thermal stability of working fluid which poses strict limitations to the maximum temperature which can be reached inside the primary heat exchanger serving the ORC module [196–198]. Fluid thermochemical decomposition is owed to the breakage of chemical bonds between the

molecules and the formation of smaller compounds, which can then react to create other hydrocarbons. Fluid overheating (hot spot) and consequent decomposition is more likely to occur in the vapour film in contact with the tube metal walls of the final part of the primary heat exchanger. As the system performance strongly relates to transport and physical properties of the working fluid, hot spots can severely reduce the net power output and the components' integrity.

The hot spot phenomenon is in some way analogous to that observed in the materials of boiler tubes, core of nuclear reactors and heat exchangers. Regarding components' degradation in power plants, [199] described the effect of long-term material overheating during the lifetime of steam boilers. In practice, the overheating of the tube metal wall induces a reaction between the steam and the tube material itself; the result is an adhesive oxide layer. This additional resistance induces the deterioration of the metal walls as the temperature raises to the maximum tolerable limit. As surveyed in [200], the occurrence of hot spot corrosion on the steam side of operating boiler tubes of fossil fuel-fired power plants is imputable to the departure from nucleate boiling which leads to acid or caustic attack and deteriorates the protective magnetite film of the tube walls. Stoppato et. al. [23] and Benato et al. [18] underline the importance of performing dynamic simulations to evaluate the effects of temperature fluctuations and components overheating during load variations and the consequent tubes' life time reduction.

Occurrence of hot spots is a well-known problem in the core of nuclear reactors when the ratio of the power density insisting on the fuel and its average value at design conditions exceed the prescribed threshold. Statistical analysis and probabilistic evaluations were performed in [201] and [202], respectively. Measurement techniques for hot spot identification in nuclear reactors were proposed by [203]. As regarding the hot spot phenomenon in heat transfer devices, [204] analysed the conditions which induce corrosion in copper alloys of condenser tubes. In [205] similar investigations for micro heat exchangers utilized in electronic devices is conducted.

In conclusion, the hot spots phenomena is a well known problem but in the literature a lacks of studies addressing the problem of hot spot formation in ORC units and practical measures to tackle this issue are still to be explored. For this reason, the following analysis is aimed at identifying the operational dynamic events that may cause grid instability and fluid thermochemical decomposition in ORC units for offshore applications.

5.2 The ORC Design Point Analysis

Figure 5.1 reports the combined cycle layout of the plant composed by the organic Rankine cycle unit recovering the exhaust gases exiting the gas turbine A and the gas turbines B and C.

Before performing a dynamic analysis it is fundamental to design and optimize the plant unit. Following the method outlined in Chapter 3.2, the multi-objective optimization procedure coupled with the genetic algorithm is utilized for the optimal design of the power generation system. The objective functions are the economic revenue, the bottoming cycle weight and the daily CO_2 emissions. A detailed design, including geometry and materials, of the heat transfer equipment is essential to evaluate the WHRU volume and weight. At this purpose, the devices' geometric quantities are included among the optimization variables. Moreover, for a correct evaluation of the CO_2 emissions over the entire year and of the profitability of the alternative investments, a part load model needs to be implemented into the optimization routine.

In Table 5.1 the organic Rankine cycle state points are listed while Figure 5.2 shows the related T–s diagram with the thermodynamic state points and the saturated dome for the ORC turbogenerator. The other main equipment parameters are listed in Table 5.2.

Table 5.1: Organic Rankine cycle state points

	T	p	ρ	h	s
1	50.00 °C	103.83 kPa	715.16 kg · m^{-3}	1.44 kJ · kg^{-1}	0.0044 kJ (kg K)$^{-1}$
2	51.53 °C	3819.48 kPa	718.01 kg · m^{-3}	7.20 kJ · kg^{-1}	0.0062 kJ (kg K)$^{-1}$
3	118.00 °C	3815.96 kPa	644.83 kg · m^{-3}	147.62 kJ · kg^{-1}	0.3985 kJ (kg K)$^{-1}$
4	224.48 °C	3756.00 kPa	416.28 kg · m^{-3}	456.42 kJ · kg^{-1}	1.0892 kJ (kg K)$^{-1}$
5	224.48 °C	3756.00 kPa	133.26 kg · m^{-3}	584.44 kJ · kg^{-1}	1.3465 kJ (kg K)$^{-1}$
6	258.72 °C	3721.37 kPa	87.345 kg · m^{-3}	701.11 kJ · kg^{-1}	1.5746 kJ (kg K)$^{-1}$
7	156.19 °C	110.29 kPa	2.2011 kg · m^{-3}	558.61 kJ · kg^{-1}	1.6477 kJ (kg K)$^{-1}$
8	70.31 °C	103.83 kPa	2.6284 kg · m^{-3}	418.25 kJ · kg^{-1}	1.2917 kJ (kg K)$^{-1}$
9	50.00 °C	103.83 kPa	2.8125 kg · m^{-3}	390.12 kJ · kg^{-1}	1.2073 kJ (kg K)$^{-1}$

The thermodynamic and transport properties of the organic working fluid are computed according to the models implemented in the open-source tool developed by Bell et al. [165].

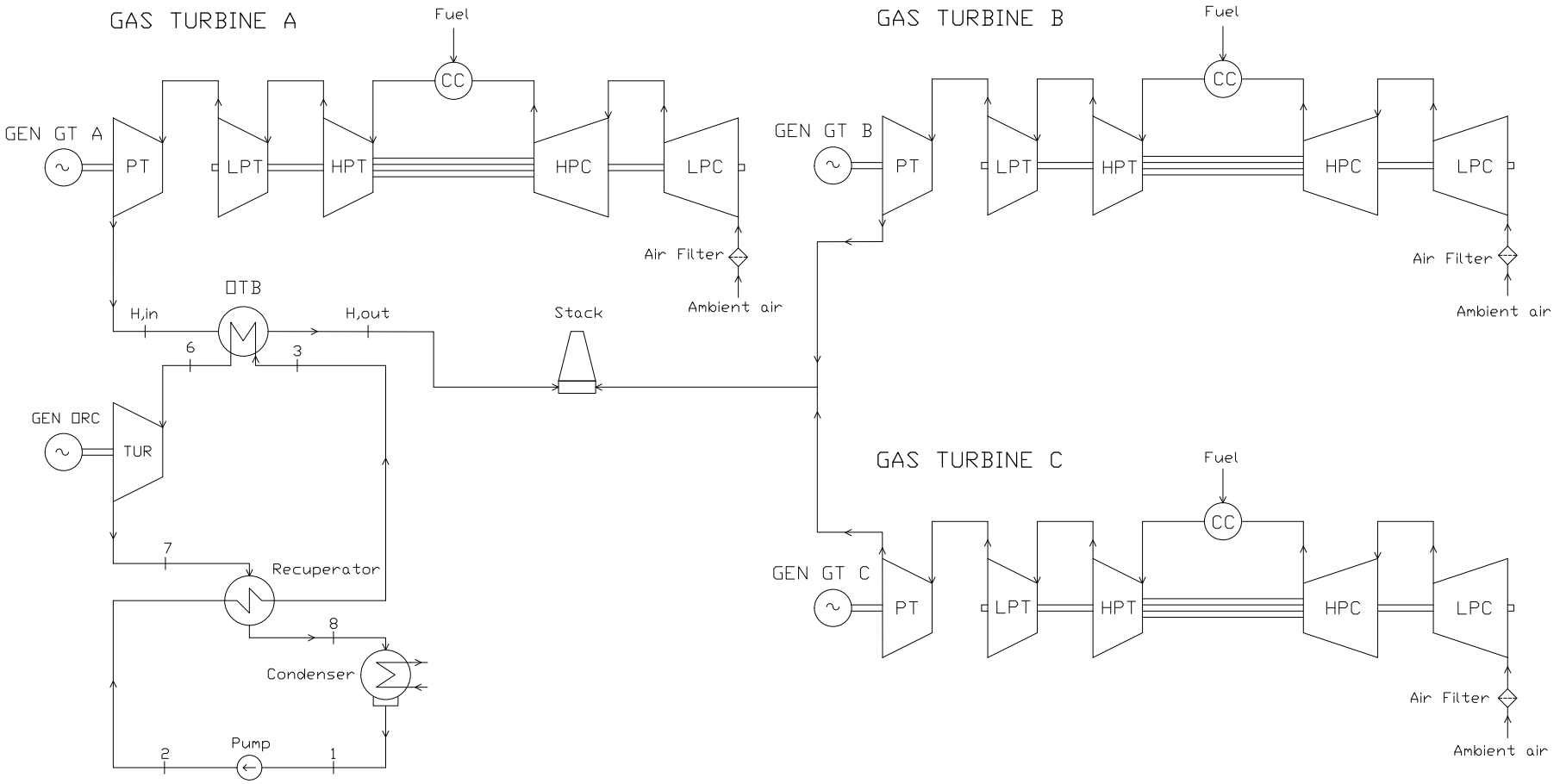

Figure 5.1: Simplified layout of the novel power system.

Table 5.2: Design-point variables utilized in the dynamic model of the organic Rankine cycle system.

Component	**Parameters**
Once-through boiler	
Number of tube rows	63
Number of tubes in parallel	64
Longitudinal and Transverse tube pitch	83 mm
Tube inner diameter	38 mm
Tube thickness	3 mm
Tube length	2.44 m
Number of fins	227 m^{-1}
Fin height	15 mm
Fin thickness	1 mm
Tube wall density	7700 $kg \cdot m^{-3}$
Tube wall specific heat capacity	500 $J \cdot kg^{-1} \cdot K^{-1}$
Fin thermal conductivity	40 $W \cdot m^{-1} \cdot K^{-1}$
Recuperator	
Volume (cold side)	1.99 m^{-3}
Volume (hot side)	20.3 m^{-3}
Weight (metal walls)	16.6 ton
UA-value	202.3 $kW \cdot K^{-1}$
Turbine	
Throat flow passage area	0.040 m^2
Isentropic efficiency	81 %
Electric generator efficiency	98 %
Pump	
Delivery pressure	3852.5 kPa
Inlet pressure	101.83 kPa
Isentropic efficiency	72 %

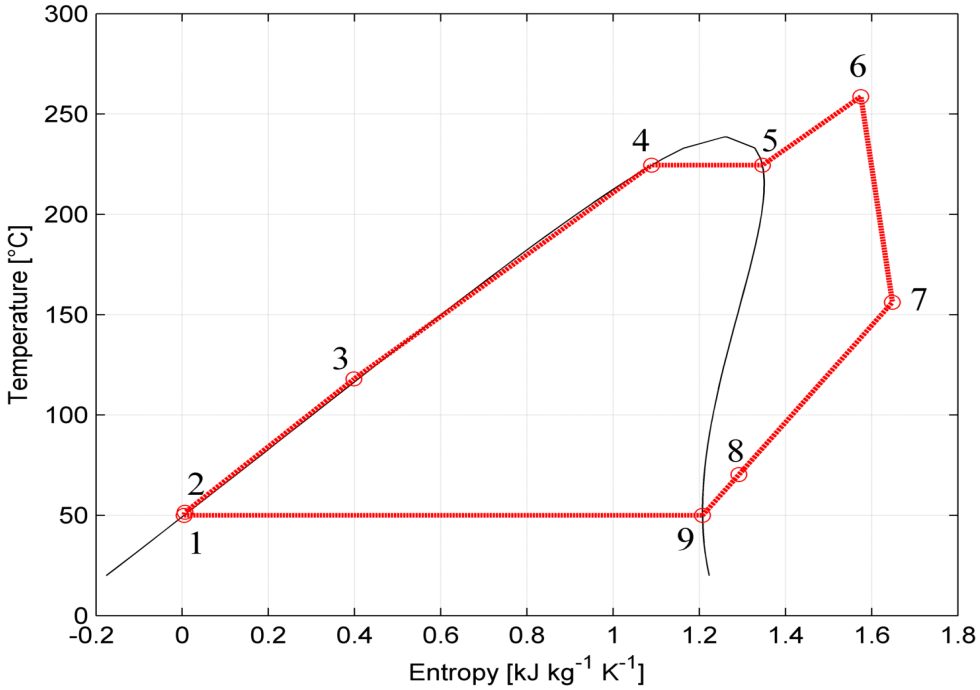

Figure 5.2: Organic Rankine cycle T–s diagram.

5.3 The Organic Rankine Cycle Model

The Modelica object diagram of the gas turbine and the organic Rankine cycle waste heat recovery unit is shown in Figure 5.3.

On the top of the Figure, the top-level interface of the gas turbine with the electric generator (GEN GT A) is depicted while the ORC unit is composed by the once through boiler (OTB); the expander (TUR) connected to the electric generator (GEN ORC) via a block that takes into account the inertia of the turbine shaft. The recuperator, the condenser and the pump complete the ORC module. The object diagram also includes the components accounting for friction losses in the heat exhangers, the blocks setting the thermodynamic state for the air and the fuel, the platform load (Load) and the feed pump control system. The pump controller is a proportional-integral (PI) controller that provides to adjust the pump speed to keep the temperature of the exhaust gases constant. This operational strategy allows to avoid corrosion problems caused by the condensation of sulfuric acid vapour at any load conditions, and to preserve the fuel flexibility of the topping unit.

The model of the gas turbine is presented and discussed in Chapter 4.2.

The model of the **once-through boiler** is readily an extension of the generic evaporator model developed and described in [39], for which the flow configura-

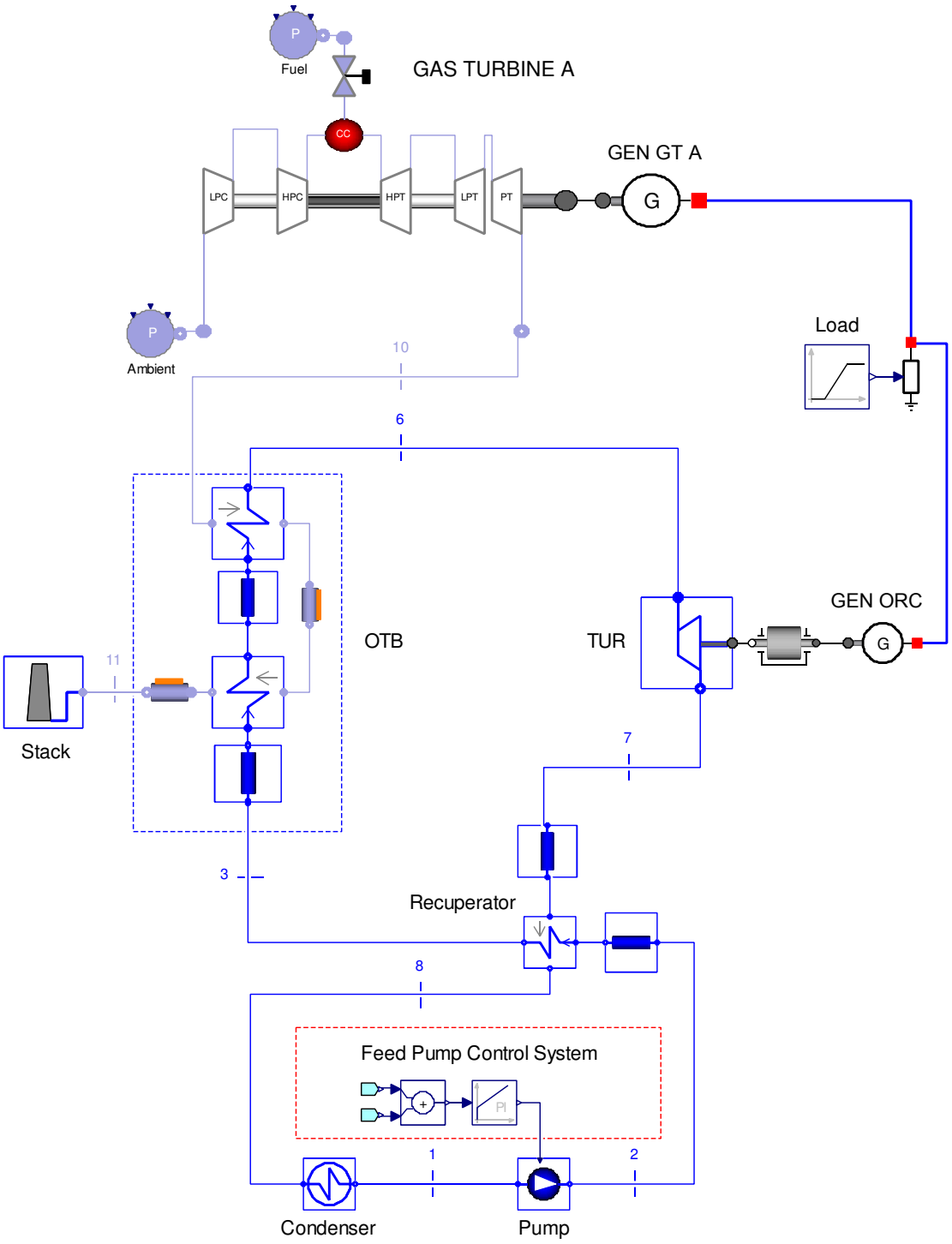

Figure 5.3: Modelica object diagram of the combined cycle unit: the SGT-500 gas turbine and the organic Rankine cycle turbogenerator.

tion, i.e. heat exchanger topology, is improved. Such generic evaporator models typically assume either parallel flow or counter-current flow configuration, while they do not resolve local fluid and wall temperatures inside tube bundles which is a requirement for the current hot spot analysis.

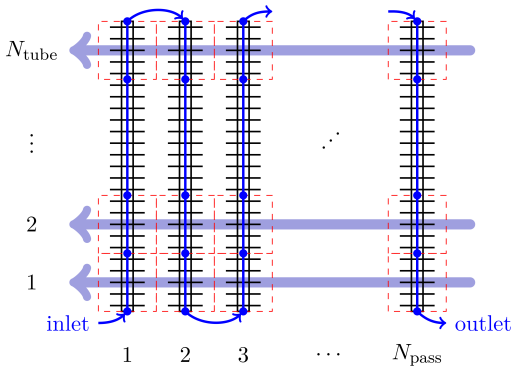

Figure 5.4: Top-view of the once-through boiler showing the discretization method.

Figure 5.4 shows a top-view of the once-through boiler with a single longitudinal tube row while Figure 5.5 displays the 3D model of the OTB unit. The OTB is recognized as a horizontal circular finned-tube bundle with counter-cross flow configuration. It is discretized in two dimensions, i.e. the exhaust gas flow direction (light purple arrows) and the organic fluid flow direction (blue arrows); N_{tube} denotes the number of cells per tube and N_{pass} denotes the number of longitudinal tubes. Temperature variations in the transverse direction of the finned-tube bundle are assumed to be negligible, and thus the longitudinal tube rows (or each cold fluid circuits) are identical from a thermodynamic perspective. Note that the total mass flow of the cold fluid is split in a series of circuits, which equal the number of transverse tubes, N_{tr}, for the current tube circuitry. Similarly, the hot fluid is divided by the number of transverse tubes and the number of cells per tube N_{tube}.

Figure 5.6 shows the Modelica object diagram of the once-through boiler. The model uses a single one-dimensional organic fluid flow model (`coldFluid`) and N_{tube} one-dimensional models (`hotFluid`) for the exhausts. The cold fluid model is connected to its pipe wall capacitance (`tubeWalls`) and a heat exchanger topology model (`extCrossFlow`). The latter essentially connects the thermal heat ports (orange rectangles in Figure 5.6) of each finite volume (dashed red rectangles in Figure 5.4), i.e. the hot fluid wall boundary with the external pipe boundary.

The tube wall model includes a one-dimensional dynamic heat balance equation in the radial direction for each finite volume, thus neglecting the small conductive thermal resistance. The flow models contain one-dimensional dynamic mass and energy balance equations, discretized by the finite volume method, assuming a

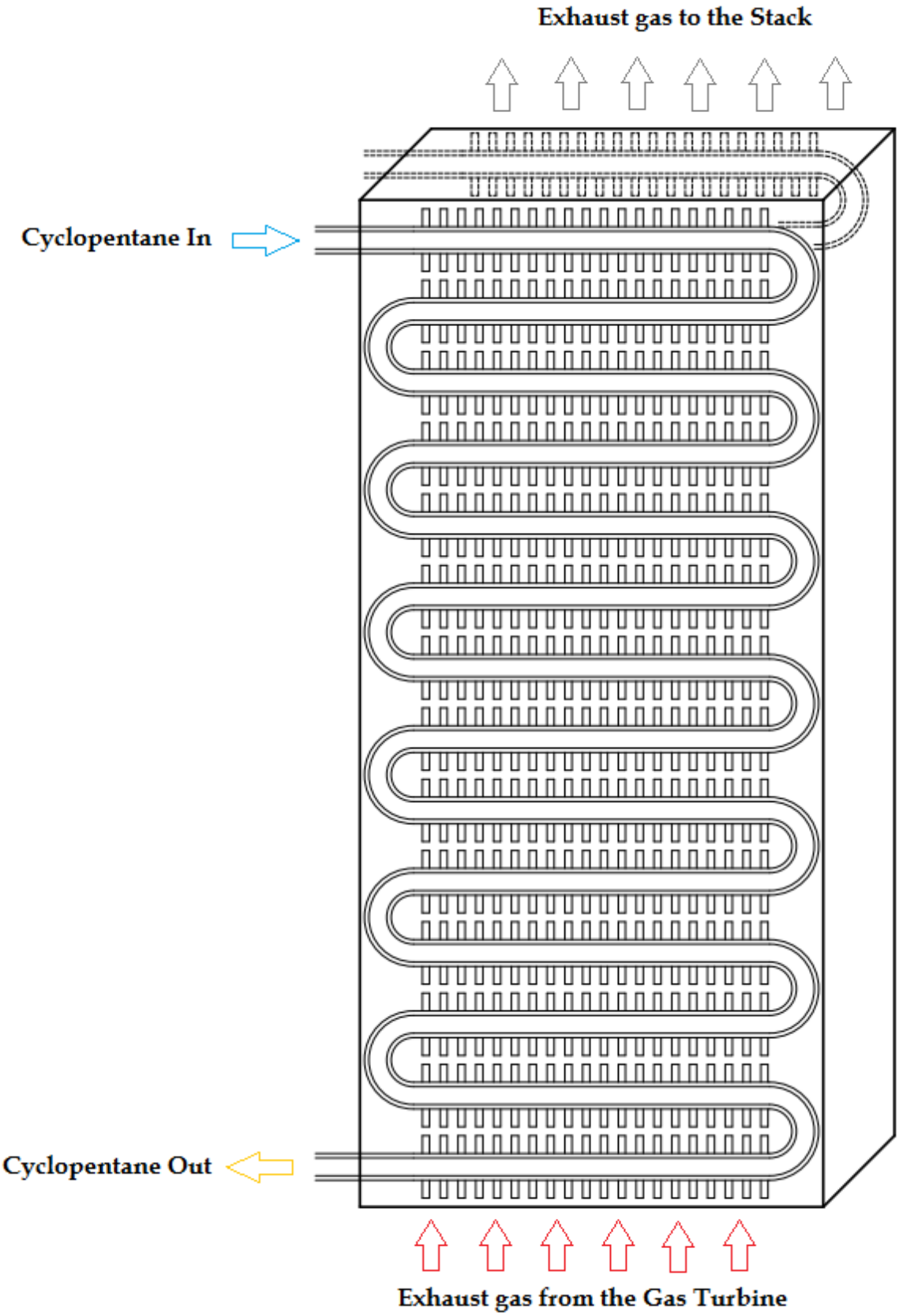

Figure 5.5: The once-through boiler 3D scheme.

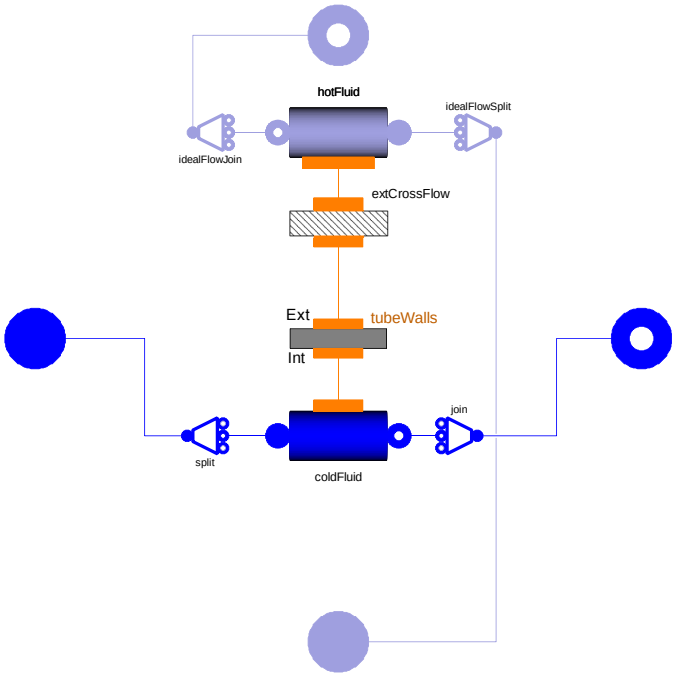

Figure 5.6: The once-through boiler Modelica object diagram.

uniform pressure distribution. The relatively small friction losses are lumped in an external component. As for the gas turbine combustion chamber, the pressure drops are estimated assuming a quadratic dependency on the volumetric flow rate. A more in-depth description of the tube wall and flow models can be found in [39]. The Modelica interface windows of the OTB where the design parameters and the correlations are set by the user are reported in Figure 5.7.

To evaluate the *heat transfer coefficient of the organic fluid flow* single phase and two-phase boiling heat transfer correlations are needed. Note that a continuous transition is required at the phase boundaries so as to ensure a smooth first derivative when entering the two-phase flow region. In this work, we used the Stepsmoother function provided by the Modelica.Fluid.Dissipation library [206], i.e. between the vapour qualities $0 \leq x < 0.05$ and $0.95 < x \leq 1$.

For single phase turbulent flow at Re $>$ 3000, the correlation proposed by Gnielinski [49] is adopted

$$\mathrm{Nu} = \frac{(f_D/8) \cdot (\mathrm{Re} - 1000) \cdot \mathrm{Pr}}{1 + 12.7 \cdot (f_D/8)^{0.5} \cdot (\mathrm{Pr}^{2/3} - 1)} \tag{5.1}$$

where the Nusselt number is $\mathrm{Nu} = h\,d/k$ and the Darcy-Weisbach friction factor is computed according to Petukhov [51].

$$f_D = (0.7904 \cdot \ln(\mathrm{Re}) - 1.64)^{-2} \tag{5.2}$$

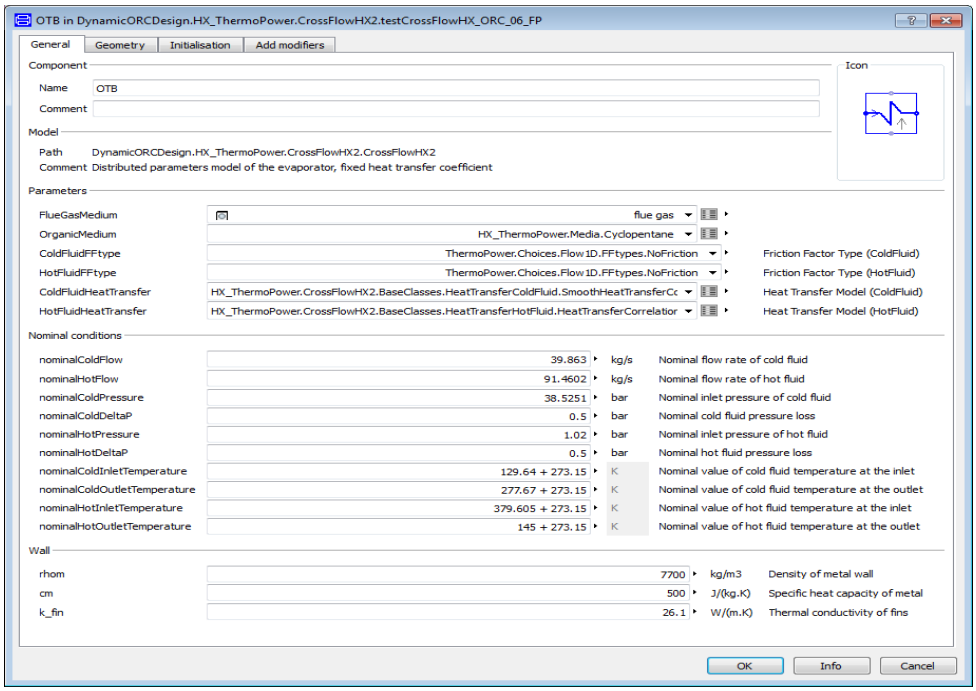

(a)

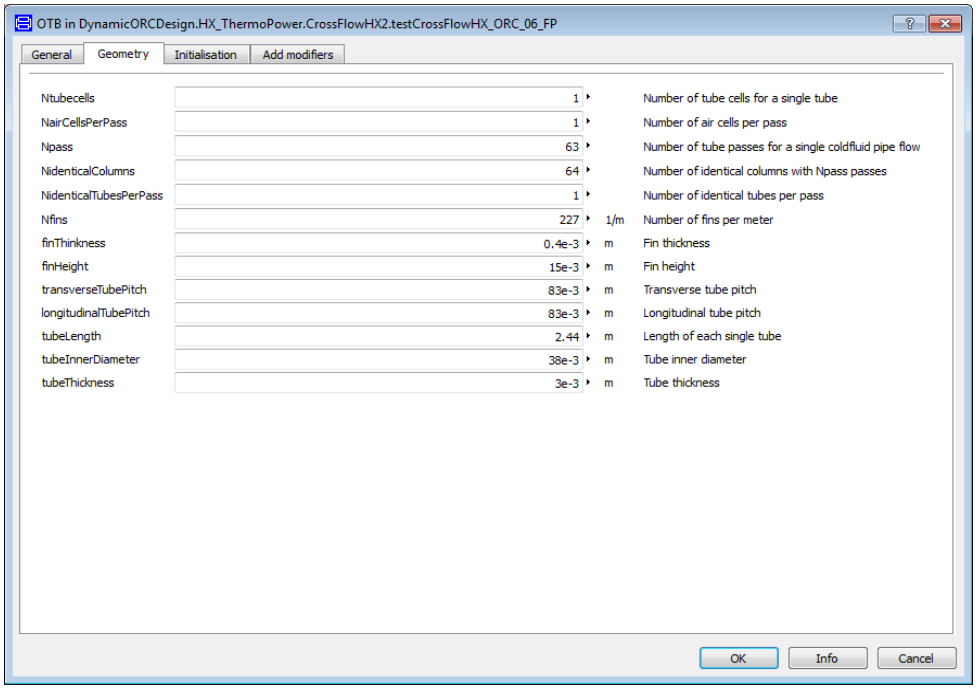

(b)

Figure 5.7: The once-through boiler Modelica windows.

For laminar flow (Re $<$ 2300), the Nusselt number equals to 3.66 assuming constant wall temperature. A simple smooth transition function is used between the laminar and turbulent Nusselt numbers.

For two-phase flow, the correlation proposed by Shah [168] is used to compute the heat transfer coefficient in local two-phase forced convective boiling. This correlation takes the largest value between the nucleate boiling heat transfer coefficient h_{nb} and the convective boiling heat transfer coefficient h_{cb}. The correlation is as follows:

For horizontal flow calculate the dimensionless parameter N by

$$N = C_o \qquad \mathrm{Fr}_L > 0.04 \tag{5.3}$$

$$N = 0.38 \cdot {\mathrm{Fr}_L}^{-0.3} \cdot C_o \qquad \mathrm{Fr}_L \leq 0.04 \tag{5.4}$$

For vertical flow, uses Equation 5.3 for all values of the liquid Froude number Fr_L. The liquid Froude number and the dimensionless parameter C_o are given by

$$\mathrm{Fr}_L = \frac{G^2}{\rho_L^2 \cdot g \cdot d} \tag{5.5}$$

$$C_o = \left(\frac{1-x}{x}\right)^{0.8} \cdot \left(\frac{\rho_G}{\rho_L}\right)^{0.5} \tag{5.6}$$

When $N > 1$, calculates h_{nb} from

$$h_{nb} = 230 \cdot h_L \cdot \mathrm{Bo}^{0.5} \qquad \mathrm{Bo} > 0.0003 \tag{5.7}$$

$$h_{nb} = h_L \cdot (1 + 46 \cdot \mathrm{Bo}^{0.5}) \qquad \mathrm{Bo} \leq 0.0003 \tag{5.8}$$

When $1 > N \geq 0.1$, calculate h_{nb} from

$$h_{nb} = h_L \cdot F \cdot \mathrm{Bo}^{0.5} \exp\left(2.74 \cdot N^{-0.1}\right) \tag{5.9}$$

When $N < 0.1$, calculate h_{nb} from

$$h_{nb} = h_L \cdot F \cdot \mathrm{Bo}^{0.5} \exp\left(2.47 \cdot N^{-0.15}\right) \tag{5.10}$$

where h_L is the liquid heat transfer coefficient calculated by the Dittus-Boelter correlation

$$\mathrm{Nu}_L = 0.023 \cdot \mathrm{Re}_L^{0.8} \cdot \mathrm{Pr}_L^{0.4} \tag{5.11}$$

$$h_L = \mathrm{Nu}_L \cdot \frac{k_L}{d} \tag{5.12}$$

$$\mathrm{Re}_L = \frac{G \cdot (1-x)d}{\mu_L} \tag{5.13}$$

$$\mathrm{Pr}_L = \frac{\mu_L \cdot c_{p,L}}{k_L} \tag{5.14}$$

The boiling number Bo is defined as

$$\mathrm{Bo} = \frac{q''}{G \cdot h_{\mathrm{LG}}} \tag{5.15}$$

and the constant F is determined as follows

$$F = 14.7 \qquad \mathrm{Bo} > 0.0011 \tag{5.16}$$

$$F = 15.43 \qquad \mathrm{Bo} \leq 0.0011 \tag{5.17}$$

The convective boiling heat transfer coefficient h_{cb} is computed by

$$h_{cb} = h_L \cdot \frac{1.8}{N^{0.8}} \tag{5.18}$$

Finally, the highest value of the two (h_{cb} and h_{nb}) is chosen for the heat transfer coefficient h.

The heat flow rate in each cold fluid cells is then computed by Newtons law of cooling as

$$q = h \cdot A \cdot (T_{wi} - T_c) \tag{5.19}$$

where subscripts "wi" and "c" denote the inner wall and cold fluid, respectively, and A is the inner tube surface area of a single cell.

The gas-side heat transfer coefficient and the fin efficiency are computed with the correlations given for staggered circular finned-tubes in the Verein Deutscher Ingenieure Heat Atlas [50].

The Nusselt number based on outer tube diameter D and for more than four tube rows is computed by

$$\mathrm{Nu} = 0.38 \cdot \mathrm{Re}_D^{0.6} \cdot \left(\frac{A}{A_{\mathrm{t0}}}\right)^{-0.15} \cdot \mathrm{Pr}^{1/3} \tag{5.20}$$

where A is the total heat transfer surface area including fins and A_{t0} is the bare tube surface area. The Reynolds number is based on the outer tube diameter and the maximum gas velocity that may occur either transversely or diagonally in between the staggered tubes. The fin efficiency for circular fins is computed by

$$\eta_f = \frac{\tanh X}{X} \tag{5.21}$$

$$X = \varphi \cdot \frac{D}{2} \cdot \sqrt{\frac{2 \cdot h}{k_f \cdot \delta}} \tag{5.22}$$

where h is the heat transfer coefficient, k_f is the thermal conductivity of the fins and δ is the fin thickness. For circular non-conic fins φ is computed by

$$\varphi = \left(\frac{D_f}{D} - 1\right) \cdot \left[1 + 0.35 \cdot \ln\left(\frac{D_f}{D}\right)\right] \tag{5.23}$$

where D_f denotes the fin diameter. Finally, the overall surface fin efficiency is calculated by

$$\eta_o = 1 - \frac{A_f}{A} \cdot (1 - \eta_f) \tag{5.24}$$

where $A_f = A - A_{\text{t0}}$, i.e the finned surface area.

The heat flow rate in each hot fluid cell is computed by Newton's law of cooling similar to the cold fluid, but including the overall surface fin efficiency as

$$q = \eta_o \cdot h \cdot A \cdot (T_{wo} - T_h) \tag{5.25}$$

where subscripts "wo" and "h" denote the outer wall and hot fluid, respectively. Note that T_c and T_h in equation 5.19 and 5.25 are taken as the cell center average value.

The organic vapour exiting the OTB enters into the **expander**. The modelled expander is a turbine because in organic Rankine cycle module with design power in the range 1–10 MW the expander is a one or two-stage axial turbine. In Figure 5.3 the component is called "TUR". In this type of machines the pressure ratio across each stage is very high, implying that the flow at the outlet of the first stage is usually supersonic. The supersonic turbine is modelled as an equivalent chocked de Laval nozzle, whose throat flow passage area is the sum of the throat areas of the nozzles that form the first stator row. An isentropic expansion is assumed from the inlet section to the throat, where sonic conditions are attained. The corresponding system of equations is listed below.

$$\begin{cases} s_{in} = s(p_{T,in}, T_{T,in}) \\ h_{S,th} = h_{T,in}(p_{T,in}, T_{T,in}) - \dfrac{1}{2} \cdot c\,(h_{S,th}, s_{in})^2 \\ \dot{m} = \rho_{S,th}(h_{S,th}, s_{in}) \cdot c\,(h_{S,th}, s_{in}) \cdot A_{th} \end{cases} \tag{5.26}$$

where s_{in} is the specific entropy at the turbine inlet, while the subscripts "S,th" and "T,in" indicate static conditions in the throat section and total conditions in the expander inlet section (i.e. total inlet pressure $p_{T,in}$ and total temperature $T_{T,in}$), respectively. The enthalpy and the speed of sound are represented with h and c, respectively, while $\dot{m}$, ρ and A_{th} are the mass flow through the nozzle, the density and the flow passage area. The throat passage area A_{th}, in the model, is assumed to be a fixed parameter obtained from the design calculation. During offdesign conditions, the relation between the mass flow rate and the turbine inlet conditions is expressed by Equation system 5.26 and, as for gas turbine, the offdesign efficiency is predicted with the correlation proposed by Schobeiri [45]:

$$\Phi = n/\sqrt{2\triangle h_{is}} \tag{5.27}$$

where Φ, n and Δh_{is} are the flow coefficients, the rotational speed and the isentropic enthalpy drop across the expander.

With the aim of improving the ORC unit efficiency, a **recuperator** is inserted after the turbine. The object diagram of the component is reported in Figure 5.8. The device is modelled by combining basic ThermoPower components: one-dimensional flow model for the vapour side (`hotFluid`), the counter-current topology block (`counterCurrent`), the tube walls (`tubeWalls` module and the one-dimensional flow model representing the liquid side (`coldFluid`).

Note that the counter-current model is fundamental in order to establish the topological correspondence between the control volumes on the tube metal walls and those of the working fluid circulating on the hot and cold side. The flow models utilize one-dimensional dynamic mass and energy balance equations (discretized following the finite volume method, and assuming a uniform pressure distribution) and the static momentum balances (lumped at both ends of the component). The tube metal wall is modelled by a one-dimensional dynamic heat balance equation, also discretized in finite volumes, neglecting the conductive thermal resistance [37]. In the present case, the heat transfer coefficient is limited by the vapour side. The liquid side heat transfer coefficient is thus specified to be sufficiently large, while the overall resistance is assumed to be equal to that of the vapour. In offdesign conditions the heat transfer coefficient is computed with the correlation proposed in [58]:

$$h = h_{des}\left(\frac{\dot{m}}{\dot{m}_{des}}\right)^{\gamma} \tag{5.28}$$

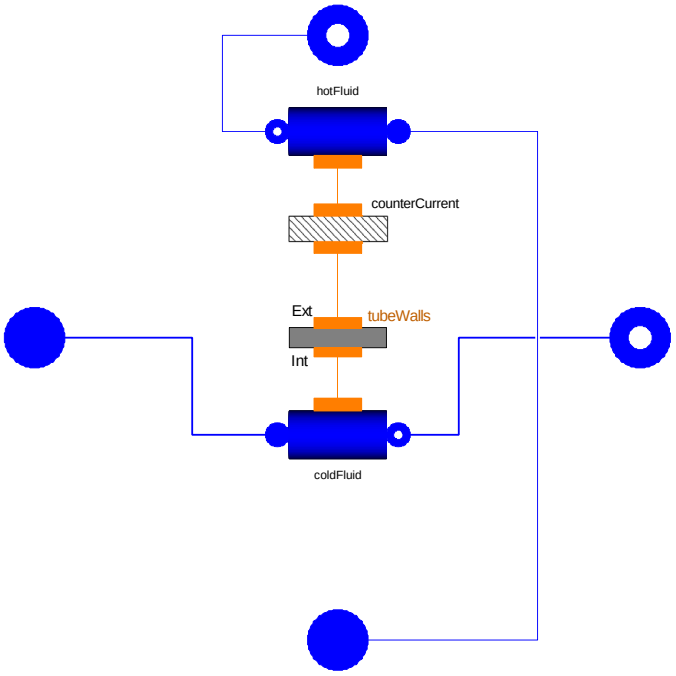

Figure 5.8: Modelica object diagram of the organic Rankine cycle shell-and-tube recuperator model.

where $\dot{m}$ is the mass flow rate of the vapour side. The subscript "*des*" refers to the value at design operating conditions, while the variable γ is the exponent of the Reynolds number. In the equation γ is posed equal to 0.6.

The **condenser** is trivially modelled as a fixed pressure component. This is justified considering the large availability of cooling sea-water, which allows the cooling circuit to be controlled in such a way that the condenser pressure is nearly constant.

The **pump** model is based on a head-capacity curve derived by fitting the data of an existing centrifugal pump designed for similar flow rates and heads. The curve can be expressed as:

$$H = H_{des} \cdot \left(b_1 + b_2 e^{\Phi}\right) \cdot \left(\frac{n}{n_{des}}\right)^2 \tag{5.29}$$

where H is the head and, b_1 and b_2 are coefficients equal to 2.462 and 0.538, respectively. The parameter ϕ is computed with the following equation:

$$\Phi = \frac{\dot{m}}{\rho} \cdot \frac{\rho_{des}}{\dot{m}_{des}} \tag{5.30}$$

where $\dot{m}$ and ρ are the mass flow rate and the density, respectively. The subscript

"*des*" refers to the values at the design point conditions.

This exponential function is selected in order to obtain a monotonic relation which increases the model robustness in comparison of the widely adopted polynomial expression.

Following the method proposed by Veres [175], the pump efficiency is a function of the coefficient F as reported in Eq. 5.31:

$$F = \Phi \cdot \frac{n_{des}}{n} \tag{5.31}$$

As shown in Figure 5.3, the ORC unit is controlled by the so called "**Feed Pump Control System**". This system provides to regulate the rotational speed of the pump and, consequently, the power produced by the ORC unit. As explained in Chapter 2.2, the platform is a stand-alone system where the alternating current is produced by the synchronous generators connected to the gas turbines and the ORC expander. Given that the topping units have the fastest load response, the control of the network frequency is managed by the gas turbine itself, while the goal of the ORC control system is to target the maximum heat recovery from the gas turbine exhaust gases. This objective can easily be fulfilled by varying the pump speed to control the exhaust gas temperature at the once-through boiler outlet section and by operating in sliding pressure mode. It is fundamental that this temperature is as low as possible, but high enough to prevent acid condensation, which might be problematic if heavy fuels are burned in the combustion chamber. The ORC proportional-integral controller is tuned in order to reach the minimum settle time of the controlled variable, to prevent speed overshooting and obtain well-damped responses for all variables.

5.4 The ORC Model Validation

The model of the ORC unit is composed by items taken from a library that was developed in order to model a 150 kW ORC turbogenerator using toulene as working fluid. The model was successfully validated for transient operation with experimental data (see [39]). Nevertheless, the once-through boiler and the recuperator need to be validated. To this purpose, in the following, the recuperator and OTB validation procedures are outlined while the validation of the other models constituting the ORC unit are described in [39].

Table 5.3: OTB geometry and operating data.

Description	**EcoVap**	**Superheater**
Number of rows	36	6
Tubes in parallel	2	2
Tubes/Row	13	13
Tube external diameter	25.0 mm	26.9 mm
Tube thickness	2.9 mm	4.2 mm
Tube length	6.0 m	6 m
Number of fins	200 m^{-1}	200 m^{-1}
Fin height	12 mm	11 mm
Transverse pitch	83 mm	83 mm
Longitudinal pitch	73 mm	73 mm
Water mass flow	2.80 kg $\cdot$ s^{-1}	2.80 kg $\cdot$ s^{-1}
Water inlet temperature	44.0 °C	-
Water outlet temperature	-	500.0 °C
Exhaust gases mass flow	20.14 kg $\cdot$ s^{-1}	20.14 kg $\cdot$ s^{-1}
Exhaust gases inlet temperature	-	592.0 °C
Exhaust gases outlet temperature	197.0 °C	-

Validation of the recuperator model

The shell and tube recuperator model is validated using an example outlined by Coulson et al. [59]. At the design point conditions, the difference between the simulation results and the data presented in the reference are withing 1 % in term of both the overall heat transfer coefficient and pressure drops.

Validation of the OTB Model

The once-through boiler model, extensively described in Chapter 5.3, is successfully validated for design and offdesign conditions with different fluids.

A model validation in steady state conditions is, firstly, performed using water as working fluid. The Modelica OTB model is compared to the once-through heat recovery steam generator outlined in [166]. Dumount and Heyen proposed a mathematical model for the simulation and design of a once-through boiler with vertical gas path and horizontal tube bundles. Table 5.3 lists the main design parameters and operating data of the above-mentioned HRSG unit.

The heat transfer coefficient on the fume side is computed by applying the correlation reported in [50] for staggered arrangement. The Gnielinski' equation is used for liquid or vapour single phase flow [50] while the Shah' equation [168] is adopted in the two phase region flow.

The difference between the heat flux computed with the Modelica model and the literature data is less then 1 %, while the steam and gas outlet temperatures differ by 3 % and 7 %, respectively.

The reason of the discrepancies is the lack of specifications in [166] about fin thickness, the exhaust gas composition and the model adopted to estimate the exhaust gas properties. This led the author to assume the missing parameters based on data available in literature, thus accepting a relatively large uncertainty in the results.

The OTB model validation at part-load and dynamic conditions is performed through the comparison between the results obtained with the OTB model built with ThermoPower library base components and the ones obtained with an OTB model built with components of the commercial library Thermal Power. Figure 5.9 reports on the left the model built with ThermoPower library and on the right the ones developed with Thermal Power components.

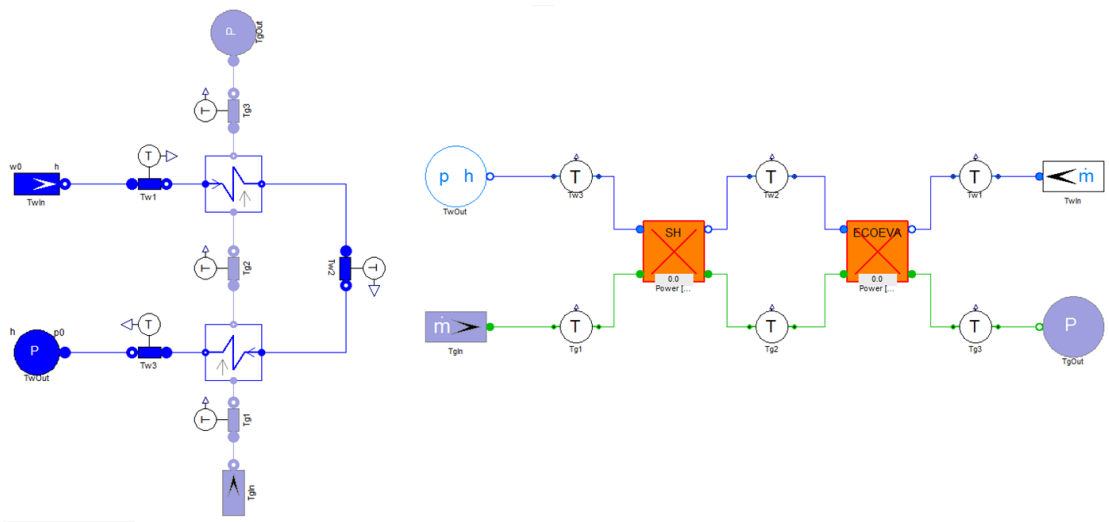

Figure 5.9: Modelica object diagram of the once-through boiler built with ThermoPower (left) and Thermal Power components (right).

A difference of 1.8 % in terms of steam and exhaust gas outlet temperatures, and less than 1 % in term of exchange heat flux is observed when the results computed with the Thermal Power OTB model are compared with the ones in the reference [166]. A difference smaller than 2 % for all the variables is observed when the results of the Modelica models are compared. Obviously, the geometry, correlations, number of fluids and wall volumes and fluids set into the Modelica components are the same in both cases, but the approach followed by the solver to compute the thermodynamic properties, heat transfer coefficients and the heat fluxes is different.

It is thus possible to conclude that the Modelica OTB model (built with ThermoPower library base components) is capable to reproduce the steady state and the dynamic characteristics with reasonable accuracy with water as working fluid.

As well-known in an ORC unit the working fluid is an organic compound, therefore, the model needs to be validated at the design point and part-load conditions with an organic fluid. The fluid (cyclopentane) and geometry computed during the design point optimization phase is imported into the OTB model and the simulation results are compared with the ones computed with an house-made Matlab model.

The two OTB models are run at steady state and offdesign with the following assumptions:

- constant heat transfer coefficients and no pressure drop;
- constant heat transfer coefficients and pressure drop;
- heat transfer coefficients computed with correlations and no pressure drop;
- heat transfer coefficients computed with correlations and pressure drop.

In all these cases the differences in the outlet cyclopentane and exhaust gas temperatures are lower than 1 % and 2 %, respectively. The reason for this discrepancies is the different way of discretizing the once-through boiler. The Modelica model is deeply discretized in terms of fluids and wall volumes, while the Matlab ones is divided only into three sections. On the one hand, a high number of volumes allows to improve the results accuracy but, on the other hand, increases the number of variables and, consequently, reduces the computational speed.

In conclusion, the heat exchanger model implemented in this work can reproduce the steady state, part-load and dynamic characteristics of the once-through boiler with satisfactory accuracy owing to a validation process involving different fluids, open source and commercial tools, and data available in public literature.

Regarding the validation of the **gas turbine** model see Chapter 4.4 for a deep explanation.

5.5 Dynamic Analysis Results

The selected case study is the gas turbine based-power system installed on the Draugen oil and gas offshore platform deeply examined in Chapter 2.2.

It is assumed that the operational range of the gas turbine spans from 20 % to 100 %; this means that the minimum load of the engine is 3 MW. This management

made allows a reasonable margin versus chocking and surging of the compressors serving the gas turbine, as suggested by the GT manufacturer.

The test case selected for the dynamic analysis is the trip of one gas turbine. According to the data provided by the engines manufacturer, the time for the gas turbine trip, i.e. the period from which the failing engine passes from a certain load to zero power, is set equal to 10 seconds. Moreover, preserving the principle of redundancy it is decided to operate the power system so that gas turbine A and the ORC unit share the load with the engine B, while the third gas turbine is on stand-by. Accordingly, the expected reference case foresees that while the normal platform load demand (19 MW) is covered by the combined cycle unit and gas turbine B at some time the engine B trips. The combined cycle unit counteracts by ramping up its load so as to match the total power consumption and to preserve the stability of the grid.

In accordance with the experimental measurements presented in [198, 207], considering the presence of oxygen and impurities, and given that the quality of construction materials is not as in a dedicated test ring, the authors assumed a maximum acceptable temperature ($T_{c,max}$) for the organic compound of 270 °C to avoid fluid decomposition. In this way the thermochemical stability of the fluid is expected to be preserved for the entire lifetime of the unit. Given the aforementioned assumptions, different load ramp rates are tested (0.3–1.0 MW $\cdot$ s^{-1}) so as to estimate the frequency and the temperature trends of cyclopentane during load changes, to detect the grid instability and the hot spot formation in order to propose possible solutions to avoid these issues.

Figure 5.10 shows the temperature trends of cyclopentane at the outlet section of the once-through boiler for different ramp rates of the combined cycle unit. Table 5.4 accordingly reports the peak temperature reached by the metal wall and by the organic compound during each transient event.

The results indicate that the temperature exceeds $T_{c,max}$ for ramp rates higher than 0.3 MW $\cdot$ s^{-1}.

Assuming an upper limit of 270 °C, the temperature of the organic compound exceeds the limit during load variations from 0.4 to 1.0 MW $\cdot$ s^{-1}.

Regarding the long-term effects of this event on thermochemical stability, it is crucial to estimate the amount of time at which the fluid goes beyond the temperature limit. Except for a ramp rate of 0.3 MW $\cdot$ s^{-1}, the time period for which the temperature at the last volume of the OTB remains larger than $T_{c,max}$ is around 8 minutes in the best case (ramp rate of 0.4 MW $\cdot$ s^{-1}) and 18 minutes for the worst scenario (ramp rate of 1.0 MW $\cdot$ s^{-1}).

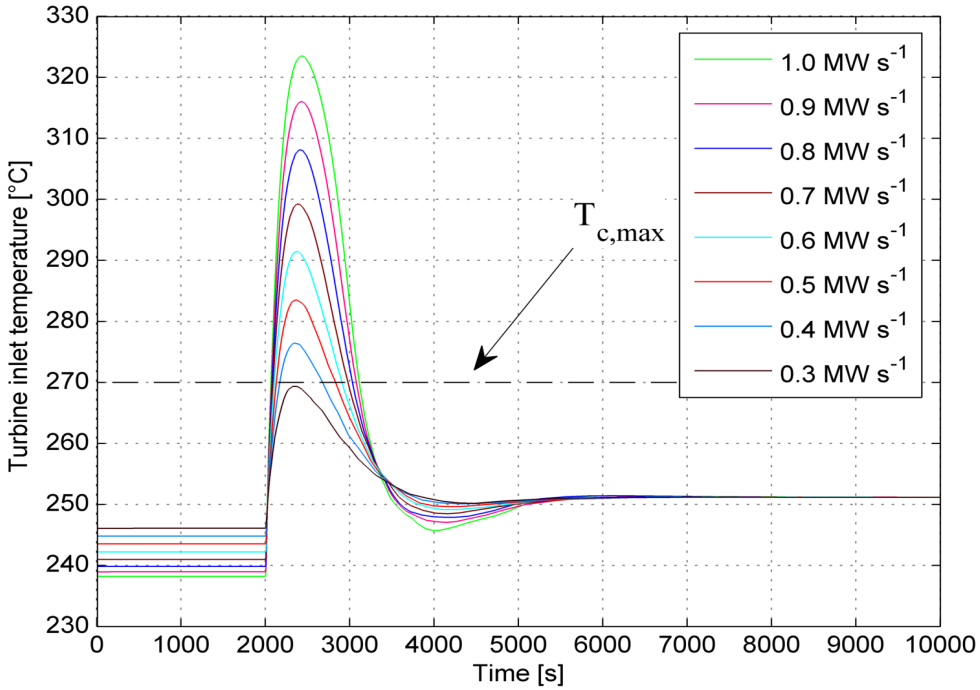

Figure 5.10: Trends of the cyclopentane temperature at the OTB exit section.

Table 5.4: Power produced by the GTs and the ORC unit before GT B' trips and GT A and ORC ramp rate. Metal wall and fluid temperatures in the hottest point of the OTB heat exchanger during the transient period, are also listed.

Load GT A + ORC	**Load GT B**	**Ramp rate**	$\mathbf{T_{wall}}$	$\mathbf{T_{fluid}}$
9 MW	10 MW	1.00 $MW \cdot s^{-1}$	331.32 °C	323.48 °C
10 MW	9 MW	0.90 MW · s^{-1}	324.95 °C	316.01 °C
11 MW	8 MW	0.80 MW · s^{-1}	318.37 °C	308.09 °C
12 MW	7 MW	0.70 MW · s^{-1}	310.89 °C	299.21 °C
13 MW	6 MW	0.60 MW · s^{-1}	304.21 °C	291.47 °C
14 MW	5 MW	0.50 MW · s^{-1}	297.41 °C	283.52 °C
15 MW	4 MW	0.40 MW · s^{-1}	291.22 °C	276.45 °C
16 MW	3 MW	0.30 MW · s^{-1}	284.90 °C	269.36 °C

When integrating an ORC turbogenerator in the power system of an oil and gas platform operating in island, frequency tolerances and recovery time have strict constrains for such stand-alone electric grid. The frequency trends are shown in Figures 5.11 and 5.12.

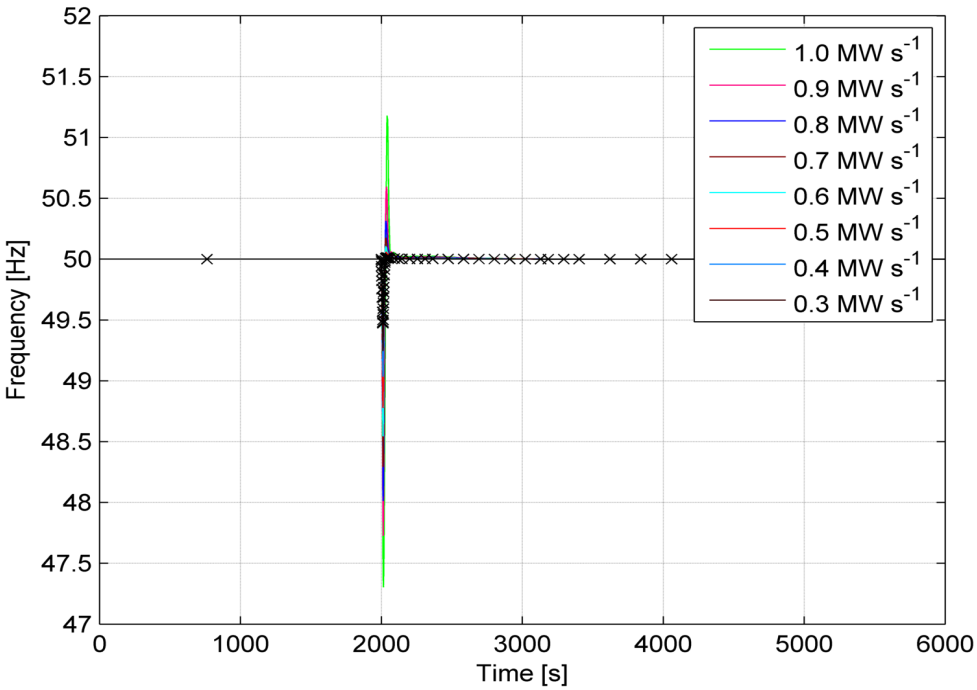

Figure 5.11: Frequency trends with the different ramp rate.

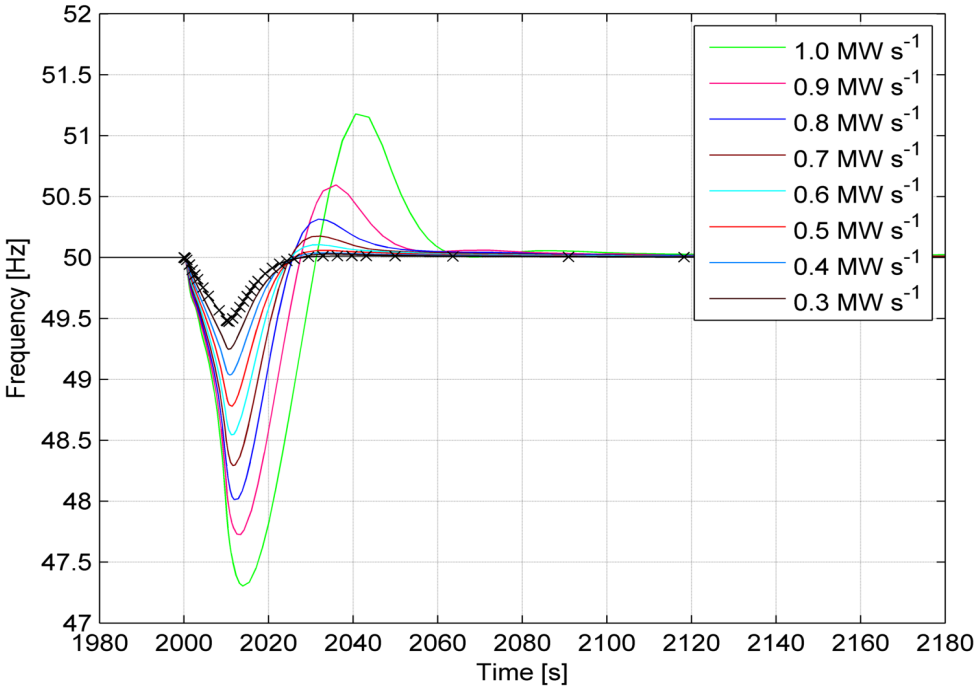

Figure 5.12: Enlargement of the frequency trends with the different ramp rate.

The frequency undershooting (overshooting) is the minimum (maximum) value that the frequency reaches during a load variation, expressed as a percentage of the reference value. The other critical dynamic metric is the rise time, defined as the time required for the frequency to return back to 99 % of the value at steady-state. Figure 5.13 shows the aforementioned quantities for the analysed cases.

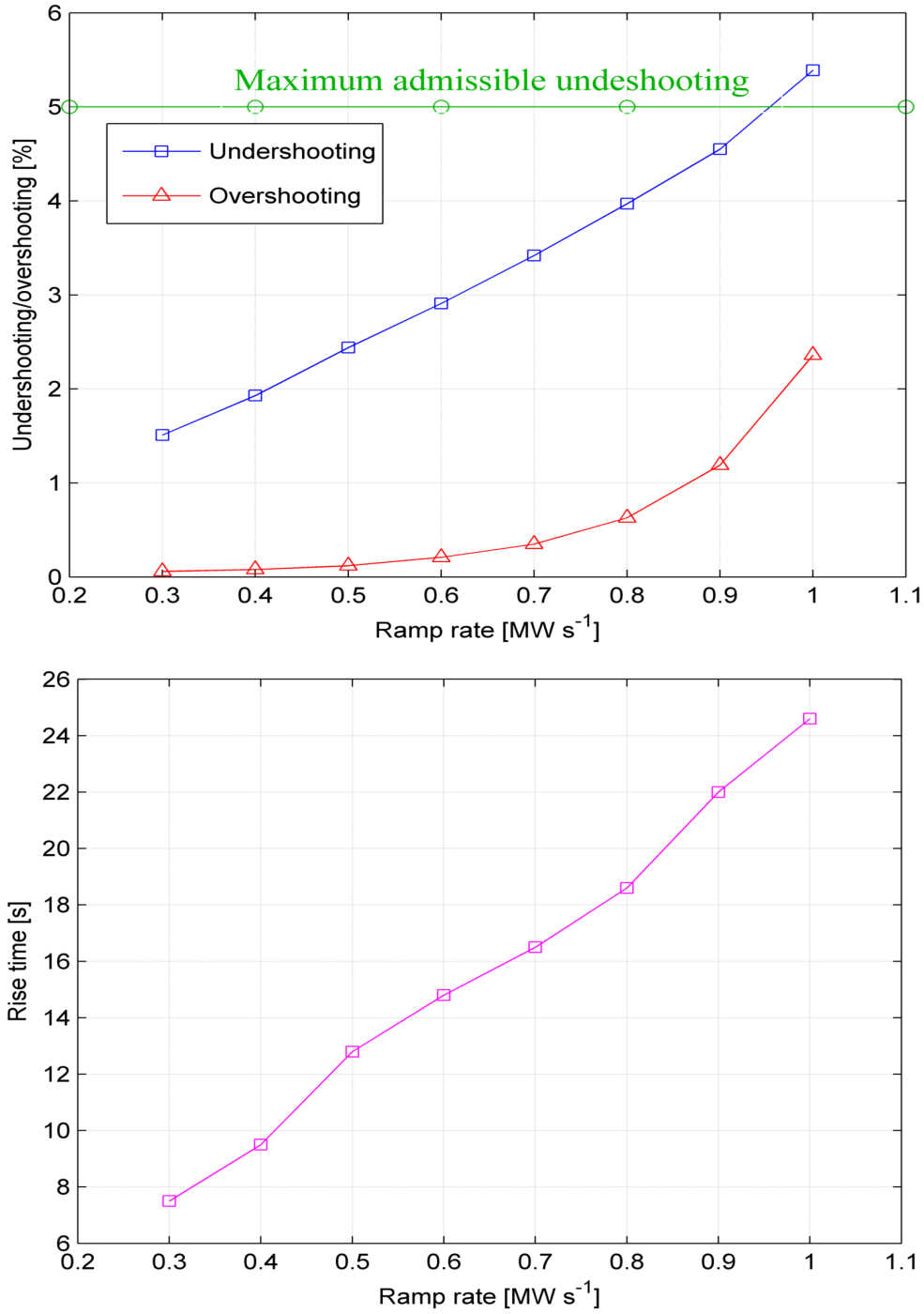

Figure 5.13: Trend of the dynamic metrics with different ramp rate.

Bearing in mind that the platform owner admits a maximum undershooting of 5 %, Table 5.4 and Figure 5.13 unveil that ramp rates equal or larger than 1.0 MW/s are not acceptable as the working fluid temperature exceeds the maximum admissible value by 23.48 °C, and the frequency undershooting is larger than 5 %. In the other cases, the calculated dynamic metrics satisfy the requirements. With the exception of load changes slower than $0.3\,\mathrm{MW} \cdot s^{-1}$, the wall and fluid temperatures at the end of the once-through boiler exceed the decomposition limit, thus increasing the risk of cyclopentane degradation.

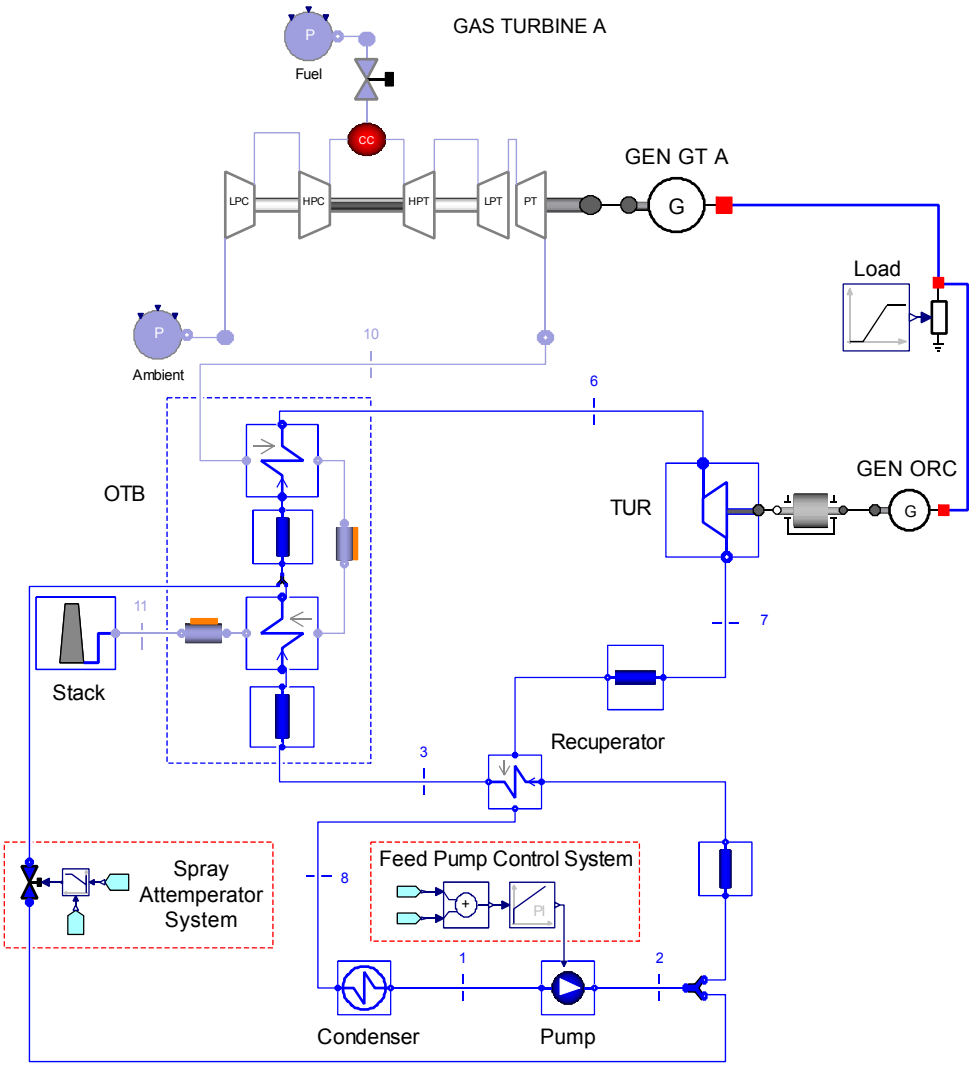

Figure 5.14: Object diagram of the combined plant with the spray attemperator system.

In order to preserve the fluid stability, a spray attemperator system is added to the plant layout (see Figure 5.14) so as to limit the temperature in the superheating section of the once-through boiler. The saturated vapour exiting the preheater-evaporator section is collected into a separator. The measurable temperature nearest to the temperature of the metal wall and of the working fluid in

the terminal part of the OTB is the turbine inlet temperature T_6. If this quantity exceeds the maximum value imposed by the user (in this case 270 °C), the spray attemperator system injects into the separator (see Figure 5.14) a certain quantity of subcooled cyclopentane extracted at the pump outlet. A dedicated valve manoeuvred by a properly tuned PI controller regulates the mass flow rate utilized for this purpose. In the PI controller the measured temperature T_6 is compared with the reference value $T_{c,max}$ and the signal deviation produces the opening/closing of the attemperator valve. As for the previous plant configuration (Figure 5.3), the pump speed is controlled to maintain the exhaust gas temperature exiting the once-through boiler at the design-point value.

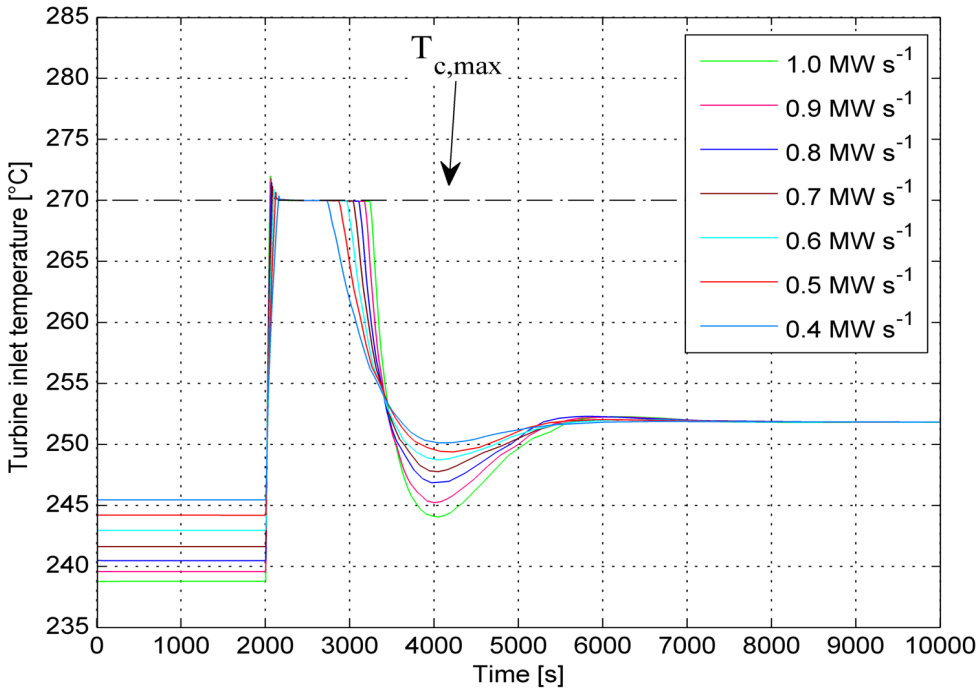

Figure 5.15: Once-through boiler outlet temperature trends with the spray attemperator system.

Figure 5.15 shows the temperature of the working fluid in the final part of the heat exchanger obtained with the new plant configuration. The ramp rate of $0.3\,\mathrm{MW} \cdot \mathrm{s}^{-1}$ is not analysed as the activation of the spray attemperator system is not needed, see Figure 5.10. It can be observed that, with the exception of the first instants of the transient, the controller can maintain the temperature at the reference value, thus preventing hot spot formation and the associated working fluid degradation.

For the sake of completeness, a comparison between the results obtained with and without the spray attemperator system for the same load ramp is presented (see Figure 5.16). The purpose is to demonstrate that the introduction of the

attemperator module does not modify significantly the dynamic response of the plant. The reference case is a ramp rate of 0.6 MW $\cdot$ s^{-1}.

As shown in Figure 5.16(a), the simulations do not reveal any appreciable difference in the two frequency trends. Figure 5.16(b) shows the variation of the mass flow rate entering the once-through boiler, while Figure 5.16(c) reports the pump speed. It is possible to notice that for the configuration with the spray attemperator the mass flow rate decreases, since a fraction of the working fluid leaving the pump deviates towards the attemperator valve so as to be injected in the separator. Maximum differences of 1.15 °C and 0.7 °C are observed for the temperature of the exhaust gases exiting the OTB and for the outlet temperature on the cold-side of the recuperator, see Figure 5.16(d) and Figure 5.16(e). Finally, Figure 5.16(f) shows the two trends for the turbine inlet pressure; for this parameter the difference is less than 20 kPa.

It should be underlined that an in-depth sensitivity analysis is conducted to understand the influence of the integration algorithm on the results, the tolerance and the number of fluid volumes in which the OTB is discretized. It is observed that variations of the resolution algorithm affect the final results by less than 1.0 %. On the other hand, reducing the tolerance from 10^{-4} to 10^{-5} or doubling the number of discretization volumes halves the computational speed of the solver. The maximum deviation for all variables involved in the simulation is lower than 1.0 %.

The tolerance selection is in any case a big issue because, as shown in Figures 5.17, 5.18 and 5.19, can generate discontinuity during the interpolation of fluid tables. For this reason, several simulations with different tolerance, fluids interpolation methods and solver algorithm are conducted in order to find the most accurate results.

5.6 Discussion and Conclusions

The design of organic Rankine cycle power modules conceived for high-temperature waste heat recovery systems needs to consider the chemical deterioration of the working fluid and the frequency fluctuations which can occur during critical transient scenarios typical of stand-alone electric grids. The methodology and tools presented are a first attempt to quantify the amplitude of dynamic events causing frequency undershooting and hot spot formation and to propose measures to tackle such operational issues.

Dynamic simulations performed at different ramp rates highlight that the most

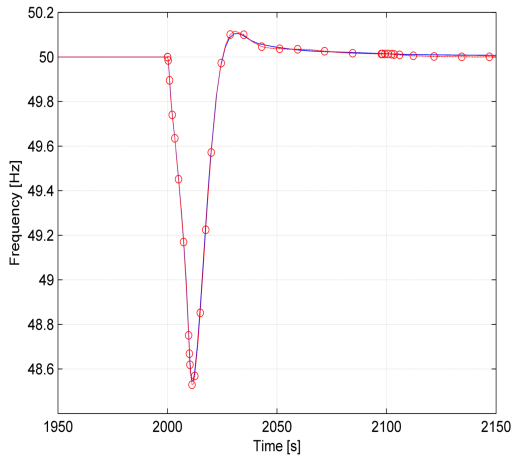

(a) Grid frequency

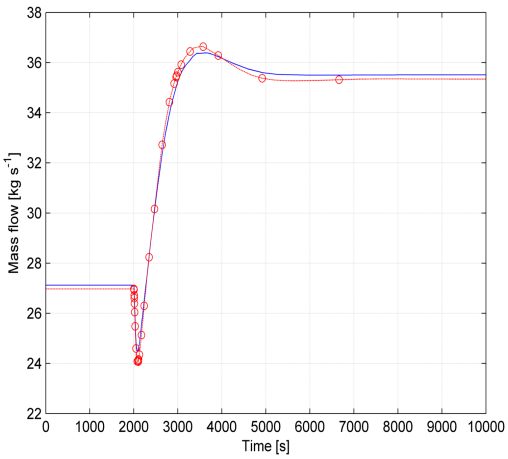

(b) Pump mass flow rate

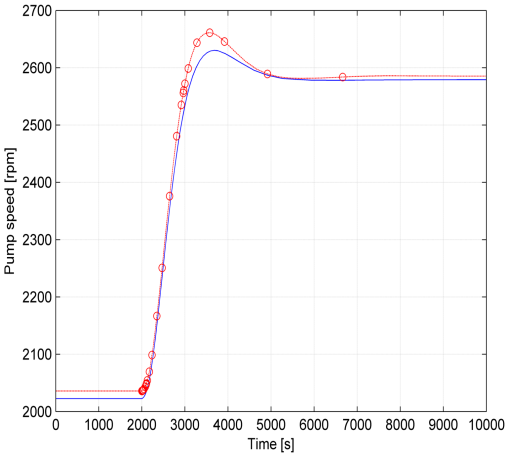

(c) Pump speed

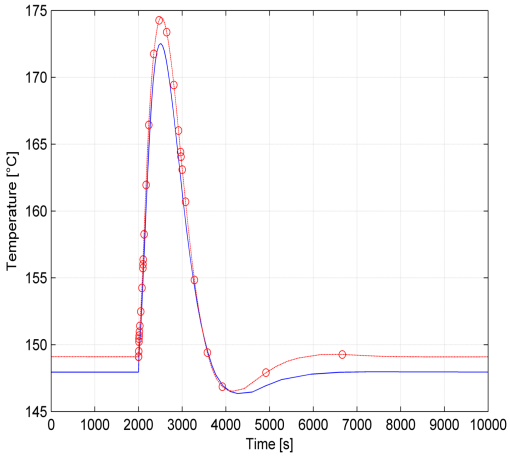

(d) OTB exhaust gases outlet temperature

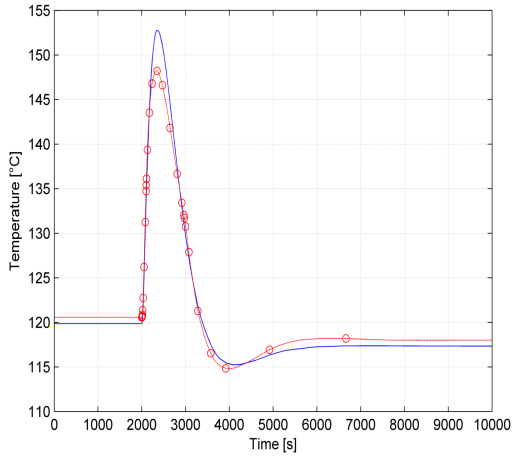

(e) OTB cyclopentane inlet temperature

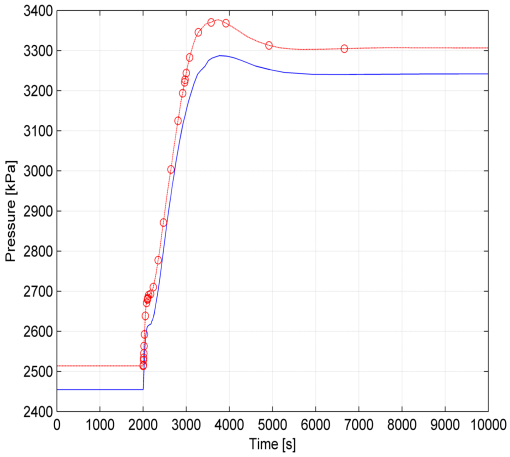

(f) OTB cyclopentane inlet pressure

Figure 5.16: Dynamic response of the combined cycle power plant for the selected test case. The continuous line indicates the parameter related to the plant without spray attemperator unit while the line with "o" marker refers to the parameters of the plant with spray attemperator system.

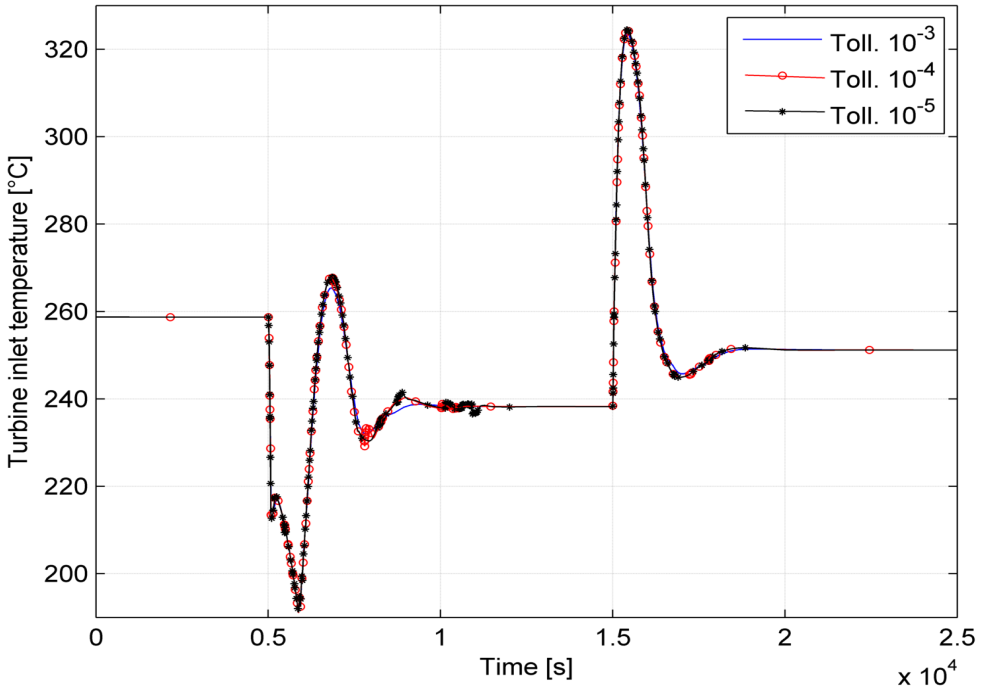

Figure 5.17: Once-through boiler outlet temperature trends with the spray attemperator system.

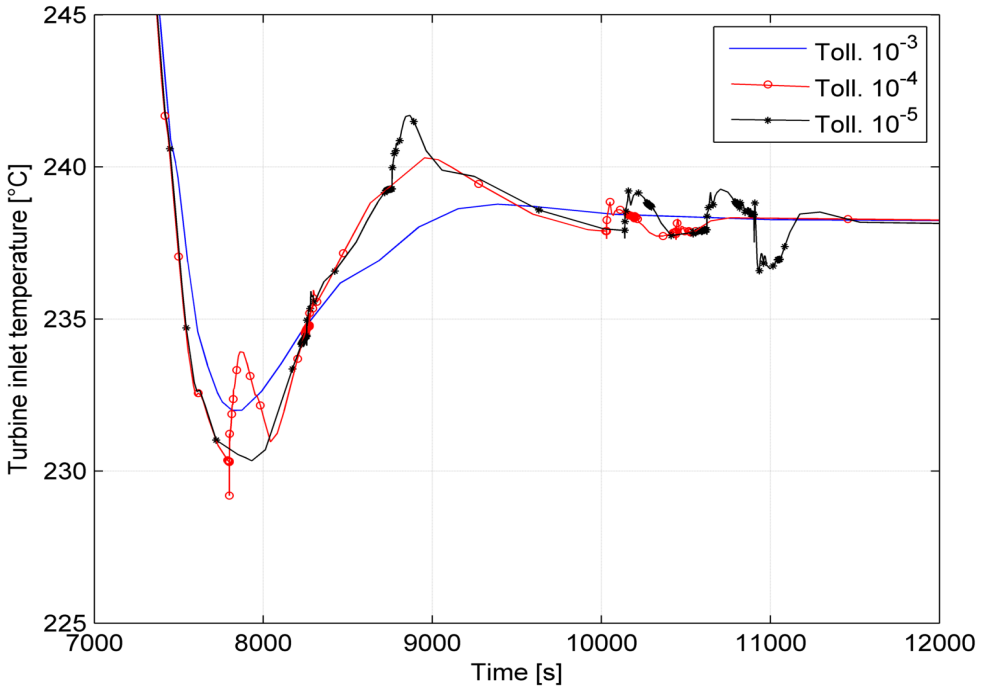

Figure 5.18: Once-through boiler outlet temperature trends with the spray attemperator system.

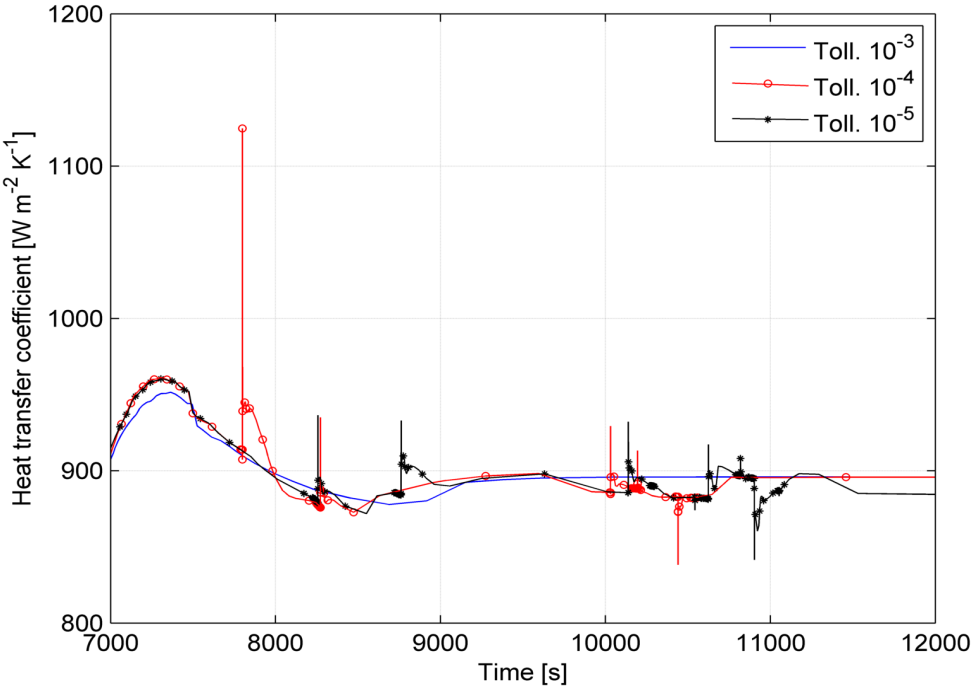

Figure 5.19: Once-through boiler outlet temperature trends with the spray attemperator system.

critical component, where hot spot phenomena are observed, is the once-through boiler. Simulation results suggest that the temperature of the working fluid exceeds the maximum admissible value for ramp rates larger than $0.3\,\mathrm{MW} \cdot \mathrm{s}^{-1}$. Such event becomes more acute during sharp load variations ($> 1.0\,\mathrm{MW} \cdot \mathrm{s}^{-1}$) owing to the longer periods (≈ 20 min) of local overheating of the organic compound.

The insertion of a spray attemperator module with a properly tuned control system has proved to be a valuable measure to maintain the temperature at the terminal section of the once-through boiler under a prefixed value. This device does not affect significantly the dynamics of the process variables and eliminates the risk of hot spot formation even during aggressive load variations by injecting a fraction of the liquid exiting the pump in the superheating section.

No effects on the grid frequency fluctuations are introduced with the insertion of the spray attemperator module. The dynamic simulations show that ramp rates higher than 0.9 MW/s provoke both not admissible frequency undershooting and thermochemical decomposition of the fluid.

In conclusion, the proposed approach and the relative solution are readily applicable to other power systems integrating organic Rankine cycle modules with gas turbines, boilers (fed by fossil and renewable fuels), fuel cells and solar units.

Chapter 6

Conclusions

System dynamic modelling and simulation is becoming a powerful and essential design tool. For this reason, this Ph.D. thesis is devoted to analyse the transient operation conditions' effects using power plant dynamic models.

In the first part of this dissertation, the dynamic analysis is the core of a procedure developed to predict lifetime reduction on traditional power plant devices. In particular, the plant dynamic model, and its capability of evaluating the trends of the main thermodynamic parameters, which describe the plant operation during transient conditions, is the base point to identify the most stressed plant devices.

Being fundamental the role played by combined cycle power plants in the scenario of the liberalized electricity market, a combined cycle power plant is selected as test case. This plant is constituted by a gas turbine and a single pressure heat recovery steam generator.

In order to test the novel procedure and identify the role played by the devices geometry, different plant models (called "TPL" and "TP"), able to simulate design, part-load and dynamic operating conditions, are built in DYMOLA environment.

A comparison among the dynamic analysis results computed with the DYMOLA models (TPL and TP) and MSM model showed that TPL model is able to predict thermodynamic variables with a higher grade of detail due to the implementation of the entire heat exchangers geometry. This brings a higher accuracy during the estimation of the devices lifetime reduction.

To sum up, the proposed procedure can be considered as a valuable innovative tool to assist power plant designers and operators in order to improve the plant's flexibility without excessively compromising the integrity of devices subjected to high thermo-mechanical stresses. Furthermore, another key factor is the user-friendly interface of the life reduction calculation tool and its short run-time in comparison with finite elements analysis tools.

The dynamic analysis is also essential in order to test the possibility of introducing innovative waste heat recovery units within an isolated grid. In particular, after a design optimization process, the dynamic behaviour of gas turbines coupled with waste heat recovery units is tested to verify the grid stability and, in the case of an ORC unit, the working fluid thermochemical stability.

The results of the design optimization process show that the organic Rankine cycle technology exhibits the highest yearly system performance with respect to SRC and ABC, thus enabling to abate CO_2 emissions and pollutants. The steam Rankine cycle technology appears to be favourable from an economic perspective as it allows to achieve the highest net present value while the use of ABC power modules is not attractive from an economic and environmental perspective compared with the other two technologies. For all the three bottoming cycle units the heat exchanger recovering the exhaust gases heat is the heaviest component, while the turbines have the largest share of the total cost of the system. In practice, the steam Rankine cycle and the organic Rankine cycle are competing technologies when targeting at the design of highly-efficient offshore platforms. Advantages in terms of applicability range and system performance seem to lead toward the use of organic Rankine cycle turbogenerators although investment costs have to be reduced to enhance the economic revenue. The implementation of air bottoming cycle units offshore does not appear to be convenient from a performance and economic perspective.

Despite the design optimization process results, a dynamic analysis of a power unit equipped with three gas turbines and an air bottoming cycle turbogenerator is performed. The ABC module is absolutely less efficient than ORC or SRC units but does not require a condensation section, a make up water system or expensive working fluid and operates with a non-flammable, non-toxic and freely available fluid. The dynamic analysis shows that a plant composed by three GTs and an ABC unit is able to cover the normal platform electricity demand but the maximum ramp rate needs to be $0.5\,\mathrm{MW} \cdot \mathrm{s}^{-1}$. Ongoing investigations are carried out to understand the role played by the recuperator inertia.

Being Organic Rankine cycle waste heat recovery units the most promising technology due to high efficiency and low costs, a dynamic analysis of the combined plant is essential to investigate the effects of load changing on the grid and working fluid thermochemical stability.

Dynamic simulations show that the design of organic Rankine cycle power modules conceived for high-temperature waste heat recovery systems needs consider-

ing the chemical deterioration of the working fluid and the frequency fluctuations which can occur during critical transient scenarios typical of stand-alone electric grids.

Dynamic analysis performed at different ramp rates highlights that the most critical component, where hot spot phenomena are observed, is the once-through boiler. Simulation results suggest that the temperature of the working fluid exceeds the maximum admissible value for ramp rates larger than $0.3\,\mathrm{MW} \cdot \mathrm{s}^{-1}$. Such event becomes more acute during sharp load variations ($> 1.0\,\mathrm{MW} \cdot \mathrm{s}^{-1}$) owing to the longer periods (≈ 20 min) of local overheating of the organic compound.

The insertion of a spray attemperator module with a properly tuned control system has proved to be a valuable measure to maintain the temperature at the terminal section of the once-through boiler under a prefixed value. This device does not affect significantly the dynamics of the process variables and eliminates the risk of hot spot formation even during aggressive load variations by injecting a fraction of the liquid exiting the pump in the superheating section. No effects on the grid frequency fluctuations are introduced with the insertion of the spray attemperator module. The dynamic simulations show that ramp rates higher than 0.9 MW/s provoke both not admissible frequency undershooting and thermochemical decomposition of the fluid.

The analysis also confirms that the proposed approach and the relative solution are readily applicable to other power systems integrating organic Rankine cycle modules with gas turbines, boilers (fed by fossil and renewable fuels), fuel cells and solar units.

To sum up, in this dissertation, two different mathematical tools are proposed. In both cases the core is the plant dynamic model. The first tool is able to predict the plant thermodynamic variables and compute the components lifetime reduction caused by load changes while the second one performs a design and optimization of different waste heat recovery units for offshore applications. The entire plant is then dynamically analysed in order to verify the grid stability and, in the case of ORC unit, the working fluid thermochemical stability.

Bibliography

[1] European Parliament and Council of the European Union. Directive 2009/28/EC, 2009.

[2] European Climate Foundation. 2030 framework for climate and energy policies., 2014. Available on: www.ec.europa.eu.

[3] European Climate Foundation. EU Roadmap 2050., 2010. Available on: www.roadmap2050.eu.

[4] European Parliament and Council. Directive 2003/54/EC: Concerning common rules for the internal market in electricity and repealing directive 96/92/EC. Directive, June 2003.

[5] European Parliament and Council. Directive 2009/72/EC: Concerning common rules for the internal market in electricity and repealing directive 2003/54/EC., July 2009.

[6] Department of Energy and International Energy Agency. International energy outlook, 2011. Available on: http://www.eia.gov.

[7] E. D. Delarue, P. J. Luickx, and W. D. D'haeseleer. The actual effect of wind power on overall electricity generation costs and co2 emissions. *ENERGY CONVERSION AND MANAGEMENT*, 50(6):1450–1456, 2009.

[8] M. Bortolini, M. Gamberi, and A. Graziani. Multi-parameter analysis for the technical and economic assessment of photovoltaic systems in the main european union countries. *Energy Conversion and Management*, 74:117, 2013.

[9] G. R. St Pierre. Advanced materials and coatings for energy conversion systems. *ENERGY CONVERSION AND MANAGEMENT*, 38(10-13):1035–1041, 1997.

[10] European Parliament and Council. Directive 2010/75/EU: Industrial emissions (integrated pollution prevention and control)., November 2010.

[11] N. Henkel, E. Schmid, and E. Gobrecht. Operational flexibility enhancements of combined cycle power plants. In *Proceedings of PowerGen Asia*, 2008.

[12] T. S. Kim. Comparative analysis on the part load performance of combined cycle plants considering design performance and power control strategy. *ENERGY*, 29(1):71–85, 2004.

[13] A. Tica, H. Gueguen, D. Dumur, D. Faille, and F. Davelaar. Design of a combined cycle power plant model for optimization. *APPLIED ENERGY*, 98:256–265, 2012.

[14] F. Alobaid, R. Postler, J. Stroehle, B. Epple, and H. G. Kim. Modeling and investigation start-up procedures of a combined cycle power plant. *APPLIED ENERGY*, 85(12):1173–1189, 2008.

[15] T. Akiyama, H. Matsumoto, and K. Asakura. Dynamic simulation and its applications to optimum operation support for advanced combined cycle plants. *ENERGY CONVERSION AND MANAGEMENT*, 38(15-17):1709–1723, 1997.

[16] S. Lu. Dynamic modelling and simulation of power plant systems. *Proceedings of the Institution of Mechanical Engineers, Part A: Journal of Power and Energy*, 213(1):7–19, 1999.

[17] P. Madejski and D. Taler. Analysis of temperature and stress distribution of superheater tubes after attemperation or sootblower activation. *Energy Conversion and Management*, 71:131, 2013.

[18] A. Benato, A. Stoppato, and S. Bracco. Combined cycle power plants: A comparison between two different dynamic models to evaluate transient behaviour and residual life. *Energy Conversion and Management*, 87:1269–1280, 2014.

[19] ASME. Asme code: Boiler and pressure vessel code - section ii, iii, 2001.

[20] British Energy. R5 assessment procedure for the high temperature response of structures, issue 3, 2003.

[21] UNI. UNI EN 12952-5:2011. Water-tube Boilers Standards., 2011.

[22] TRD. TRD 301 annex1 calculation for cyclic loading due to pulsating internal pressure or combined changes of internal pressure and temperature.

[23] A. Stoppato, A. Benato, and A. Mirandola. Assessment of stresses and residual life of plant components in view of life-time extension of power plants. In *Proceedings of ECOS 2012 - The 25th International Conference on Efficiency, Cost, Optimization and Simulation of Energy Conversion Systems and Processes*, volume 4, pages 104–113, June 26-29 2012.

[24] S. Bracco, G. Crosa, and A. Trucco. Dynamic simulator of a combined cycle power plant: Focus on the heat recovery steam generator. *Proceedings of ECOS 2007*, I:189–196, 2007.

[25] P. Heusser, V. Pocajt, and N. Baumann. Key to metals database. Available on: <http://keytometals.com/>.

[26] MATLAB User's Guide. The mathworks. *Inc., Natick, MA*, 5, 1998.

[27] Mathworks. Matlab r2013, 2013. Available on: http://www.mathworks.it/help/matlab/.

[28] European Committee For Standardization. En 13345 part 3, unfired pressure vessels, clause 17; simplified assessment of fatigue life, and clause 18; detailed assessment of fatigue life, May 2002.

[29] ASTM. Astm e 1049: 85 standard practices for cycle counting in fatigue analysis, 1997.

[30] H. Elmqvist, D. Bruck, and M. Otter. *Dymola - User's Manual*. Lund, Sweden, 1996.

[31] Dassault Systemes AB. Dymola, 2014. Available on: www.3ds.com.

[32] P. Fritzson and V. Engelson. Modelica - a unified object-oriented language for system modeling and simulation. In *ECOOP 98 - Object-Oriented Programming*, pages 67–90. Springer, 1998.

[33] H. Elmqvist, S. E. Mattsson, and M. Otter. Modelica: The new object-oriented modeling language. In *12th European Simulation Multiconference*, 1998.

[34] P. Fritzson. *Principles of Object-Oriented Modeling and Simulation with Modelica 2.1*. John Wiley & Sons, Inc., Piscataway, United States of America, 2003. ISBN: 9780470937617.

[35] Modelon AB. Thermal power library, 2014. Available on: www.3ds.com.

[36] F. Casella, M. Otter, K. Proelss, C. Richter, and H. Tummescheit. The modelica fluid and media library for modeling of incompressible and compressible thermo-fluid pipe networks, 2006.

[37] F. Casella and A. Leva. Modelling of thermo-hydraulic power generation processes using Modelica. *Mathematical and Computer Modeling of Dynamical Systems*, 12(1):19–33, Feb. 2006.

[38] F. Casella and A. Leva. Thermopower library: Open library for thermal power plant simulation., 2014.

[39] F. Casella, T. Mathijssen, P. Colonna, and J. Van Buijtenen. Dynamic modeling of ORC power systems. *Journal of Engineering for Gas Turbines and Power*, 135:1–12, 2012.

[40] G. Lozza. *Turbine a gas e cicli combinati*. Progetto Leonargo - Società editrice esculapio srl, 2006.

[41] Siemens AG Energy Sector. Gas turbines, 2014. Available on: www.energy.siemens.com.

[42] J. Kurzke. *Component map collection 2, Compressor and turbine maps for gas turbine performance computer programs.* Germany, 2004. Available on: www.gasturb.de.

[43] J. Kurzke. How to create a performance model of a gas turbine from a limited amount of information. In *Proceedings of ASME Turbo Expo 2005*, pages 145–153, Reno-Tahoe, United States of America, June 2005.

[44] A. Stodola. *Dampf- und Gasturbinen: Mit einem Anhang über die Aussichten der Wärmekraftmaschinen*. Springer Berlin, Berlin, Germany, 1922. ISBN: 7352997563.

[45] M. Schobeiri. *Turbomachinery flow physics and dynamic performance*. Springer Berlin, Berlin, Germany, 2005. ISBN: 9783540223689.

[46] F. Haglind and B. Elmegaard. Methodologies for predicting the part-load performance of aero-derivative gas turbines. *Energy*, 34(10):1484–1492, 2009.

[47] S. M. Camporeale, A. Dumas, and B. Fortunato. Dynamic modelling of recuperative gas turbine. In *Proceedings of the Institution of Mechanical*

Engineers, Part A: Journal of Power and Energy, volume 3, pages 231–225. Professional Engineering Publishing, 2000.

[48] W. Wagner and B. Rukes. IAPWS-IF97: The new industrial formulation. *BRENNSTOFF-WARME-KRAFT*, 50(3):42, 1998.

[49] V. Gnielinski. New equation for heat and mass transfer in turbulent pipe and channel flow. *International Chemical Engineering*, 16:359–368, 1976.

[50] Verein Deutscher Ingenieure. *VDI-Wärmeatlas: Berechnungsblätter für den Wärmeübergang*. Springer-Verlag, Berlin, Germany, 1953. ISBN: 9783540412014.

[51] B. S. Petukhov. Heat transfer and friction in turbulent pipe flow with variable physical properties. *Advances in heat transfer*, 6(503):i565, 1970.

[52] H. Hausen. Equation for calculation of heat transmission in crosscurrent on boiler tubes. *CHEMIE INGENIEUR TECHNIK*, 42(16):1058–&, 1970.

[53] P. K. Konakov, S. S. Filimonov, and B. A. Khrustalev. Calculation of heat exchange in boiler furnaces. *Teploenergetika*, 4(8):48–53, 1957.

[54] ESCOA. *ESCOA Turb-X HF Rating Instructions*. ESCOA, 1979.

[55] A. Nir. Heat transfer and friction factor correlations for crossflow over staggered finned tube banks. *Heat Transfer Engineering*, 12(1):43–58, 1991.

[56] C. Weirman. Correlations ease the selection of finned tubes. *Oil Gas J*, 74(36):94–100, 1976.

[57] L. Pierobon, E. Casati, F. Casella, F. Haglind, and P. Colonna. Design methodology for flexible energy conversion systems accounting for dynamic performance. *Energy*, 68:667–679, 2014.

[58] F. P. Incropera, A. S. Lavine, and D. P. DeWitt. *Fundamentals of heat and mass transfer*. John Wiley and Sons, 2011. ISBN: 9780471457282.

[59] J. M. Coulson, J. F. Richardson, and J. R. Backhurst. *Coulson and Richardson's Chemical Engineering*. Chemical engineering. Butterworth-Heinemann, Oxford, Great Britain, 1999. ISBN: 9780750644440.

[60] A. Ongiro, V. I. Ugursal, A. M. AlTaweel, and J. D. Walker. Modeling of heat recovery steam generator performance. *APPLIED THERMAL ENGINEERING*, 17(5):427–446, 1997.

[61] P. J. Dechamps. Modeling the transient-behavior of heat-recovery steam-generators. *PROCEEDINGS OF THE INSTITUTION OF MECHANICAL ENGINEERS PART A-JOURNAL OF POWER AND ENERGY*, 209(4):265–273, 1995.

[62] N. Hegde, I. Han, T. W. Lee, and R. P. Roy. Flow and heat transfer in heat recovery steam generators. *JOURNAL OF ENERGY RESOURCES TECHNOLOGY-TRANSACTIONS OF THE ASME*, 129(3):232–242, 2007.

[63] F. Alobaid, S. Pfeiffer, B. Epple, C. Y. Seon, and H. G. Kim. Fast start-up analyses for benson heat recovery steam generator. *ENERGY*, 46(1):295–309, 2012.

[64] S. Sanaye and M. Rezazadeh. Transient thermal modelling of heat recovery steam generators in combined cycle power plants. *INTERNATIONAL JOURNAL OF ENERGY RESEARCH*, 31(11):1047–1063, 2007.

[65] F. C. Knopf. *Modeling, analysis, and optimization of process and energy systems*. Wiley, 2012.

[66] M. Holmgren. X steam for matlab, 2006. Available on: www.x-eng.com.

[67] J. I. Steinfeld. Climate change and energy options: Decision making in the midst of uncertainty. *ACS Division of Fuel Chemistry, Preprints*, 45(1):139–142, 2000.

[68] K. S. Ng, N. Zhang, and J. Sadhukhan. Techno-economic analysis of polygeneration systems with carbon capture and storage and co2 reuse. *CHEMICAL ENGINEERING JOURNAL*, 219:96–108, 2013.

[69] M. De Paepe. Situation of the ORCNext project. In *International Symposium on Advanced Waste Heat Valorization Technologies*, Kortrijk, Belgium, September 13 – 14 2012.

[70] U.S. Department of Energy. Waste heat recovery: Technology and opportunities in u.s. industry. Technical report, U.S. Department of Energy, 2008.

[71] F. Campana, M. Bianchi, L. Branchini, A. De Pascale, A. Petto, M. Baresi, A. Fermi, N. Rossetti, and R. Vescovo. ORC waste heat recovery in European energy intensive industries: Energy and GHG savings. *Energy Conversion and Management*, 76:244–252, 2013.

[72] T. V. Nguyen, L. Pierobon, B. Elmegaard, F. Haglind, P. Breuhaus, and M. Voldsund. Exergetic assessment of energy systems on North Sea oil and gas platforms. *Energy*, 62(0):23 – 36, 2013.

[73] Ministry of the Environment. The Government is following up on the Climate Agreement, 2013. Available on: www.regjeringen.no/en/dep/md/press-centre/Press-releases/2012/the-government-is-following-up-on-the-cl.html?id=704137.

[74] L. Pierobon, A. Benato, E. Scolari, F. Haglind, and A. Stoppato. Waste heat recovery technologies for offshore platforms. *Applied Energy*, 136(0):228 – 241, 2014.

[75] Eoos. The Eoos Project, 2010. Available on: http://eoos.no/index.html.

[76] Shell Norge. Available on: <http://www.shell.no/>.

[77] A. Benato, A. Stoppato, L. Pierobon, and F. Haglind. Dynamic performance of a combined gas turbine and air bottoming cycle plant for off-shore applications. In *Proceedings of the ASME 2014 12th Biennial Conference on Engineering Systems Design and Analysis*, June 25-27 2014.

[78] Siemens AG Energy Sector. SGT-500 Industrial Gas Turbine, 2011. Available on: http://www.energy.siemens.com.

[79] Siemens AG Energy Sector. Gas turbine sgt-500, 2014. Available on: http://www.energy.siemens.com/hq/en/fossil-power-generation/gas-turbines/sgt-500.htm.

[80] T. V. Nguyen, T. Jacyno, and P. Breuhaus. Thermodynamic analysis of an upstream petroleum plant operated on a mature field. *Energy*, 68:454, 2014.

[81] R. J. Krane and Ed. ASME. *Thermodynamics and the Design, Analysis, and Improvement of Energy Systems 1995*. ASME, 1995.

[82] B. F. Tchanche, G. Lambrinos, A. Frangoudakis, and G. Papadakis. Low-grade heat conversion into power using organic rankine cycles - a review of various applications. *Renewable and Sustainable Energy Reviews*, 15(8):3963–3979, 2011.

[83] E. Wali. Optimum working fluids for solar powered rankine-cycle cooling of buildings. *SOLAR ENERGY*, 25(3):235–241, 1980.

[84] M. Badami and M. Mura. Preliminary design and controlling strategies of a small-scale wood waste rankine cycle (rc) with a reciprocating steam engine (se). *ENERGY*, 34(9):1315–1324, 2009.

[85] P. Kloster. Energy optimization on offshore installations with emphasis on offshore combined cycle plants. In *Offshore Europe Conference*, pages 1–9, Aberdeen, Great Britain, 7-9 September 1999. Society of Petroleum Engineers.

[86] L. O. Nord and O. Bolland. Steam bottoming cycles offshore-challenges and possibilities. *Journal of Power Technologies*, 92(3):201–207, 2012.

[87] W. M. Farrell. Air cycle thermodynamic conversion system, 1988.

[88] W. M. Farrell. Air cycle thermodinamic convertion system, 1992.

[89] J. Pettersen. Bunnprosesser for gassturbin-hraftverk (bottoming cycles for gas turbine power plant. Diploma thesis, Norwegian institute of technology, 1987.

[90] Y. S. H. Najjar and M. S. Zaamout. Performance analysis of gas turbine air-bottoming combined system. *Energy Conversion and Management*, 37(4):399 – 403, 1996.

[91] M. Korobitsyn. Industrial applications of the air bottoming cycle. *Energy Conversion and Management*, 43(9):1311 – 1322, 2002.

[92] M. Ghazikhani, M. Passandideh-Fard, and M. Mousavi. Two new high-performance cycles for gas turbine with air bottoming. *Energy*, 36(1):294 – 304, 2011.

[93] M. Ghazikhani, I. Khazaee, and E. Abdekhodaie. Exergy analysis of gas turbine with air bottoming cycle. *Energy*, 72(0):599 – 607, 2014.

[94] C. Carcasci, F. Costanzi, and B. Pacifici. Performance analysis in off-design condition of gas turbine air-bottoming combined system. *Energy Procedia*, 45(0):1037 – 1046, 2014. ATI 2013 - 68th Conference of the Italian Thermal Machines Engineering Association.

[95] O. Bolland, M. Forde, and B. Hånde. Air bottoming cycle: use of gas turbine waste heat for power generation. *Journal of engineering for gas turbines and power*, 118:359–368, 1996.

[96] H. J. Richter. Thermodynamics and the design, analysis, and improvement of energy systems. *American Society of Mechanical Engineers, Advanced Energy Systems Division (Publication) AES*, 30, 1993.

[97] M. Korobitsyn. Industrial applications of the air bottoming cycle. *ENERGY CONVERSION AND MANAGEMENT*, 43(9-12):1311–1322, 2002.

[98] K. A. Tveitaskog and F. Haglind. Optimization of advanced liquid natural gas-fuelled combined cycle machinery systems for a high-speed ferry. *PROCEEDINGS OF THE ASME TURBO EXPO 2012, VOL 5*, pages 329–338, 2012.

[99] W. M. Kays and A. L. London. *Compact heat exchangers*. McGraw-Hill, New York, United States of America, 1984. ISBN: 9780070333918.

[100] O. Genceli. *Heat exchangers*. Birsen Book Company, Turkey, 1999. ISBN: 9789755112183.

[101] F. P. Incropera, D. P. DeWitt, T. L. Bergman, and A. S. Lavine. *Fundamentals of Heat and Mass Transfer*. John Wiley & Sons, Inc., Jefferson City, United States of America, 6 edition, 2007. ISBN: 9780470501979.

[102] K. L. Douglas. *Handbook of sulfuric acid manufacturing*. Engineering, 1961.

[103] T. C. Hung, T. Y. Shai, and S. K. Wang. A review of organic rankine cycles (orcs) for the recovery of low-grade waste heat. *ENERGY*, 22(7):661–667, 1997.

[104] W. C. Andersen and T. J. Bruno. Rapid screening of fluids for chemical stability in organic rankine cycle applications. *INDUSTRIAL and ENGINEERING CHEMISTRY RESEARCH*, 44(15):5560–5566, 2005.

[105] M. S. Orosz. Small scale solar orc system for distributed power in lesotho. *29th ISES Biennial Solar World Congress 2009, ISES 2009*, 2:1042–1048, 2009.

[106] A. M. Delgado-Torres and L. Garcia-Rodriguez. Analysis and optimization of the low-temperature solar organic rankine cycle (ORC). *ENERGY CONVERSION AND MANAGEMENT*, 51(12):2846–2856, 2010.

[107] T. Guo, H. X. Wang, and S. J. Zhang. Selection of working fluids for a novel low-temperature geothermally-powered orc based cogeneration system. *ENERGY CONVERSION AND MANAGEMENT*, 52(6):2384–2391, 2011.

[108] R. Rayegan and Y. X. Tao. A procedure to select working fluids for solar organic rankine cycles (orcs). *RENEWABLE ENERGY*, 36(2):659–670, 2011.

[109] E. Bocci, M. Villarini, L. Bove, S. Esposto, and V. Gasperini. Modeling small scale solar powered orc unit for standalone application. *Mathematical Problems in Engineering*, page 124280, 2012.

[110] Z. Wang, S. He, J. Li, and G. Song. Modeling and testing a screw expander integrated into a trilateral flash cycle. *MANUFACTURING SCIENCE AND TECHNOLOGY, PTS 1-8*, 383-390(383-390):727–733, 2012.

[111] A. Amoresano, S. Meo, and G. Langella. Cycle efficiency optimization for orc solar plants. *International Review of Mechanical Engineering*, 7(5):888–894, 2013.

[112] F. Ferrara, A. Luongo, and A. Gimelli. Small-scale concentrated solar power (csp) plant: Orcs comparison for different organic fluids. *Energy Procedia*, 45:217–226, 2013.

[113] H. Ozcan and I. Dincer. Thermodynamic analysis of an integrated sofc, solar orc and absorption chiller for tri-generation applications. *FUEL CELLS*, 13(5):781–793, 2013.

[114] R. Marshall. Ocean thermal energy conversion. *Sunworld*, 9(4):119–121, 128, 1985.

[115] G. C. Nihous. A preliminary assessment of ocean thermal energy conversion resources. *Journal of Energy Resources Technology*, 129(1):10–17, 2007.

[116] R. Magesh. Otec technology- a world of clean energy and water. *WCE 2010 - World Congress on Engineering 2010*, 2:1618–1623, 2010.

[117] A. Etemadi, A. Emdadi, O. AsefAfshar, and Y. Emami. Electricity generation by the ocean thermal energy. *Energy Procedia*, 12:936–943, 2011.

[118] W. min Liu, F. Y. Chen, Y. Q. Wang, and J. G. Zhang. Progress of closed-cycle otec and study of a new cycle of otec. *Advanced Materials Research*, 354-355(1):275–278, 2011.

[119] A. Borsukiewicz-Gozdur and W. Nowak. Maximising the working fluid flow as a way of increasing power output of geothermal power plant. *APPLIED THERMAL ENGINEERING*, 27(11-12):2074–2078, 2007.

[120] L. Y. Bronicki. Organic rankine cycles in geothermal power plants 25 years of ormat experience. *Transactions - Geothermal Resources Council*, 31:499–502, 2007.

[121] M. Aneke, B. Agnew, and C. Underwood. Performance analysis of the chena binary geothermal power plant. *APPLIED THERMAL ENGINEERING*, 31(10):1825–1832, 2011.

[122] T. Guo, H. X. Wang, and S. J. Zhang. Fluids and parameters optimization for a novel cogeneration system driven by low-temperature geothermal sources. *ENERGY*, 36(5):2639–2649, 2011.

[123] Z. Huan-lai, S. Shang-ming, H. Chun-bo, and F. Xiao-meng. Study on the oilfield produced water geothermal resource utilization. *Advanced Materials Research*, 524-527(2):1284–1288, 2012.

[124] T. Li, J. Zhu, and W. Zhang. Cascade utilization of low temperature geothermal water in oilfield combined power generation, gathering heat tracing and oil recovery. *APPLIED THERMAL ENGINEERING*, 40:27–35, 2012.

[125] T. Li, J. Zhu, and W. Zhang. Comparative analysis of series and parallel geothermal systems combined power, heat and oil recovery in oilfield. *APPLIED THERMAL ENGINEERING*, 50(1):1132–1141, 2013.

[126] P. Thonhofer, E. Reisenhofer, and I. Obernberger. Description and evaluation of the new orc process. *Euroheat and Power/Fernwarme International*, 31(10):18–25, 2002.

[127] I. Obernberger and M. Gaia. Biomass-power-heat coupling based on the orc process - state-of-the-art and possibilities for process optimization, biomasse - kraft-warme-kopplung auf basis des orc-prozesses - stand der technik und molichkeiten der prozessoptimierung. *VDI Berichte*, 1(1891):131–148, 2005.

[128] I. Obernberger, F. Biedermann, P. Thonhofer, M. Gaia, and R. Bini. New small scale organic rankine cycle (orc) technology (200 kw electrical) for decentralized biomass power and heat coupling facility, neue klein-orc-technologie (200 kwel) fur dezentrale biomasse-kwk-anlagen. *VDI Berichte*, 1(2044):133–149, 2008.

[129] A. Rentizelas, S. Karellas, E. Kakaras, and I. Tatsiopoulos. Comparative techno-economic analysis of orc and gasification for bioenergy applications. *ENERGY CONVERSION AND MANAGEMENT*, 50(3):674–681, 2009.

[130] G. Qiu, Y. Shao, J. Li, H. Liu, and S. B. Riffat. Experimental investigation of a biomass-fired orc-based micro-chp for domestic applications. *FUEL*, 96(1):374–382, 2012.

[131] V. Chawla and P. S. Bundela. Sustainable development through waste heat recovery. *American Journal of Environmental Sciences*, 6(1):83–89, 2010.

[132] M. Aneke, B. Agnew, and C. Underwood. Power generation from waste heat in a food processing application. *Applied Thermal Engineering*, 36:171, 2012.

[133] B. F. Tchanche, S. Quoilin, S. Declaye, G. Papadakis, and V. Lemort. Economic feasibility study of a small scale organic rankine cycle system in waste heat recovery application. *PROCEEDINGS OF THE ASME 10TH BIENNIAL CONFERENCE ON ENGINEERING SYSTEMS DESIGN AND ANALYSIS, 2010, VOL 1*, pages 249–256, 2010.

[134] J. Bao and L. Zhao. A review of working fluid and expander selections for organic rankine cycle. *Renewable and Sustainable Energy Reviews*, 24:325, 2013.

[135] T. C. Hung. Waste heat recovery of organic rankine cycle using dry fluids. *Energy Conversion and Management*, 42(5):539–553, 2001.

[136] B. T. Liu, K. H. Chien, and C. C. Wang. Effect of working fluids on organic rankine cycle for waste heat recovery. *ENERGY*, 29(8):1207–1217, 2004.

[137] N. B. Desai and S. Bandyopadhyay. Process integration of organic rankine cycle. *ENERGY*, 34(10):1674–1686, 2009.

[138] S. Quoilin. *Sustainable energy convertion through the use of organic Rankine cylces for waste heat recovery and solar applications.* PhD thesis, University of Liege, 2011.

[139] G. Qiu. Selection of working fluids for micro-chp systems with orc. *RENEWABLE ENERGY*, 48:565–570, 2012.

[140] B. F. Tchanche, M. Pétrissans, and G. Papadakis. Heat resources and organic rankine cycle machines. *Renewable and Sustainable Energy Reviews*, 39:1185, 2014.

[141] S. B. Riffat, V. M. Nguyen, and P. S. Doherty. Development of a prototype low-temperature rankine cycle electricity generation system. *Applied Thermal Engineering*, 21(2):169–181, 2001.

[142] A. Hoshi and T. S. Saitoh. Proposed solar rankine cycle system with phase change steam accumulator and cpc solar collector. *Proceedings of the Intersociety Energy Conversion Engineering Conference*, pages 725–730, 2002.

[143] A. M. Abu-Zour, S. B. Riffat, and M. Gillott. New design of solar collector integrated into solar louvres for efficient heat transfer. *APPLIED THERMAL ENGINEERING*, 26(16):1876–1882, 2006.

[144] X. D. Wang, L. Zhao, and J. L. Wang. Experimental investigation on the low-temperature solar rankine cycle system using r245fa. *ENERGY CONVERSION AND MANAGEMENT*, 52(2):946–952, 2011.

[145] E. H. M. Kane. *Integration et optimisation thermoeconomique et environemique de centrales thermiques solaires hybrides*. PhD thesis, Ecole Polytechnique Federale de Lausane, 2002.

[146] V. Lemort. Contribution to the characterization of scroll machines in compressor and expander modes. 2008.

[147] S. Quoilin, V. Lemort, and J. Lebrun. Experimental study and modeling of an organic rankine cycle using scroll expander. *APPLIED ENERGY*, 87(4):1260–1268, 2010.

[148] A. I. Kalina. Combined cycle system with novel bottoming cycle. *MECHANICAL ENGINEERING*, 106(7):88–88, 1984.

[149] A. I. Kalina and M. Tribus. Advances in kalina cycle technology (1980-1991) .1. development of a practical cycle. *ENERGY FOR THE TRANSITION AGE*, pages 97–110, 1992.

[150] A. I. Kalina and M. Tribus. Advances in kalina cycle technology (1980-1991) .2. iterative improvements. *ENERGY FOR THE TRANSITION AGE*, pages 111–124, 1992.

[151] L.J. Peletz and M.C. Tanca. Refurbishing conventional power plants for kalina cycle operation, March 14 2000. US Patent 6,035,642.

[152] X. Zhang, M. He, and Y. Zhang. A review of research on the kalina cycle. *RENEWABLE and SUSTAINABLE ENERGY REVIEWS*, 16(7):5309–5318, 2012.

[153] T. Coetsee. Kalina cycle. *Process and Control Engineering*, 46(5):34–36, 1993.

[154] L. Lazzeri, F. Diotti, M. Bruzzone, and M. Scala. Applications of kalina cycle to geothermal applications. *Proceedings of the American Power Conference*, 57-1:370–373, 1995.

[155] L. J. Peletz, C. Bozzuto, and D. Norris. Repowering a pulverized coal unit with system 19 kalina cycle. *IEEE Power Engineering Review*, 17(6):6–, 1997.

[156] Z. Jialing, L. Zhiyong, Z. Wei, and F. Wencheng. Kalina cycle of geothermal power production. *Science and Technology Review*, 30(32):46–50, 2012.

[157] I. K. Smith. Development of the trilateral flash cycle system .part 1. fundamental considerations. *PROCEEDINGS OF THE INSTITUTION OF MECHANICAL ENGINEERS PART A-JOURNAL OF POWER AND ENERGY*, 207(A3):179–194, 1993.

[158] I. K. Smith and R. P. M. da Silva. Development of the trilateral flash cycle system. part 2: Increasing power output with working fluid mixtures. *Proceedings of the Institution of Mechanical Engineers, Part A: Journal of Power and Energy*, 208(2):135–144, 1994.

[159] A. Date, F. Alam, A. Khaghani, and A. Akbarzadeh. Investigate the potential of using trilateral flash cycle for combined desalination and power generation integrated with salinity gradient solar ponds. *INTERNATIONAL ENERGY CONGRESS 2012*, 49:42–49, 2012.

[160] Y. Yang, L. Yang, X. Du, Y. Zhou, and C. Guo. Supercritical CO2 rankine cycle using low and medium temperature heat sources. *ASME 2013 7th Int. Conf. on Energy Sustainability Collocated With the ASME 2013 Heat Transfer Summer Conf. and the ASME 2013 11th Int. Conf. on Fuel Cell Science, Engineering and Technology, ES 2013*, 2013.

[161] Y. M. Kim, C. G. Kim, and D. Favrat. Transcritical or supercritical CO2 cycles using both low- and high-temperature heat sources. *ENERGY*, 43(1):402–415, 2012.

[162] H. Yamaguchi, X. R. Zhang, K. Fujima, M. Enomoto, and N. Sawada. Solar energy powered Rankine cycle using supercritical CO2. *APPLIED THERMAL ENGINEERING*, 26(17-18):2345–2354, 2006.

[163] J. Wang, Z. Sun, Y. Dai, and S. Ma. Parametric optimization design for supercritical CO_2 power cycle using genetic algorithm and artificial neural network. *APPLIED ENERGY*, 87(4):1317–1324, 2010.

[164] K. C. Cotton. *Evaluating and improving steam turbine performance*. Cotton Fact, Rexford, United States of America, 1998. ISBN: 9780963995513.

[165] I. H. Bell, J. Wronski, S. Quoilin, and V. Lemort. Pure and pseudo-pure fluid thermophysical property evaluation and the open-source thermophysical property library CoolProp. *Industrial & Engineering Chemistry Research*, 53(6):2498–2508, 2014.

[166] M. N. Dumont and G. Heyen. Mathematical modelling and design of an advanced once-through heat recovery steam generator. *Computers & Chemical Engineering*, 28(5):651–660, 2004.

[167] V. Gnielinski. On heat transfer in tubes. *International Journal of Heat and Mass Transfer*, 63(0):134 – 140, 2013.

[168] M. M. Shah. Chart correlation for saturated boiling heat transfer: equations and further study. *ASHRAE Transaction*, 88(1):185–196, 1982.

[169] L. Friedel. Pressure drop during gas/vapor-liquid flow in pipes. *International Chemical Engineering*, 20(3):352–367, 1980.

[170] S. Z. Rouhani and E. Axelsson. Calculation of void volume fraction in the subcooled and quality boiling regions. *International Journal of Heat and Mass Transfer*, 13(2):383–393, 1970.

[171] S. Haaf. *Wärmeübertragung in Luftkühlern*. Springer Verlag, Berlin, Germany, 1988. ISBN: 9783540154778.

[172] D. Q. Kern. *Process heat transfer*. McGraw-Hill, New York, United States of America, 1950. ISBN: 9780070341906.

[173] R. M. Manglik and A. E. Bergles. Heat transfer and pressure drop correlations for the rectangular offset strip fin compact heat exchanger. *Experimental Thermal and Fluid Science*, 10(2):171–180, 1995.

[174] M. Yousefi, R. Enayatifar, and A. N. Darus. Optimal design of plate-fin heat exchangers by a hybrid evolutionary algorithm. *International Communications in Heat and Mass Transfer*, 39(2):258 – 263, 2012.

[175] J. P. Veres. Centrifugal and axial pump design and off-design performance prediction. Technical report, NASA, Sunnyvale, United States of America, 1994. Technical Memorandum 106745.

[176] A. Bejan and M. J. Moran. *Thermal design and optimization*. John Wiley & Sons, Inc., Hoboken, United States of America, 1996. ISBN: 9780471584674.

[177] A. Valero, M. A. Lozano, L. Serra, G. Tsatsaronis, J. Pisa, C. Frangopoulos, and M. R. von Spakovsky. CGAM problem: definition and conventional solution. *Energy*, 19(3):279–286, 1994.

[178] M. A. Lozano, A. Valero, and L. Serra. Theory of exergetic cost and thermoeconomic optimization. In *Proceedings of the International Symposium ENSEC*, pages 339 – 350, Cracow, Poland, July 5 - 9 1993.

[179] Z. T. Lian, K. J. Chua, and S. K. Chou. A thermoeconomic analysis of biomass energy for trigeneration. *Applied Energy*, 87(1):84–95, 2010.

[180] S. G. Hall, S. Ahmad, and R. Smith. Capital cost targets for heat exchanger networks comprising mixed materials of construction, pressure ratings and exchanger types. *Computers & chemical engineering*, 14(3):319–335, 1990.

[181] M. Astolfi, M. C. Romano, P. Bombarda, and E. Macchi. Binary ORC (Organic Rankine Cycles) power plants for the exploitation of medium–low temperature geothermal sources–Part B: Techno-economic optimization. *Energy*, 66:435–446, 2014.

[182] Inflationdata web site. Inflation data, 2014. Available on: inflationdata.com/Inflation.

[183] L. Pierobon, T. V. Nguyen, U. Larsen, F. Haglind, and B. Elmegaard. Multi-objective optimization of organic Rankine cycles for waste heat recovery: Application in an offshore platform. *Energy*, 58(0):538–549, 2013.

[184] C. Bonacina, A. Cavallini, and L. Mattarolo. *Trasmissione del calore*. Cleup, Padova, Italy, 1992. ISBN: 9788871789200.

[185] M. P. Boyce. *Gas turbine engineering handbook*. Butterworth-Heinemann, Oxford, Great Britain, 2012. ISBN: 9780123838421.

[186] L. Pierobon, F. Haglind, R. Kandepu, A. Fermi, and N. Rossetti. Technologies for waste heat recovery in off-shore applications. In *Proceedings of*

ASME 2013 International Mechanical Engineering Congress & Exposition, pages 1–10, San Diego, California, November 2013.

[187] S. Quoilin, M. V. D. Broek, S. Declaye, P. Dewallef, and V. Lemort. Techno-economic survey of organic Rankine cycle (ORC) systems. *Renewable and Sustainable Energy Reviews*, 22:168–186, 2013.

[188] L. Pierobon and F. Haglind. Design and optimization of air bottoming cycles for waste heat recovery in off-shore platforms. *Applied Energy*, 118:156, 2014.

[189] A. Bejan. *Advanced engineering thermodynamics*. Wiley, 2006.

[190] H. S. Leff. Thermal efficiency at maximum work output: new results for old heat engines. *American Journal of Physics*, 55(7):602–610, 1987.

[191] A. Fakheri. A general expression for the determination of the log mean temperature correction factor for shell and tube heat exchangers. *JOURNAL OF HEAT TRANSFER-TRANSACTIONS OF THE ASME*, 125(3):527–530, 2003.

[192] O. Frank. *Simplified design procedure for tubular exhangers. Practical aspects of heat transfer.* Chem. Eng. Prog. Tech. Manual., 1978.

[193] F. Carchedi and G. R. Wood. Design and development of a 12:1 pressure ratio compressor for the Ruston 6-MW gas turbine. *Journal for Engineering for Power*, 104:823 – 831, 1982.

[194] L. Pierobon, K. Iyengar, P. Breuhaus, R. Kandepu, M. Hana, and F. Haglind. Dynamic performance of power generation systems for off-shore oil and gas platforms. In *Proceedings of ASME Turbo Expo 2014*, 2014.

[195] S. Sanaye and H. Hajabdollahi. Thermal-economic multi-objective optimization of plate fin heat exchanger using genetic algorithm. *APPLIED ENERGY*, 87(6):1893–1902, 2010.

[196] L. Calderazzi and P. Colonna di Paliano. Thermal stability of r-134a, r-141b, r-13i1, r-7146, r-125 associated with stainless steel as a containing material. *International Journal of Refrigeration*, 20(6):381 – 389, 1997.

[197] A. S. Hill, R. C. Striebich, M. Vangsness, K. Wohlwend, L. Q. Maurice, and T. Edwards. Thermal stability of energetic hydrocarbon fuels for use in combined cycle engines. *Journal of Propulsion and Power*, 17(6):1258–1262, 2001.

[198] M. Pasetti, C. M. Invernizzi, and P. Iora. Thermal stability of working fluids for organic rankine cycles: An improved survey method and experimental results for cyclopentane, isopentane and n-butane. *Applied Thermal Engineering*, 73(1):762 – 772, 2014.

[199] A. Tanzer. Discussion of 'an overheat boiler tube failure'. *Journal of Failure Analysis and Prevention*, 6(2):31–32, 2006.

[200] D. N. French. *Metallurgical failures in fossil fired boilers.* Wiley, United States of America, 1983. ISBN: 0471558397.

[201] A. Amendola. Hot spot expectation in nuclear reactor core thermal design. *Nuclear Science and Engineering*, 49:106–108, 1972.

[202] X. Zhang, M. Y. Yu, and B. Shen. Hot spot formation outside of the fusion-fuel core. *Physics of Plasmas*, 12(12):1–4, 2005.

[203] A. Gandini. Hot point detection method. *Annals of Nuclear Energy*, 38:2843–2847, 2011.

[204] R. Francis. Hot spot corrosion in condenser tube: its causes and prevention. *British Corrosion Journal*, 22:199–201, 1987.

[205] R. S. Prasher, J. Dirner, J. Y. Chang, A. Myers, D. Chau, S. Prstic, D. He, and R. S. Prasher. Effect of localized hotspot on the thermal performance of two-phase microchannel heat exchanger. *Proceedings of the ASME/Pacific Rim Technical Conference and Exhibition on Integration and Packaging of MEMS, NEMS, and Electronic Systems: Advances in Electronic Packaging 2005*, PART A:99–104, 2005.

[206] J. Eiden, O. Enger, N. Peci, S. Rutkowski, T. Vahlenkamp, and S. Wischhusen. Fluid.dissipation library, 2013.

[207] D. M. Ginosar, L. M. Petkovic, and D. P. Guillen. Thermal stability of cyclopentane as an organic Rankine cycle working fluid. *Energy & Fuels*, 25(9):4138–4144, 2011.

Author's Publications

Journals

- Benato A., Stoppato A., Mirandola A., Influenza delle Variazioni di Carico sulla Vita degli Impianti Termoelettrici, La Termotecnica, March 2013, Pages 1-4.

- Stoppato A., Cavazzini G., Benato A., Influenza degli Impianti Alimentati da Fonti Rinnovabili sulle Strategie di Gestione del Sistema Energetico, Atti e Memorie dell'Accademia Galileiana di Scienze, Lettere ed Arti in Padova. Parte II. Memorie della Classe di Scienze Matematiche e Naturali, ISSN 1592-1743.

- Benato A., Stoppato A., Bracco S., Combined Cycle Power Plant: a Comparison Between Two Different Dynamic Models to Evaluate Transient Behaviour and Residual Life, Energy Conversion and Management, Volume 87, November 2014, Pages 1269-1280.

- Pierobon L., Benato A., Scolari E., Haglind F., Stoppato A., Waste Heat Recovery Technologies for Off-shore Platforms, Applied Energy, Volume 136, December 2014, Pages 228-241.

Conferences

- Stoppato A., Benato A., Mirandola A., Assessment of Stresses and Residual Life of Plant Components in View of Life-Time Extension of Power Plants, In Proceedings of ECOS 2012 − The 25th International Conference On Efficiency, Cost, Optimization, Simulation And Environmental Impact Of Energy Systems, Pages 1-10, June 26-29, 2012, Perugia, Italy.

- Benato A., Stoppato A., Mirandola A., Influenza delle Variazioni di Carico sulla Vita degli Impianti Termoelettrici, In Proceedings of ATI 2012 − 67th

National Congress of The Associazione Termotecnica Italiana; Pages 1-10, September 11-14, 2012, Trieste, Italy.

- Benato A., Bracco S., Stoppato A., A Comparison between Two Different Approaches aimed at Simulating the Behaviour of Combined Cycles in Transient Conditions, Accepted as Archival at 8th Conference on Sustainable Development of Energy, Water and Environment Systems; September 22-27, 2013, Dubrovnik, Croatia.

- Stoppato A., Benato A., Destro N., Mirandola A., Optimal Design and Management of a Cogeneration System with Energy Storage, In Proceedings of ECOS 2014 − The 27th International Conference on Efficiency, Cost, Optimization, Simulations and Environmental Impact of Energy Systems, June 15-19, 2014, Turku, Finland.

- Benato A., Stoppato A., Bracco S., Dynamic Behaviour Analysis of a Single Pressure Heat Recovery Steam Generator during Cycling Operation, In Proceedings of ECOS 2014 − The 27th International Conference on Efficiency, Cost, Optimization, Simulations and Environmental Impact of Energy Systems, June 15-19, 2014, Turku, Finland.

- Stoppato A., Cavazzini G., Benato A., Destro N., Optimal Design and Management of a Hybrid Photovoltaic Pump Hydro Energy Storage System, In proceedings of The ASME 2014 − 12th Biennial Conference on Engineering Systems Design and Analysis, June 25-27, 2014, Copenhagen, Denmark.

- Benato A., Pierobon L., Stoppato A., Haglind F., Dynamic Performance of a Combined Gas Turbine and Air Bottoming Cycle Plant for Off-shore Applications, In proceedings of The ASME 2014 − 12th Biennial Conference on Engineering Systems Design and Analysis, June 25-27, 2014, Copenhagen, Denmark.

Book Chapters

- Mirandola A., Stoppato A., Benato A., Steam Power Generation, Handbook of Clean Energy Systems, Published by John Wiley & Sons, Ltd., The Atrium, Southern Gate, Chichester, West Sussex, PO19 8SQ, United Kingdom.

- Stoppato A., Benato A., Mirandola A., Gas Turbines and Combined Cycle Gas Turbine, Compendium of Energy Science and Technology (in 10 Vols), Vol. 9, Published by Stadium Press LLC, USA.

Other Publications

- Benato A., Micropompa: Caratteristiche di una Pompa Innovativa RSP (Micropump: Characteristics of an Innovative Rotary Shaft Pump), Bachelor Degree Thesis, 2007, University of Padova, Padova, Italy.
- Benato A., Performance Analysis of a 1.5 kW Horizontal-Axis Wind Turbine (HAWT), Master Degree Thesis, 2010, University of Padova, Padova, Italy.
- Benato A., Influenza delle Variazioni di Carico sulla Vita dei Componenti degli Impianti Termoelettrici, Scientific Report, 2011, University of Padova, Padova, Italy.

Other Works Accepted for Publication

- Benato A., Pierobon L., Kaern M. R., Haglind F., Stoppato A., Analysis of hot spots in boiler of organic Rankine cycle units during transient operation, Applied Energy.
- Benato A., Stoppato A., Bracco S., Dynamic Behaviour Analysis of a Single Pressure Heat Recovery Steam Generator during Cycling Operation, Energy Conversion and Management.
- Stoppato A., Benato A., Destro N., Mirandola A., Optimal Design and Management of a Cogeneration System with Energy Storage, Energy and Buildings.